

Cover Page



Universiteit Leiden



The following handle holds various files of this Leiden University dissertation:
<http://hdl.handle.net/1887/59461>

Author: Yamamoto, Y.

Title: Systems pharmacokinetic models to the prediction of local CNS drug concentrations in human

Issue Date: 2017-11-21

**SYSTEMS PHARMACOKINETIC
MODELS TO THE PREDICTION OF LOCAL
CNS DRUG CONCENTRATIONS IN HUMAN**

Yumi Yamamoto

Ph.D. Thesis, Leiden University, November 2017

The research presented in this thesis was performed within the framework of project no. D2-501 of the former Dutch Top Institute Pharma, currently Lygature (Leiden, the Netherlands) at the Division of Pharmacology of the Leiden Academic Centre for Drug Research (LACDR), Leiden University, Leiden, the Netherlands.

Financial support for the printing of this thesis was provided by:
Leiden Academic Centre for Drug Research (LACDR)

Cover and Layout:	Design Your Thesis, Rotterdam, the Netherlands
Printing:	Ridderprint B.V., Ridderkerk, the Netherlands
ISBN:	978-94-6299-684-7

©2017 Yumi Yamamoto. No part of this thesis may be reproduced or transmitted in any form or by any mean without written permission of the author and the publisher holding the copyright of the published articles.

SYSTEMS PHARMACOKINETIC MODELS TO THE PREDICTION OF LOCAL CNS DRUG CONCENTRATIONS IN HUMAN

PROEFSCHRIFT

ter verkrijging van
de graad van Doctor aan de Universiteit Leiden
op gezag van Rector Magnificus prof.mr. C.J.J.M. Stolker,
volgens besluit van het College voor Promoties
te verdedigen op dinsdag 21 november 2017
klokke 13:45 uur

door

Yumi Yamamoto
geboren te Tokio, Japan
in 1980

Promotor: Prof. Dr. M. Danhof

Co-promotor: Dr. E.C.M. de Lange

Promotiecommissie: Prof. Dr. H. Irth, voorzitter
Prof. Dr. J.A. Bouwstra, secretaris
Prof. Dr. A. Rostami, University of Manchester
Prof. Dr. R. Masereeuw, Universiteit Utrecht
Prof. Dr. J. Burggraaf, Universiteit Leiden
Prof. Dr. O.C. Meijer, Universiteit Leiden
Prof. Dr. T. Hankemeier, Universiteit Leiden

Everything that humans can imagine is a possibility in reality

- Willy Karen-

Aan allen die mij dierbaar zijn

TABLE OF CONTENTS

CHAPTER 1	Scope and intent of investigations	9
CHAPTER 2	Microdialysis: the key to physiologically based model prediction of human CNS target site concentrations	19
CHAPTER 3	A generic multi-compartmental CNS distribution model structure for 9 drugs allows prediction of human brain target site concentrations	57
CHAPTER 4	Predicting drug concentration-time profiles in multiple CNS compartments using a comprehensive physiologically based pharmacokinetic model	105
CHAPTER 5	Prediction of human CNS pharmacokinetics using a physiologically based pharmacokinetic modeling approach	141
CHAPTER 6	General discussion and future perspectives	181
APPENDIX	English summary	197
	Nederlandse samenvatting	205
	Acknowledgements	215
	Curriculum vitae	217
	List of publications	219



Scope and intent of investigations

Development of drugs for central nervous system (CNS)-associated diseases has suffered from high attrition rates (1,2) due to safety and efficacy issues (3). To improve the prediction of CNS drug effects, knowledge of the CNS target-site pharmacokinetics (PK) of especially the unbound drug is indispensable (4). However, measuring drug concentrations in the CNS of healthy volunteers or patients has major practical and ethical constraints. Plasma concentrations are therefore still the mainstay in the selection of optimal dose regimens in clinical CNS drug development, even though these concentrations may differ substantially from the local concentrations in the CNS. The differences in drug concentrations between plasma and CNS originate from the barrier properties of the blood-brain barrier (BBB) and the processes that govern intra-brain distribution (5). Therefore, it is important to search for robust approaches that can aid in the prediction of CNS target-site PK to improve CNS drug development.

The ultimate aim of the research described in this thesis is to develop a comprehensive mathematical PK model for the prediction of concentration-time profiles of (unbound) small molecule drugs in multiple CNS compartments in humans. This model is created in a step-wise manner in chapters 3, 4 and 5.

Chapter 2 starts with a summary review of the CNS systems properties and processes (physiological characteristics) that are relevant for the prediction of CNS PK, both in healthy and in disease conditions. In addition, an overview on experimental techniques and approaches to obtain direct or indirect information on CNS concentrations is given. Finally, state-of-the-art model-based approaches to predict CNS PK are provided. This chapter forms the base knowledge for the models developed in the successive chapters of this thesis.

The CNS consists of several major physiological components such as the brain vasculature, the cells that form the BBB and the blood-cerebrospinal fluid-barrier (BCSFB), the brain parenchymal cells, the brain extracellular fluid (brain_{ECF}) and several spaces filled with cerebrospinal fluid (CSF). In addition, physiological flows such as the cerebral blood flow, brain_{ECF} bulk flow and CSF flow exist. These physiological CNS components and the physicochemical properties of the drug, govern in concert the rate and extent of drug transport across the BBB and BCSFB and its intra-brain distribution, which can display substantial variations among different drugs. While the drug properties are a given, CNS systems characteristics are condition dependent, and single or multiple CNS systems characteristics may be altered by diseases. Alterations in CNS systems characteristics may have a significant impact on CNS drug distribution (6–24) and must therefore be considered in drug development.

Currently available experimental techniques and approaches to measure CNS drug concentrations have focused mostly on steady state conditions, and often do not distinguish between total and unbound drug concentrations. As, even in chronic dosing, drug concentrations in plasma and CNS will vary over time, and transport processes are time-dependent, time-course concentration data are crucial to properly understand and predict CNS PK. In addition, information on unbound drug concentrations is a prerequisite not only because it drives the drug effects, but also the different transport processes. Microdialysis is a highly valuable technique, as it allows the *in vivo* measurement of unbound drug concentration kinetics, at different CNS locations (25–30). However, though minimally invasive, the use of microdialysis in humans is highly restricted. Therefore, approaches that can predict time-dependent and CNS location-dependent unbound drug concentration in human are of great relevance. Of all the mathematical PK modeling approaches that have been proposed to predict CNS PK (28–42), so far none has captured enough CNS systems complexity, which indicates the need for the development of more comprehensive CNS PK models.

Chapter 3 describes the development of a multi-compartmental CNS PK model. By the use of microdialysis unbound drug concentration-time data (in rat plasma, brain_{ECP} and two CSF sites) for nine drugs with wide range of drug physiochemical properties, and rat CNS system characteristics taken from literature, a generic multi-compartmental CNS PK model structure is identified. The model consists of plasma and main CNS physiological compartments (brain_{ECP}, the brain intracellular fluid (brain_{ICF}), and four different CSF sites) that can adequately describe the *in vivo* rat PK data of the nine different drugs. Subsequent scaling of the model from rat to human makes it possible to predict unbound drug concentration-time profiles in human CNS at multiple locations. This generic CNS PK model structure is then used further for the development of comprehensive physiologically based pharmacokinetic (PBPK) models for rat and human CNS in the next two chapters.

Chapter 4 describes the development of a comprehensive rat CNS PBPK model, which includes descriptors of multiple CNS physiological compartments and drug distribution processes in the CNS. In contrast to the generic multi-compartmental CNS PK model (Chapter 3), the comprehensive CNS PBPK model is able to predict unbound drug PK profiles in multiple CNS physiological compartments in the rat without the need to have PK data from *in vivo* animal studies. This is possible on the basis of information of drug-specific parameters that can be obtained either by *in silico* predictions or *in vitro* studies. The predictive performance of the model is evaluated using detailed unbound drug concentration-time profiles from ten small molecule drugs in rat plasma, brain_{ECP}, two CSF sites, and total brain tissue.

Chapter 5 describes the scaling of the comprehensive CNS PBPK model developed in Chapter 4 from rat to human. The predictive value of this model is evaluated using unbound drug concentration-time data in brain_{ECF} and/or CSF from three drugs, which are obtained from human subjects under physiological CNS conditions. Furthermore, the model is applied to investigate the underlying factors that may explain altered CNS PK in pathophysiological CNS conditions in patients with traumatic brain injury and epilepsy.

Chapter 6 summarizes and discusses the results presented in this thesis on the prediction of unbound drug concentration-time profiles in multiple CNS compartments in human. Furthermore, this chapter provides future perspectives towards a comprehensive PBPK-Pharmacodynamic model to predict drug efficacy in human CNS.

REFERENCES

1. Kola I, Landis J. Can the pharmaceutical industry reduce attrition rates? *Nat Rev Drug Discov.* 2004;3:1–5.
2. Hurko O, Ryan JL. Translational Research in Central Nervous System Drug Discovery. *J Am Soc Exp Neurother.* 2005;2(4):671–82.
3. Arrowsmith J, Miller P. Trial Watch: Phase II and Phase III attrition rates 2011–2012. *Nat Rev Drug Discov.* 2013;12(8):569–569.
4. Danhof M, de Lange ECM, Della Pasqua OE, Ploeger BA, Voskuyl RA. Mechanism-based pharmacokinetic-pharmacodynamic (PK-PD) modeling in translational drug research. *Trends Pharmacol Sci.* 2008;29(4):186–91.
5. Hammarlund-Udenaes, M Paalzow L, de Lange E. Drug equilibration across the blood-brain barrier—pharmacokinetic considerations based on the microdialysis method. *Pharm Res.* 1997;14(2):128–34.
6. Serot JM, Béné MC, Foliguet B, Faure GC. Altered choroid plexus basement membrane and epithelium in late-onset Alzheimer's disease: An ultrastructural study. *Ann N Y Acad Sci.* 1997;826:507–9.
7. Aanerud J, Borghammer P, Chakravarty MM, Vang K, Rodell AB, Jónsdóttir KY, et al. Brain energy metabolism and blood flow differences in healthy aging. *J Cereb Blood Flow Metab.* 2012;32(7):1177–87.
8. Shimada A, Hasegawa-Ishii S. Senescence-accelerated Mice (SAMs) as a Model for Brain Aging and Immunosenescence. *Aging Dis.* 2011;2(5):414–35.
9. Silverberg GD, Miller MC, Messier AA, Majmudar S, Machan JT, Donahue JE, et al. Amyloid deposition and influx transporter expression at the blood-brain barrier increase in normal aging. *J Neuropathol Exp Neurol.* 2010;69(1):98–108.
10. Greve MW, Zink BJ. Pathophysiology of traumatic brain injury. *Mt Sinai J Med.* 2009;76(2):97–104.
11. Chodobski A, Zink BJ, Szmydynger-Chodobska J. Blood-Brain Barrier Pathophysiology in Traumatic Brain Injury. *Transl Stroke Res.* 2011;2(4):492–516.
12. Pop V, Sorensen DW, Kamper JE, Ajao DO, Murphy MP, Head E, et al. Early brain injury alters the blood-brain barrier phenotype in parallel with b-amyloid and cognitive changes in adulthood. *J Cereb Blood Flow Metab.* 2013;33:205–14.
13. Appel S, Duke ES, Martinez AR, Khan OI, Dustin IM, Reeves-Tyer P, et al. Cerebral blood flow and fMRI BOLD auditory language activation in temporal lobe epilepsy. *Epilepsia.* 2012;53(4):631–8.
14. Bednarczyk J, Lukasiuk K. Tight junctions in neurological diseases. *Acta Neurobiol Exp.* 2011;71(4):393–408.

15. Lazarowski A, Czornyj L, Lubienieki F, Girardi E, Vazquez S, D’Giano C. ABC transporters during epilepsy and mechanisms underlying multidrug resistance in refractory epilepsy. *Epilepsia*. 2007;48:140–9.
16. Löscher W, Potschka H. Role of multidrug transporters in pharmacoresistance to antiepileptic drugs. *J Pharmacol Exp Ther*. 2002;301(1):7–14.
17. Palmer JC, Baig S, Kehoe PG, Love S. Endothelin-converting enzyme-2 is increased in Alzheimer’s disease and up-regulated by Abeta. *Am J Pathol*. 2009;175(1):262–70.
18. Bowman G, Quinn J. Alzheimer’s disease and the blood–brain barrier: past, present and future. *Aging health*. 2008;4(1):47–57.
19. Cipolla MJ, Sweet JG, Chan S-L. Cerebral vascular adaptation to pregnancy and its role in the neurological complications of eclampsia. *J Appl Physiol*. 2011;110(2):329–39.
20. Dutheil F, Jacob A, Dauchy S, Beaune P, Scherrmann J-M, Declèves X, et al. ABC transporters and cytochromes P450 in the human central nervous system: influence on brain pharmacokinetics and contribution to neurodegenerative disorders. *Expert Opin Drug Metab Toxicol*. 2010;6(10):1161–74.
21. Hsu JL, Jung TP, Hsu CY, Hsu WC, Chen YK, Duann JR, et al. Regional CBF changes in Parkinson’s disease: A correlation with motor dysfunction. *Eur J Nucl Med Mol Imaging*. 2007;34(9):1458–66.
22. van Vliet EA, Araújo SDC, Redeker S, van Schaik R, Aronica E, Gorter JA. Blood-brain barrier leakage may lead to progression of temporal lobe epilepsy. *Brain*. 2007;130(2):521–34.
23. Ingrisch M, Sourbron S, Morhard D, Ertl-Wagner B, Kümpfel T, Hohlfeld R, et al. Quantification of Perfusion and Permeability in Multiple Sclerosis. *Invest Radiol*. 2012;47(4):252–8.
24. Weiss N, Miller F, Cazaubon S, Couraud PO. The blood-brain barrier in brain homeostasis and neurological diseases. *Biochim Biophys Acta*. 2009;1788(4):842–57.
25. Hammarlund-Udenaes M, Paalzow LK, de Lange ECM. Drug equilibration across the blood-brain barrier - Pharmacokinetic considerations based on the microdialysis method. *Pharm Res*. 1997;14(2):128–34.
26. Hammarlund-Udenaes M. The use of microdialysis in CNS drug delivery studies: Pharmacokinetic perspectives and results with analgesics and antiepileptics. *Adv Drug Deliv Rev*. 2000;45(2–3):283–94.
27. de Lange ECM, Danhof M, de Boer AG, Breimer DD. Critical factors of intracerebral microdialysis as a technique to determine the pharmacokinetics of drugs in rat brain. *Brain Res*. 1994;666(1):1–8.
28. Westerhout J, Ploeger B, Smeets J, Danhof M, de Lange ECM. Physiologically based pharmacokinetic modeling to investigate regional brain distribution kinetics in rats. *AAPS J*. 2012;14(3):543–53.

29. Westerhout J, Smeets J, Danhof M, de Lange ECM. The impact of P-gp functionality on non-steady state relationships between CSF and brain extracellular fluid. *J Pharmacokinet Pharmacodyn*. 2013;40(3):327–42.
30. Westerhout J, van den Berg D-J, Hartman R, Danhof M, de Lange ECM. Prediction of methotrexate CNS distribution in different species - Influence of disease conditions. *Eur J Pharm Sci*. 2014;57:11–24.
31. Collins JM, Dedrick RL. Distributed model for drug delivery to CSF and brain tissue. *Am J Physiol*. 1983;245(3):303–10.
32. Ooie T, Terasaki T, Suzuki H, Sugiyama Y. Kinetic Evidence for Active Efflux Transport across the Blood-Brain Barrier of Quinolone Antibiotics. *J Pharmacol Exp Ther*. 1997;283(1):293–304.
33. Takasawa K, Terasaki T, Suzuki H, Ooie T, Sugiyama Y. Distributed model analysis of 3'-azido-3'-deoxythymidine and 2',3'-dideoxyinosine distribution in brain tissue and cerebrospinal fluid. *J Pharmacol Exp Ther*. 1997;282(3):1509–17.
34. Hansen DK, Scott DO, Otis KW, Lunte SM. Comparison of in vitro BBMEC permeability and in vivo CNS uptake by microdialysis sampling. *J Pharm Biomed Anal*. 2002;27:945–58.
35. Bourasset F, Scherrmann JM. Carrier-mediated processes at several rat brain interfaces determine the neuropharmacokinetics of morphine and morphine-6-beta-D-glucuronide. *Life Sci*. 2006;78(20):2302–14.
36. Liu X, Smith BJ, Chen C, Callegari E, Becker SL, Chen X, et al. Use of a Physiologically Based Pharmacokinetic Model to Study the Time to Reach Brain Equilibrium: An Experimental Analysis of the Role of Blood-Brain Barrier Permeability, Plasma Protein Binding, and Brain Tissue Binding. *J Pharmacol Exp Ther*. 2005;313(3):1254–62.
37. Kielbasa W, Stratford RE. Exploratory Translational Modeling Approach in Drug Development to Predict Human Brain Pharmacokinetics and Pharmacologically Relevant Clinical Doses. *Drug Metab Dispos*. 2012;40(5):877–83.
38. Fenneteau F, Turgeon J, Couture L, Michaud V, Li J, Nekka F. Assessing drug distribution in tissues expressing P-glycoprotein through physiologically based pharmacokinetic modeling: model structure and parameters determination. *Theor Biol Med Model*. 2009;36:495–522.
39. Ball K, Bouzom F, Scherrmann J-M, Walther B, Declèves X. Physiologically Based Pharmacokinetic Modelling of Drug Penetration Across the Blood-Brain Barrier--Towards a Mechanistic IVIVE-Based Approach. *AAPS*. 2013;15(4):913–32.
40. Badhan RKS, Chenel M, Penny JI. Development of a Physiologically-Based Pharmacokinetic Model of the Rat Central Nervous System. *Pharmaceutics*. 2014;6(1):97–136.
41. Trapa PE, Belova E, Liras JL, Scott DO, Steyn SJ. Insights from an Integrated Physiologically Based Pharmacokinetic Model for Brain Penetration. *J Pharm Sci*. 2016;105(2):965–71.

42. Gaohua L, Neuhoff S, Johnson TN, Rostami-hodjegan A, Jamei M. Development of a permeability-limited model of the human brain and cerebrospinal fluid (CSF) to integrate known physiological and biological knowledge: Estimating time varying CSF drug concentrations and their variability using in vitro data. *Drug Metab Pharmacokinet*. 2016;31(3):224–33.



Microdialysis: the key to physiologically based model prediction of human CNS target site concentrations

Y Yamamoto, M Danhof, E C M de Lange

Modified of the AAPS journal 2017; 19(4): 891-909

ABSTRACT

Despite the enormous research efforts that have been put into the development of central nervous system (CNS) drugs, the success rate in this area is still disappointing. To increase the successful rate in the clinical trials, first the problem of predicting human CNS drug distribution should be solved.

As it is the unbound drug that equilibrates over membranes and is able to interact with targets, especially knowledge on unbound extracellular drug concentration-time profiles in different CNS compartments is important. The only technique able to provide such information *in vivo* is microdialysis. Also, obtaining CNS drug distribution data from human subjects is highly limited and therefore we have to rely on preclinical approaches combined with physiologically based pharmacokinetic (PBPK) modeling, taking unbound drug CNS concentrations into account. The next step is then to link drug concentrations in local CNS to target interaction kinetics and CNS drug effects.

In this review, system properties and small molecule drug properties that together govern CNS drug distribution are summarized. Furthermore, the currently available approaches on prediction of CNS pharmacokinetics are discussed, including *in vitro*, *in vivo*, *ex vivo* and *in silico* approaches, with special focus on the powerful combination of *in vivo* microdialysis and PBPK modeling. Also, sources of variability on drug kinetics in the CNS are discussed. Finally, remaining gaps and challenges are highlighted and future directions are suggested.

INTRODUCTION

There is a huge unmet medical need for central nervous system (CNS) disease therapies because of the growing of chronic and complex diseases associated with aging. However development of CNS drugs is one of the most challenging tasks for the pharmaceutical industry (1). Actually, drug development for CNS drugs has suffered a higher attrition rate compared to that of other therapeutic areas drugs; it has been reported that only around 8-9% of CNS drugs that entered phase 1 were approved to launch (2). And around 50% of the attrition of potential CNS drugs has resulted due to a lack of efficacy and safety issues in phase 2 (2,3). Knowledge of human CNS drug concentrations forms the basis for understanding exposure-response relationships therefore the lack of appropriate consideration of these target-site drug concentrations is one of the factors contributing to this high degree of attrition.

Obtaining the target-site concentrations of CNS drugs is not straightforward because plasma concentrations do not adequately reflect CNS exposure, primarily due to the presence of the blood-brain barrier (BBB) and the blood-cerebrospinal fluid barriers (BCSFB), and additional specific physiological characteristics of the CNS. Furthermore, significant variation in the rate and extent of mechanisms that govern target-site pharmacokinetics (PK), target engagement and signal transduction is known to exist, due to differences in system conditions such as species, gender, genetic background, age, diet, disease and drug treatment (4). Moreover, with regard to CNS drug action there is a lack of sufficiently established clinical biomarkers and proof-of-concept (5). Thus, it is clear that there is a need for more predictive approaches. These predictive approaches have to be interconnected to the system conditions and must be performed using adequate (including bound and unbound drug) concentrations. Also processes should preferably not be studied in isolation and then combined, but instead studied in conjunction with each other as this will provide insight about the interdependencies of these processes (4). Since measurement on CNS target-site concentration in the clinical setting is highly restricted, we have to develop an approach based on integrated preclinical data that is translatable to human.

Even though drug properties have been investigated well, information of CNS system properties (CNS physiology and biochemistry) is sparse and has a large variability. Drug PK in the CNS is determined by their interaction. System properties depend on the condition of the system, which means that we have to use approaches to distinguish between system and drug properties, as this would allow us to translate the model to other species and also other disease conditions, by using physiologically based pharmacokinetic (PBPK) modeling.

Currently many more or less complex semi-PBPK models have been published for CNS drug distribution. At present, 3 preclinical translational models have been validated with human CNS concentration profiles (6–8). In these models, however, the parameters were estimated using *in vivo* data to describe CNS distribution of individual drug in animals. Ultimate goal of the PBPK modeling is to build a generic PBPK model in which the parameters are derived from *in vitro* and/or *in silico* data. To achieve this, *in vivo* data is needed to validate the generic PBPK model. Furthermore, an investigation is needed on the relationship between drug physicochemical properties and CNS distribution.

In this review, system properties and small molecule drug properties that together govern CNS drug distribution are summarized, followed by currently available approaches on prediction of drug PK in the CNS, including *in vitro*, *in vivo*, *ex vivo* and *in silico* approaches, with special focus on the powerful combination of *in vivo* microdialysis and PBPK modeling. Also, sources of variability on drug kinetics in the CNS are discussed. Finally, remaining gaps and challenges will be discussed and future directions will be provided.

INTERACTION BETWEEN CNS SYSTEM- AND DRUG PROPERTIES

Many CNS system properties and drug specific properties are known to influence drug kinetics in the brain, as shown in **Figure 1**. Here we focus on the relevant factors from each that contribute to the drug kinetics, and summarize their function.

CNS system properties

Physiological compartments, flows and pH

The CNS is a complex system composed of many physiological components and flows (**Figure 2**): Physiological compartments are the BBB, the BCSFB, brain extracellular fluid (brain_{ECF}), cerebral blood, brain parenchymal cells, and the cerebrospinal fluid (CSF) in the ventricles, the cisterna magna, and the subarachnoid space (4). There are pH differences among the compartments (9–15). Then there are the CNS fluid flows that include the cerebral blood flow, brain_{ECF} bulk flow, and CSF flow. All relevant physiological parameter values are summarized in **Table I**.

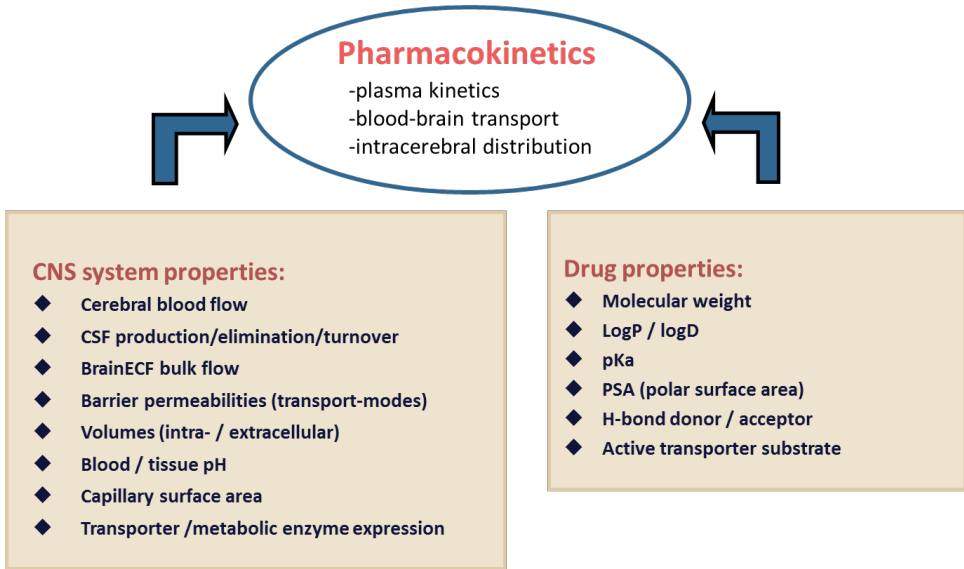


Figure 1. System and drug properties which govern drug kinetics in brain. The figure is modified from de Lange (4).

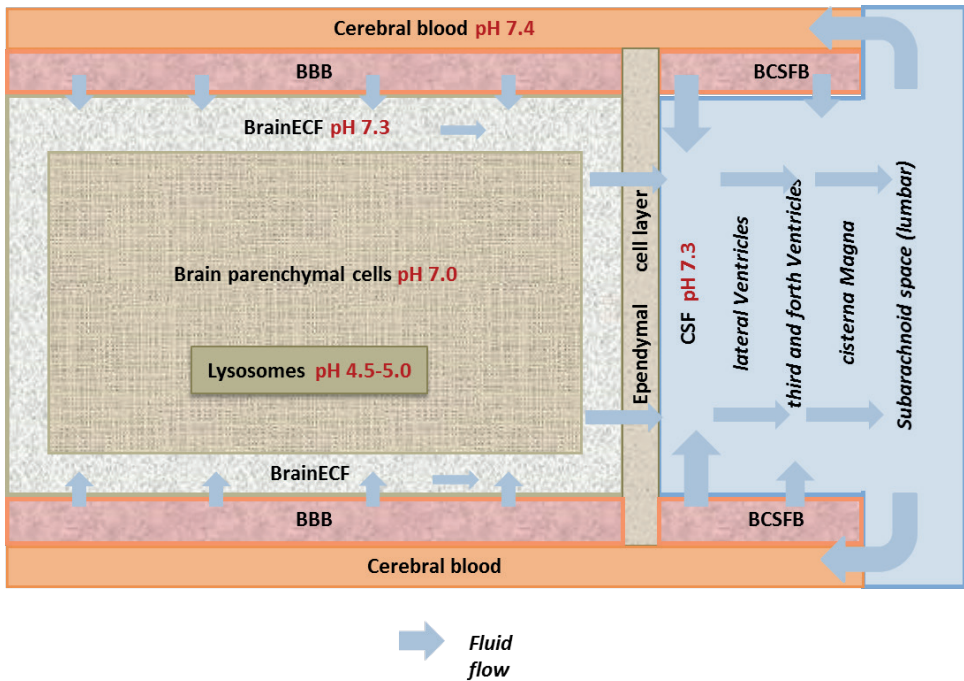


Figure 2. Brain physiological components and flow. The figure is modified from de Lange (4).

Active transporters

The localization of transporters, and their expression level are also important factors to determine drug distribution in the brain. Transporters are present at the BBB and at the BCSFB, also on the membrane of brain parenchyma. Active transporters on the BBB and BCSFB consist of facilitated transport and ATP-dependent transport. The solute carrier (SLC) family, such as organic anion-transporting polypeptide (OATP) and organic anion transporters (OATs) are categorized as a facilitated transport, while ABC transporters, such as P-glycoprotein (P-gp), multidrug resistance protein (MRPs) and breast cancer-resistant protein (BCRP) are categorized as an ATP-dependent transport (16). **Table II** summarizes an overview of transporters with their localization, and their endogenous and exogenous substrates.

Metabolic enzymes

Presence and localization of enzymes in the brain are also important factors to determine drug kinetics in the brain. In the brain the following enzymes are found: oxidoreductases such as cytochrome P450 (CYPs) and monoamine oxidase (MAO), membrane-bound and soluble catechol-O-methyltransferase (COMT), and transferases such as uridine 5-diphospho (UDP) -glucuronosyltransferases (UGTs) and phenol sulfotransferase (PST) (17). In **Table III**, an overview is provided of the different enzymes with their localization, and examples of their endogenous and exogenous substrates.

Table I. Values of CNS system properties for rat and human

	Parameter	Human	Refs	Rat	Refs
Volumes	BBB volume	8.25 mL (calculated using thickness endothelial cell of 550 nm)	(18)	5.02 μ L	(19)
	BCSFB volume	107.25 mL (calculated using thickness 14.3 μ m of endothelial cell)	(20)	37.5 μ L	(19)
	Brain volume	1400 g	(21)	1.8 g, 1880 μ L	(22,23)
	Brain _{ECF} volume	240-280 mL	(24,25)	290 μ L	(26)
	Brain _{ICF} volume	960 mL	(25)	1440 μ L	(25)
	CSF volume	130-150 mL	(27,28)	250 μ L	(22)
	CSF _{LV} volume	20-25 mL	(27,29)	50 μ L	(30,31)
	CSF _{TFV} volume	20-25 mL	(27,29)	50 μ L	(30,31)
	CSF _{CM} volume	7.5 mL	(32,33)	17 μ L	(32,33)
	CSF _{SAS} volume	90-125 mL	(27,29)	180 μ L	(34,35)
Flows	cerebral blood flow	610-860 mL/min	(36-38)	1.1-1.3 mL/min	(39,40)
	brain _{ECF} flow	0.15-0.2 mL/min (50% of CSF production)	(28)	0.00018-0.00054 mL/min	(41)
	CSF flow	0.3-0.4 mL/min	(28)	0.0022 mL/min	(26,42)
Surfaces	BBB SA	12-18 m ²	(18)	155-263 cm ²	(43,44)
	BCSFB SA	6-9 m ² (assumed 50% of BBB SA)	(18)	25-75 cm ² (assumed 50% of BBB SA)	(43,45)
	brain ECF/ICF SA	228 m ²	Calculated ^{a)}	3000 cm ²	(19)
	brain ICF/lysosome SA	12 m ²	Calculated ^{a)}	162 cm ²	Calculated ^{a)}
pH	Plasma	7.4	(12)	7.4	(9)
	Brain _{ECF}	NA		7.3	(10)
	Brain _{ICF}	7.0	(13)	7.0	(10)
	lysosome	4.5-5.0	(14)	5.0	(10)
	CSF	7.3	(12)	7.3	(11)

^{a)} Calculation was performed based on an assumption that the brain cells and lysosome are spherical.

brain_{ECF}; a brain extracellular fluid compartment, brain_{ICF}; a brain intracellular fluid compartment, CSF_{LV}; a compartment of cerebrospinal fluid in lateral ventricle, CSF_{TFV}; a compartment of cerebrospinal fluid in the third and fourth ventricle, CSF_{CM}; a compartment of cerebrospinal fluid in the cisterna magna, CSF_{SAS}; a compartment of cerebrospinal fluid in the subarachnoid space, SA; surface area

Table II. Transporters in the CNS

Transporter (Gene name in human) (Gene name in rat)	Tissue	Location			Substrates			Function		
		Human	Rat	Refs	Endogenous	Refs	Exogenous	Refs	Function	Refs
P-gp (ABCB1) (Abcb1a)	BBB	luminal membrane of the BCEC	luminal membrane of the BCEC	(46–48)			antineoplastic agents, anticancer drugs, corticoids, analgesics, hydrophobic neutral or cationic compounds		efflux	(51)
	BCSFB		apical side of the CPEC	(52)	cytokines	(49)			influx/ efflux	(52–54)
	BP	adjacent pericytes and astrocytes	astrocytes	(48,55)					efflux	(55)
MRPs (ABCC1) (Abcc1)	BBB	luminal and abluminal membranes of the BCEC	luminal and abluminal membranes of the BCEC	(52,56–58)	conjugated metabolites such as glutathione- and glucuronide- conjugates		anticancer drugs, organic anion compounds, 17 β -estradiol-d-17 β - glucuronide		efflux/ influx	(54,60)
	BCSFB	luminal and abluminal membranes of the CPEC	luminal and abluminal membranes of the CPEC	(61,62)		(59)			efflux	(63)
	BP	astrocytes and microglial cells	astrocytes and microglial cells	(60)						
OTAPs (SLCO, formerly SLC21A) (Slco1a/b)	BBB		luminal and abluminal membranes of the BCEC (Oatp1a4 and Oatp1a5 and OATP2)	(16,64,65)					efflux/ influx	(61)
	BCSFB		luminal membrane of the CPEC (Oatp1a4 and Oatp1a5, OATP2)	(16,64)	amphipathic organ anions	(16)	opioid peptides, E217bG	(66)		
	BBB		brush border membrane of the CPEC (OATP1)	(16)						
OATs (SLC22A) (Slc22a)	BBB		abluminal membrane of the BCEC	(16)	organic anions	(67)			efflux/ influx	(16,61)
	BCSFB									

BBB; blood–brain barrier; BCSFB; Blood–cerebrospinal fluid barrier; BP; brain parenchymal cells; BCEC; brain capillary endothelial cells; CPEC; choroid plexus epithelial cells

Table III. Metabolic enzymes in the CNS

Enzyme	Human		Rat		Endogenous Substrates	Refs	Exogenous substrates	Refs
	Location	Refs	Enzyme	Location				
CYPs								
CYP1A1		(68)	CYP1A1		Melatonin, estradiol, arachidonic acid, progesterone, all-trans-retinal acid	(69)		
CYP1A2		(68)	(CYP1A2)					
CYP1B1	cerebral microvessels at the BBB	(68,70)			Melatonin, estradiol	(69)		
			CYP2B		Arachidonic acid, testosterone, serotonin, anandamide, all-trans-retinoic acid,	(69)	Propofol	(71)
CYP2B6	pyramidal neurons of the frontal cortex and astrocytes surrounding cerebral blood vessels	(68,72)			17- β estradiol, anandamide, arachidonic acid, estrone, serotonin, testosterone	(69)	Bupropion, diazepam, ketamine, methadone, meperidine, nicotine, pentobarbital, phencyclidine, propofol, sertraline selegiline, tramadol	(69)
CYP2C		(68)	CYP2C		Testosterone, progesterone, arachidonic acid, serotonin, harmaline, harmine, linoleic acid, melatonin, all-trans-retinoic acid	(69)		
			CYP2C13					
			CYP2D	neuron, glia cells, choroid plexus	5-methoxytryptamine, octopamine, synephrine, tyramine, progesterone, anandamide, harmaline, harmine	(69)		

Table III. (continued)

Enzyme	Human		Rat		Endogenous Substrates	Refs	Exogenous substrates	Refs
	Location	Refs	Enzyme	Location				
CYPs								
CYP2D6					5-methoxytryptamine, anandamide, progesterone, tyramine	(69)	Mirtazapine, brofaromine, clomipramine, codeine, citalopram, clozapine, desipramine, dextromethorphan, ethylmorphine, fluoxetine, fluvoxamine, haloperidol, hydrocodone, imipramine, mianserin, mirtazapine, nergoline, nortryptaline, oxycodone, paroxetine, perphenazine, risperidone, tramadol, tranylcypromine, venlafaxine, zuclopenthixol	(74–76)
						(68)		
						(68)		
CYP2E		(68)						
CYP3A		(68)			Arachidonic acid, linoleic acid, oleic acid, 17- β -estradiol, estrone, prostaglandin	(68)	Enflurane, felbamate, halothane, isoflurane, sevoflurane, trimethadione	(69)
CYP3A51		(68)						
						(68)		
						(68)		
						(68)		
COMT								
membrane-bound	prefrontal cortex	(77)	membrane-bound	prefrontal cortex	Dopamine	(77)		(78)
soluble	prefrontal cortex	(77)	soluble	prefrontal cortex		(77)		

Table III. (continued)

Enzyme	Human		Rat		Endogenous Substrates	Refs	Exogenous substrates	Refs
	Location	Refs	Enzyme	Location				
MAO								
MAOA	Adrenergic neurons	(79)	MAOA		Noradrenaline, adrenaline, dopamine, β-phenylethylamine and serotonin	(83)		
MAOB	Astrocytes and serotonergic neurons	(84)	MAOB					
UGT								
UGT2B7								
UGT1A6		(86)	UGT1A6			(87,88)	Morphine	(85)
Miscellaneous								
membrane-bound epoxide hydrolase		(86)						
benzoxresorufin-0-deethylase		(86)						
PST		(89–91)						

Small molecule drug properties and interaction with the CNS system

A combination of CNS system properties and drug properties determines drug PK in the CNS, including the CNS target-site. Important physicochemical properties for determination of drug PK in the CNS are summarized in **Figure 1**.

Physicochemical properties of a drug, such as lipophilicity, size, charge, hydrogen bonding potential and polar surface area (PSA), are important determinants for drug distribution in the CNS. Many studies have investigated the influence of individual physicochemical properties on the BBB penetration in isolation. However, as physicochemical properties are highly inter-correlated, it is more appropriate to consider these properties in combination.

First of all it should be noted that it is the unbound and neutral form of drug molecules that is able to diffuse across barriers like the BBB and BCSFB, depending on the concentration gradient of the unbound and neutral form of the drug on either side of a membrane. Lipophilicity relates to the BBB permeability, as transcellular diffusion rate (92,93). Furthermore, as a rule of thumb, higher lipophilicity increases drug binding to brain tissue. Molecular size is an important factor for paracellular drug diffusion rate, and also has an impact on transcellular diffusion rate at the BBB (92,94,95). The degree of ionization depends on the pKa of the drug and actual pH in a body compartment. Thus, the BBB permeability rate is influenced by lipophilicity, size and pKa of a drug. (92,96). Using quantitative structure-activity relationship (QSAR) modeling, it has been shown that the descriptors for the prediction of BBB penetration, are different for different charge classes (97). As there are pH differences between plasma, brain_{ECF} and CSF (**Figure 2**), charge is an important factor for CNS drug disposition (98).

The hydrogen bonding potential reflects the necessary energy for a molecule to move out of the aqueous phase into the lipid phase of a membrane. Recent studies have shown that the relationship between chemical structure and $K_{p,uu,brain}$ (the ratio of the unbound concentration in the brain over that in plasma at equilibrium which measures the extent of CNS distribution) was dominated by hydrogen bonding (99).

PSA is generally defined as the sum of the van der Waals surface areas of oxygen and nitrogen atoms. Therefore, PSA of a compound can be related to its hydrogen bonding potential. Some studies have shown that PSA is highly correlated with the permeability coefficient of membranes (93,100,101). A recent study for $K_{p,uu,brain}$ has been shown that PSA is one of the important factors to predict the $K_{p,uu,brain}$ for each compound (102).

BBB and BCSFB transport

Protein binding. It is generally accepted that unbound drug in plasma is able to cross the BBB and BCSFB. Two major proteins in plasma are albumin and α 1-acid glycoprotein (103). For passive diffusion, the free concentration gradient between plasma and brain determines the rate of transport. The extent of BBB and BCSFB transport are investigated using $K_{p,uu,brain}$: If there is only diffusion, $K_{p,uu,brain}$ is 1. If there is active transport processes, then $K_{p,uu,brain}$ is larger than 1 (active in) or $K_{p,uu,brain}$ is smaller than 1 (active out).

Ionization of the drug in plasma and in the brain. There are similar pH differences among the CNS physiological compartments in human and in rat (**Table I**). Because of the pH differences, the ratio of neutral form of a compound among the compartments is different. It is generally accepted that neutral form can pass the barriers, therefore ionization that is determined by the pKa of a compounds and pH in the physiological compartments will have an impact on drug disposition in the brain.

Cerebral blood flow- flow versus permeability limited transport rate. Lipophilic compounds usually have a large permeability coefficient, therefore a permeability surface area product (PA), which is determined by the permeability coefficient and surface area of tissue, becomes large. If the PA is larger than the physiological cerebral blood flow, then the physiological cerebral blood flow determines the transport rate of the compound.

Modes of BBB transport- different modes. The combination of transport modes at the BBB, BSCFB and membrane of brain parenchyma determines the rate and extent of drug exchange at the BBB, BCSFB and membrane of brain parenchyma (104,105). Therefore, the operative transport mechanism(s) may differ for each drug. Each transport mode is summarized in **Table IV**.

Active transporter function. Active transporters mediate influx and efflux of drug transport. The magnitude of interaction of active transport is drug and species dependent (106). The functions of individual transporters are summarized in **Table II**.

Table IV. Blood-brain barrier main modes of transport and their characteristics

BBB/BCSFB transport mode	Characteristics	Concentration-dependent transport kinetics?	Drug concentration-gradient dependent?	Consumes energy?
Paracellular	Passive; Between tight junctions of the BCEC and the CPEC	No	Yes	No
Transcellular	Passive; Across the membranes of the BCEC and the CPEC	No	Yes	No
Facilitated	Passive;	Yes	Yes	No
Active influx	Active;	Yes	No	Yes
Active efflux	Active;	Yes	No	Yes
Transcytosis	Receptor (specific, low capacity) or absorptive mediated (non-specific, high capacity)	No	No	Yes

BCEC; brain capillary endothelial cells, CPEC; choroid plexus epithelial cells

Brain distribution and elimination

Extra-intracellular distribution. Once having crossed the BBB, the drug is distributed by brain_{ECF} bulk flow into the CSF compartments. At the same time, the drug in brain_{ECF} is transported to brain parenchymal cell intracellular fluid (brain_{ICF}). It should be noted that also on the brain parenchyma cell membranes active transport may occur (105).

Tissue binding. Tissue binding can occur as being specific at the target or non-specific to tissue components.

Lysosomal trapping. In the brain parenchyma cells, there is a physiological pH gradient between the intracellular compartment (cytoplasm) and the lysosome compartment (**Figure 2**). Especially basic compounds are known to be trapped in the lysosomes (10).

Drug dispersion within CSF. Some studies have shown that intrathecally administered drugs distribute faster than what can be accounted only by molecular diffusion (107,108). Thus, it is thought that molecular diffusion makes only a small contribution to the total drug dispersion within CSF. This leads to the need to take into account also the convection due to oscillatory CSF flow to adequately explain this dispersion (109). Recently the drug dispersion has been considered to be enhanced by the CSF pulsatility (heart rate and CSF stroke volume), and it leads to high inter- and intra-patient variability in drug distribution in the brain (109,110).

Elimination from the brain. Apart from transport across the BBB and BCSFB as discussed earlier, drug may leave the brain via the BBB, but also via CSF reflux into the blood stream at the level of the arachnoid villi.

Metabolism. In the brain, several metabolic enzymes are present. Enzyme interaction with drugs is important information not only on the drug PK profile but also on the drug pharmacological effect in the brain since it may create active metabolites. Presence and localization of several enzymes have been reported in the brain (**Table III**), although their activity is reported to be relatively small compared to the liver (17,86).

CURRENT APPROACHES TO INVESTIGATE CNS DRUG DISTRIBUTION

Since obtaining a human drug target-site concentration in the brain is not feasible in most of the clinical studies, quantitative prediction of target-site concentration is important. To achieve this, we need information from *in vitro*, *ex vivo*, *in vivo*, and *in silico* approaches. Here we summarize the current approaches to obtain the necessary information to predict human drug target-site concentration.

In silico approaches

For decades, QSAR studies have been performed using $K_{p,brain}$ (total concentration ratio of the brain to plasma) or $\log BB$, either of which may not reflect the relevant drug exposure in the brain to assess the drug efficacy since drug efficacy is influenced by binding of compounds to plasma proteins and brain tissue. Eventually $\log BB$ was replaced by the PA, as an estimate of the net BBB influx clearance (111). However, it has been argued that the PA cannot predict the unbound drug concentration in the CNS by itself. Recently the most relevant parameter $K_{p,uu,brain}$ has been used, with QSAR being conducted to model this parameter (99,102,112,113). Other than $K_{p,uu,brain}$, physiological meaningful parameter, $V_{u,brain}$ (the volume of distribution of the unbound drug in the brain) or $K_{p,uu,cell}$ (unbound concentration ration between $brain_{ECF}$ and $brain_{ICF}$) are also reported using molecular descriptors (102).

In vitro approaches

In vitro approaches to investigate the BBB permeability have been conducted using BBB models (114). BBB models can be classified into non-cell based surrogate models, such as parallel artificial membrane permeability assay (PAMPA), and cell-based models such as primary cultures cells, immortalized brain endothelial cells or human-derived stem cells (115). Although primary cultured cells from human tissue have been reported, acquiring human brain tissue is difficult as it can only be obtained postmortem and should be fresh enough (116). Therefore alternative models based on immortalized brain endothelial cells or human-derived stem cells are often used (117,118). Even though these models have been developed for measuring the BBB permeability, an ideal cell culture model of the BBB is yet to be developed. Furthermore, reliable *in vitro*-*in vivo* correlation data is needed to enable the use of *in vitro* results for the prediction of *in vivo* permeability. However, *in vitro* results have not been consistent in their ability to predict *in vivo* permeability, probably because of different *in vitro* models, and different sets of compounds used in the *in vitro* studies (119).

Currently, the biopharmaceutics classification system (BCS) and biopharmaceutics drug distribution classification system (BDDCS) are used for CNS drugs. The BDDCS is a modification of BCS that utilizes drug metabolism to predict drug disposition and potential drug-drug interactions in the brain (120). However, this classification approach needs to be further investigated because of inconsistencies. For example, it was proposed that 98% of BDDCS class 1 drugs would be able to get into the brain even though the drugs were P-gp substrates based on *in vitro* studies (121), while it has also been reported that the *in vitro* efflux ratio reflects the *in vivo* brain penetration regardless of the class in BDDCS (122).

Ex vivo approaches

As mentioned before, it is the unbound drug molecules that are able to pass membranes and to interact with the target (22). Thus, measuring unbound drug concentrations is very important. $V_{u,brain}$ or $F_{u,brain}$ (the unbound fraction in the brain) are used to investigate unbound fraction of drugs in the brain. $F_{u,brain}$ can be derived from brain homogenate (123), and $V_{u,brain}$ can be obtained from the brain slice technique (124). The brain slice method is more physiologically relevant because the cell-cell interactions, pH gradients and active transport systems are all conserved (34).

In vivo approaches

Microdialysis can be considered as a key technique to examine time-dependent information regarding unbound drug concentrations. With microdialysis both the rate and extent of drug transport and distribution processes can be determined (125,126). Thus, it can be used to obtain $K_{p,uu,brain}$ in conjunction with the rate of transport processes. Moreover, this can be done at multiple locations and this feature has shown that even for a drug like acetaminophen that is not subjected to any active transport, substantial differences in pharmacokinetic profiles exist in different brain compartments (6). While there is some limit to use this water-based technique for the highly lipophilic drugs, lots of microdialysis experiments have contributed to a boost in the understanding on drug exchange across the BBB (125,127,128). Especially the use of microdialysis at multiple brain locations have provided insight into the relative contribution of CNS distribution and elimination processes to the local (differences in) PK of a compound (6,7,129).

Positron emission tomography (PET) is a valuable non-invasive *in vivo* monitoring technique that can be used to visualize drug CNS distribution in living animals and human. However, the PET technique cannot distinguish parent compounds from their metabolites, or bound and unbound drug. Furthermore it may also encounter difficulties in obtaining useful data when a very high non-specific binding (NSB) to non-target proteins and phospholipid membranes occurs (130). Recently a novel Lipid Membrane Binding Assay (LIMBA) was established as a fast and reliable tool for identifying compounds with unfavorably high NSB in the brain tissue (55).

Combinatory mapping approach

Combinatory mapping is an approach that combines three compound-specific parameters obtained from *in vitro*, *ex vivo* and *in vivo* data: $K_{p,brain}$, $V_{u,brain}$ and $F_{u,plasma}$, for calculation of $K_{p,uu,brain}$ (132). This approach can be used not only to obtain $K_{p,uu,brain}$ but also to understand unbound drug disposition in the cell cytosol, and the lysosomes. Recently, this approach has been extended to predict drug exposure in different brain regions such as frontal cortex, striatum, hippocampus, brainstem, cerebellum and hypothalamus, in which also the impact of transporters and receptors in each region was taken into account (133). Although this approach is useful to support the selection of potential CNS drugs in drug discovery, it has two limitations. The first limitation is that it can only predict the parameters at steady state. The second limitation is that the approach cannot be translated to predict the parameters, for instance, inter-

species or inter-disease conditions because the processes to obtain the parameters in this approach are not connected with system properties which will be changed in these conditions.

CONDITION DEPENDENCY AND PBPK MODELING

Condition dependency

Drug distribution into and within the brain depends on the interaction between system and drug properties. Drug properties remain the same, whatever the species and conditions are in which the drug has been administered. This indicates that interspecies variability in drug distribution into and within the brain is the result of differences in physiological and biochemical parameters. Factors which cause variation in drug PK include: genetic background, species differences, gender, age, diet, disease states, drug treatment (4). Factors which cause variation in drug pharmacodynamics include: seasonal effect (134), age (135), gender (136), species (137). Effects of these conditions on CNS system properties are summarized in **Table V**.

(Semi-) PBPK modeling

PBPK models need to be informed on system and on drug properties to model the interaction and predict the drug PK in different compartments. Especially as obtaining PK data from the human brain is highly restricted, working in the PBPK model framework is valuable as it can be translated to predict the target-site concentrations in inter-species and inter-disease situations (4). Some translational research has been reported by using an animal (semi-) PBPK model for CNS drugs but it is relatively sparse and ranges from simple to more advanced (**Table VI**).

For remoxipride, Stevens et al. have shown that drug concentration in brain_{ECF} which was measured with microdialysis, represented the target-site concentrations, because these concentrations could be directly linked to the effect of remoxipride on plasma prolactin levels in an advanced mechanism-based model (138). After scaling to human, this indeed could also be concluded for human CNS remoxipride effects on human plasma prolactin levels. This underscores the importance of having information on PK at the CNS target region.

Table V. Sources of variability in CNS pharmacokinetics

Parameter	Location	Source of variability	Effect	Refs
Protein binding		aging	lower	(139)
		pathophysiological condition	higher with disease induced evaluation of plasma protein	(140,141)
Cerebral blood flow		aging	lower	(142)
		pathophysiological condition	lower in the multi-infarct group	(143)
		diurnal variation	change	(144)
BBB	membrane lipid	aging	change	(145)
		diet	change	(146)
		pathophysiological condition	change in several disease conditions, such as Alzheimer's disease and schizophrenia	(147–149)
	paracellular diffusion	stress	increase with hypoxic stress	(150)
		pathophysiological condition	increase (due to loose of tight junctions)	see below
	tight junction	pathophysiological condition	disruption of the tight junctions by ischaemic brain stroke	(151)
			opening of the tight junctions in AD patients	(152)
			opening of tight junctions in multiple sclerosis patients	(153)
	facilitated transport	diet	decreased in hypoglycemia condition	(154)
		pathophysiological condition	upregulation in the brain tumor	(155)
	vesicle based transport	pathophysiological condition	increase in experimental autoimmune encephalomyelitis	(156)
active transporters	pathophysiological condition	see below	see below	
Brain _{ECF}		pathophysiological condition	volume is enlarged in the patient with vasogenic type of brain	(157)
			blockade of brain ECF flow in AD patient	(42)
Brain Parenchyma		aging	shrunk	(158)
BCSFB		aging	thinner	(159)
		pathophysiological condition	decrease in Alzheimer patients	(159)
CSF		aging	decrease in CSF production, increase in CSF outflow resistance	(160)
		pathophysiological condition	decrease in CSF production, CSF turnover and increase in CSF volume in AD patients	(161)
			increased resistance to CSF absorption and CSF pressure in the patients with normal-pressure hydrocephalus	(162)
Brain metabolic enzymes		aging	increase in the CYP2D6 enzyme level	(163)
		gender	higher MAO activity in women	(82)
		pathophysiological condition	higher MAOB activity in AD patients	(164)
			difference of COMT expression in schizophrenia patients	(77)
		gene	deficiency of CYP2D6 enzyme	(74)
			change of COMT function	(165,166)
smoking and alcoholism	change of CYP2B6 and CYP2E1 levels	(72,167)		

Table V. (continued)

Parameter	Location	Source of variability	Effect	Refs
Transporter		aging	decrease in P-gp activity	(168)
			decrease in glucose transporter activity	(169)
		pathophysiological condition	upregulation of P-gp and MRPs in epileptogenic brain	(170)
			upregulation of P-gp and MRP1 in the brain tumor	(171)
			Alteration of the levels of glutamate transporter in the various brain disorders, including cerebral ischemia, amyotrophic lateral sclerosis, AD, AIDS, traumatic brain injury, schizophrenia, and epilepsy (seizure)	(172,173)
		diurnal variation	change in P-gp activity	(174)

REMAINING GAPS AND CHALLENGES ON PBPK MODELING, TOWARDS A GENERIC PBPK MODEL

The ultimate aim is to have a CNS PBPK model that can predict human brain compartment concentrations on the basis of the compounds physicochemical properties, which can be determined by *in vitro* measurements, or *in silico* prediction. Thus, in the overview in **Table VI** it can be seen that we still have a number of gaps in the currently available (semi-) PBPK models of CNS drugs. Most of the models require *in vivo* data on the compound(s), and most of the predictions have not been validated on human data. Thus, it can be seen that there is a need for further development of a generic, fully PBPK model for CNS drug distribution (185–187).

To have a PBPK model that would predict CNS drug distribution based the physicochemical properties of an individual drug, for different species and in different conditions, a number of challenges remain:

- Having a PBPK model structure with all relevant compartment/parameters, as physiological parameter values reported are sparse and variable (see **Table I**).
- Having drug physicochemical parameter values determined from *in vitro*, and/or *in silico*, or even some *in vivo* measurements, which may not necessarily be correct. For example, *in vitro* or *in vivo* data may depend on the experimental setting, while *in silico* information really depends on the data availability, used to obtain the equation.
- Obtaining human data sets for validating the model predictive performance is typically very difficult.
- Having information on pathophysiological changes in human CNS system properties in (the many) disease conditions. For example, BBB characteristics may change in Alzheimer's disease, multiple sclerosis, and pharmacoresistant epilepsies (188).

DISCUSSION AND CONCLUSION

PK of drugs in the CNS is governed by a combination of CNS system physiology and drug properties. This means that variability in CNS system physiological parameters (condition dependency) may lead to variability of CNS drug PK. Therefore, it is important to explicitly distinguish between system physiology and drug properties, by either changing conditions and investigating the PK of one drug, or investigating the PK of different drugs in the same condition.

The currently available predictive approaches are based on total drug plasma and total tissue concentrations at equilibrium (SS), while more recent approaches include, at best, unbound plasma SS concentrations. However, as body processes are based on the interaction with the unbound drug and are time-dependent, it is crucial to measure the unbound drug in each compartment as a function of time (Mastermind Research Approach (MRA)) (4), for which microdialysis has been proven the key technique. Using the MRA, microdialysis will provide lots of valuable data that pave the way towards a generic CNS PBPK model.

One microdialysis experiment in a single freely-moving animal can provide a lot of data points, obtained under the same experimental condition of the animal, and thereby revealing the interrelationships of processes. With this microdialysis has already contributed to reduction and refinement in the use of animals. Furthermore, all this information can further be “condensed” into a generic PBPK model, and will thereby help in the reduction in the future use of animals (189).

In order to be able to predict CNS drug effects in human, next steps would be the development of a full PBPK CNS drug distribution model, and combining it with target binding kinetics, receptor occupancy and signal transduction (190,191), and including system changes by human disease condition.

REFERENCES

1. Kola I, Landis J. Can the pharmaceutical industry reduce attrition rates? *Nat Rev Drug Discov.* 2004;3:1–5.
2. Hurko O, Ryan JL. Translational Research in Central Nervous System Drug Discovery. *J Am Soc Exp Neurother.* 2005;2(4):671–82.
3. Cook D, Brown D, Alexander R, March R, Morgan P, Satterthwaite G, et al. Lessons learned from the fate of AstraZeneca's drug pipeline: a five-dimensional framework. *Nat Rev Drug Discov.* 2014;13(6):419–31.
4. de Lange ECM. The mastermind approach to CNS drug therapy: translational prediction of human brain distribution, target site kinetics, and therapeutic effects. *Fluids Barriers CNS.* 2013;10(1):1–16.
5. Palmer AM, Stephenson FA. CNS Drug Discovery: Challenges and Solutions. *Drug News Perspect.* 2005;18(1):51–7.
6. Westerhout J, Ploeger B, Smeets J, Danhof M, de Lange ECM. Physiologically based pharmacokinetic modeling to investigate regional brain distribution kinetics in rats. *AAPS J.* 2012;14(3):543–53.
7. Westerhout J, van den Berg D-J, Hartman R, Danhof M, de Lange ECM. Prediction of methotrexate CNS distribution in different species - Influence of disease conditions. *Eur J Pharm Sci.* 2014;57:11–24.
8. Gaohua L, Neuhoff S, Johnson TN, Rostami-hodjegan A, Jamei M. Development of a permeability-limited model of the human brain and cerebrospinal fluid (CSF) to integrate known physiological and biological knowledge: Estimating time varying CSF drug concentrations and their variability using in vitro data. *Drug Metab Pharmacokinet.* 2016;31(3):224–33.
9. Mutch W, Hansen A. Extracellular pH changes during spreading depression and cerebral ischemia: mechanisms of brain pH regulation. *J Cereb blood flow Metab.* 1984;4(1):17–27.
10. Fridén M, Bergström F, Wan H, Rehngren M, Ahlin G, Hammarlund-Udenaes M, et al. Measurement of unbound drug exposure in brain: Modeling of pH partitioning explains diverging results between the brain slice and brain homogenate methods. *Drug Metab Dispos.* 2011;39(3):353–62.
11. Shu C, Shen H, Teuscher NS, Lorenzi PJ, Keep RF, Smith DE. Role of PEPT2 in peptide/mimetic trafficking at the blood-cerebrospinal fluid barrier: studies in rat choroid plexus epithelial cells in primary culture. *J Pharmacol Exp Ther.* 2002;301(3):820–9.
12. Shen DD, Artru AA, Adkison KK. Principles and applicability of CSF sampling for the assessment of CNS drug delivery and pharmacodynamics. *Adv Drug Deliv Rev.* 2004;56(12):1825–57.
13. Jwnsen KE, Thomsen C, Henriksen O. In vivo measurement of intracellular pH in human brain during different tensions of carbon dioxide in arterial blood. A ³¹P-NMR study. *Acta Physiol Scand.* 1988;134(2):295–8.

14. Mindell JA. Lysosomal acidification mechanisms. *Annu Rev Physiol.* 2012;74:69–86.
15. Touitou E, Barry BW. *Enhancement in Drug Delivery.* CRC Press; 2006.
16. Kushihara H, Sugiyama Y. Active Efflux across the Blood-Brain Barrier: Role of the Solute Carrier Family. *J Am Soc Exp Neurother.* 2005;2:73–85.
17. Minn A, Ghersi-Egea J-F, Perrin R, Leininger B, Siest G. Drug metabolizing enzymes in the brain and cerebral microvessels. *Brain Res Rev.* 1991;16(1):65–82.
18. Wong AD, Ye M, Levy AF, Rothstein JD, Bergles DE, Searson PC. The blood-brain barrier: an engineering perspective. *Front Neuroeng.* 2013;6:1–22.
19. Trapa PE, Belova E, Liras JL, Scott DO, Steyn SJ. Insights from an Integrated Physiologically Based Pharmacokinetic Model for Brain Penetration. *J Pharm Sci.* 2016;105(2):965–71.
20. Serot JM, Bénédicte MC, Foliguet B, Faure GC. Morphological alterations of the choroid plexus in late-onset Alzheimer's disease. *Acta Neuropathol.* 2000;99(2):105–8.
21. Dekaban AS, Sadowsky D. Changes in brain weights during the span of human life: relation of brain weights to body heights and body weights. *Ann Neurol.* 1978;4(4):345–56.
22. Hammarlund-Udenaes M, Fridén M, Syvänen S, Gupta A. On The Rate and Extent of Drug Delivery to the Brain. *Pharm Res.* 2008;25(8):1737–50.
23. Kawakami J, Yamamoto K, Sawada Y, Iga T. Prediction of brain delivery of ofloxacin, a new quinolone, in the human from animal data. *J Pharmacokinetic Biopharm.* 1994;22(3):207–27.
24. Begley DJ, Bradbury MW, Kreuter J. *The Blood-Brain Barrier and Drug Delivery to the CNS.* New York: Marcel Dekker, Inc. 2000.
25. Thorne RG, Hrabe S, Nicholson C, Robert G. Diffusion of Epidermal Growth Factor in Rat Brain Extracellular Space Measured by Integrative Optical Imaging. *J Neurophysiol.* 2004;92(6):3471–81.
26. Cserr H, Cooper D, Suri P, Patlak C. Efflux of radiolabeled polyethylene glycols and albumin from rat brain. *Am J Physiol.* 1981;240(4):319–28.
27. Sakka L, Coll G, Chazal J. Anatomy and physiology of cerebrospinal fluid. *Eur Ann Otorhinolaryngol Head Neck Dis.* 2011 Dec;128(6):309–16.
28. Kimelberg HK. Water homeostasis in the brain: basic concepts. *Neuroscience.* 2004 Jan;129(4):851–60.
29. Pardridge WM. Drug transport in brain via the cerebrospinal fluid. *Fluids Barriers CNS.* 2011;8(7):1–7.
30. Condon P, Wyper D, Grant R, Patterson J, Hadley D, Teasdale G, et al. Use of magnetic resonance imaging to measure intracranial cerebrospinal fluid volume. *Lancet.* 1986;327(8494):1355–7.
31. Kohn MI, Tanna NK, Herman GT, Resnick SM, Mozley PD, Gur RE, et al. Analysis of brain and cerebrospinal fluid volumes with MR imaging. Part I. Methods, reliability, and validation. *Radiology.* 1991;178(1):115–22.

32. Robertson EG. Developmental defects of the cisterna magna and dura mater. *J Neurol Neurosurg Psychiatry*. 1949;12(1):39–51.
33. Adam R, Greenberg JO. The mega cisterna magna. *J Neurosurg*. 1978;48(2):190–2.
34. Bass NH, Lundborg P. Postnatal development of bulk flow in the cerebrospinal fluid system of the albino rat: clearance of carboxyl-(14C)inulin after intrathecal infusion. *Brain Res*. 1973;52:323–32.
35. Levinger IM. The cerebral ventricles of the rat. *J Anat*. 1971;108(3):447–51.
36. Stange K, Greitz M, Ingvar T, Hindmarsh T, Sollevi A. Global cerebral blood flow during infusion of adenosine in humans: assessment by magnetic resonance imaging and positron emission tomography. *Acta Physiol Scand*. 1997;160(2):117–22.
37. Ito H, Inoue K, Goto R, Kinomura S, Taki Y, Okada K, et al. Database of normal human cerebral blood flow measured by SPECT: I. Comparison between I-123-IMP, Tc-99m-HMPAO, and Tc-99m-ECD as referred with O-15 labeled water PET and voxel-based morphometry. *Ann Nucl Med*. 2006;20(2):131–8.
38. Fagerholm U. The highly permeable blood-brain barrier: an evaluation of current opinions about brain uptake capacity. *Drug Discov Today*. 2007;12(23–24):1076–82.
39. Harashima H, Sawada Y, Sugiyama Y, Iga T, Hanano M. Analysis of nonlinear tissue distribution of quinidine in rats by physiologically based pharmacokinetics. *J Pharmacokinet Biopharm*. 1985;13(4):425–40.
40. Peng B, Andrews J, Nestorov I, Brennan B, Nicklin P, Rowland M. Tissue distribution and physiologically based pharmacokinetics of antisense phosphorothioate oligonucleotide ISIS 1082 in rat. *Antisense Nucleic Acid Drug Dev*. 2001;11(1):15–27.
41. Abbott NJ. Prediction of blood-brain barrier permeation in drug discovery from in vivo, in vitro and in silico models. *Drug Discov Today Technol*. 2004;1(4):407–16.
42. Abbott NJ. Evidence for bulk flow of brain interstitial fluid: significance for physiology and pathology. *Neurochem Int*. 2004;45(4):545–52.
43. Skipor J, Thiery JC. The choroid plexus-cerebrospinal fluid system: Undervaluated pathway of neuroendocrine signaling into the brain. *Acta Neurobiol Exp*. 2008;68(3):414–28.
44. Kumar G, Smith QR, Hokari M, Parepally J, Duncan MW. Brain uptake, pharmacokinetics, and tissue distribution in the rat of neurotoxic N-butylbenzenesulfonamide. *Toxicol Sci*. 2007;97(2):253–64.
45. Strazielle N, Ghersi-Egea JF. Choroid plexus in the central nervous system: biology and physiopathology. *J Neuropathol Exp Neurol*. 2000;59(7):561–74.
46. Schinkel AH. P-Glycoprotein, a gatekeeper in the blood–brain barrier. *Adv Drug Deliv Rev*. 1999;36(2–3):179–94.
47. Tsuji A, Tamai I. Blood-brain barrier function of P-glycoprotein. *Adv Drug Deliv Rev*. 1997;25(2–3):287–98.

48. Bendayan R. In Situ Localization of P-glycoprotein (ABCB1) in Human and Rat Brain. *J Histochem Cytochem.* 2006;54(10):1159–67.
49. Löscher W, Potschka H. Role of drug efflux transporters in the brain for drug disposition and treatment of brain diseases. *Prog Neurobiol.* 2005;76(1):22–76.
50. Schinkel AH, Jonker JW. Mammalian drug efflux transporters of the ATP binding cassette (ABC) family: An overview. *Adv Drug Deliv Rev.* 2003;55:3–29.
51. Shapiro AB, Ling V. Stoichiometry of coupling of rhodamine 123 transport to ATP hydrolysis by P-glycoprotein. *Eur J Biochem.* 1998;254:189–93.
52. Rao VV, Dahlheime JL, Bardgett ME, Snyder AZ, Finch RA, Sartorelli AC, et al. Choroid plexus epithelial expression of MDR1 P glycoprotein and multidrug resistance-associated protein contribute to the blood-cerebrospinal-fluid drug-permeability barrier. *Med Sci.* 1999;96(7):3900–5.
53. Cordon-Cardo C, O'Brien JP, Casals D, Rittman-Grauer L, Biedler JL, Melamed MR, et al. Multidrug-resistance gene (P-glycoprotein) is expressed by endothelial cells at blood-brain barrier sites. *Proc Natl Acad Sci U S A.* 1989;86(2):695–8.
54. Kassem NA, Deane R, Segal MB, Chen R, Preston JE. Thyroxine (T4) transfer from CSF to choroid plexus and ventricular brain regions in rabbit: contributory role of P-glycoprotein and organic anion transporting polypeptides. *Brain Res.* 2007;1181:44–50.
55. Ronaldson PT, Bendayan M, Gingras D, Piquette-Miller M, Bendayan R. Cellular localization and functional expression of P-glycoprotein in rat astrocyte cultures. *J Neurochem.* 2004;89(3):788–800.
56. Miller DS. Regulation of ABC transporters at the blood-brain barrier. *Clin Pharmacol Ther.* 2015;97(4):395–403.
57. Löscher W, Potschka H. Blood-brain barrier active efflux transporters: ATP-binding cassette gene family. *NeuroRx.* 2005;2(1):86–98.
58. Nies AT, Jedlitschky G, König J, Herold-Mende C, Steiner HH, Schmitt H-P, et al. Expression and immunolocalization of the multidrug resistance proteins, MRP1–MRP6 (ABCC1–ABCC6), in human brain. *Neuroscience.* 2004;129(2):349–60.
59. Hipfner DR, Deeley RG, Cole SPC. Structural, mechanistic and clinical aspects of MRP1. *Biochim Biophys Acta.* 1999;1461:359–76.
60. Hirrlinger J, König J, Dringen R. Expression of mRNAs of multidrug resistance proteins (Mrps) in cultured rat astrocytes, oligodendrocytes, microglial cells and neurones. *J Neurochem.* 2002;82:716–9.
61. Westerhout J, Danhof M, de Lange ECM. Preclinical Prediction of Human Brain Target Site Concentrations : Considerations in Extrapolating to the Clinical Setting. *J Pharm Sci.* 2011;100(9):3577–93.
62. Begley DJ. ABC transporters and the blood-brain barrier. *Curr Pharm Des.* 2004;10(12):1295–312.

63. Wijnholds J, de Lange ECM, Scheffer GL, van den Berg DD, Mol CAAM, van der Valk M, et al. Multidrug resistance protein 1 protects the choroid plexus epithelium and contributes to the blood-cerebrospinal fluid barrier. *J Clin Invest*. 2000;105(3):279–85.
64. Gao B, Stieger B, Noé B, Fritschy JM, Meier PJ. Localization of the organic anion transporting polypeptide 2 (Oatp2) in capillary endothelium and choroid plexus epithelium of rat brain. *J Histochem Cytochem*. 1999;47(10):1255–64.
65. Angeletti RH, Novikoff PM, Juvvadi SR, Fritschy J-M, Meier PJ, Wolkoff AW. The choroid plexus epithelium is the site of the organic anion transport protein in the brain. *Neurobiology*. 1997;94:283–6.
66. Gao B, Hagenbuch B, Kullak-Ublick GA, Benke D, Aguzzi A, Meier PJ. Organic Anion-Transporting Polypeptides Mediate Transport of Opioid Peptides across Blood-Brain Barrier. *J Pharmacol Exp Ther*. 2000;294(1):73–39.
67. Sekine T, Cha SH, Endou H. The multispecific organic anion transporter (OAT) family. *Pflugers Arch*. 2000;440(3):337–50.
68. Miksys SL, Tyndale RF. Drug-metabolizing cytochrome P450s in the brain. *J psychiatry Neurosci*. 2002;27(6):406–15.
69. Miksys S, Tyndale RF. Cytochrome P450-mediated drug metabolism in the brain. *J Psychiatry Neurosci*. 2013;38(3):152–63.
70. Declèves X, Jacob A, Yousif S, Shawahna R, Potin S, Scherrmann J. Interplay of drug metabolizing CYP450 enzymes and ABC transporters in the blood-brain barrier. *Curr Drug Metab*. 2011;12(8):732–41.
71. Favetta P, Degoute CS, Perdrix JP, Dufresne C, Bouliou R, Guitton J. Propofol metabolites in man following propofol induction and maintenance. *Br J Anaesth*. 2002;88(5):653–8.
72. Miksys S, Lerman C, Shields PG, Mash DC, Tyndale RF. Smoking, alcoholism and genetic polymorphisms alter CYP2B6 levels in human brain. *Neuropharmacology*. 2003;45(1):122–32.
73. Miksys S, Rao Y, Sellers EM, Kwan M, Mendis D, Tyndale RF. Regional and cellular distribution of CYP2D subfamily members in rat brain. *Xenobiotica*. 2000;30(6):547–64.
74. Zanger UM, Raimundo S, Eichelbaum M. Cytochrome P450 2D6: Overview and update on pharmacology, genetics, biochemistry. *Naunyn Schmiedebergs Arch Pharmacol*. 2004;369(1):23–37.
75. D'empaire I, Guico-Pabia CJ, Preskorn SH. Antidepressant Treatment and Altered CYP2D6 Activity. *J Psychiatr Pract*. 2011;17(5):330–9.
76. Leysen J, Janssen P, Megens A, Schotte A. Risperidone: a novel antipsychotic with balanced serotonin-dopamine antagonism, receptor occupancy profile, and pharmacologic activity. *J Clin Psychiatry*. 1994;55:5–12.

77. Matsumoto M, Weickert CS, Beltaifa S, Kolachana B, Chen J, Hyde TM, et al. Catechol O-methyltransferase (COMT) mRNA expression in the dorsolateral prefrontal cortex of patients with schizophrenia. *Neuropsychopharmacology*. 2003;28(8):1521–30.
78. Huotari M, Gogos JA, Karayiorgou M, Koponen O, Forsberg M, Raasmaja A, et al. Brain catecholamine metabolism in catechol-O-methyltransferase (COMT)-deficient mice. *Eur J Neurosci*. 2002;15:246–56.
79. Pintar JE, Breakefield XO. Monoamine Oxidase (MAO) Activity as a Determinant in Human Neurophysiology. *Behav Genet*. 1982;12(1):53–68.
80. Bogdanski DF, Weissbach H, Udenfriend S. The distribution of serotonin, 5-hydroxytryptophan decarboxylase, and monoamine oxidase in brain. *J Neurochem*. 1957;1:272–8.
81. Luine VN, Khylichevskaya RI, Mcewen BS. Effect of gonadal steroids on activities of monoamine oxidase and choline acetylase in rat brain. *Brain Res*. 1975;86:293–306.
82. Robinson DS, Davis JM, Nies A, Ravaris CL, Sylwester D, Burlington V. Relation of Sex and Aging to Monoamine Oxidase Activity of Human Brain, Plasma, and Platelets. *Arch Gen Psychiat*. 1971;24:536–9.
83. Nagatsu T. Progress in Monoamine Oxidase (MAO) Research in Relation to Genetic Engineering. *Neurotoxicology*. 2004;25(1–2):11–20.
84. Levitt P, Pintar JE, Breakefieldt XO. Immunocytochemical demonstration of monoamine oxidase B in brain astrocytes and serotonergic neurons. *Neurobiology*. 1982;79:6385–9.
85. Ohno S, Kawana K, Nakajin S. Contribution of UDP-glucuronosyltransferase 1A1 and 1A8 to morphine-6-glucuronidation and its kinetic properties. *Drug Metab Dispos*. 2008;36(4):688–94.
86. Ghersi-Egea JF, Leninger-Muller B, Suleman G, Siest G, Minn A. Localization of Drug-Metabolizing Enzyme Activities to Blood-Brain Interfaces and Circumventricular Organs. *J Neurochem*. 1994;62:1089–96.
87. King CD, Rios GR, Assouline JA, Tephly TR. Expression of UDP-Glucuronosyltransferases (UGTs) 2B7 and 1A6 in the Human Brain and Identification of 5-Hydroxytryptamine as a Substrate. *Arch Biochem Biophys*. 1999;365(1):156–62.
88. Suleman FG, Abid A, Gradinaru D, Daval J-L, Magdalou J, Minn A. Identification of the Uridine Diphosphate Glucuronosyltransferase Isoform UGT1A6 in Rat Brain and in Primary Cultures of Neurons and Astrocytes. *Arch Biochem Biophys*. 1998;358(1):63–7.
89. Foldes A, Meek JL. Rat brain phenolsulfotransferase-Partial purification and some properties. *Biochim. Biophys. Acta* 1973. *Biochim Biophys Acta*. 1973;327:365–74.
90. Meek JL, Neff NH. Biogenic amines and their metabolites as substrates for phenol sulphotransferase (EC 2.8.2.1) of brain and liver. *J Neurochem*. 1973;21(9):1–9.
91. Renskers KJ, Feor KD, Roth JA. Sulfation of Dopamine and Other Biogenic Amines by Human Brain Phenol Sulfotransferase. *J Neurochem*. 1980;34(6):1362–8.

92. Levin VA. Relationship of octanol/water partition coefficient and molecular weight to rat brain capillary permeability. *J Med Chem.* 1980;23(6):682–4.
93. van de Waterbeemd er al H, van de Waterbeemd H, Camenisch G, Folkers G, Raevsky OA. Estimation of Caco-2 Cell Permeability using Calculated Molecular Descriptors. *Quant Struct-Act Relat.* 1996;15:480–90.
94. Lipinski C a., Lombardo F, Dominy BW, Feeney PJ. Experimental and computational approaches to estimate solubility and permeability in drug discovery and development settings. *Adv Drug Deliv Rev.* 2012;64:4–17.
95. Chan OH, Stewart BH. Physicochemical and drug- delivery considerations for oral drug bioavailability. *Drug Discov Today.* 1996;1(11):461–73.
96. Upton RN. Regional pharmacokinetics I. physiological and physicochemical basis. *Biopharm Drug Dispos.* 1990;11(8):647–62.
97. Shayanfar A, Soltani S, Jouyban A. Prediction of Blood-Brain Distribution : Effect of Ionization. *Biol Pharm Bull.* 2011;34(2):266–71.
98. Macintyre AC, Cutler DJ. The potential role of lysosomes in tissue distribution of weak bases. *Biopharm Drug Dispos.* 1988;9:513–26.
99. Fridén M, Winiwarter S, Jerndal G, Bengtsson O, Wan H, Bredberg U, et al. Structure-brain exposure relationships in rat and human using a novel data set of unbound drug concentrations in brain interstitial and cerebrospinal fluids. *J Med Chem.* 2009;52(20):6233–43.
100. Palm K, Luthman K, Ungell A-L, Strandlund G, Beigi F, Lundahl P, et al. Evaluation of dynamic polar molecular surface area as predictor of drug absorption: comparison with other computational and experimental predictors. *J Med Chem.* 1998;41(27):5382–92.
101. Krarup LH, Christensen IT, Hovgaard L, Frokjaer S. Predicting drug absorption from molecular surface properties based on molecular dynamics simulations. *Pharmaceutical Res.* 1998;15(7):972–8.
102. Loryan I, Sinha V, Mackie C, van Peer A, Drinkenburg WH, Vermeulen A, et al. Molecular properties determining unbound intracellular and extracellular brain exposure of CNS drug candidates. *Mol Pharm.* 2015;12(2):520–32.
103. Peletier LA, Benson N, van der Graaf PH. Impact of plasma-protein binding on receptor occupancy: An analytical description. *J Theor Biol.* 2009;256(2):253–62.
104. Abbott NJ, Rönnbäck L, Hansson E. Astrocyte-endothelial interactions at the blood-brain barrier. *Nat Rev Neurosci.* 2006;7(41–53).
105. Lee G, Dallas S, Hong M, Bendayan R. Drug Transporters in the Central Nervous System : Brain Barriers and Brain Parenchyma Considerations. *Pharmacol Rev.* 2001;53(4):569–96.
106. Ohtsuki S, Terasaki T. Contribution of carrier-mediated transport systems to the blood-brain barrier as a supporting and protecting interface for the brain; importance for CNS drug discovery and development. *Pharm Res.* 2007;24(9):1745–58.

107. Plassat R, Verbe BP, Menei P, Menegalli D, Mathe J, Richard I. Treatment of spasticity with intrathecal Baclofen administration long-term follow-up, review of 40 patients. *Spinal Cord*. 2004;42:686–93.
108. Kroin JS. The Distribution of Medication along the Spinal Canal after Chronic Intrathecal Administration. *Neurosurgery*. 1993;33:226–30.
109. Hettiarachchi HDM, Hsu Y, Harris TJ, Penn R, Linninger AA. The effect of pulsatile flow on intrathecal drug delivery in the spinal canal. *Ann Biomed Eng*. 2011;39(10):2592–602.
110. Hsu Y, Hettiarachchi HDM, Zhu DC, Linninger AA. The Frequency and Magnitude of Cerebrospinal Fluid Pulsations Influence Intrathecal Drug Distribution. *Anesth Analg*. 2012;115(2):386–94.
111. Pardridge WM. Log(BB), PS products and in silico models of drug brain penetration. *Drug Discov Today*. 2004;9(9):392–3.
112. Chen H, Winiwarter S, Fridén M, Antonsson M, Engkvist O. In silico prediction of unbound brain-to-plasma concentration ratio using machine learning algorithms. *J Mol Graph Model*. 2011;29(8):985–95.
113. Loryan I, Fridén M, Hammarlund-Udenaes M. The brain slice method for studying drug distribution in the CNS. *Fluids Barriers CNS*. 2013;10(6):1–9.
114. Helms HC, Abbott NJ, Burek M, Cecchelli R, Couraud P-O, Deli MA, et al. In vitro models of the blood-brain barrier: An overview of commonly used brain endothelial cell culture models and guidelines for their use. *J Cereb Blood Flow Metab*. 2016;36(5):862–90.
115. Bicker J, Alves G, Fortuna A, Falcão A. Blood-brain barrier models and their relevance for a successful development of CNS drug delivery systems: A review. *Eur J Pharm Biopharm*. 2014;87(3):409–32.
116. Bernas MJ, Cardoso FL, Daley SK, Weinand ME, Campos AR, Ferreira AJG, et al. Establishment of primary cultures of human brain microvascular endothelial cells to provide an in vitro cellular model of the blood-brain barrier. *Nat Protoc*. 2010;5(7):1265–72.
117. Weksler BB, Subileau EA, Perrière N, Charneau P, Holloway K, Leveque M, et al. Blood-brain barrier-specific properties of a human adult brain endothelial cell line. *FASEB J*. 2005;19(13):1872–4.
118. Cecchelli R, Aday S, Sevin E, Almeida C, Culot M, Dehouck L, et al. A stable and reproducible human blood-brain barrier model derived from hematopoietic stem cells. *PLoS One*. 2014;9(6):1–11.
119. Stanimirovic DB, Bani-Yaghoub M, Perkins M, Haqqani AS. Blood-brain barrier models: in vitro to in vivo translation in preclinical development of CNS-targeting biotherapeutics. *Expert Opin Drug Discov*. 2015;10(2):141–55.
120. Larregieu CA, Benet LZ. Distinguishing between the permeability relationships with absorption and metabolism to improve BCS and BDDCS predictions in early drug discovery. *Mol Pharm*. 2014;11(4):1335–44.

121. Broccatelli F, Larregieu CA, Cruciani G, Oprea TI, Benet LZ. Improving the prediction of the brain disposition for orally administered drugs using BDDCS. *Adv Drug Deliv Rev.* 2012;64(1):95–109.
122. Kikuchi R, De Morais SM, Kalvass JC. In vitro P-glycoprotein efflux ratio can predict the in vivo brain penetration regardless of biopharmaceutics drug disposition classification system class. *Drug Metab Dispos.* 2013;41(12):2012–7.
123. Kalvass JC, Maurer TS. Influence of nonspecific brain and plasma binding on CNS exposure: Implications for rational drug discovery. *Biopharm Drug Dispos.* 2002;23(8):327–38.
124. Friden M, Gupta A, Antonsson M, Bredberg U, Hammarlund-Udenaes M. In Vitro Methods for Estimating Unbound Drug Concentrations in the Brain Interstitial and Intracellular Fluids. *Drug Metab Dispos.* 2007;35:1711–9.
125. Hammarlund-Udenaes M, Paalzow LK, de Lange ECM. Drug equilibration across the blood-brain barrier - Pharmacokinetic considerations based on the microdialysis method. *Pharm Res.* 1997;14(2):128–34.
126. Hammarlund-Udenaes M. The use of microdialysis in CNS drug delivery studies: Pharmacokinetic perspectives and results with analgesics and antiepileptics. *Adv Drug Deliv Rev.* 2000;45(2–3):283–94.
127. Elmquist W, Sawchuk R. Application of microdialysis in pharmacokinetic studies. *Pharm Res.* 1997;14(3):267–88.
128. de Lange ECM, Danhof M, de Boer AG, Breimer DD. Methodological considerations of intracerebral microdialysis in pharmacokinetic studies on drug transport across the blood-brain barrier. *Brain Res Brain Res Rev.* 1997;25(1):27–49.
129. Westerhout J, Smeets J, Danhof M, de Lange ECM. The impact of P-gp functionality on non-steady state relationships between CSF and brain extracellular fluid. *J Pharmacokinet Pharmacodyn.* 2013;40(3):327–42.
130. Neuwelt E, Abbott NJ, Abrey L, Banks WA, Blakley B, Davis T, et al. Strategies to advance translational research into brain barriers. *Lancet Neurol.* 2008;7(1):84–96.
131. Assmus F, Seelig A, Gobbi L, Borroni E, Glaentzlin P, Fischer H. Label-free assay for the assessment of nonspecific binding of positron emission tomography tracer candidates. *Eur J Pharm Sci.* 2015;79:22–35.
132. Loryan I, Sinha V, Mackie C, van Peer A, Drinkenburg W, Vermeulen A, et al. Mechanistic Understanding of Brain Drug Disposition to Optimize the Selection of Potential Neurotherapeutics in Drug Discovery. *Pharm Res.* 2014;32(8):2203–19.
133. Loryan I, Melander E, Svensson M, Payan M, König F, Jansson B, et al. In-depth neuropharmacokinetic analysis of antipsychotics based on a novel approach to estimate unbound target-site concentration in CNS regions: link to spatial receptor occupancy. *Mol Psychiatry.* 2016;1–10.
134. Murbach Freire C, Marques M, Costa M. Effects of seasonal variation on the central nervous system activity of *Ocimum gratissimum* L. essential oil. *J Ethnopharmacol.* 2006;105:161–6.

135. Bowie MW, Slattum PW. Pharmacodynamics in older adults: a review. *Am J Geriatr Pharmacother.* 2007;5(3):263–303.
136. Bigos KL, Pollock BG, Stankevich BA, Bies RR. Sex differences in the pharmacokinetics and pharmacodynamics of antidepressants: an updated review. *Gend Med.* 2009;6(4):522–43.
137. Oksenberg D, Marsters S, O'Dowd BF, Jin H, Havlik S, Peroutka SJ, et al. A single amino-acid difference confers major pharmacological variation between human and rodent 5-HT1B receptors. *Nature.* 1992;360:161–3.
138. Stevens J, Ploeger BA, van der Graaf PH, Danhof M, de Lange ECM. Systemic and direct nose-to-brain transport pharmacokinetic model for remoxipride after intravenous and intranasal administration. *Drug Metab Dispos.* 2011;39(12):2275–82.
139. Grandison MK, Boudinot FD. Age-related changes in protein binding of drugs: implications for therapy. *ClinPharmacokinet.* 2000;38(3):271–90.
140. Greenblatt D. Reduced serum albumin concentration in the elderly: a report from the Boston Collaborative Drug Surveillance Program. *J Am Geriatr Soc.* 1979;27(1):20–2.
141. Piafsky KM, Borgå O, Odar-Cederlöf I, Johansson C, Sjöqvist F. Increased Plasma Protein Binding of Propranolol and Chlorpromazine Mediated by Disease-Induced Elevations of Plasma α 1 Acid Glycoprotein. *new Engl Juornal pf Med.* 1978;299:1435–9.
142. Shaw TG, Mortel KF, Meyer JS, Rogers RL, Hardenberg J, Cutaia MM. Cerebral blood flow changes in benign aging and cerebrovascular disease. *Neurology.* 1984;34(7):855.
143. Kim SG. Quantification of Relative Cerebral Blood-Flow Change By Flow- Sensitive Alternating Inversion-Recovery (Fair) Technique - Application To Functional Mapping. *Magn Reson Med.* 1995;34(3):293–301.
144. Braun AR, Balkin TJ, Wesensten NJ, Carson RE, Varga M, Baldwin P, et al. Regional cerebral blood flow throughout the sleep-wake cycle An H2 15O PET study. *Brain.* 1997;120:1173–97.
145. Giusto NM, Salvador GA, Castagnet PI, Pasquaré SJ, Ilincheta de Boschero MG. Age-Associated Changes in Central Nervous System Glycerolipid Composition and Metabolism. *Neurochem Res.* 2002;27(11):1513–23.
146. Yehuda S, Rabinovitz S, Carasso RL, Mostofsky DI. The role of polyunsaturated fatty acids in restoring the aging neuronal membrane. *Neurobiol Aging.* 2002;23:843–53.
147. Uauy R, Dangour AD. Nutrition in Brain Development and Aging: Role of Essential Fatty Acids. *Nutr Rev.* 2006;64(5):24–33.
148. Yehuda S, Rabinovitz S, Mostofsky DI. Essential fatty acids and the brain: From infancy to aging. *Neurobiol Aging.* 2005;26:98–102.
149. Assies J, Lieverse R, Vreken P, Wanders RJA, Dingemans PMJA, Linszen DH. Significantly reduced docosahexaenoic and docosapentaenoic acid concentrations in erythrocyte membranes from schizophrenic patients compared with a carefully matched control group. *Biol Psychiatry.* 2001;49(6):510–22.

150. Mark KS, Davis TP. Cerebral microvascular changes in permeability and tight junctions induced by hypoxia-reoxygenation. *Am J Physiol Heart Circ Physiol.* 2002;282(4):1485–94.
151. Sandoval KE, Witt KA. Blood-brain barrier tight junction permeability and ischemic stroke. *Neurobiol Dis.* 2008;32(2):200–19.
152. Marco S, Skaper SD. Amyloid beta-peptide1-42 alters tight junction protein distribution and expression in brain microvessel endothelial cells. *Neurosci Lett.* 2006;401:219–24.
153. Plumb J, McQuaid S, Mirakhur M, Kirk J. Abnormal endothelial tight junctions in active lesions and normal-appearing white matter in multiple sclerosis. *Brain Pathol.* 2002;12:154–69.
154. Blomqvist G, Hospital K, Brain M. Facilitated transport of glucose from blood to brain in man on cerebral glucose utilization. *Eur J Nucl Med.* 1991;18:834–7.
155. Miyagawa T, Oku T, Uehara H, Desai R, Beattie B, Tjuvajev J, et al. “Facilitated” amino acid transport is upregulated in brain tumors. *J Cereb blood flow Metab.* 1998;18(5):500–9.
156. Claudio L, Kress Y, Norton WT, Brosnan CF. Increased vesicular transport and decreased mitochondrial content in blood-brain barrier endothelial cells during experimental autoimmune encephalomyelitis. *Am J Pathol.* 1989;135(6):1157–68.
157. Reulen HJ, Graham R, Spatz M, Klatzo I. Role of pressure gradients and bulk flow in dynamics of vasogenic brain edema. *J Neurosurg.* 1977;46(1):24–35.
158. Resnick SM, Pham DL, Kraut MA, Zonderman AB, Davatzikos C. Longitudinal Magnetic Resonance Imaging Studies of Older Adults : A Shrinking Brain. *J Neurosci.* 2003;23(8):3295–301.
159. Serot JM, Béné MC, Foliguet B, Faure GC. Altered choroid plexus basement membrane and epithelium in late-onset Alzheimer’s disease: An ultrastructural study. *Ann N Y Acad Sci.* 1997;826:507–9.
160. May C, Kaye JA, Atack JR, Schapiro MB, Friedland RP, Rapoport SI. Cerebrospinal fluid production is reduced in healthy aging. *Neurology.* 1990;40:500–3.
161. Silverberg GD, Mayo M, Saul T, Rubenstein E, McGuire D. Alzheimer’s disease, normal-pressure hydrocephalus, and senescent changes in CSF circulatory physiology: a hypothesis. *Lancet Neurol.* 2003;2:506–11.
162. Johanson CE, Duncan JA, Klinge PM, Brinker T, Stopa EG, Silverberg GD. Multiplicity of cerebrospinal fluid functions: New challenges in health and disease. *Cerebrospinal Fluid Res.* 2008 Jan;5(10):1–32.
163. Mann A, Miksys SL, Gaedigk A, Kish SJ, Mash DC, Tyndale RF. The neuroprotective enzyme CYP2D6 increases in the brain with age and is lower in Parkinson’s disease patients. *Neurobiol Aging.* 2012;33(9):2160–71.
164. Orelund L, Gottfries C-G. Brain and brain monoamine oxidase in aging and in dementia of Alzheimer’s type. *Prog Neuro-Psychopharmacology Biol Psychiatry.* 1986;10:533–40.

165. Chen J, Lipska BK, Halim N, Ma QD, Matsumoto M, Melhem S, et al. Functional Analysis of Genetic Variation in Catechol-O-Methyltransferase (COMT): Effects on mRNA, Protein, and Enzyme Activity in Postmortem Human Brain. *Am J Hum Genet.* 2004;75:807–21.
166. Meyer-Lindenberg A, Nichols T, Callicott JH, Ding J, Kolachana B, Buckholtz J, et al. Impact of complex genetic variation in COMT on human brain function. *Mol Psychiatry.* 2006;11(9):867–77.
167. Howard LA, Miksys S, Hoffmann E, Mash D, Tyndale RF. Brain CYP2E1 is induced by nicotine and ethanol in rat and is higher in smokers and alcoholics. *Br J Pharmacol.* 2003;138(7):1376–86.
168. Toornvliet R, van Berckel BNM, Luurtsema G, Lubberink M, Geldof AA, Bosch TM, et al. Effect of age on functional P-glycoprotein in the blood-brain barrier measured by use of (R)-[¹¹C] verapamil and positron emission tomography. *Clin Pharmacol Ther.* 2006;79(6):540–8.
169. Vorbrodth AW, Dobrogowska DH, Meeker HC, Carp RI. Immunogold study of regional differences in the distribution of glucose transporter (GLUT-1) in mouse brain associated with physiological and accelerated aging and scrapie infection. *J Neurocytol.* 1999;28:711–9.
170. Aronica E, Gorter JA, Jansen GH, van Veelen CW, van Rijen PC, Leenstra S, et al. Expression and cellular distribution of multidrug transporter proteins in two major causes of medically intractable epilepsy: focal cortical dysplasia and glioneuronal tumors. *Neuroscience.* 2003;118(2):417–29.
171. Spiegl-Kreinecker S, Buchroithner J, Elbling L, Steiner E, Wurm G, Bodenteich A, et al. Expression and functional activity of the ABC-transporter proteins P-glycoprotein and multidrug-resistance protein 1 in human brain tumor cells and astrocytes. *J Neurooncol.* 2002;57(1):27–36.
172. Danbolt NC. Glutamate uptake. *Prog Neurobiol.* 2001;65(1):1–105.
173. Holmes GL. Seizure-induced neuronal injury. *Neurology.* 2002;59(9):3–6.
174. Kervezee L, Hartman R, van den Berg D-J, Shimizu S, Emoto-Yamamoto Y, Meijer JH, et al. Diurnal variation in P-glycoprotein-mediated transport and cerebrospinal fluid turnover in the brain. *AAPS J.* 2014;16(5):1029–37.
175. Collins JM, Dedrick RL. Distributed model for drug delivery to CSF and brain tissue. *Am J Physiol.* 1983;245(3):303–10.
176. Ooie T, Terasaki T, Suzuki H, Sugiyama Y. Kinetic Evidence for Active Efflux Transport across the Blood-Brain Barrier of Quinolone Antibiotics. *J Pharmacol Exp Ther.* 1997;283(1):293–304.
177. Takasawa K, Terasaki T, Suzuki H, Ooie T, Sugiyama Y. Distributed model analysis of 3'-azido-3'-deoxythymidine and 2,3'-dideoxyinosine distribution in brain tissue and cerebrospinal fluid. *J Pharmacol Exp Ther.* 1997;282(3):1509–17.
178. Hansen DK, Scott DO, Otis KW, Lunte SM. Comparison of in vitro BBMEC permeability and in vivo CNS uptake by microdialysis sampling. *J Pharm Biomed Anal.* 2002;27:945–58.

179. Bourasset F, Scherrmann JM. Carrier-mediated processes at several rat brain interfaces determine the neuropharmacokinetics of morphine and morphine-6-beta-D-glucuronide. *Life Sci.* 2006;78(20):2302–14.
180. Liu X, Smith BJ, Chen C, Callegari E, Becker SL, Chen X, et al. Use of a Physiologically Based Pharmacokinetic Model to Study the Time to Reach Brain Equilibrium: An Experimental Analysis of the Role of Blood-Brain Barrier Permeability, Plasma Protein Binding, and Brain Tissue Binding. *J Pharmacol Exp Ther.* 2005;313(3):1254–62.
181. Kielbasa W, Stratford RE. Exploratory Translational Modeling Approach in Drug Development to Predict Human Brain Pharmacokinetics and Pharmacologically Relevant Clinical Doses. *Drug Metab Dispos.* 2012;40(5):877–83.
182. Fenneteau F, Turgeon J, Couture L, Michaud V, Li J, Nekka F. Assessing drug distribution in tissues expressing P-glycoprotein through physiologically based pharmacokinetic modeling: model structure and parameters determination. *Theor Biol Med Model.* 2009;36:495–522.
183. Ball K, Bouzom F, Scherrmann J-M, Walther B, Declèves X. Physiologically Based Pharmacokinetic Modelling of Drug Penetration Across the Blood-Brain Barrier--Towards a Mechanistic IVIVE-Based Approach. *AAPS.* 2013;15(4):913–32.
184. Badhan RKS, Chenel M, Penny JI. Development of a Physiologically-Based Pharmacokinetic Model of the Rat Central Nervous System. *Pharmaceutics.* 2014;6(1):97–136.
185. Wagner C, Zhao P, Pan Y, Hsu V, Grillo J, Huang SM, et al. Application of Physiologically Based Pharmacokinetic (PBPK) Modeling to Support Dose Selection : Report of an FDA Public Workshop on PBPK. *Clin Pharmacol Ther.* 2015;4(4):226–30.
186. Shepard T, Scott G, Cole S, Nordmark A, Bouzom F. Physiologically Based Models in Regulatory Submissions: Output From the ABPI/MHRA Forum on Physiologically Based Modeling and Simulation. *CPT Pharmacometrics Syst Pharmacol.* 2015;4:221–5.
187. European Medicines Agency. Concept paper on qualification and reporting of physiologically-based pharmacokinetic (PBPK) modelling and analyses. 2014; Available from: http://www.ema.europa.eu/docs/en_GB/document_library/Scientific_guideline/2014/06/WC500169452.pdf
188. Erdő F, Denes L, de Lange ECM. Age-associated physiological and pathological changes at the blood-brain barrier. *J Cereb Blood Flow Metab.* 2017;37(1):4–24.
189. Kilkenny C, Browne W, Cuthill IC, Emerson M, Altman DG. Animal Research: Reporting In Vivo Experiments: The ARRIVE Guidelines. *J Gene Med.* 2010;12(8):561–3.
190. de Witte WEA, Danhof M, van der Graaf PH, de Lange ECM. In vivo Target Residence Time and Kinetic Selectivity: The Association Rate Constant as Determinant. *Trends Pharmacol Sci.* 2016;37(10):831–42.
191. de Witte WEA, Wong YC, Nederpelt I, Heitman LH, Danhof M, van der Graaf PH, et al. Mechanistic models enable the rational use of in vitro drug-target binding kinetics for better drug effects in patients. *Expert Opin Drug Discov.* 2016;11(1):45–63.



A generic multi-compartmental CNS distribution model structure for 9 drugs allows prediction of human brain target site concentrations

Y Yamamoto, P A Väitalo, D-J van den Berg, R Hartman, W van den Brink, Y C Wong, D R Huntjens, J H Proost, A Vermeulen, W Krauwinkel, S Bakshi, V Aranzana-Climent, S Marchand, C Dahyot-Fizelier, W Couet, M Danhof, J G C van Hasselt, E C M de Lange

Pharmaceutical Research 2017; 34(2): 333-351

ABSTRACT

Purpose: Predicting target site drug concentration in the brain is of key importance for the successful development of drugs acting on the central nervous system. We propose a generic mathematical model to describe the pharmacokinetics in brain compartments, and apply this model to predict human brain disposition.

Methods: A mathematical model consisting of several physiological brain compartments in the rat was developed using rich concentration-time profiles from 9 structurally diverse drugs in plasma, brain extracellular fluid, and two cerebrospinal fluid compartments. The effect of active drug transporters was also accounted for. Subsequently, the model was translated to predict human concentration-time profiles for acetaminophen and morphine, by scaling or replacing system- and drug-specific parameters in the model.

Results: A common model structure was identified that adequately described the rat pharmacokinetic profiles for each of the 9 drugs across brain compartments, with good precision of structural model parameters (relative standard error <37.5 %). The model predicted the human concentration-time profiles in different brain compartments well (symmetric mean absolute percentage error <90 %).

Conclusions: A multi-compartmental brain pharmacokinetic model was developed and its structure could adequately describe data across 9 different drugs. The model could be successfully translated to predict human brain concentrations.

INTRODUCTION

Central nervous system (CNS) drug development suffers from 91% attrition rate and especially the success rate in phase II is very low (1,2). The primary reasons for attrition are safety issues (3). Although the underlying physiological and pharmacological reasons for such failures are often not fully known they are likely related to a lack of knowledge or failure to account for a combination of on- and off-target site concentrations, target interaction and downstream signal processing. The first step in this cascade, obtaining quantitative insight into CNS target site concentration kinetics, is already a major challenge, and has been suggested as a major factor contributing to failure of novel drug candidates (4). During clinical drug development, typically only drug plasma concentrations are considered as marker for drug exposure, because quantifying drug concentrations in the brain is challenging. Hence, the ability to predict brain concentrations based on plasma data is highly relevant to further optimize CNS drug development.

The prediction of brain target-site concentrations is controlled by several factors. First, the poorly penetrable blood-brain barrier (BBB) and the blood-cerebrospinal barrier (BCSFB) (5) limit passage of drugs from the systemic circulation into the brain. These barriers are associated with limited passive diffusion, and in addition various active transport and drug metabolism processes that systemically administered drugs need to pass. Second, the brain can be further subdivided into several distinct physiological compartments, including the brain extracellular fluid (ECF), brain intracellular fluid (ICF), and multiple cerebrospinal fluid (CSF) compartments. The specific disposition characteristics across these specific compartments further determines drug target-site concentrations. Third, CNS drug target-site concentrations are mediated by physiological flows including the microvascular blood flow, and brain ECF and CSF flows. Lastly, drug protein binding and the localized pH in specific sub-compartments further affect ultimate brain target-site concentrations.

Passive drug transport processes are mediated through a combination of drug permeability properties, trans-membrane transport routes, and the surface areas of the BBB (SA_{BBB}) and BCSFB (SA_{BCSFB}) (5). Active drug transport is mediated by transport proteins such as P-glycoprotein (P-gp), multidrug resistance-associated protein (MRPs), organic anion transporters (OATs), and organic anion transporting polypeptides (OATPs). Even though the function and localization of these transporters has been extensively investigated in *in-vitro* and *in-vivo* studies, their precise functions is in some cases not fully understood (6).

Several experimental preclinical models have been developed to assess drug distribution to brain compartments. These models differ in terms of temporal and spatial resolution, and in their consideration of drug protein binding (7–10). For example, the combinatorial mapping approach has been recently introduced using unbound drug concentration with the brain slice technique (10,11). This approach can predict unbound drug CNS exposure at steady state in multiple brain compartments, but does not allow temporal characterization of drug concentration changes. Positron emission tomography (PET) is sometimes used also clinically, as a non-invasive imaging method to visualize spatiotemporal drug distribution in the brain. However, PET scan signals cannot distinguish parent compounds from their metabolites, or bound and unbound drug compounds in the brain (12). Finally, microdialysis allows serial sampling in multiple physiological compartments of unbound drug concentrations, hence is suited to characterize the time profile of drug concentrations in the brain (13).

In order to capture the time profile and complexity of interacting factors governing drug distribution across brain compartments as determined by microdialysis methods, mathematical modeling represents an indispensable tool. Specifically, physiologically based pharmacokinetic (PBPK) models are of interest, as these models aim to distinguish between system- and drug-specific parameters, allowing for translational predictions by scaling or replacing system- or drug-specific parameters from the rat to man (14). Several (semi-) PBPK models for CNS drug distribution have been published, with different levels of complexity (15–20). However, these models did not yet include validations of predicted human CNS concentrations (21). Recently, Gaohoa et al published a CNS PBPK model, which consists of four compartments such as brain blood volume, brain mass, cranial CSF and spinal CSF. This model was validated with human acetaminophen and phenytoin data. However, a limitation of this model is the lack of consideration of a brain extracellular fluid compartment (brain_{ECF}), which is of critical importance for prediction of receptor binding kinetics for drugs acting on membrane bound receptors and ultimately drug efficacy (22).

Previously we have developed separate semi-physiological CNS PBPK models for three drugs based on microdialysis experiments in rats, which included unbound drug concentration-time profiles across multiple brain compartments (23–25). These models described the data well, but resulted in different individual model structures for each of these drugs.

The purpose of the current work was to develop a more generally applicable model structure that can be used to predict drug target site concentration-time profiles in human brain compartments based on rat pharmacokinetic (PK) studies. To this aim, we

used published and newly generated datasets for a larger number of drugs, and we performed rigorous model validation on external datasets. Furthermore, the impact of key drug transporters was also included in our model. Finally, we investigated the performance of the developed model structure to predict human brain concentration-time profiles for acetaminophen and morphine.

MATERIALS AND METHODS

Data for model development

An overview of experimental data for 9 compounds with different physicochemical characteristics used for model development is provided in **Table I**. The physicochemical characteristics of the 9 compounds are provided in **Table SI**. Data on 6 compounds were previously published, as indicated in **Table I**. For 3 compounds (paliperidone, phenytoin and risperidone), data were newly produced after single intravenous administration, as described below.

For some of the drugs, active transport inhibitors were co-administered intravenously to characterize the effect of P-gp, MRP, OATs and OATPs, as indicated in **Table I**. The transport inhibitors included were probenecid as an inhibitor of MRPs, OATs and OATPs, and GF120918 or tariquidar as inhibitor of P-gp.

Data for external model validation

For an external validation of the model, we used two separate rat datasets for acetaminophen and remoxipride, as indicated in **Table I**. The acetaminophen data was previously published, the remoxipride data was newly generated as described in the experimental section. For acetaminophen and remoxipride, two separate experimental datasets were available. For each drug, one of these datasets was used for model development, whilst the second dataset was used for external validation. The external validation with these second sets of data allows assessment of the robustness of our model predictions with respect to a different experiment and variation in experimental design.

Table I. Summary of the rat brain distribution data for model development and external validation

	Model development												External validation	
	Published data						Newly produced data						Published data	Newly produced data
	Acetaminophen	Atenolol	Methotrexate	Morphine	Morphine	Quinidine	Remoxipride	Paliperidone	Phenytoin	Risperidone	Acetaminophen	Remoxipride		
Study design														
Species	rat	rat	rat	rat	rat	rat	rat	rat	rat	rat	rat	rat	rat	
Nr of animals	16	5	23	65	18	41	29	21	14	16	8	65		
Dosage, mg/kg (infusion time, min)	16 (10)	10 (1)	40, 80 (10)	4, 10, 40 (10)	10, 40 (10)	10, 20 (10)	4, 8, 16 (30)	0.5 (20)	20, 30, 40 (10)	2 (20)	200 ^a (1)	0.7, 5.2, 14 (10)		
Nr of samples (sampling times, min)	67 (0-240)	32 (0-120)	186 (0-300)	825 (0-360)	306 (0-190)	313 (0-360)	189 (0-240)	182 (0-360)	109 (0-480)	124 (0-360)	67 (0-180)	290 (0-240)		
	592 (0-240)	106 (0-120)	1065 (0-300)	238 (0-360)	299 (0-180)	1678 (0-360)	125 (0-240)	660 (0-240)	152 (0-480)	436 (0-240)	72 (0-180)	489 (0-240)		
Active transport inhibitor	-	-	probencid ^b	GF120918 ^c	-	tariquidar	-	tariquidar	tariquidar ^c , probencid ^b	tariquidar ^c	-	-		
Dosage of active transport inhibitor, mg/kg (infusion time, min)	-	-	150 (10)	6 (cont.) ^d	-	15 (10)	-	15 (10)	15 (10), 150 (10)	15 (10)	-	-		
Data														
plasma	X	X	X	X	X	X	X	X	X	X	X	X		
brain _{ECF}	X	X	X	X	X	X	X	X	X	X	X	X		
CSF _{LV}	X		X			X						X		
CSF _{CM}	X		X			X		X		X		X		
References	(23)	(26)	(25)	(27)	(28)	(24)	(29)				(30)			

brain_{ECF}: a brain extracellular fluid compartment, CSF_{LV}: a compartment of cerebrospinal fluid in the lateral ventricle, CSF_{CM}: a compartment of cerebrospinal fluid in the cisterna magna

^a, mg; ^b, inhibitor of MRPs, OATs and OATPs; ^c, inhibitor of P-gp; ^d, continuous infusion

Animals

Animal study protocols were approved by the Animal Ethics Committee of Leiden University and all animal experiments were performed in accordance with the Dutch Law of Animal Experimentation (for approval numbers see **Table SII**). Male Wistar rats (225-275 g, Charles River, The Netherlands) were housed in groups for a few days (5-13 days) under standard environmental conditions with ad libitum access to food (Laboratory chow, Hope Farms, Woerden, The Netherlands) and acidified water. Between surgery and experiments, the animals were kept individually in Makrolon type 3 cages for 7 days to recover from surgical procedures.

Surgery

Rats were anesthetized (5% isoflurane for induction, 1-2% as maintenance), and subsequently received cannulas in the femoral artery for serial blood sampling, and in the femoral vein for drug administration, respectively. Subsequently, microdialysis guides were inserted into different brain locations. The animals were allowed to recover for 1 week before the experiments were performed. One day before the experiment, the microdialysis dummies were replaced by microdialysis probes. For details on guides, probes and locations see **Table SII**.

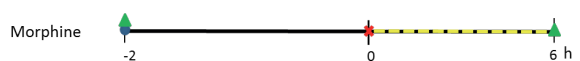
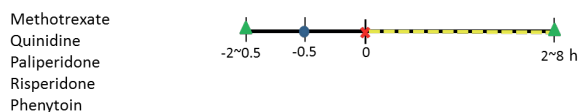
Microdialysis and drug administration

Experiments generally started at 9:00 a.m. to minimize the influence of circadian rhythms. Microdialysis probes were continuously flushed with microdialysis perfusion fluid (PF) until equilibration before the start of drug administration. Drugs were administered at $t = 0$ h by intravenous infusion through the cannula implanted in the femoral vein. For the quantification of active drug transport, the active transport inhibitor was administered before the drug's administration. The general procedure of microdialysis is depicted in **Figure 1**. Dosage and infusion time for each drug and the active transport inhibitor were summarized in **Table I**, and the composition of microdialysis PF and flow rate of microdialysis PF are summarized in **Table SII**.

No active transport inhibitor



Single active transport inhibitor



Double active transport inhibitor



- ▲ Start/end of the microdialysis
- ✖ Administration of the compounds
- Administration of the active transport inhibitors
- Microdialysate sampling

Figure 1. Microdialysis procedures for the compounds used for the development of the multi-compartmental brain PK model.

Bioanalytical methods

The developed analytical methods for risperidone, paliperidone, phenytoin and remoxipride are described below.

Chemicals and Reagents

For all procedures, nanopure lab water (18.2 MΩ cm) was used. All chemicals used were obtained from Sigma Aldrich (Zwijndrecht, The Netherlands), and analytical grade unless stated otherwise. The internal standards risperidone-D4 and paliperidone-D4 were purchased from Toronto Research Chemicals (Toronto, Ontario, Canada). Remoxipride-HCl was obtained from TOCRIS (Bristol, United Kingdom). Tariquidar (TQD, XR9576) was obtained from Xenova group PLC (Cambridge, United Kingdom). Ammonium formate, ammonium bicarbonate (ULC/MS grade), acetonitrile (LC-MS grade), methanol, isopropanol, and formic acid (ULC/MS grade) were obtained from Biosolve B.V. (Valkenswaard, The Netherlands). Sodium hydroxide was obtained from Baker (Deventer, The Netherlands).

Sample preparation of plasma

- Risperidone and paliperidone

The calibration curve was in a range of 5 to 1000 ng/ml. Quality controls (QC's) were prepared in blank rat plasma at three different concentration levels and stored at -20 °C. The lower limit of quantification (LLOQ) for both risperidone and paliperidone was 5 ng/ml. To 20 µl of plasma, 20 µl of internal standard solution (risperidone-D4 and paliperidone-D4) and 20 µl water (or 20 µl calibration solution in the case of the calibration curve) were added. After brief vortexing, 1 ml of acetonitrile was added. Brief vortexing and subsequent centrifugation at 10,000 g led to a clear supernatant, which was transferred to a glass tube and evaporated in the vortex evaporator (Labconco, Beun de Ronde, Breda, The Netherlands). The residue was redissolved in 200 µl of 2 % methanol, 10 mM ammonium formate, pH 4.1 and processed in according to the solid phase extraction (SPE)- liquid chromatography (LC) method.

- Phenytoin

20 µl of plasma sample was mixed with 20 µl of water in an Eppendorf vial. An aliquot of 40 µl acetonitrile was added for protein precipitation. After centrifugation at 11,000 g for 10 minutes, 40 µl of supernatant was mixed with 40 µl ammonium acetate buffer (pH 5.0). Calibration was performed by adding 20 µl of calibration solution to 20 µl of blank plasma, using the same clean-up procedure. The calibration solutions ranged from 0.2 to 100 µg/ml. 30 µl was injected into the high-performance liquid chromatography (HPLC) system. The LLOQ was 250 ng/ml.

- Remoxipride

Sample preparation was performed according to Stevens et al (29). Briefly, 20 µl of sample was mixed with 20 µl of water and 20 µl internal standard (raclopride). Proteins were precipitated with 6% perchloric acid and centrifugation. After addition of sodium carbonate, 10 µl was injected into the SPE-LC system.

Sample preparation for microdialysates

- Risperidone and paliperidone

The calibration curve for the microdialysis samples was prepared in buffered PF (composition in **Table SII**). The concentrations were in the range of 0.1 to 20 ng/ml. QC's were prepared using a different batch of buffered PF. Before injection of 10 µl into the LC system, the microdialysate samples were diluted with internal standard solution in a ratio of 1:1 v/v. The internal standard solution consisted of 100 ng/ml risperidone-D4 and paliperidone-D4 in nanopure water. The LLOQs for risperidone and paliperidone were 0.4 and 0.2 ng/ml, respectively.

- *Phenytoin*

Calibration curves were made in minimal PF at a concentration range of 25 to 5000 ng/ml. QC's were prepared using a different batch of buffered PF. Of a typical sample that consisted of 40 µl of microdialysate, 30 µl was injected into the HPLC system. The LLOQ was 25 ng/ml.

- *Remoxipride*

Calibration curves were prepared in buffered PF. The calibration range was from 1 to 200 ng/ml. QC's were prepared using a different batch of buffered PF. Samples were mixed in a 1:1 v/v ratio with the internal standard raclopride (100 ng/ml) before injection of 5 µl into the LC system. The LLOQ was 0.5 ng/ml.

Chromatography

- *Paliperidone and risperidone*

SPE-LC method. For plasma samples the SPE-method was applied. The SPE system consisted of a Hyphere C8 HD, SE column (10x2 mm) (Spark Holland, Emmen, The Netherlands) in a cartridge holder and served for the clean-up of the sample. The cartridge holder was connected to a Gynkotech gradient pump (Thermo Scientific, Breda, The Netherlands) and a Waters 717 autosampler (Waters, Etten-Leur, The Netherlands). The MS Surveyor pump from Thermo Scientific (Breda, The Netherlands) provided the flow for the LC column, which was the same type as in the LC-method. The sample was injected onto the SPE, which was preconditioned with 2 % methanol (pH 4.1). After 1 minute of flushing, the SPE was switched into the LC system. After 4 minutes, the SPE was cleaned with 98 % methanol (pH 4.1) for 2 minutes and reconditioned with 2 % methanol (pH 4.1). The flow of the SPE pump was 0.75 ml/min. The flow of the LC system was 0.25 ml/min. The gradient was from 10 to 90 % methanol (1 - 8.5 minutes after injection). The SPE column was used for a maximum of 240 injections.

LC-method. For microdialysates, LC-Method was applied. The separation of the active compounds was possible using Hyper Clone HPLC column (3 µm BDS C18 130Å) from Phenomenex (Utrecht, The Netherlands) placed at 40°C. The LC system was used at a flow of 0.25 ml/min using a linear gradient from 20 to 74 % methanol (1 - 6 minutes after injection). Before the next injection, the column was re-equilibrated with 20 % methanol for two minutes.

- *Phenytoin*

HPLC method and detection. For both plasma and microdialysates samples an HPLC method was used. The mobile phase consisted of 15 mM ammonium acetate adjusted to pH 5.0 with acetic acid and acetonitrile in a 2:1 ratio (v/v). Separation was achieved using an Altima HP C18-Amide HPLC column (5 μ m, 150 x 4.6mm) from Grace Alltech (Breda, The Netherlands). The injector was from Waters (Etten-Leur, The Netherlands). The LC pump (LC-10 ADVP) was obtained from Shimadzu ('s-Hertogenbosch, The Netherlands). The ultraviolet (UV) detector (Spectroflow 757) was obtained from Applied Biosystems (Waltham, Massachusetts) and was used at a wavelength of 210 nm. Data acquisition was achieved using Empower software from Waters (Etten-Leur, The Netherlands).

- *Remoxipride*

SPE-LC Method. For the precipitated plasma samples, on-line SPE was combined with HPLC and mass spectrometry according to Stevens et al (29). Briefly, a pretreated sample was loaded into a Hysphere GP resin cartridge column (10x2 mm) from Spark Holland (Emmen, The Netherlands) at pH 8.3 and flushed for one minute. Elution was performed using a low pH and an Altima HP C18 column (150x1.0 mm, 5 μ m).

LC-Method. For microdialysates, a Kinetex 2.6 μ m column (50x2.0 mm, XB-C-18) from Phenomenex (Utrecht, The Netherlands) was used at a flow of 0.6 ml/min and placed at 40 °C. The system was a Nexera-X2 UHPLC system, consisting of two ultra high performance liquid chromatography (UHPLC) pumps delivering the high pressure gradient. A SIL-30AC auto sampler was used to inject 5 μ l of the microdialysis sample. The flow was diverted for the first 0.5 minute, while a gradient from 10 to 90 % methanol in 1.5 minute served to elute both remoxipride and raclopride to the mass spectrometer.

Mass spectrometry

For risperidone, paliperidone and remoxipride, mass spectrometry was used to measure the concentrations. The mass spectrometer was a TSQ Quantum Ultra from Thermo Fisher Scientific (Breda, the Netherlands) and was used in MS/MS mode. Electrospray was used for ionization in the positive mode, nitrogen served as the desolvation gas and argon was used as collision gas. Data acquisition for both remoxipride and risperidone and paliperidone was performed using LCQuan 2.5 software from Thermo Scientific (Breda, The Netherlands).

Risperidone and paliperidone had the following transitions (m/z): 411.2→191.1 (risperidone), 415.2→195.1 (paliperidone), 415.2→195.1 (risperidone-D4), 431.2→211.1 (paliperidone-D4). The scan width was set at 0.2 m/z, the scan time was 0.05 seconds. Collision was performed at fixed voltages between 27 and 38 V, using a skimmer offset of 2 V.

The transitions (m/z) were 371→242.8 for remoxipride and 247.0→ 84.0, 112, 218.8 for raclopride. The skimmer offset was 18 and collision was performed between at fixed voltages between 24 and 45 V. Scan width and scan time were the same as above.

Determination of fraction unbound in plasma

To determine the free fraction of paliperidone and risperidone in plasma samples, Centrifree Ultrafiltration Devices from Merck Millipore (Amsterdam, The Netherlands) were used to separate the free from the protein bound risperidone and paliperidone in pooled plasma samples. Both the ultrafiltrate and the original pooled plasma sample (without ultrafiltration step) were measured. The free fraction was calculated according to the following Equation 1:

$$\text{Free fraction} = \frac{\text{Ultrafiltrate concentration}}{\text{Pooled plasma concentration}} \quad (1)$$

For phenytoin and remoxipride, the free fraction in plasma was calculated using a protein binding constant of 91 % and 26 % respectively which were obtained from literature (31,32).

Determination of in-vivo recovery (retro dialysis) (33)

The *in-vivo* recovery of paliperidone, risperidone, phenytoin and remoxipride was calculated using the compound concentration in the dialysate (C_{dial}) and in PF (C_{in}) according to the following Equation 2:

$$\text{In vivo recovery} = \frac{C_{\text{in}} - C_{\text{dial}}}{C_{\text{in}}} \quad (2)$$

Brain microdialysis data of paliperidone, risperidone, phenytoin and remoxipride were corrected for *in-vivo* recovery to obtain brain_{ECF} and CSF data.

The *in-vivo* recovery and free fraction for the 9 compounds are summarized in **Table SII**.

Human data

Table II summarizes the clinical concentration data for acetaminophen and morphine used to assess model performance to predict human concentrations. These data consisted of two clinical studies for acetaminophen and two studies for morphine. All studies were published, except for study 1 for acetaminophen that consists of newly generated data (see in **Table II**).

Acetaminophen

Acetaminophen human plasma samples and CSF samples were obtained at Poitiers University Hospital. Seven patients who had a traumatic brain injury (TBI) were enrolled in the clinical study. They were treated with a 30 min intravenous infusion of 1 g of acetaminophen. CSF samples were collected from a compartment of cerebrospinal fluid in the lateral ventricle (CSF_{LV}) by external-ventricular drainage (EVD) to control the intracranial overpressure (named CSF_{EVD}) (34). All clinical studies were conducted according to the Declaration of Helsinki, and written informed consent was obtained from each subject after the approval of the institutional review board at the medical institute. The demographic data is summarized in **Table SIII**. Acetaminophen concentrations at the start of the study (some patients already received acetaminophen before) were used as an initial value in the plasma compartment. The volume of EVD samples and EVD flow rate during a certain time interval were experimentally determined (**Table SIV**).

A second human acetaminophen PK dataset (study 2) in plasma and in CSF subarachnoid space (CSF_{SAS}) was obtained from the literature, and was based on patients with nerve-root compression pain (35).

For both datasets, total plasma concentrations for acetaminophen were converted to free plasma concentrations using the free fraction obtained from literature (36).

Morphine

Morphine human concentration-time profiles in plasma and in brain_{ECF} were obtained from the physiologically "normal" side of the brain and also from the "injured" side of the brain of TBI patients (37,38). For both datasets, the unbound plasma concentrations were already reported in the original publications (37,38).

Software

The PK analysis was performed using NONMEM version 7.3 (ICON Development Solutions, Hanover, MD, USA) (39). For the brain PK modeling of rat data, the extended least squares estimation method was applied. Other analyses were performed by

using the first-order conditional estimation method with interaction (FOCE-I). The compartmental models were defined using the ADVAN6 differential equation solver in NONMEM (39). The plots and the statistical analysis were conducted using R (Version 3.2.5; R Foundation for Statistical Computing, Vienna, Austria) (40).

Table II. Summary of the human acetaminophen and morphine data

Study design		Acetaminophen		Morphine	
		Study 1	Study 2	Study 1	Study 2
Condition of patients		human with traumatic brain injury	human with nerve-root compression pain	human with traumatic brain injury	human with traumatic brain injury
Nr of patients		7	1 (mean values)	2	1
Dosage		1 g, 30 min infusion	2g (propacetamol), short infusion	10 mg, 10min infusion	10 mg, 10min infusion
Nr of samples (sampling time, h)	plasma	38 (0-6h)	11 (0-12h)	23 (0-3h)	11 (0-3h)
	brain ECF or CSF	54 (0-5.5h)	11 (0-13h)	74 (0-3h)	37 (0-3h)
data references		Newly generated	(35)	(38)	(37)
Data					
plasma		X	X	X	X
brain _{ECF}				X ("normal" and "injured" brain tissue)	X ("normal" and "injured" brain tissue)
CSF _{EVD}		X			
CSF _{SAS}			X		
f _p ^a		85%	85%	-	-
f _p references		(36)	(36)	(38)	(37)

brain_{ECF}: a brain extracellular fluid compartment, CSF_{EVD}: a compartment of cerebrospinal fluid in EVD, CSF_{SAS}: a compartment of cerebrospinal fluid in the subarachnoid space

^a free fraction in plasma

Model development

Separate models describing plasma and brain concentration-time profiles for all 9 compounds were developed whereby plasma- and brain-related parameters were estimated simultaneously. A naïve pooling approach was used (41), i.e. inter-individual variability in each compound's data was not quantified, because of the highly standardized experimental settings combined with the homogeneous nature of the animals within each study.

The structural model that was used as a starting point was based on our previously developed models (23–25). To develop a more generally applicable model structure with parameters that can be precisely estimated across drugs, we systematically assessed the following two model structure characteristics.

First, a combined drug dispersion parameter was estimated to capture the CSF and ECF flow and turbulence flow of the drug molecules (42,43).

Second, drug transfer across the BCSFB was excluded. SA_{BCSFB} is 2-15 times smaller than SA_{BBB} (44–46), suggesting that drug exchange at BCSFB can be ignored from the model.

We evaluated for each drug the validity of the changes to the basic model with regard to a single or two different flow rates for drug dispersion and drug transport at the BCSFB.

Quantification of active drug transport

For the 6 compounds, data were obtained using co-administration of inhibitors of active transport. For all these compounds, the effect of the active transport inhibitors was tested on drug exchange at the BBB (Q_{PL_ECF}) and plasma clearance (CL_{PL}), and in combination, as a categorical covariate. (Eq.3)

$$P = P_{PAT} \times (1 + \theta_{cov} \cdot Cov) \quad (3)$$

where P_{PAT} represents the parameter including passive and active transport (net transport), P represents the parameter which takes into account the active transport inhibitors if there is any such effect, Cov is the value of the covariate (0: without an active transport inhibitor, 1: with an active transport inhibitor), θ_{cov} represents the effect of the active transport inhibitor.

Model evaluation

The systematic inclusion of aforementioned factors was guided by a likelihood ratio test, by an adequate parameter estimation precision, by assessment of the parameter correlation matrix to ensure parameter identifiability, and by the graphical evaluation of plots for observations versus predictions and weighted residuals versus time and versus predictions. The likelihood ratio test is based on the assumption that changes in the NONMEM objective function values (OFV, $-2 \log$ likelihood) are asymptotically chi-square distributed. A decrease of OFV ≥ 3.84 was considered statistically significant ($p < 0.05$). For a clear assessment of model predictions and observations we also computed the following metrics (Eq.4 and 5).

$$PE = \frac{Y_{OBS,ij} - Y_{PRED,ij}}{(Y_{OBS,ij} + Y_{PRED,ij})/2} \quad (4)$$

$$SMAPE = \frac{1}{N} \sum_{k=1}^N |PE| \times 100 \quad (5)$$

where PE is a prediction error, and SMAPE is symmetric mean absolute percentage error (47). $Y_{OBS,ij}$ is the j th observation of the i th subject, $Y_{PRED,ij}$ is the j th prediction of the i th subject. N is number of observations. In the cases where we did not estimate inter-individual variability, e.g. for all brain PK data, $Y_{PRED,ij}$ equals the mean population prediction $Y_{PRED,j}$.

External model validation

Validation of the brain PK model was performed by investigating the quality of the prediction of external rat data. The prediction was done as follows, 1) estimating plasma-related parameters (CL_{PL} , $Q_{PL-PER1}$, V_{PL} and $V_{PL-PER1}$) using the external rat plasma data, 2) fixing the brain-related parameters (Q_{PL-ECF} , Q_{DIFF} , V_{ECF} , V_{LV} , V_{TFV} , V_{CM} and V_{SAS}) to the values which were estimated from the brain PK model and 3) predicting the brain_{ECF} or CSF concentrations using estimated rat plasma-related parameters and fixed brain-related parameters.

Plasma PK analysis of external rat data

The plasma-related parameters including inter-individual variability on these parameters and residual errors were estimated using the external rat plasma data. We used a mixed effects modeling approach to investigate the predictability of the brain concentration based on each plasma concentration. The same plasma model structure, which was obtained from the brain PK model was applied for each compound. Inter-individual variability were tested on each PK parameter using an exponential model (Eq. 6).

$$\theta_i = \theta \times e^{\eta_i} \quad (6)$$

where θ_i represents the parameters of the i th subject, θ represents the population mean value of the parameter, and η_i is the random effect of the i th subject under the assumption of a normal distribution with a mean value of 0 and variance of ω^2 .

A proportional error model and the mixed error model (Eq. 7-8) were tested for the residual errors:

$$C_{ij} = Y_{PRED,ij} \times (1 + \varepsilon_{ij}) \quad (7)$$

$$C_{ij} = Y_{PRED,ij} \times (1 + \varepsilon_{1,ij}) + \varepsilon_{2,ij} \quad (8)$$

where C_{ij} represents the j th observed concentration of the i th subject, $Y_{PRED,ij}$ represents the j th predicted concentration of the i th subject, and ε_{ij} is the random effect of the j th observed concentration of the i th subject under the assumption of a normal distribution with a mean value of 0 and variance of σ^2 .

Model selection was guided by a likelihood ratio test with $p < 0.05$ and by the precision of the parameter estimates.

Handling of the brain-related parameter values

For Q_{PL_ECP} , Q_{DIFF} the same values, which were estimated from the brain PK model, were used for acetaminophen and remoxipride, respectively. V_{ECP} , V_{LV} , V_{TFV} , V_{CM} and V_{SAS} are system-specific parameters, therefore, the same rat physiological values were used, indicated in **Table III**.

Prediction of brain_{ECF} and CSF concentrations of external data

Simulations were performed 200 times for each compound. The 95 % prediction interval (using the calculated 2.5 % tile and 97.5 % tile) and the median of the simulated concentrations were plotted together with the external data. Accuracy of the mean population prediction for brain PK data was evaluated with SMAPE mentioned above (Eq. 5).

Translation of the model to humans

The translational prediction was performed by the following steps, 1) estimating plasma-related parameters (CL_{PL} , $Q_{PL-PER1}$, V_{PL} and $V_{PL-PER1}$) using human plasma data, 2) replacing brain-related system-specific parameters (V_{ECF} , V_{LV} , V_{TFW} , V_{CM} and V_{SAS}) by human values, 3) applying allometric scaling to the brain-related drug-specific parameters which were estimated with the rat *in-vivo* data (Q_{PL-ECF} and Q_{DIFF}), 4) adding clinical sampling procedure related fixed parameters which were obtained from the EVD into the model (Q_{LV-EVD} and V_{EVD}) and 5) predicting the brain_{ECF} and CSF concentrations using estimated human plasma PK parameters, replacing system-specific parameters, scaling drug-specific parameters and using clinical sampling procedure related fixed parameters. The details of the translational methods for each parameter are explained in **Figure 2**.

Human plasma PK analysis

Plasma-related parameters including inter-individual variability and residual errors were estimated using the human data using the equations 6-8. A 1-compartment, 2-compartment and 3-compartment model were tested. Model selection was guided by a likelihood ratio test with $p < 0.05$, by the precision and correlation between parameter estimates and by the graphical evaluation of plots for observations versus predictions and weighted residuals versus time and versus predictions.

Replacement of the system-specific parameters

System-specific parameters in the brain distribution rat model (V_{ECF} , V_{LV} , V_{TFW} , V_{CM} and V_{SAS}) were replaced with the human physiological values, which are available from literature (48–54) (see **Table IV**).

Scaling of the drug-specific parameters

Drug-specific parameters (CL_{PL-ECF} and Q_{DIFF}) were scaled to human values using allometric principles following Equation 9 (18).

$$P_{human} = P_{rat} \times \left(\frac{BW_{human}}{BW_{rat}} \right)^{0.75} \quad (9)$$

where P_{human} is the scaled human parameter, P_{rat} is the estimated rat parameter from the model, BW_{human} is the average human body weight (70 kg), and BW_{rat} is the average rat body weight (250 g).

Adding clinical sampling procedure related fixed parameters

In addition to those parameters which were used in the rat brain PK model, we have data obtained from the EVD approach, therefore the EVD compartment was added into the translated brain distribution model (see **Figure 2**). To describe the PK of acetaminophen in the EVD compartment, the values of flow rate from CSF_{LV} to CSF_{EVD} ($Q_{\text{LV,EVD}}$) and the volume of EVD compartment (V_{EVD}) were added into the model. The values of $Q_{\text{LV,EVD}}$ and V_{EVD} for each patient are obtained from EVD approach and available in **Table SIV**.

Prediction of human brain_{ECF} and CSF concentrations

Simulations were performed using the same methods as we mentioned for the external model validation.

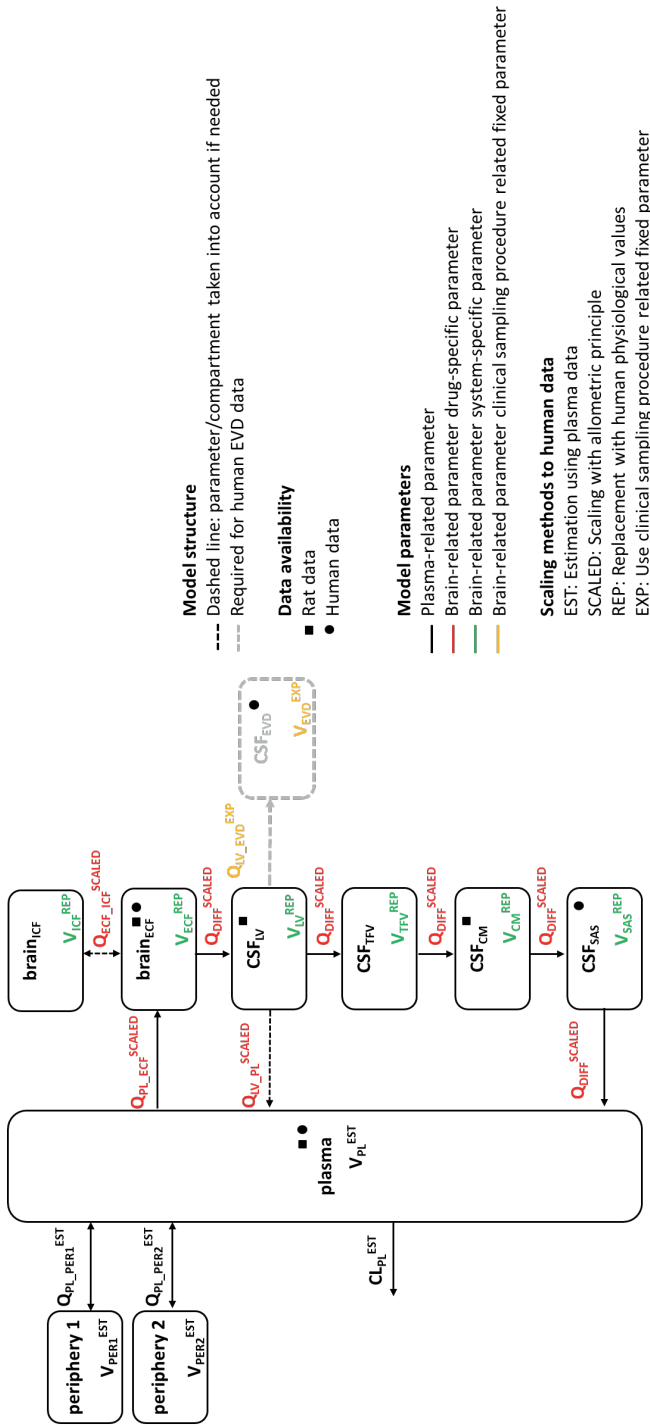


Figure 2. The brain PK model structure and translational methods for each parameter. The brain PK model consists of plasma, brain_{ICF}, brain_{ECF}, CSF_{LV}, CSF_{TV}, CSF_{CM} and CSF_{SAS}, which consists of 4 different categories parameters (colors). The scaling method on each parameter is indicated with color coding.

Table IV. Parameter values used for the translational prediction to humans

	Translational methods	Unit	Parameter estimates (RSE, %)	
			Acetaminophen	Morphine
Plasma-related parameters				
CL_{PL}	estimation from human PK data	mL/min	562 (20.1)	3070 (15.8)
Q_{PL_PER1}	estimation from human PK data	mL/min	2060 (31.1)	3030 (0.60)
V_{PL}	estimation from human PK data	mL	9880 (41.1)	16000 (35.3)
V_{PER1}	estimation from human PK data	mL	51900 (18.3)	95400 (2.50)
Brain-related parameters				
Drug-specific parameters				
Q_{PL_ECF}	allometric scaling	mL/min	1.92 FIX	0.513 FIX
Q_{DIFF}	allometric scaling	mL/min	3.81 FIX	1.37 FIX
System-specific parameters				
V_{ECF}^a (48)	replacement	mL	240 FIX	240 FIX
V_{LV}^a (49–51)	replacement	mL	22.5 FIX	22.5 FIX
V_{TFV}^a (49–51)	replacement	mL	22.5 FIX	22.5 FIX
V_{CM}^a (52,53)	replacement	mL	7.5 FIX	7.5 FIX
V_{SAS}^a (54)	replacement	mL	90 FIX	90 FIX
Clinical sampling procedure related fixed parameters				
Q_{LV_EVD}	use the fixed parameter	mL/min	values are in supplemental table IV	
V_{EVD}	use the fixed parameter	mL		
Standard deviations of inter-individual variability (estimated from human PK data)				
$\omega_{CL_{PL}}$			0.490 (30.2)	0.271 (19.9)
$\omega_{Q_{PL_PER1}}$			NA	NA
$\omega_{V_{PL}}$			NA	0.596 (20.0)
$\omega_{V_{PER1}}$			0.235 (22.5)	NA
Standard deviations of residual error (estimated from human PK data)				
σ_{plasma}			0.250 (8.20)	0.0960 (22.9)

CL_{PL} : clearance from the central compartment, Q_{PL_PER1} : inter-compartmental clearance between the central compartment and the peripheral compartment 1, V_{PL} : distribution volume of the central compartment, V_{PER1} : distribution volume of the peripheral compartment 1, Q_{PL_ECF} : clearance from the central compartment to brain, Q_{DIFF} : drug diffusion rate in brain and CSF, V_{ECF} : distribution volume of brain, V_{LV} : distribution volume of CSF, V_{TFV} : distribution volume of CSF, V_{CM} : distribution volume of CSF, V_{SAS} : distribution volume of CSF, Q_{LV_EVD} : flow from CSF, V_{EVD} : volume of CSF.

^a: physiological values

RESULTS

The analysis work flow is depicted in **Figure 3**. The developed multi-compartmental brain PK model adequately described the data for the 9 compounds, as can be observed from the selected observed and predicted concentration-time profiles (**Figure 4A**) and the prediction error plots for all of the 9 compounds (**Figure 4B**). The prediction errors were mostly within 2 standard deviations of zero, i.e. no systematic differences between observations and predictions were found. No specific trend across time, also with respect to the presence or absence of active transport inhibitors, were observed. More extensive plots for individual observations versus predictions and weighted residuals versus time across drugs, dose levels and active transport inhibitors, are provided in the supplemental material (**Figure S1 and S2**).

We identified a generally applicable model structure (**Figure 2**) with physiologically relevant compartments. The final model consists of plasma, brain_{ECF}, brain intracellular fluid compartment (brain_{ICF}), CSF_{LV} compartment of CSF in third and fourth ventricle (CSF_{TFV}), compartment of CSF in cisterna magna (CSF_{CM}) and CSF_{SAS}, which included processes for drug exchange at the BBB (Q_{PL_ECF}) and drug dispersion through brain_{ECF} and CSF compartments (Q_{DIFF}). The parameter estimates were obtained with good precision, and are summarized in **Table III**.

A single drug dispersion rate (Q_{DIFF}) was shown to be sufficient for describing the sum of the drug distribution in the brain_{ECF} and CSF for the 9 compounds. Q_{DIFF} was comparable among the compounds, and ranged between 0.0598 mL/min for methotrexate to 0.0133 mL/min for phenytoin, and could be precisely identified (RSE <15.0 %), suggesting this parameter could be potentially considered to represent a system-specific parameter.

The parameter representing drug transfer at the BBB (Q_{PL_ECF}) was critical to quantify drug exchange between blood and brain. Q_{PL_ECF} was substantially different between drugs, ranging from 0.0354 mL/min for quinidine to 0.00109 mL/min for methotrexate.

On the other hand, drug exchange at BCSFB was identified only for methotrexate, and could not be identified for the other 8 compounds. For methotrexate, the efflux transport at BCSFB (Q_{LV_PL}) was 0.105 mL/min.

Among the 9 compounds, clearance between brain_{ECF} and brain_{ICF} (Q_{ECF_ICF}) could be estimated for paliperidone and quinidine: Q_{ECF_ICF} is 0.0250 mL/min for quinidine, and 0.0126 mL/min for paliperidone, implying for quinidine a slightly faster uptake into brain_{ICF} after crossing the BBB (**Table III**).

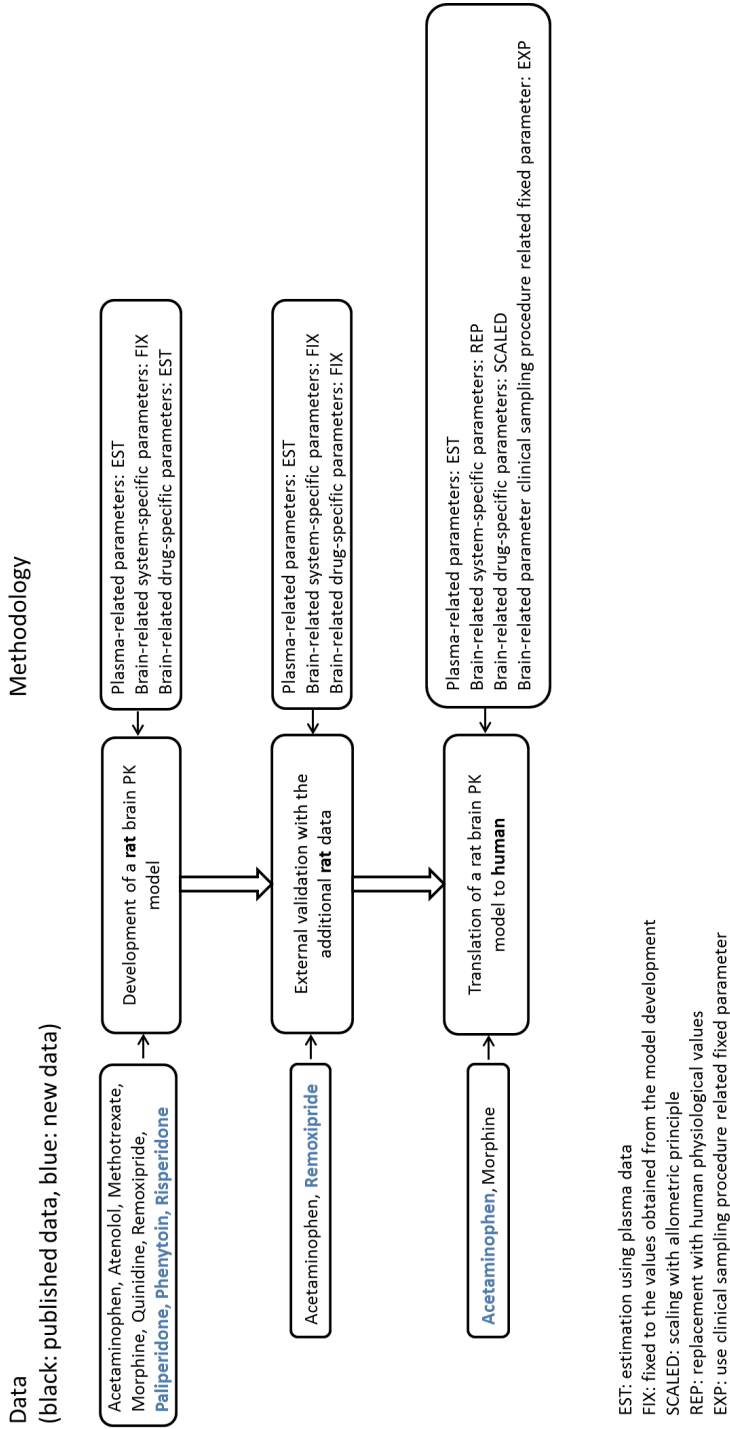


Figure 3. Schematic flow chart of the analysis.

For morphine, $\text{brain}_{\text{ECF}}$ concentration displayed a nonlinear relationship with dose and plasma concentrations. A categorical dose effect was therefore estimated. Continuous linear or nonlinear concentration-dependent effects to account for this effect were not supported by the data.

No statistically significant impact of P-gp and the combination of MRPs, OATs and OATPs on CL_{PL} could be identified, whereas those transporters were identified to act as efflux transporters at the BBB for our compounds. The P-gp function was quantified on the data of morphine, paliperidone, phenytoin, quinidine, and risperidone, and the impact of the combination of MRPs, OATs and OATPs was quantified on the data of methotrexate, as a categorical covariate on $\text{Q}_{\text{PL_ECF}}$. The presence of P-gp inhibitors increased the $\text{Q}_{\text{PL_ECF}}$ values of morphine, paliperidone, phenytoin, quinidine, and risperidone by 162 %, 43.4 %, 35.5 %, 443 % and 124 % respectively. The presence of the inhibitor of MRPs, OATs and OATPs increased the $\text{Q}_{\text{PL_ECF}}$ values of methotrexate by 409 %.

The developed model adequately predicted the external rat acetaminophen and remoxipride data. **Figure 5** presents the prediction results for the external rat data of acetaminophen and remoxipride using the developed multi-compartmental brain PK model. Prediction of the acetaminophen concentration-time profile in $\text{brain}_{\text{ECF}}$ using the final model captured the external acetaminophen concentration in $\text{brain}_{\text{ECF}}$ well (SMAPE<61%). Prediction of the remoxipride concentration-time profile in $\text{brain}_{\text{ECF}}$, CSF_{LV} and CSF_{CM} using the final model also captured the external remoxipride concentrations in $\text{brain}_{\text{ECF}}$, CSF_{LV} and CSF_{CM} concentrations well (SMAPE<67 %, 77%, 56%, respectively).

The model was successfully scaled to predict concentration-time profiles of acetaminophen and morphine in human brain compartments. **Table IV** summarizes the parameter values that were used for the prediction of human plasma, CSF_{EVD} , CSF_{SAS} and $\text{brain}_{\text{ECF}}$. In **Figure 6**, the human predictions versus human observations are depicted. The acetaminophen human CSF_{SAS} concentration in the patients with nerve-root compression pain and CSF_{EVD} concentration in the patients with TBI were predicted relatively well (SMAPE<90 % and 66 % respectively), even though there is a slightly faster elimination in CSF_{SAS} . Morphine $\text{brain}_{\text{ECF}}$ concentrations in the physiologically “normal” brain tissue of TBI patients were predicted very well (SMAPE<35 %). However, morphine $\text{brain}_{\text{ECF}}$ concentrations were underpredicted when the $\text{brain}_{\text{ECF}}$ concentrations were taken from “injured” brain tissue of TBI patients (SMAPE<56 %).

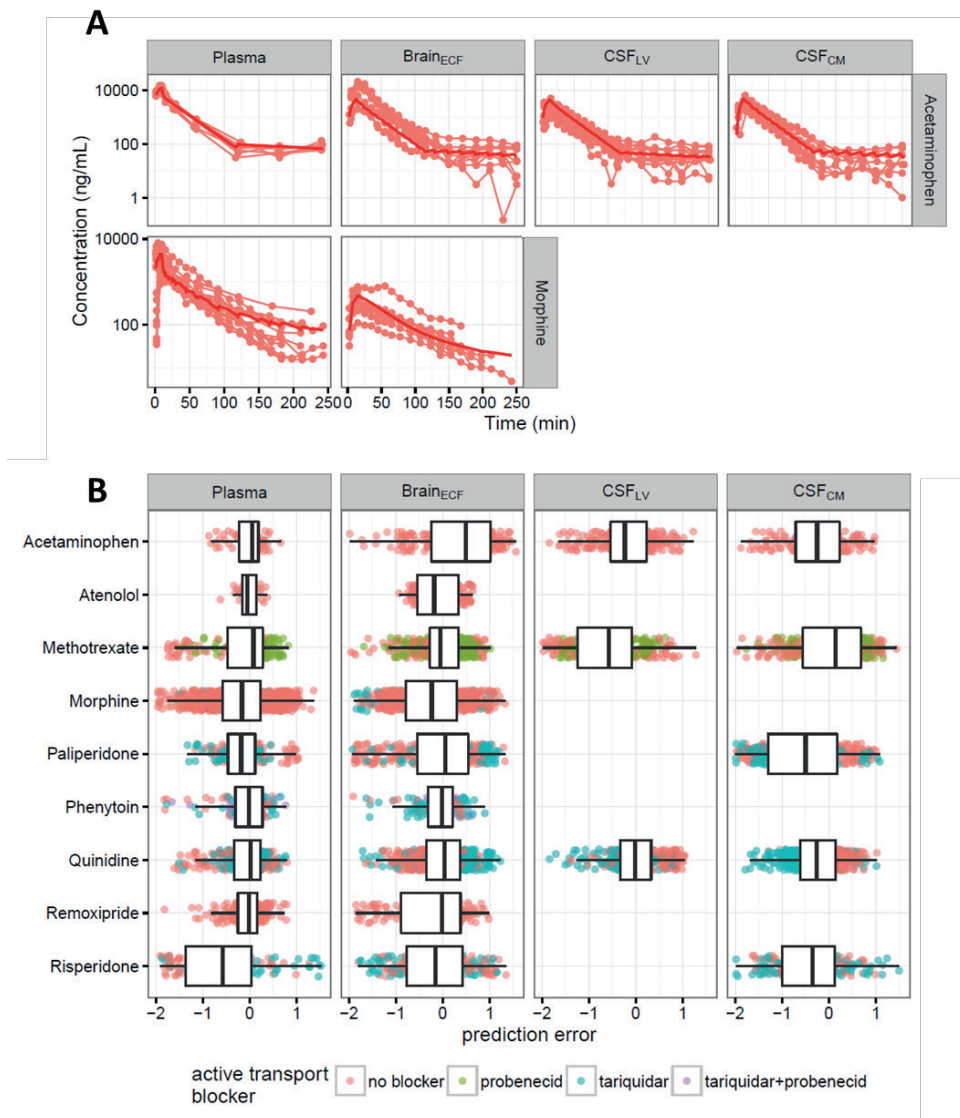


Figure 4. Prediction of the multi-compartmental brain PK model. (A) Individual observed drug concentrations (lines and circles) and mean model prediction (solid lines). Unbound concentration (ng/mL) versus time (min) profiles for acetaminophen and morphine. (B) Box-whisker plots for the prediction errors across all 9 drugs evaluated. The plots were stratified by brain compartments (panels) and by active transport blockers (colors).

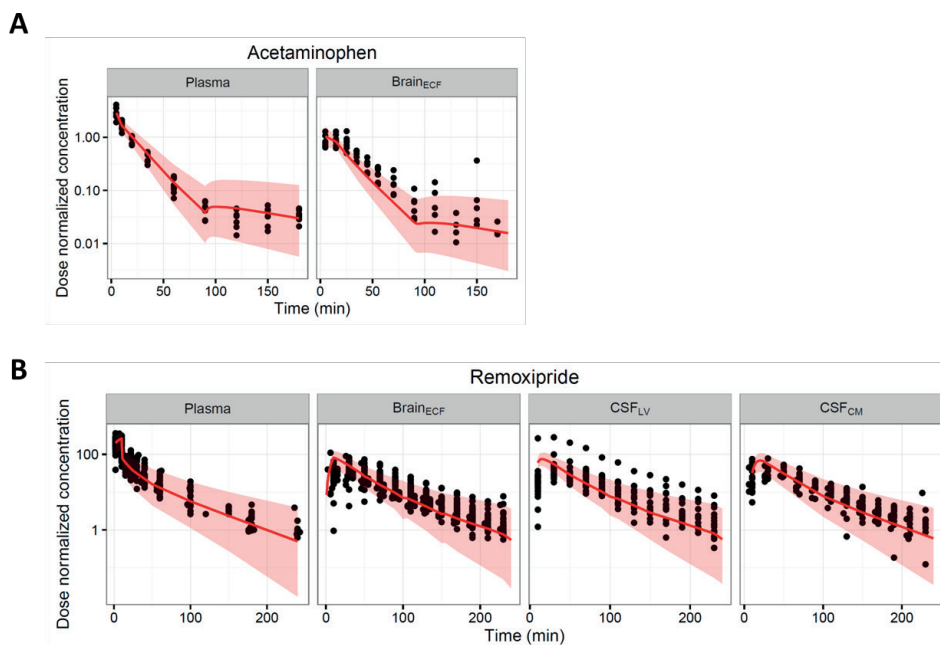


Figure 5. Model prediction versus external acetaminophen and morphine data in rat. Individual concentration-time profile of the external data (circles) and prediction from the brain PK model (red lines: median, shaded area is 95 % prediction interval). (A) Acetaminophen data were obtained after 200 mg administration, (B) remoxipride data were obtained from the dose group of 0.7, 5.2 and 14 mg/kg. The x-axis represents the time in minutes and the y-axis represents the dose-normalized acetaminophen and remoxipride concentration. The panels are stratified by brain compartments and compounds.

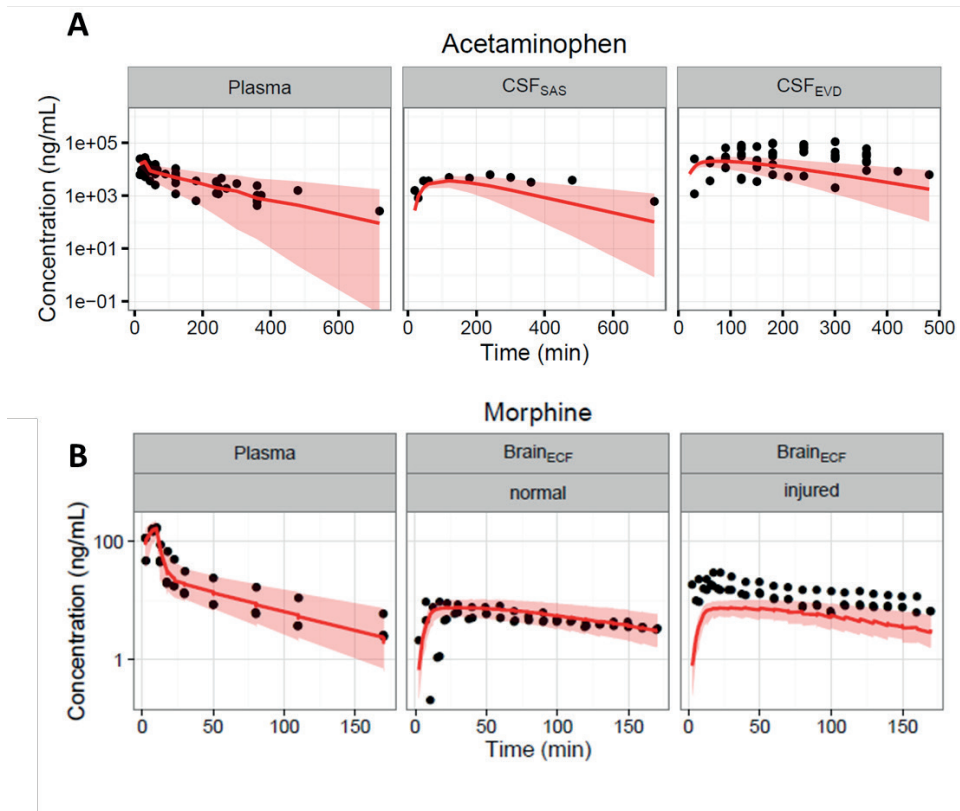


Figure 6. Human brain_{ECF} and CSF concentration-time profiles (circles) and prediction from the translational model (red lines: median, shaded area is 95 % prediction interval). (A) Acetaminophen data was obtained from plasma, CSF_{SAS} and CSF_{EVD}, (B) morphine data was obtained from plasma and brain_{ECF} in “normal” brain and “injured” brain. The x-axis represents the time in minutes and the y-axis represents the acetaminophen and morphine concentration in ng/ml. The panels are stratified by brain compartments and brain conditions.

DISCUSSION

The developed multi-compartmental brain PK model could describe the data of the 9 compounds in the rat adequately in the absence and presence of active transport blockers (**Figure 4**). After scaling of the model, human brain concentration-time profiles of acetaminophen and morphine could be adequately predicted in several physiological compartments under normal physiological conditions.

The model structure we have derived differs from the ones published earlier by: (i) a combined drug dispersion parameter was estimated to capture the CSF and brain_{ECF} flow and turbulence flow of the drug molecules; and (ii) drug transfer across the BCSFB was excluded (23–25). The final model has four different CSF compartments. This model is developed to predict human brain concentration profiles using rat data. In our analysis, rat data was sampled from CSF_{LV} and CSF_{CM}. Since in rats it is anatomically easier to access the CSF_{CM} compartment to obtain drug concentration by microdialysis and by the cisternal puncture methods, there are more data available from CSF_{CM} (59). Through keeping the CSF_{CM} compartment in the model structure, it will be easier to apply the model to additional compounds' data obtained in animals. Furthermore, substantial differences between CNS compartments may exist, such as a concentration difference between CSF_{LV} and CSF_{CM} for methotrexate and quinidine in rat (24,25). Thus, to predict the drug target-site concentration, the location of the CSF sampling site should be taken into account. For human, in clinical studies most CSF samples are taken from other CSF compartments, such as CSF_{SAS} and CSF_{LV} where samples are taken by EVD. Hence, we think that our model structure is a minimal, necessary model structure for translation.

We found that the brain intracellular fluid compartment (brain_{ICF}) is required for the description of drug distribution of quinidine and paliperidone, and likely associated with the lipophilic basic nature of quinidine (pKa 13.9, log P 3.4) and paliperidone (pKa 13.7, log P 1.8). For other compounds with a less distinct lipophilic-basic nature, such as for acetaminophen and phenytoin, we have shown that brain_{ICF} was not required for the description of concentration-time profiles in the brain. However, for a generally applicable brain PK model, inclusion of this compartment would still be required since prediction of intracellular drug concentrations would be of relevance for CNS drug development as well as prediction of extracellular drug concentrations. Our model and the microdialysis methodology used only allow quantification of extracellular concentrations. However, in combination with PBPK modeling based principles to predict intracellular partitioning, our model will be of significant relevance as it provides the required predictions for unbound extracellular drug concentration kinetics.

A drug exchange parameter across the BCSFB ($Q_{LV,PL}$) was identified for methotrexate only, even though it could not be identified for the other 8 compounds. This suggests that an additional efflux transporter might be present at the BCSFB for which methotrexate is a substrate. It is known that methotrexate is indeed a substrate of various transporters, such as RFC1, MRP, BCRP, OATP and OAT transporters (25), which are not involved in the drug transfer of the other 8 compounds. This result indicates that drug transport at BCSFB still needs to be investigated using data on compounds which are substrates for those transporters. The current model delineates the process that can be used to arrive to the best-performing model for such drugs. We took care to design the modeling process such that the total number of models that need to be fitted is minimal.

We identified a drug dispersion rate parameter that captures drug dispersion from brain_{ECF} to CSF. The median estimated drug dispersion flow was 0.0237 mL/min. The magnitude of the drug dispersion rate was approximately 10 times faster than the reported physiological CSF flow rate alone (60), and about 100 times faster than the reported physiological brain ECF bulk flow rate (55,61). Since similar values across drugs were identified, the parameter may be considered a system-specific parameter that could be fixed in further analyses (see **Table III**), to allow for estimation of other processes of interest.

P-gp transport for quinidine, risperidone, paliperidone, morphine and phenytoin was confirmed as efflux transporter at the BBB which were in line with literature (62,63). P-gp transporter effects were not identified at the BCSFB for these 5 P-gp substrates, i.e. CSF concentrations for these compounds were well-described solely by the BBB mediated P-gp transport. The role and contribution of P-gp transporters at the BCSFB is still inconsistent, and both efflux and influx processes have been reported (64–66). Our results however suggest that the function of P-gp may be ignored, since its potential magnitude likely is negligible compared to transport at the BBB, and drug dispersion processes prevail. Nonetheless, overall, we envision that the combination of our dynamical modeling approach with the incorporation of *in-vitro* assays to characterize active transport across the BBB or BCSFB, may be a fruitful direction to further characterize and disentangle the precise contribution to the brain drug disposition of different drug transport.

The developed model adequately predicted the external acetaminophen and remoxipride rat data, confirming the reliability of the model. Both of these drugs were also used for model development, but the experiments were different and applied somewhat different designs. Since we aimed to generate mean predictions, the variation in numbers of animals is expected to result in limited bias in the modeling. Furthermore,

sampling time points were very informatively distributed and any inter-experimental differences in these time points are therefore also considered to be of limited impact on model development. The external validation results indicated that the model is robust with respect to variations in experimental designs and conditions (i.e. the number of rats, sampling times, infusion times, and flow rates of microdialysis).

We consider the developed model structure suited for translational predictions of human brain (target site) concentrations such as required during drug development. The predictive performance in human data ranged between SMAPE of 35-90 %. Even though errors <90% may appear large, such <two-fold error is not considered unacceptable when compared to for instance QSAR studies, which are used to predict unbound brain partition coefficients of drugs in drug development (67,68). Secondly, the prediction error is likely inflated because of the use of human data obtained from patients with traumatic brain injury or with nerve-root compression pain. Therefore, larger variability in their physiological condition is expected.

Body weight in combination with allometric scaling was used to scale the parameters to humans, and this resulted in adequate predictions of human brain concentrations for physiologically “normal” brains. Different translational methods for estimation of CNS PK parameters have been reported in the literature. For instance, system-based scaling was applied using volume of brain tissue or brain endothelial surface area (25,69), but allometric scaling using body weight (our approach) was supported by work from others in the literature (70–73). Based on our current approach, reasonable predictions were obtained. Therefore, we suggest that the allometric scaling approach may indeed be appropriate although it would be worthwhile to investigate alternative approaches.

Our model was developed based on healthy rats and then translated to human data that was partly based on patients with severe brain injuries. Indeed, observed human morphine concentrations in brain_{ECF} obtained from the “injured” side of the brain of the TBI patients was higher than the prediction from the translational model (**Figure 6**). It is known that the BBB permeability is increased after TBI, which may be the reason for the under-prediction of our translational model for those data (74,75). Therefore, for predictions in patients with pathological conditions that alter the integrity of BBB or BCSFB barriers, or brain fluid flows, our model should be further extended with additional physiological details.

CONCLUSION

A multi-compartmental brain PK model structure was developed across a wide range of drugs with different physicochemical properties. The model structure was shown to be of relevance for the scaling of brain concentrations in humans. As such, the developed model structure can be used to inform the prediction of relevant target site concentrations in humans and aid in the translational development of CNS targeted drugs.

REFERENCES

1. Kola I, Landis J. Can the pharmaceutical industry reduce attrition rates? *Nat Rev Drug Discov.* 2004;3:1–5.
2. Hurko O, Ryan JL. Translational Research in Central Nervous System Drug Discovery. *J Am Soc Exp Neurother.* 2005;2(4):671–82.
3. Cook D, Brown D, Alexander R, March R, Morgan P, Satterthwaite G, et al. Lessons learned from the fate of AstraZeneca's drug pipeline: a five-dimensional framework. *Nat Rev Drug Discov.* 2014;13(6):419–31.
4. Danhof M, de Jongh J, de Lange ECM, Della Pasqua O, Ploeger BA, Voskuyl RA. Mechanism-Based Pharmacokinetic-Pharmacodynamic Modeling: Biophase Distribution, Receptor Theory, and Dynamical Systems Analysis. *Annu Rev Pharmacol Toxicol.* 2007;47(1):357–400.
5. de Lange ECM. The mastermind approach to CNS drug therapy: translational prediction of human brain distribution, target site kinetics, and therapeutic effects. *Fluids Barriers CNS.* 2013;10(1):1–16.
6. Westerhout J, Danhof M, de Lange ECM. Preclinical Prediction of Human Brain Target Site Concentrations : Considerations in Extrapolating to the Clinical Setting. *J Pharm Sci.* 2011;100(9):3577–93.
7. Hammarlund-Udenaes M, Fridén M, Syvänen S, Gupta A. On The Rate and Extent of Drug Delivery to the Brain. *Pharm Res.* 2008;25(8):1737–50.
8. Abbott NJ. Prediction of blood-brain barrier permeation in drug discovery from in vivo, in vitro and in silico models. *Drug Discov Today Technol.* 2004;1(4):407–16.
9. de Lange ECM, Hammarlund-Udenaes M. Translational aspects of blood-brain barrier transport and central nervous system effects of drugs: from discovery to patients. *Clin Pharmacol Ther.* 2015;97(4):380–94.
10. Loryan I, Fridén M, Hammarlund-Udenaes M. The brain slice method for studying drug distribution in the CNS. *Fluids Barriers CNS.* 2013;10(6):1–9.
11. Loryan I, Sinha V, Mackie C, van Peer A, Drinkenburg W, Vermeulen A, et al. Mechanistic Understanding of Brain Drug Disposition to Optimize the Selection of Potential Neurotherapeutics in Drug Discovery. *Pharm Res.* 2014;32(8):2203–19.
12. Neuwelt E, Abbott NJ, Abrey L, Banks WA, Blakley B, Davis T, et al. Strategies to advance translational research into brain barriers. *Lancet Neurol.* 2008;7(1):84–96.
13. Hammarlund-Udenaes M. The use of microdialysis in CNS drug delivery studies: Pharmacokinetic perspectives and results with analgesics and antiepileptics. *Adv Drug Deliv Rev.* 2000;45(2–3):283–94.
14. van Hasselt JGC, van der Graaf PH. Towards integrative systems pharmacology models in oncology drug development. *Drug Discov Today Technol.* 2015;15:1–8.

15. Collins JM, Dedrick RL. Distributed model for drug delivery to CSF and brain tissue. *Am J Physiol.* 1983;245(3):303–10.
16. Liu X, Smith BJ, Chen C, Callegari E, Becker SL, Chen X, et al. Use of a Physiologically Based Pharmacokinetic Model to Study the Time to Reach Brain Equilibrium: An Experimental Analysis of the Role of Blood-Brain Barrier Permeability, Plasma Protein Binding, and Brain Tissue Binding. *J Pharmacol Exp Ther.* 2005;313(3):1254–62.
17. Kielbasa W, Kalvass JC, Stratford R. Microdialysis evaluation of atomoxetine brain penetration and central nervous system pharmacokinetics in rats. *Drug Metab Dispos.* 2009;37(1):137–42.
18. Kielbasa W, Stratford RE. Exploratory Translational Modeling Approach in Drug Development to Predict Human Brain Pharmacokinetics and Pharmacologically Relevant Clinical Doses. *Drug Metab Dispos.* 2012;40(5):877–83.
19. Badhan RKS, Chenel M, Penny JI. Development of a Physiologically-Based Pharmacokinetic Model of the Rat Central Nervous System. *Pharmaceutics.* 2014;6(1):97–136.
20. Ball K, Bouzom F, Scherrmann J-M, Walther B, Declèves X. Comparing translational population-PBPK modelling of brain microdialysis with bottom-up prediction of brain-to-plasma distribution in rat and human. *Biopharm Drug Dispos.* 2014;25(8):485–99.
21. Deo AK, Theil F-P, Nicolas J-M. Confounding parameters in preclinical assessment of blood-brain barrier permeation: an overview with emphasis on species differences and effect of disease states. *Mol Pharm.* 2013;10(5):1581–95.
22. Gaohua L, Neuhoff S, Johnson TN, Rostami-hodjegan A, Jamei M. Development of a permeability-limited model of the human brain and cerebrospinal fluid (CSF) to integrate known physiological and biological knowledge: Estimating time varying CSF drug concentrations and their variability using in vitro data. *Drug Metab Pharmacokinet.* 2016;31(3):224–33.
23. Westerhout J, Ploeger B, Smeets J, Danhof M, de Lange ECM. Physiologically based pharmacokinetic modeling to investigate regional brain distribution kinetics in rats. *AAPS J.* 2012;14(3):543–53.
24. Westerhout J, Smeets J, Danhof M, de Lange ECM. The impact of P-gp functionality on non-steady state relationships between CSF and brain extracellular fluid. *J Pharmacokinet Pharmacodyn.* 2013;40(3):327–42.
25. Westerhout J, van den Berg D-J, Hartman R, Danhof M, de Lange ECM. Prediction of methotrexate CNS distribution in different species - Influence of disease conditions. *Eur J Pharm Sci.* 2014;57:11–24.
26. de Lange ECM, Danhof M, de Boer AG, Breimer DD. Critical factors of intracerebral microdialysis as a technique to determine the pharmacokinetics of drugs in rat brain. *Brain Res.* 1994;666(1):1–8.

27. Groenendaal D, Freijer J, de Mik D, Bouw MR, Danhof M, de Lange ECM. Population pharmacokinetic modelling of non-linear brain distribution of morphine: influence of active saturable influx and P-glycoprotein mediated efflux. *Br J Pharmacol.* 2007;151(5):701–12.
28. Bouw MR, Gårdmark M, Hammarlund-Udenaes M. Pharmacokinetic-pharmacodynamic modelling of morphine transport across the blood-brain barrier as a cause of the antinociceptive effect delay in rats - a microdialysis study. *Pharm Res.* 2000;17(10):1220–7.
29. Stevens J, Ploeger BA, van Der Graaf PH, Danhof M, de Lange ECM. Systemic and direct nose-to-brain transport pharmacokinetic model for remoxipride after intravenous and intranasal administration. *Drug Metab Dispos.* 2011;39(12):2275–82.
30. Stevens J, Suidgeest E, van der Graaf PH, Danhof M, de Lange ECM. A new minimal-stress freely-moving rat model for preclinical studies on intranasal administration of CNS drugs. *Pharm Res.* 2009;26(8):1911–7.
31. Srikanth CH, Chaira T, Sampathi S, Sreekumar VB, Bambal RB. Correlation of in vitro and in vivo plasma protein binding using ultracentrifugation and UPLC-tandem mass spectrometry. *Analyst.* 2013;138(20):6106–16.
32. Widman M, Nilsson L, Bryske B, Lundström J. Disposition of remoxipride in different species. Species differences in metabolism. *Arzneimittelforschung.* 1993;43(3):287–97.
33. Stähle L, Segersvärd S, Ungerstedt U. A comparison between three methods for estimation of extracellular concentrations of exogenous and endogenous compounds by microdialysis. *J Pharmacol Methods.* 1991;25(1):41–25.
34. Dey M, Jaffe J, Stadnik A, Awad IA. External ventricular drainage for intraventricular hemorrhage. *Curr Neurol Neurosci Rep.* 2012;12(1):24–33.
35. Bannwarth B, Netter P, Lopicque F, Gillet P, Péré P, Boccard E, et al. Plasma and cerebrospinal fluid concentrations of paracetamol after a single intravenous dose of propacetamol. *Br J Clin Pharmacol.* 1992;34(1):79–81.
36. Gazzard B, Ford-Hutchinson A, Smith M, Williams R. The binding of paracetamol to plasma proteins of man and pig. *J Pharm Pharmacol.* 1973;25(12):964–7.
37. Bouw R, Ederoth P, Lundberg J, Ungerstedt U, Nordström C-H, Hammarlund-Udenaes M. Increased blood-brain barrier permeability of morphine in a patient with severe brain lesions as determined by microdialysis Case report. *Acta Anaesthesiol Scand.* 2001;45(3):390–2.
38. Ederoth P, Tunblad K, Bouw R, Lundberg CJ, Ungerstedt U, Nordstrom CH, et al. Blood-brain barrier transport of morphine in patients with severe brain trauma. *Br J Clin Pharmacol.* 2003;57(4):427–35.
39. Beal S, Sheiner L, Boeckmann A, Bauer R. NONMEM User's Guides. Icon Development Solutions, Ellicott City. 2010.
40. R Core Team. R: A Language and Environment for Statistical Computing, R Foundation for Statistical Computing. 2013. Available from: <http://www.R-project.org/>.

41. Sheiner LB, Beal SL. Evaluation of methods for estimating population pharmacokinetics parameters. I. Michaelis-Menten model: routine clinical pharmacokinetic data. *J Pharmacokinet Biopharm.* 1980;8(6):553–71.
42. Hettiarachchi HDM, Hsu Y, Harris TJ, Penn R, Linninger AA. The effect of pulsatile flow on intrathecal drug delivery in the spinal canal. *Ann Biomed Eng.* 2011;39(10):2592–602.
43. Hladky SB, Barrand MA. Mechanisms of fluid movement into, through and out of the brain: evaluation of the evidence. *Fluids Barriers CNS.* 2014;11(26):1–32.
44. Skipor J, Thiery JC. The choroid plexus-cerebrospinal fluid system: Undervaluated pathway of neuroendocrine signaling into the brain. *Acta Neurobiol Exp.* 2008;68(3):414–28.
45. Kumar G, Smith QR, Hokari M, Parepally J, Duncan MW. Brain uptake, pharmacokinetics, and tissue distribution in the rat of neurotoxic N-butylbenzenesulfonamide. *Toxicol Sci.* 2007;97(2):253–64.
46. Strazielle N, Ghersi-Egea JF. Choroid plexus in the central nervous system: biology and physiopathology. *J Neuropathol Exp Neurol.* 2000;59(7):561–74.
47. Makridakis S. Accuracy concerns measures : theoretical and practical concerns. *Int J Forecast.* 1993;9:527–9.
48. Begley DJ, Bradbury MW, Kreuter J. *The Blood-Brain Barrier and Drug Delivery to the CNS.* New York: Marcel Dekker, Inc. 2000.
49. Condon P, Wyper D, Grant R, Patterson J, Hadley D, Teasdale G, et al. Use of magnetic resonance imaging to measure intracranial cerebrospinal fluid volume. *Lancet.* 1986;327(8494):1355–7.
50. Kohn MI, Tanna NK, Herman GT, Resnick SM, Mozley PD, Gur RE, et al. Analysis of brain and cerebrospinal fluid volumes with MR imaging. Part I. Methods, reliability, and validation. *Radiology.* 1991;178(1):115–22.
51. Dickey CC, Shenton ME, Hirayasu Y, Fischer I, Voglmaier MM, Niznikiewicz MA, et al. Large CSF volume not attributable to ventricular volume in schizotypal personality disorder. *Am J Psychiatry.* 2000;157(1):48–54.
52. Robertson EG. Developmental defects of the cisterna magna and dura mater. *J Neurol Neurosurg Psychiatry.* 1949;12(1):39–51.
53. Adam R, Greenberg JO. The mega cisterna magna. *J Neurosurg.* 1978;48(2):190–2.
54. Pardridge WM. Drug transport in brain via the cerebrospinal fluid. *Fluids Barriers CNS.* 2011;8(7):1–7.
55. Cserr H, Cooper D, Suri P, Patlak C. Efflux of radiolabeled polyethylene glycols and albumin from rat brain. *Am J Physiol.* 1981;240(4):319–28.
56. Thorne RG, Hrabe S, Nicholson C, Robert G. Diffusion of Epidermal Growth Factor in Rat Brain Extracellular Space Measured by Integrative Optical Imaging. *J Neurophysiol.* 2004;92(6):3471–81.
57. Levinger IM. The cerebral ventricles of the rat. *J Anat.* 1971;108(3):447–51.

58. Bass NH, Lundborg P. Postnatal development of bulk flow in the cerebrospinal fluid system of the albino rat: clearance of carboxyl-(14C)inulin after intrathecal infusion. *Brain Res.* 1973;52:323–32.
59. Mahat MYA, Ahamed NFA, Chandrasekaran S, Rajagopal S, Narayanan S, Surendran N. An improved method of transcutaneous cisterna magna puncture for cerebrospinal fluid sampling in rats. *J Neurosci Methods.* 2012;211(2):272–9.
60. Cserrl H. Potassium exchange between cerebrospinal fluid, plasma, and brain. *Am J Physiol.* 1965;209:1219–26.
61. Abbott NJ. Evidence for bulk flow of brain interstitial fluid: significance for physiology and pathology. *Neurochem Int.* 2004;45(4):545–52.
62. Schinkel AH. P-Glycoprotein, a gatekeeper in the blood–brain barrier. *Adv Drug Deliv Rev.* 1999;36(2–3):179–94.
63. Tsuji A, Tamai I. Blood-brain barrier function of P-glycoprotein. *Adv Drug Deliv Rev.* 1997;25(2–3):287–98.
64. Rao VV, Dahlheime JL, Bardgett ME, Snyder AZ, Finch RA, Sartorelli AC, et al. Choroid plexus epithelial expression of MDR1 P glycoprotein and multidrug resistance-associated protein contribute to the blood-cerebrospinal-fluid drug-permeability barrier. *Med Sci.* 1999;96(7):3900–5.
65. Cordon-Cardo C, O'Brien JP, Casals D, Rittman-Grauer L, Biedler JL, Melamed MR, et al. Multidrug-resistance gene (P-glycoprotein) is expressed by endothelial cells at blood-brain barrier sites. *Proc Natl Acad Sci U S A.* 1989;86(2):695–8.
66. Kassem NA, Deane R, Segal MB, Chen R, Preston JE. Thyroxine (T4) transfer from CSF to choroid plexus and ventricular brain regions in rabbit: contributory role of P-glycoprotein and organic anion transporting polypeptides. *Brain Res.* 2007;1181:44–50.
67. Chen H, Winiwarter S, Fridén M, Antonsson M, Engkvist O. In silico prediction of unbound brain-to-plasma concentration ratio using machine learning algorithms. *J Mol Graph Model.* 2011;29(8):985–95.
68. Loryan I, Sinha V, Mackie C, van Peer A, Drinkenburg WH, Vermeulen A, et al. Molecular properties determining unbound intracellular and extracellular brain exposure of CNS drug candidates. *Mol Pharm.* 2015;12(2):520–32.
69. Johnson M, Kozielska M, Reddy VP, Vermeulen A, Barton HA, Grimwood S, et al. Translational Modeling in Schizophrenia: Predicting Human Dopamine D2 Receptor Occupancy. *Pharm Res.* 2016;33(4):1003–17.
70. Li CH, Stratford RE, de Mendizabal NV, Cremers TI, Pollock BG, Mulsant BH, et al. Prediction of brain clozapine and norclozapine concentrations in humans from a scaled pharmacokinetic model for rat brain and plasma pharmacokinetics. *J Transl Med.* 2014;12(1):1–11.
71. Melhem M. Perspectives in Pharmacology Translation of Central Nervous System Occupancy from Animal Models : Application of Pharmacokinetic / Pharmacodynamic Modeling. *J Pharmacol Exp Ther.* 2013;347:2–6.

72. Stevens J, Ploeger BA, Hammarlund-Udenaes M, Osswald G, van Der Graaf PH, Danhof M, et al. Mechanism-based PK-PD model for the prolactin biological system response following an acute dopamine inhibition challenge: Quantitative extrapolation to humans. *J Pharmacokinet Pharmacodyn.* 2012;39(5):463–77.
73. Lu Y, Barton HA, Leung L, Zhang L, Hajos-Korcsok E, Nolan CE, et al. Cerebrospinal fluid β -amyloid turnover in the mouse, dog, monkey and human evaluated by systematic quantitative analyses. *Neurodegener Dis.* 2013;12(1):36–50.
74. Beaumont A, Marmarou A, Hayasaki K, Barzo P, Fatouros P, Corwin F, et al. The Permissive Nature of Blood Brain Barrier (BBB) Opening in Edema Formation Following Traumatic Brain Injury. *Acta Neurochir Suppl.* 2000;76:125–9.
75. Başkaya MK, Rao AM, Doğan A, Donaldson D, Dempsey RJ. The biphasic opening of the blood-brain barrier in the cortex and hippocampus after traumatic brain injury in rats. *Neurosci Lett.* 1997;226(1):33–6.
76. Stain F, Barjavel MJ, Sandouk P, Plotkine M, Scherrmann J-M, Bhargava HN. Analgesic Response and Plasma and Brain Extracellular Pharmacokinetics of Morphine and Morphine-6-f3-D-Glucuronide in the Rat Fluid of opiates effects. *J Pharmacol Exp Ther.* 1995;274(2):852–7.

SUPPLEMENTARY FIGURES

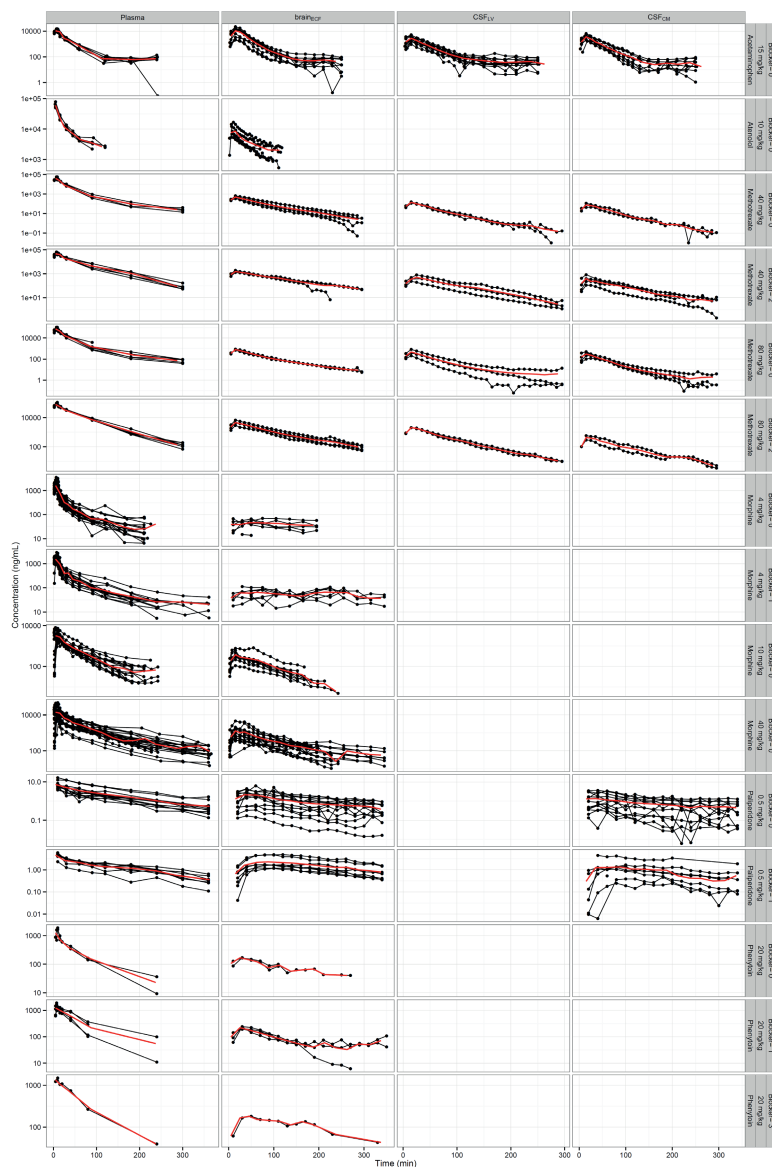


Figure S1. Model prediction (solid lines) versus observation (lines and circles) of the 9 compounds in rat for each dose and without and with co-administration of active transport blockers. The x-axis represents the time in minutes and the y-axis represents the concentration of the 9 compounds in ng/ml. The panel is stratified by brain compartments and by active transport blockers (colors).

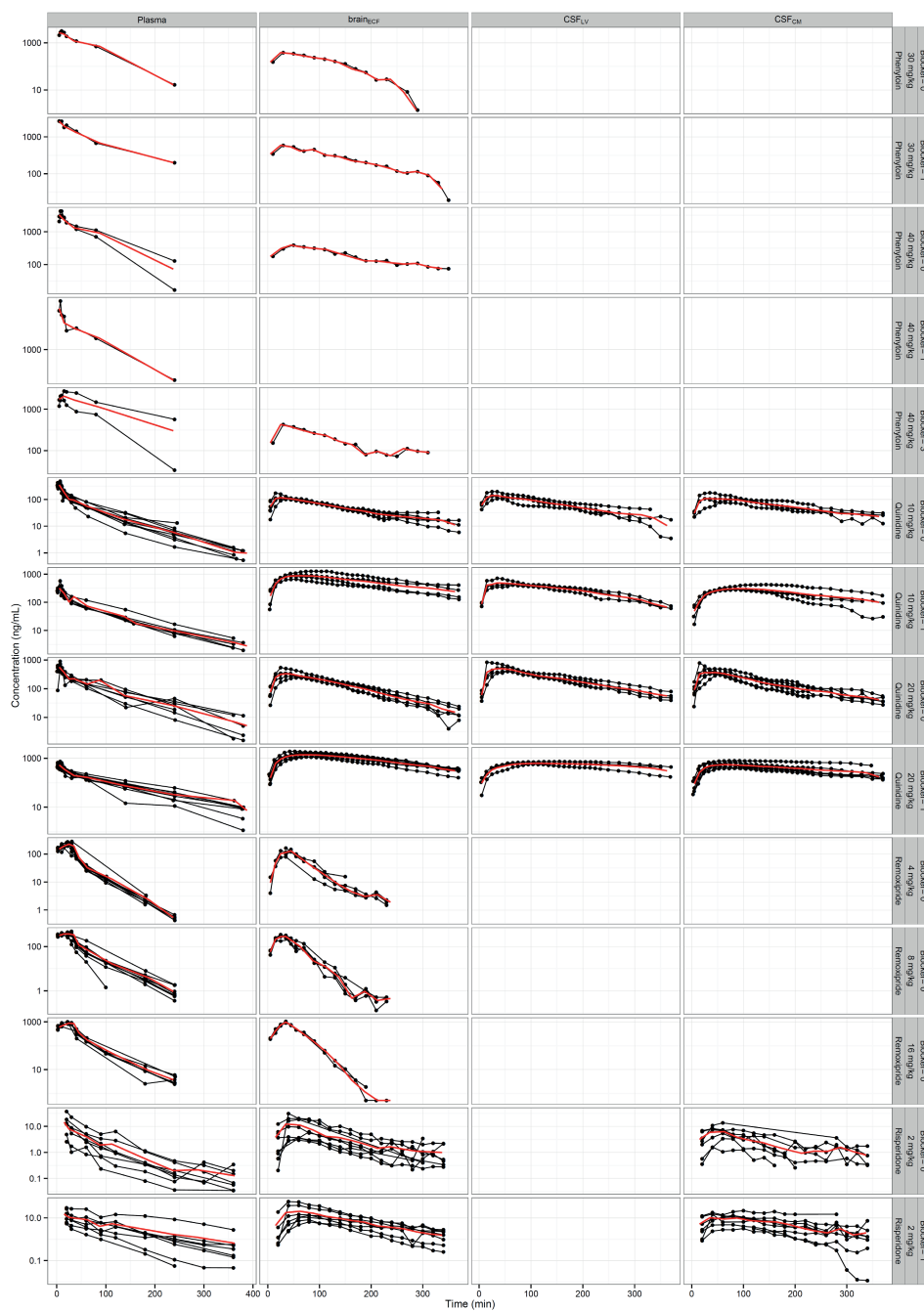


Figure S1. (continued)

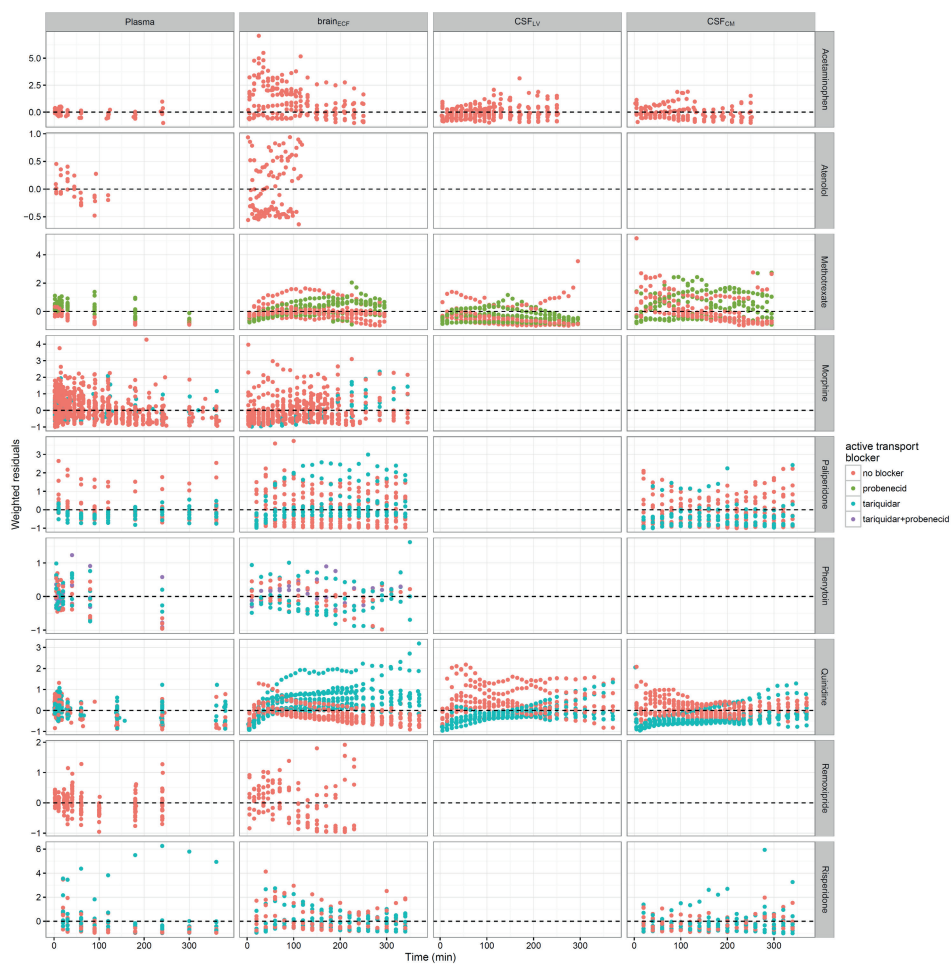


Figure S2. Weighted residuals versus time of the 9 compounds in rat. The x-axis represents the time in minutes and the y-axis represents the weighted residuals of the 9 compounds. The panel is stratified by brain compartments and by active transport blockers (colors).

SUPPLEMENTARY TABLES

Table S1. Physicochemical properties of the 9 compounds

	Molecular weight	PSA	log P	log D (pH 7.4)	No. of H donors	No. of H acceptors	pKa (Acid)	pKa (Base)
Acetaminophen	151	49	0.5	0.5	2	2	9.5	-4.4
Atenolol	266	85	0.2	-1.7	3	4	14.1	9.7
Methotrexate	454	211	-1.9	-2.5	5	12	3.4	2.8
Morphine	285	53	0.9	-0.4	2	4	10.3	9.1
Paliperidone	426	82	1.8	2.1	1	5	13.7	8.8
Phenytoin	252	58	2.47	2.5	2	2	9.47	-9
Quinidine	324	46	3.4	2.0	1	4	13.9	9.1
Remoxipride	371	51	2.1	0.7	1	4	13.1	8.4
Risperidone	410	62	2.5	2	0	4		8.8

from DrugBank (<http://www.drugbank.ca/>)

Table SII. Summary of the *in vivo* experimental setting in rat data

	Model development											External validation		
	Published data					Newly produced data						Published data	Newly produced data	
	Acetaminophen	Atenolol	Methotrexate	Morphine	Morphine	Morphine	Quinidine	Remoxipride	Paliperidone	Phenytoin	Risperidone	Acetaminophen	Remoxipride	
Study design														
plasma sampling points	-5, 2, 7, 10, 15, 30, 60, 120, 180, 240 min	0, 5, 15, 30, 45, 60, 90, 120 min	-5, 2, 7, 9, 10, 12, 17, 30, 90, 180, 300 min	15 samples up to 360 min	0, 8, 20, 70, 130, 190 min	-5, 2, 7, 10, 12, 17, 30, 60, 140, 240, 360 min	-5, 5, 10, 20, 35, 60, 90, 120, 150, 240 min	-15, 10/20, 30, 60, 90, 120, 180, 240, 300, 360 min	10 samples up to 480 min	10 samples up to 480 min	-15, 10/20, 30, 60, 90, 120, 180, 240, 300, 360 min	0, 5, 10, 20, 35, 60, 90, 120, 150, 180 min	0, 2, 7, 10, 16, 22, 40, 150 and 240 min	
dialysate sampling points	every 10 min up to 120 min, every 20 min from 120 to 240 min	up to 120 min	every 10 min up to 300 min	25 and 30 dialysate samples up to 360 min	every 5 min during infusion, 10 min from 10 to 60 min, every 20 min from 60 to 180 min	every 10 min up to 240 min, every 20 min from 240 to 360 min	every 10 min up to 120 min, every 20 min from 120 to 240 min	every 20 min up to 240 min	every 10 min up to 480 min	every 20 min up to 240 min	every 10 min up to 60 min, every 20 min from 60 to 180 min	every 20 min up to 240 min		
DEC approval number	07068	02112	10094	03008	n.a. (from literature)	07142	06132	12049	11092	12049	06023	13186		
Microdialysis setting														
probe material	A	B	C	D	n.a. (from literature)	C	A	C	C	C	A	C		
probe supplier	E	F	E	E	E	E	E	E	E	E	E	E		
PF	G	H	G	H	H	G	H	H	H	H	H	H		
flow rate	2 μ L/min	7 μ L/min	2 μ L/min	2 μ L/min	2 μ L/min	2 μ L/min	2 μ L/min	1 μ L/min	2 μ L/min	1 μ L/min	2 μ L/min	1 μ L/min		

Table SII. (continued)

	Model development										External validation	
	Published data					Newly produced data					Published data	Newly produced data
	Acetaminophen	Atenolol	Methotrexate	Morphine	Morphine	Quinidine	Remoxipride	Paliperidone	Phenytoin	Risperidone	Acetaminophen	Remoxipride
f_p (%)	81%	91%	45%	83%	83%	14%	74%	8%	9%	7%	81%	74%
<i>in vivo</i> recovery (loss %)	Brain _{ECF} : 12.0 % CSF _{UV} : 8.10% CSF _{CM} : 8.60 %	Brain _{ECF} : 13.0 %	Without probenecid: Brain _{ECF} : 22.1 % F _{UV} : 28.1% CSF _{CM} : 35.9 % With probenecid: Brain _{ECF} : 7.10 % F _{UV} : 16.9% CSF _{CM} : 21.6 %	Brain _{ECF} (4mg/kg): 16.1 % Brain _{ECF} (40mg/kg): 20.3 %	Plasma: 40.9 % Brain _{ECF} : 8.40 %	Brain _{ECF} : 9.10 % CSF _{UV} : 2.90% CSF _{CM} : 3.50 %	Brain _{ECF} : 18.0 % CSF _{CM} : 10.0 %	Brain _{ECF} : 18.0 % CSF _{CM} : 10.0 %	Brain _{ECF} : 35.0 %	Brain _{ECF} : 22.0 % CSF _{CM} : 10.0 %	Brain _{ECF} : 12.0 % CSF _{UV} : 8.10% CSF _{CM} : 8.60 %	Brain _{ECF} : 11.0 % CSF _{UV} : 7.00 % CSF _{CM} : 5.00 %
<i>in-vivo</i> recovery references	(23)	(26)	(25)	(27)	(28)	(24)	(72)				(30)	(32)
f_p references	(23)	(31)	(25)	(76)	(76)	(24)	(32)		(31)		(30)	(32)

A: Polycarbonate, B: Cellulose acetate, C: Polyarylethersulphone (PAES), D: polycarbonate-poly-ether (PC-PE) co-polymeric membrane, E: CMA Microdialysis AB, Kista, Sweden, F: Home made, G: 140.3 mM sodium, 2.7 nM potassium, 1.2 mM calcium, 1.0 mM magnesium and 147.7 mM chloride, H: NaCl 145 mM, KCl 0.6 mM, MgCl₂ 1.0 mM, CaCl₂ 1.2 mM and ascorbic acid 0.2 mM in 2 mM phosphate buffer (pH 7.4)
PF: microdialysis perfusion fluid, f_p : free fraction in plasma

Table SIII. Demographic data of the patients in the acetaminophen study (study 1)

Patient	1	2	3	4	5	6	7
Gender	M	F	F	F	F	M	F
age (year)	51	49	76	62	54	79	42
height (cm)	178	170	160	155	160	175	168
weight (kg)	64	65	56.5	70	56	74	57
number of doses before inclusion	43	22	14	29	5	18	25
reason of admission	SAH	SAH	SAH	SAH	SAH	SAH	SAH

SAH; subarachnoid hemorrhage
M: male, F: female

Table SIV. Acetaminophen EVD experimental data

Patient 1		
	EVD volume	flow
	(mL)	(mL/h)
baseline	4	4
0-0.5h	4	8
0.5-1h	4	8
1h-1.5h	5	10
1.5-2h	8.5	17
2-2.5h	1.5	3
2.5-3h	4	8
3-3.5h	3.5	7
3.5-4h	7	7
4-5h	2	2
5-6h	13	13
6-7h	3	3
7-8h	7	7

Patient 2		
	EVD volume	flow
	(mL)	(mL/h)
baseline	18	9
0-0.5h	6.5	13
0.5-1h	5	10
1h-1.5h	5	10
1.5-2h	3	6
2-3h	12	24
3-0-4h	15	30
4-5h	10	10
5-6h	15	15
6-7h	10	10
7-8h	6	6

Patient 3		
	EVD volume	flow
	(mL)	(mL/h)
baseline	17	17
0-1h	8	8
1-2h	13	13
2-3h	4	4
3-4h	12	12
4-5h	6	6
5-6h	15	15

Patient 4		
	EVD volume	flow
	(mL)	(mL/h)
baseline	14.5	14.5
0-1h	12	nd
1h-1.5	4	8
1.5-2h	6.5	13
2-2.5h	1.6	3.2
2.5-3h	6.5	13
3-4h	19	19
4-5h	16.5	16.5
5-6h	16	16

Patient 5		
	EVD volume	flow
	(mL)	(mL/h)
baseline	21	21
0-1h	11	nd
1h-1.5	5	10
1.5-2h	5	10
2-2.5h	5.5	11
2.5-3h	8	16
3-4h	14	14
4-5h	14	14
5-6h	7	7

Patient 6		
	EVD volume	flow
	(mL)	(mL/h)
baseline	9	9
0-1h	5.5	nd
1h-1.5	6	12
1.5-2h	0.75	1.5
2-2.5h	4.5	9
2.5-3h	3	6
3-4h	7.5	7.5
4-5h	8	8
5-6h	12	12

Patient 7		
	EVD volume	flow
	(mL)	(mL/h)
baseline	12	12
0-1h	4.75	nd
1h-1.5	4.6	9.2
1.5-2h	0.75	1.5
2-2.5h	2.75	5.5
2.5-3h	5.5	11
3-4h	17	17
4-5h	13	13
5-6h	14	14



Predicting drug concentration-time profiles in multiple CNS compartments using a comprehensive physiologically based pharmacokinetic model

Y Yamamoto, P A Väitalo, D R Huntjens, J H Proost, A Vermeulen,
W Krauwinkel, M W Beukers, D-J van den Berg, R Hartman, Y
C Wong, M Danhof, J G C van Hasselt, E C M de Lange

Accepted for publication in CPT: Pharmacometrics & Systems Pharmacology

ABSTRACT

Drug development targeting the central nervous system (CNS) is challenging due to poor predictability of drug concentrations in various CNS compartments. We developed a generic physiologically based pharmacokinetic (PBPK) model for prediction of drug concentrations in physiologically relevant CNS compartments. System-specific and drug-specific model parameters were derived from literature and *in silico* predictions. The model was validated using detailed concentration-time profiles from 10 drugs in rat plasma, brain extracellular fluid, two cerebrospinal fluid sites, and total brain tissue. These drugs, all small molecules, were selected to cover a wide range of physicochemical properties. The concentration-time profiles for these drugs were adequately predicted across the CNS compartments (symmetric mean absolute percentage error for the model prediction was < 91%).

In conclusion, the developed PBPK model can be used to predict temporal concentration profiles of drugs in multiple relevant CNS compartments, which we consider valuable information for efficient CNS drug development.

INTRODUCTION

The development of drugs targeting diseases of the central nervous system (CNS) represents one of the most significant challenges in the research of new medicines (1). Characterization of exposure-response relationships at the drug target-site may be of critical importance to reduce attrition. However, unlike for many other drugs, prediction of target-site concentrations for CNS drugs is complex, among other factors, due to the presence of the blood-brain barrier (BBB) and the blood-cerebrospinal fluid barrier (BCSFB). Moreover, direct measurement of human brain concentrations is highly restricted for ethical reasons. Therefore, new approaches that can robustly predict human brain concentrations of novel drug candidates based on *in vitro* and *in silico* studies are of great importance.

Several pharmacokinetic (PK) models to predict CNS exposure have been published with different levels of complexity (2). The majority of these models depends on animal data. Furthermore, these models have typically not been validated against human CNS drug concentrations (2). We previously published a general multi-compartmental CNS PK model structure, which was developed using PK data obtained from rats (3).

Quantitative structure-property relationship (QSPR) models can be used to predict drug BBB permeability and $K_{p,uu,brain_{ECF}}$ (unbound brain extracellular fluid-to-plasma concentration ratio) (4–6) without performing novel experiments, but these QSPR models have not taken into account the time course of CNS distribution. Therefore, there exists an unmet need for approaches to predict drug target-site concentration-time profiles without the need of *in vivo* animal experiments.

Physiologically based pharmacokinetic (PBPK) modelling represents a promising approach for the prediction of CNS drug concentrations. Previously such models have been widely used to predict tissue concentrations (7). PBPK models typically distinguish between drug-specific and system-specific parameters, therefore enabling predictions across drugs and species. However, PBPK models for the CNS have been of limited utility due to a lack of relevant physiological details for mechanism of transport across the BBB and BCSFB, and for drug distribution within the CNS (2).

Capturing the physiological compartments, flows and transport processes in a CNS PBPK model is critically important to predict PK profiles in the CNS. The CNS comprises of multiple key physiological compartments (2), including brain extracellular fluid ($brain_{ECF}$), brain intracellular fluid ($brain_{ICF}$), and multiple cerebrospinal fluid (CSF) compartments. The $brain_{ECF}$ and $brain_{ICF}$ compartments are considered highly relevant target-sites for

CNS drugs, while CSF compartments are often used to measure CNS-associated drug concentrations, if $\text{brain}_{\text{ECF}}$ and $\text{brain}_{\text{ICF}}$ information cannot be obtained. Furthermore, cerebral blood flow (CBF) and physiological flows within the CNS, such as the $\text{brain}_{\text{ECF}}$ flow and CSF flows, influence drug distribution across CNS compartments. Next to binding to protein and lipids, pH-dependent distribution in subcellular compartments such as trapping of basic compounds in lysosomes needs to be considered. With regard to the transfer processes across the BBB and BCSFB, passive diffusion via the paracellular and transcellular pathways, and active transport by influx and/or efflux transporters need to be addressed.

At both BBB and BCSFB barriers, the cells are interconnected by tight junctions, which limit drug exchange via the paracellular pathway (8). Paracellular and transcellular diffusion depend on the aqueous diffusivity coefficient and membrane permeability of the compound, which can be related to the physicochemical properties. The combination of these transport routes may differ between individual drugs, which complicates the prediction of plasma-brain transport.

System-specific information on physiological parameters can be used in scaling between species. Many of these system-specific parameters can or have been obtained from *in vitro* and *in vivo* experiments. Drug-specific parameters can be derived by *in vitro* and QSPR approaches, and can be used for the scaling between drugs. A comprehensive CNS PBPK model can integrate system- and drug-specific parameters to potentially enable the prediction of the brain distribution of drugs, without the need to conduct *in vivo* animal studies.

The purpose of the current work is to develop a comprehensive PBPK model to predict drug concentration-time profiles in the multiple physiologically relevant compartments in the CNS, based on system-specific and drug-specific parameters without the need to generate *in vivo* data. We specifically consider the prediction of PK profiles in the CNS during pathological conditions, which may have distinct effects on paracellular diffusion, transcellular diffusion and active transport. Therefore, we include a range of such transport mechanisms in our CNS PBPK model. This model is evaluated using previously published detailed multilevel brain and CSF concentration-time data for 10 drugs with highly diverse physicochemical properties.

MATERIALS AND METHODS

We first empirically modelled plasma PK using available plasma PK data, which was used as the basis for the CNS PBPK model. This CNS model was based entirely on parameters derived from literature and *in silico* predictions. Model development was performed using NONMEM version 7.3.

Empirical plasma PK model

Plasma PK models were systematically developed using *in vivo* data with a mixed-effects modeling approach. One-, two- and three-compartment models were evaluated. Inter-individual variability and inter-study variability were incorporated on each PK parameter using exponential models. Proportional and combined additive-proportional residual error models were considered. Model selection was guided by the likelihood ratio test ($p < 0.05$), precision of the parameter estimates, and standard goodness of fit plots (9).

CNS PBPK model development

A generic PBPK model structure was developed based on the previously published generic multi-compartmental CNS distribution model (**Figure 1**) (3), which consists of plasma, brain_{ECF}, brain_{ICF}, CSF in the lateral ventricle (CSF_{LV}), CSF in the third and fourth ventricle (CSF_{TFV}), CSF in the cisterna magna (CSF_{CM}) and CSF in the subarachnoid space (CSF_{SAS}) compartments. We added new components; (1) an acidic subcellular compartment representing lysosomes to account for pH-dependent drug distribution, (2) a brain microvascular compartment (brain_{MV}) to account for CBF *versus* permeability rate-limited kinetics, and (3) separation of passive diffusion at the BBB and BCSFB into its transcellular and paracellular components.

System-specific parameters

Physiological values of the distribution volumes of all the CNS compartments, flows, surface area (SA) of the BBB (SA_{BBB}), SA of the BCSFB (SA_{BCSFB}), SA of the total brain cell membrane (BCM) (SA_{BCM}) and the width of BBB (Width_{BBB}) were collected from literature. SA_{BCSFB} was divided into SA_{BCSFB1}, which is a surface area around CSF_{LV} and SA_{BCSFB2}, which is a surface area around CSF_{TFV}. The lysosomal volume was calculated based on the volume ratio of lysosomes to brain intracellular fluid of brain parenchyma cells (1:80) (10), and SA of the lysosomes (SA_{LYSO}) is calculated by obtaining lysosome number per cell using the lysosomal volume and the diameter of each lysosome (11). Transcellular and paracellular diffusion were separately incorporated into the models, therefore the ratio of SA_{BBB} and SA_{BCSFB} for transcellular diffusion and paracellular diffusion were required for the calculation. Based on electron microscopic cross-section pictures of

brain capillary, the length of a single brain microvascular endothelial cell was estimated to be around 17 μm and the length of the intercellular space was estimated to be around 0.03 μm (12). The presence of tight junctions in the intercellular space of the BBB and BCSFB significantly reduces paracellular transport (8). Therefore, correcting for the effective pore size for paracellular diffusion is important. The transendothelial electrical resistance (TEER) is reported to be around 1800 $\Omega\text{ cm}^2$ at the rat BBB (13), whereas the TEER is around 20-30 $\Omega\text{ cm}^2$ at the rat BCSFB (14). According to a study on the relationship between TEER and the pore size (15), the pore size at the BBB and BCSFB can be assumed to be around 0.0011 μm and 0.0028 μm , respectively. Thus, it was expected that 99.8% of total SA_{BBB} and 99.8% of total SA_{BCSFB} is used for the transcellular diffusion (SA_{BBBt} and SA_{BCSFBt} respectively), whereas 0.006% of total SA_{BBB} and 0.016% of total SA_{BCSFB} are used for paracellular diffusion (SA_{BBBp} and SA_{BCSFBp} respectively). Note that, due to the presence of tight junction proteins, not all intercellular space can be used for paracellular diffusion.

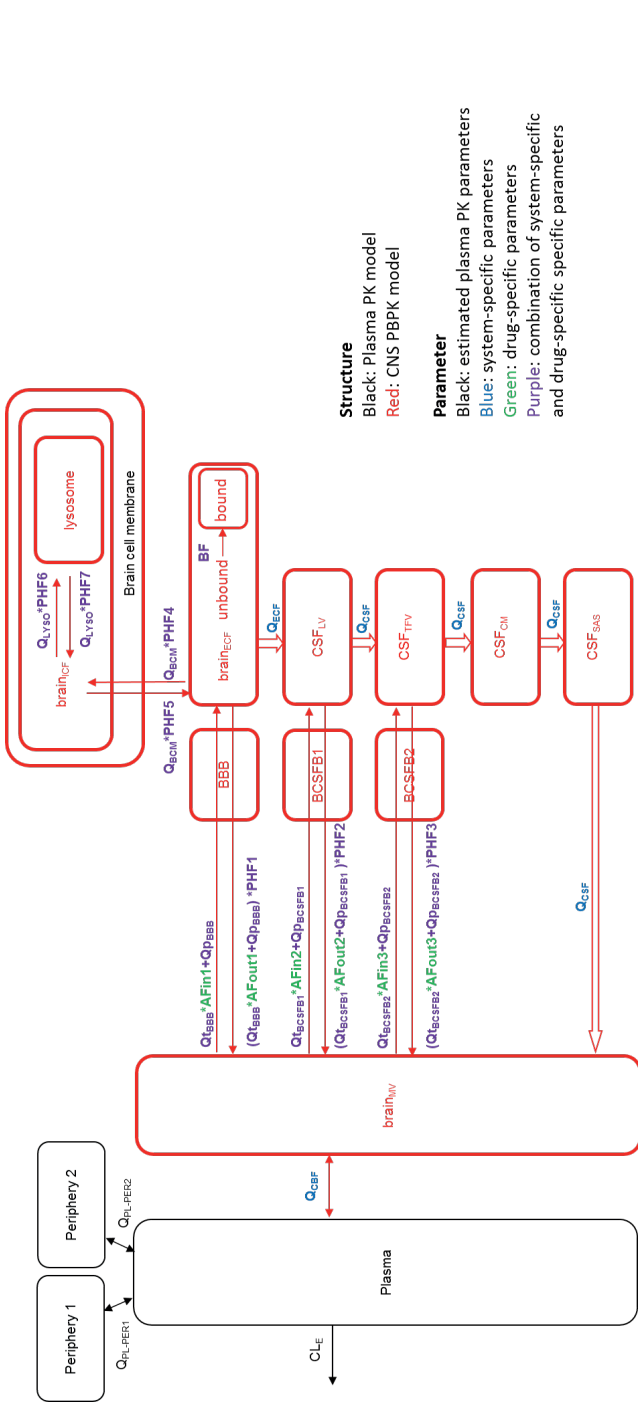


Figure 1. The developed model structure.

The model consists of a plasma PK model and a CNS PBPK model with estimated plasma PK parameters, and system-specific and drug-specific parameters (colors) for CNS. Peripheral compartment 1 and 2 were used in cases where the plasma PK model required them to describe the plasma data adequately. Brain_{IV}: brain intravascular, BBB: blood-brain barrier, BCSFB: blood-CSF barrier, brain_{ICF}: brain extra cellular fluid, brain_{ICF}: brain intra cellular fluid, CSF_{LV}: CSF in the lateral ventricle, CSF_{TIV}: transcellular diffusion clearance at the BBB, Qp_{BBB}: paracellular diffusion CSF_{SAS}: CSF in the subarachnoid space, Q_{GBF}: cerebral blood flow, Q_{TBBB}: transcellular diffusion clearance at the BBB, Qp_{BBB}: paracellular diffusion clearance at the BBB, Q_{TBCSFB1}: transcellular diffusion clearance at the BCSFB1, Qp_{BCSFB1}: paracellular diffusion clearance at the BCSFB1, Q_{TBCSFB2}: transcellular diffusion clearance at the BCSFB2, Qp_{BCSFB2}: paracellular diffusion clearance at the BCSFB2, Q_{BCM}: passive diffusion clearance at the brain cell membrane, Q_{LYSO}: passive diffusion clearance at the lysosomal membrane, Q_{ECF}: brain_{ECF} flow, Q_{CSF}: CSF flow, AFin 1-3: asymmetry factor into the CNS compartments 1-3, AFout1-3: asymmetry factor out of the CNS compartments 1-3, PHF1-7: pH-dependent factor 1-7, BF: binding factor.

Drug-specific parameters

Aqueous diffusivity coefficient. The aqueous diffusivity coefficient was calculated using the molecular weight of each compound with the following equation (16).

$$\log Daq = -4.113 - 0.4609 \times \log MW \quad (1)$$

where Daq is the aqueous diffusivity coefficient (in cm^2/s) and MW is the molecular weight (in g/mol).

Permeability. Transmembrane permeability was calculated using the $\log P$ of each compound with the following equation (17).

$$\log P_0^{\text{transcellular}} = 0.939 \times \log P - 6.210 \quad (2)$$

where $P_0^{\text{transcellular}}$ is the transmembrane permeability (in cm/s), $\log P$ is the *n*-octanol lipophilicity value.

Active transport. The impact of the net effect of active transporters on the drug exchange at the BBB and BCSFB was incorporated into the model using asymmetry factors (AFin1-3 and AFout1-3). The AFs were calculated from $K_{p,uu,brain_{ECP}}$, $K_{p,uu,CSF_{LV}}$ (unbound CSF_{LV} -to-plasma concentration ratio) and $K_{p,uu,CSF_{CM}}$ (unbound CSF_{CM} -to-plasma concentration ratio), such that they produced the same $K_{p,uu}$ values within the PBPK model at the steady state. The AFs were therefore dependent on both the $K_{p,uu}$ values and the structure and parameters of the PBPK model. If the $K_{p,uu}$ values were larger than 1 (i.e. net active influx), then AFin1, AFin2 and AFin3 were derived from $K_{p,uu,brain_{ECP}}$, $K_{p,uu,CSF_{LV}}$ and $K_{p,uu,CSF_{CM}}$, respectively, while AFout1-3 were fixed to 1. If the $K_{p,uu}$ values were smaller than 1 (i.e. net active efflux), then AFout1, AFout2 and AFout3 were derived from $K_{p,uu,brain_{ECP}}$, $K_{p,uu,CSF_{LV}}$ and $K_{p,uu,CSF_{CM}}$, respectively, while AFin1-3 were fixed to 1. In the analysis, $K_{p,uu,brain_{ECP}}$, $K_{p,uu,CSF_{LV}}$ and $K_{p,uu,CSF_{CM}}$ were derived from previous *in vivo* animal experiments (3). The steady state differential equations in the PBPK model were solved using the Maxima Computer Algebra System (<http://maxima.sourceforge.net>) to obtain algebraic solutions for calculating AFs from the $K_{p,uu}$ values. The detailed algebraic solutions for each AF are provided in **Supplementary Material S1**.

Combined system-specific and drug-specific parameters

Passive diffusion across the brain barriers. Passive diffusion clearance at the BBB and BCSFB (Q_{BBB} and Q_{BCSFB} , respectively) was obtained from a combination of paracellular and transcellular diffusion, Qp and Qt , respectively (Eq.3).

$$Q_{BBB/BCSFB}(mL/min) = Qp_{BBB/BCSFB} + Qt_{BBB/BCSFB} \quad (3)$$

where $Q_{BBB/BCSFB}$ represents the passive diffusion clearance at the BBB/BCSFB, $Qp_{BBB/BCSFB}$ represents the paracellular diffusion clearance at the BBB/BCSFB, and $Qt_{BBB/BCSFB}$ represents the transcellular diffusion clearance at the BBB/BCSFB.

The paracellular diffusion clearance was calculated with the aqueous diffusivity coefficient (Daq), $Width_{BBB/BCSFB}$ and SA_{BBBp} or SA_{BCSFBp} using equation 4.

$$Qp_{BBB/BCSFB}(mL/min) = \frac{Daq}{Width_{BBB/BCSFB}} \times SA_{BBBp/BCSFBp} \quad (4)$$

The transcellular diffusion clearance was calculated with the transmembrane permeability and SA_{BBBt} or SA_{BCSFBt} using equation 5.

$$Qt_{BBB/BCSFB}(mL/min) = \frac{1}{2} * P_0^{transcellular} \times SA_{BBBt/BCSFBt} \quad (5)$$

where the factor 1/2 is the correction factor for passage over two membranes instead of one membrane in transcellular passage.

Active transport across the brain barriers. To take into account the net effect of the active transporters at the BBB and BCSFB, AFs were added on $Qt_{BBB/BCSFB}$ (Eq.6 and 7).

$$Q_{BBB/BCSFB_in}(mL/min) = Qp_{BBB/BCSFB} + Qt_{BBB/BCSFB} * AF_{in} \quad (6)$$

$$Q_{BBB/BCSFB_out_withoutPHF}(mL/min) = Qp_{BBB/BCSFB} + Qt_{BBB/BCSFB} * AF_{out} \quad (7)$$

where $Q_{BBB/BCSFB_in}$ represents the drug transport clearance from brain_{MV} to brain_{ECF}/CSFs, and $Q_{BBB/BCSFB_out_withoutPHF}$ represents the drug transport clearance from brain_{ECF}/CSFs to brain_{MV} without taking into account the pH-dependent kinetics (to be taken into account separately; see below).

Cellular and subcellular distribution. Passive diffusion at the BCM (Q_{BCM}) and at the lysosomal membrane (Q_{LYSO}) was described with the transmembrane permeability together with SA_{BCM} or SA_{LYSO} , respectively (Eq.8 and 9).

$$Q_{BCM}(mL/min) = P_0^{transcellular} \times SA_{BCM} \quad (8)$$

$$Q_{LYSO}(mL/min) = P_0^{transcellular} \times SA_{LYSO} \quad (9)$$

where Q_{BCM} represents the passive diffusion clearance at the BCM, and Q_{LYSO} represents the passive diffusion clearance at the lysosomal membrane.

pH-dependent partitioning. We considered the differences in pH in plasma (pH 7.4) and in relevant CNS compartments, namely brain_{ECF} (pH_{ECF} 7.3), CSF (pH_{CSF} 7.3), brain_{ICF} (pH_{ICF} 7.0), and lysosomes (pH_{LYSO} 5.0) (18). The impact of pH differences on the passive diffusion clearance from brain_{ECF} to brain_{MV} (PHF1), from CSF_{LV} to brain_{MV} (PHF2), from CSF_{TFV} to brain_{MV} (PHF3), from brain_{ECF} to brain_{ICF} (PHF4), from brain_{ICF} to brain_{ECF} (PHF5), from brain_{ICF} to lysosomes (PHF6), and from lysosomes to brain_{ICF} (PHF7) were described by pH-dependent factors, which were defined as the ratio of the un-ionized fraction of each compound at the pH in a particular compartment and the un-ionized fraction in plasma. The PHFs were calculated from the pKa of each compound and the pH of a particular compartment. The equations are developed using the classical Henderson-Hasselbalch equation(19,20), and are based on the assumption that there is no active transport.

$$PHF_{base1} = PHF_{base4} = \frac{10^{pKa-7.4+1}}{10^{pKa-pH_{ECF}+1}} \quad (10)$$

$$PHF_{base2} = PHF_{base3} = \frac{10^{pKa-7.4+1}}{10^{pKa-pH_{CSF}+1}} \quad (11)$$

$$PHF_{base5} = PHF_{base6} = \frac{10^{pKa-7.4+1}}{10^{pKa-pH_{ICF}+1}} \quad (12)$$

$$PHF_{base7} = \frac{10^{pKa-7.4+1}}{10^{pKa-pH_{LYSO}+1}} \quad (13)$$

$$PHF_{acid1} = PHF_{acid4} = \frac{10^{7.4-pKa+1}}{10^{pH_{ECF}-pKa+1}} \quad (14)$$

$$PHF_{acid2} = PHF_{acid3} = \frac{10^{7.4-pKa+1}}{10^{pH_{CSF}-pKa+1}} \quad (15)$$

$$PHF_{acid5} = PHF_{acid6} = \frac{10^{7.4-pKa+1}}{10^{pH_{ICF}-pKa+1}} \quad (16)$$

$$PHF_{acid7} = \frac{10^{7.4-pKa+1}}{10^{pH_{LYSO}-pKa+1}} \quad (17)$$

where $PHF_{base\ 1-7}$ are PHF1-7 for basic compounds, $PHF_{acid\ 1-7}$ are PHF1-7 for acidic compounds, and 7.4 is the pH in the plasma compartment.

The impact of pH differences on the drug distribution among $brain_{ECF}$, CSF, $brain_{ICF}$ and lysosomes was added on Q_{BCM} and Q_{LYSO} using PHFs with the following equations 18-24, based on the assumption that the transport clearance is proportional to the un-ionized fraction of each compound.

$$Q_{BBB_out}(mL/min) = Q_{BBB_out_withoutPHF} \times PHF1 \quad (18)$$

$$Q_{BCSFB1_out}(mL/min) = Q_{BCSFB_withoutPHF} \times PHF2 \quad (19)$$

$$Q_{BCSFB2_out}(mL/min) = Q_{BCSFB_withoutPHF} \times PHF3 \quad (20)$$

$$Q_{BCM_in}(mL/min) = Q_{BCM} \times PHF4 \quad (21)$$

$$Q_{BCM_out}(mL/min) = Q_{BCM} \times PHF5 \quad (22)$$

$$Q_{LYSO_in}(mL/min) = Q_{LYSO} \times PHF6 \quad (23)$$

$$Q_{LYSO_out}(mL/min) = Q_{LYSO} \times PHF7 \quad (24)$$

where Q_{BBB_out} represents the drug transport clearance from $brain_{ECF}$ to $brain_{MV}$, Q_{BCSFB1_out} represents the drug transport clearance from CSF_{LV} to $brain_{MV}$, Q_{BCSFB2_out} represents the drug transport clearance from CSF_{TFV} to $brain_{MV}$, Q_{BCM_in} represents the drug transport clearance from $brain_{ECF}$ to $brain_{ICF}$, and Q_{BCM_out} represents the drug transport clearance from $brain_{ICF}$ to $brain_{ECF}$, Q_{LYSO_in} represents the drug transport clearance from $brain_{ICF}$ to lysosomes, and Q_{BCM_out} represents the drug transport clearance from lysosomes to $brain_{ICF}$.

Drug binding. Drug binding to brain tissue components was taken into account in the model using a binding factor (BF) under the assumption that drug binding to the tissue happens instantly. The BF was calculated from Kp (total brain-to-plasma concentration

ratio) by solving the BF that results in the same K_p value in the model, using the Maxima program as described above (**Supplementary Material S1**). The K_p for each compound was calculated using the compounds' log P , the composition of brain tissue and plasma, $f_{u,p}$ (free fraction in plasma) and $f_{u,b}$ (free fraction in brain) with the following equation (21).

$$K_p = \frac{[10^{\log P} \times (V_{nlb} + 0.3 \times V_{phb}) + 0.7 \times V_{phb} + V_{wb} / f_{u,b}]}{[10^{\log P} \times (V_{nlp} + 0.3 \times V_{php})] + 0.7 \times V_{php} + V_{wp} / f_{u,p}} \quad (25)$$

where V_{nlb} , V_{phb} , V_{wb} , V_{nlp} , V_{php} , and V_{wp} represent the rat volume fractions of brain neutral lipids (0.0392), brain phospholipids (0.0533), brain water (0.788), plasma neutral lipids (0.00147), plasma phospholipids (0.00083), and plasma water (0.96), respectively (22).

***In vivo* data collection for model evaluation**

In vivo data obtained from multiple brain locations were used to evaluate the developed model (3,23–30). An overview of experimental design and data for 10 compounds with substantially different physicochemical characteristics is provided in **Table I**. All data were previously published, except the remoxipride total brain tissue data. General animal surgery procedure, experimental protocol and bioanalytical methods for remoxipride total brain tissue data are described in **Supplementary Material S2**, and experimental protocol details for each drug are summarized in **Supplementary Table SI**.

Table I. Summary of rat multilevel brain and CSFs data for model evaluation

Study design	Acetaminophen	Atenolol	Methotrexate	Morphine	Morphine	Paliperidone	Phenytoin	Quinidine	Raclopride	Remoxipride	Remoxipride	Risperidone
Nr of animals	16	5	23	65	18	21	14	41	19	29	65	16
Dosage, mg/kg (infusion time, min)	15 (10)	10 (1)	40, 80 (10)	4, 10, 40 (10)	10, 40 (10)	0.5 (20)	20, 30, 40 (10)	10, 20 (10)	0.56 (10)	4, 8, 16 (30)	0.7, 5.2, 14 (10)	2 (20)
Data												
Plasma	X	X	X	X	X	X	X	X	X	X	X	X
brain _{ECF}	X	X	X	X	X	X	X	X	X	X	X	X
CSF _{LV}	X		X					X			X	
CSF _{CM}	X		X			X		X		X (new data)	X (new data)	X
Total brain tissue								X	X	X (new data)	X (new data)	
References	(24)	(25)	(23)	(26)	(27)	(3)	(3)	(28)	(29)	(30) (except total brain tissue data)	(3) (except total brain tissue data)	(3)

brain_{ECF}: brain extracellular fluid compartment, CSF_{LV}: cerebrospinal fluid compartment in the lateral ventricle, CSF_{CM}: cerebrospinal fluid compartment in the cisterna magna

Evaluation of the PBPK model

The PBPK model performance was evaluated by the comparison of model predictions with the concentration-time profiles in brain_{ECP}, CSF_{LV}, CSF_{CM} and total brain tissue of 10 compounds. We performed 200 simulations for each compound including random effect estimates for the plasma PK model. Based on these, we calculated the prediction error (PE) and symmetric mean absolute percentage error (SMAPE) (Eq. 26 and 27).

$$PE = \frac{Y_{OBS,ij} - Y_{PRED,ij}}{(Y_{OBS,ij} + Y_{PRED,ij})/2} \quad (26)$$

$$SMAPE = \frac{1}{N} \sum_{k=1}^N |PE| \times 100 \quad (27)$$

where $Y_{OBS,ij}$ is the j th observation of the i th subject, $Y_{PRED,ij}$ is the j th mean prediction of the i th subject, and N is the number of observations.

RESULTS

Plasma PK model

The estimated parameters for the descriptive plasma PK models were obtained with good precision and summarized in **Table II**. The models describe plasma concentration-time profiles very well for all compounds except risperidone (**Supplementary Figure S1**). For remoxipride, a small under-prediction was observed at later time points.

CNS PBPK model

The values of the system-specific and drug-specific parameters are summarized in **Table III** and **Table IV**, respectively. The combined system-specific and drug-specific parameters are summarized in **Table V**. Overall, the developed generic PBPK model could adequately predict the rat data in brain_{ECP}, CSF_{LV}, CSF_{CM} and total brain tissue. **Figure 2** shows the PE for each compound and each CNS compartment. The PE for risperidone brain_{ECP} and CSF_{CM} showed modest under-prediction. For the other drugs, the PEs were distributed within two standard deviations and no specific trends were observed across time, compounds and CNS locations. The SMAPEs for the model prediction in brain_{ECP}, CSF_{LV}, CSF_{CM} and total brain tissue were 72, 71, 69 and 91%, respectively, indicating that the model could predict concentration-time profiles in these compartments with less than two-fold prediction error. The concentration-time plots of individual predictions *versus* observations across drugs and dose levels, are provided (**Supplementary Figure S1**).

Table II. Parameter estimates for plasma pharmacokinetics of the 10 compounds

		Parameter estimates (RSE, %)									
		Acetaminophen	Atenolol	Methotrexate	Morphine	Paliperidone	Phenytoin	Quinidine	Raclopride	Remoxipride	Risperidone
CL_{PL}	mL/min	15.8 (9.10)	7.13 (20.6)	8.04 (15.9)	22.6 (7.70)	196 (13.0)	36.0 (8.90)	162 (4.10)	46.4 (4.30)	42.2 (4.90)	886 (33.2)
Q_{PL_PER1}	mL/min	33.8 (33.7)	NA	28.5 (30.7)	30.8 (10.0)	61.5 (86.2)	265 (12.7)	829 (6.80)	13.4 (27.5)	33.8 (20.7)	NA
Q_{PL_PER2}	mL/min	NA	NA	3.33 (34.8)	7.21 (10.2)	NA	NA	NA	69.2 (7.50)	14.0 (10.1)	NA
V_R	mL	49.5 (59.0)	256 (27.0)	28.0 (55.0)	152 (11.1)	26400 (12.6)	943 (21.5)	670 (13.3)	48.9 (16.3)	83.7 (18.3)	43100 (28.1)
V_{PER1}	mL	363 (33.1)	NA	111 (14.6)	530 (9.10)	3580 (35.8)	2050 (7.50)	11300 (3.20)	684 (19.2)	253 (10.9)	NA
V_{PER2}	mL	NA	NA	83.5 (34.9)	1200 (10.8)	NA	NA	NA	493 (18.3)	757 (4.00)	NA
fraction		0.693 (19.6)	NA	NA	NA	NA	NA	NA	NA	NA	NA
inter individual variability^{a)}											
$\omega_{CL_{PL}}$	%	NA	NA	37.4 (46.8)	17.8 (9.5)	42.0 (62.5)	73.8 (12.5)	23.9 (15.3)	14.4 (29.8)	31.0 (12.0)	72.5 (38.7)
$\omega_{Q_{PL_PER1}}$	%	NA	NA	NA	28.8 (29.4)	NA	NA	24.3 (28.2)	NA	25.1 (12.1)	NA
$\omega_{Q_{PL_PER2}}$	%	NA	NA	42.5 (42.0)	86.7 (19.3)	NA	NA	NA	NA	76.7 (13.5)	NA
$\omega_{V_{PL}}$	%	NA	NA	40.4 (75.5)	80.6 (17.2)	47.5 (81.4)	75.0 (27.2)	NA	NA	64.1 (32.9)	53.7 (78.8)
$\omega_{V_{PER1}}$	%	51.8 (86.0)	NA	NA	46.0 (15.3)	NA	NA	12.8 (26.6)	NA	NA	NA
$\omega_{V_{PER2}}$	%	NA	NA	NA	NA	NA	NA	NA	NA	NA	NA
inter occasional variability^{b)}											
$\omega_{_study1}$	%	NA	NA	NA	42.7 (16.2)	NA	NA	NA	NA	NA	NA
$\omega_{_study2}$	%	NA	NA	NA	29.7 (30.5)	NA	NA	NA	NA	NA	NA
residual error^{c)}											
$\sigma_{_plasma\ proportional}$	%	23.7 (35.0)	48.6 (56.1)	15.1 (17.2)	24.6 (8.80)	22.7 (15.6)	13.0 (10.6)	24.5 (7.70)	14.1 (8.60)	31.0 (11.2)	47.2 (49.1)
$\sigma_{_plasma\ additive}$	ng/mL	NA	NA	5400 (42.6)	NA	NA	NA	NA	NA	NA	0.0244 (27.6)

CL_{PL} : clearance from the central compartment, Q_{PL_PER1} : inter-compartmental clearance between the central compartment and the peripheral compartment 1, Q_{PL_PER2} : inter-compartmental clearance between the central compartment and the peripheral compartment 2, V_{PL} : distribution volume of the central compartment, V_{PER1} : distribution volume of the peripheral compartment 1, V_{PER2} : distribution volume of the peripheral compartment 2, fraction: percentage of the drug which is reabsorbed by enterohepatic circulation, RSE: relative standard error.

a) and b) $\theta_i = \theta_0 \times e^{\omega_i}$ ($\eta_i + \eta_j$), where θ_0 represents the parameters of the i th subject and j th study, θ represents the population mean value of the parameter, η_i is the random effect of the i th subject under the assumption of a normal distribution with a mean value of 0 and variance of ω_i^2 , and η_j is the random effect of the j th study under the assumption of a normal distribution with a mean value of 0 and variance of ω_j^2 .

c) $C_j = Y_{j_obs} \times (1 + \epsilon_j)$ or $C_j = Y_{j_pred} \times (1 + \epsilon_j)$, where C_j represents the j th observed concentration of the i th subject, Y_{j_obs} represents the j th individual prediction of the i th subject, and ϵ_j is the random effect of the j th observed concentration of the i th subject under the assumption of a normal distribution with a mean value of 0 and variance of σ^2 .

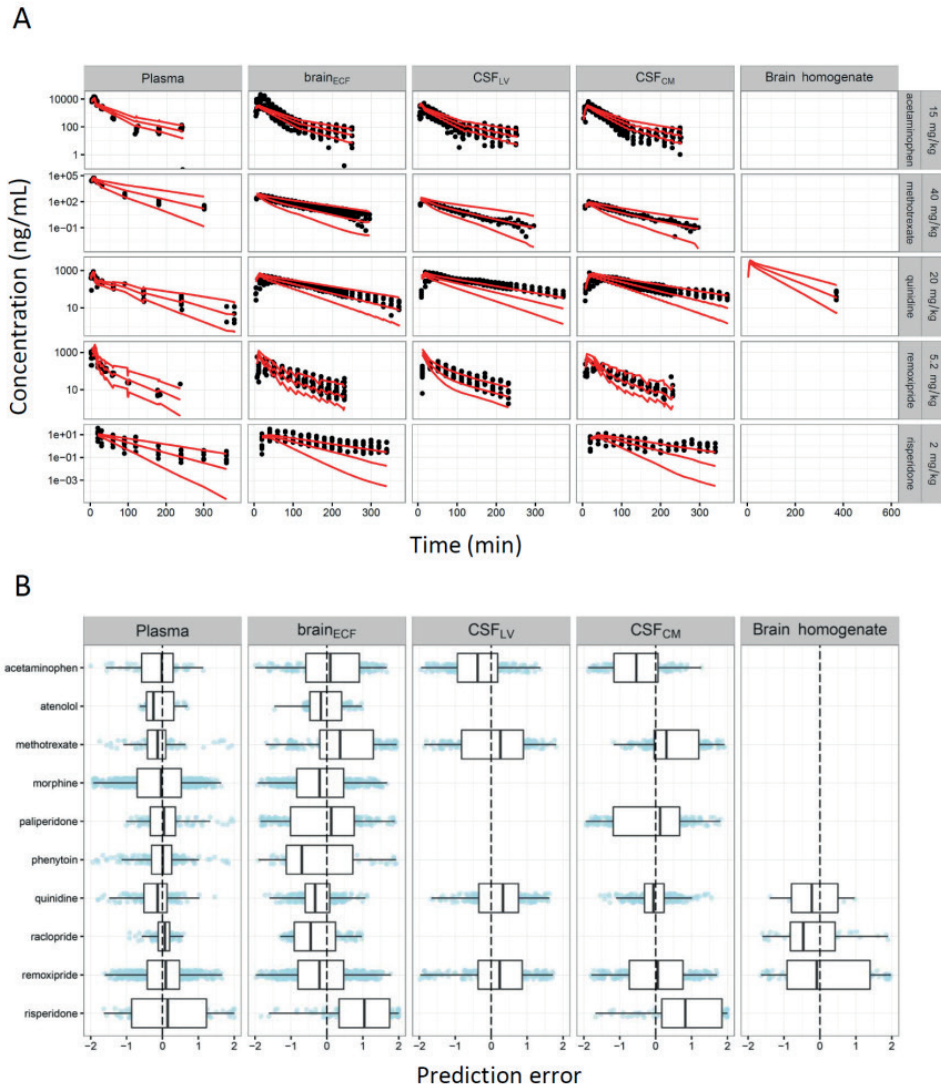


Figure 2. Prediction accuracy of the PBPK model. The plots were stratified by the CNS compartments (panels). (A) Selected individual observed drug concentrations (dots) and 95 % prediction interval (red lines). (B) Box-whisker plots for the prediction errors (PE) across all 10 drugs evaluated. Blue dots are PE for each observation.

Table III. System-specific parameters of the PBPK model

	Description	Parameter	Value	Reference
Volumes	Brain	V_{tot}	1880 μ l	(31)
	Brain _{ECF}	$V_{brain_{ECF}}$	290 μ l	(32)
	Brain _{ICF}	$V_{brain_{ICF}}$	1440 μ l	(33)
	Total lysosome	V_{LYSO}	18 μ l	calculated ^{d)}
	CSF _{LV}	$V_{CSF_{LV}}$	50 μ l	(34,35)
	CSF _{TFV}	$V_{CSF_{TFV}}$	50 μ l	(34,35)
	CSF _{CM}	$V_{CSF_{CM}}$	17 μ l	(36,37)
	CSF _{SAS}	$V_{CSF_{SAS}}$	180 μ l	(34,38)
	Brain microvascular	V_{MV}	60 μ l	(39)
Flows	Cerebral blood flow	Q_{CBF}	1.2 mL/min	(40)
	Brain _{ECF} flow	Q_{ECF}	0.0002 mL/min	(41)
	CSF flow	Q_{CSF}	0.0022 mL/min	(32)
Surface areas	BBB	SA_{BBB}	263 cm ² a)	(42)
	BCSFB	SA_{BCSFB}	25 cm ² b,c)	(43)
	Total BCM	SA_{BCM}	3000 cm ²	(44)
	Total lysosomal membrane	SA_{LYSO}	1440 cm ²	calculated ^{d)}
Width	BBB	$Width_{BBB}$	0.3-0.5 μ m (0.5 was used in the model)	(45)

CSF, cerebrospinal fluid; BBB, blood-brain barrier; BCSFB, blood-cerebrospinal barrier; BCM, brain cell membrane

^{a)} 99.8 % of SA_{BBB} are used for transcellular diffusion, and 0.006 % of SA_{BBB} are used for paracellular diffusion, ^{b)} 99.8 % of SA_{BCSFB} are used for transcellular diffusion and 0.016 % of SA_{BCSFB} are used for paracellular diffusion, ^{c)} SA_{BCSFB1} and SA_{BCSFB2} are assumed to be 12.5cm² and 12.5cm², respectively, ¹⁾ based on the volume ratio of lysosomes to brain_{ICF} (1:80)(10), ^{d)} based on the lysosome number per cell which was calculated using the total lysosomal volume and diameter of each lysosome (0.5-1.0 μ m)(11).

Table IV. Drug-specific parameters of the PBPK model

		Acetaminophen	Atenolol	Methotrexate	Morphine	Paliperidone	Phenytion	Quinidine	Raclopride	Remoxipride	Risperidone
Drug specific parameters											
Transmembrane permeability	cm/min	1.1*10 ⁻⁴	5.7*10 ⁻⁵	6.1*10 ⁻⁷	2.5*10 ⁻⁴	0.0018	0.0077	0.058	6.6*10 ⁻⁴	0.0035	0.0082
	Aqueous diffusivity coefficient (Paracellular diffusion)	4.6*10 ⁻⁴	3.5*10 ⁻⁴	2.8*10 ⁻⁴	3.4*10 ⁻⁴	2.8*10 ⁻⁴	3.6*10 ⁻⁴	3.2*10 ⁻⁴	3.1*10 ⁻⁴	3.0*10 ⁻⁴	2.9*10 ⁻⁴
AF	AFin1	1.0	1.0	1.0	1.0	1.0	1.0	1.2	1.0	1.0	1.0
	AFin2	1.0	1.0	1.0	1.0	1.0	1.0	1.4	1.0	1.0	1.0
	AFin3	1.0	1.0	1.0	1.0	1.0	1.0	1.4	1.0	1.0	1.0
	AFout1	12	40	4.6*10 ⁴	11 ^{a)} , 20 ^{b)}	3.0	4.2	1.0	1.4	1.7	1.3
AFout2	29	82	4.7*10 ⁵	20 ^{a)} , 38 ^{b)}	3.7	7.6	1.0	1.1	1.7	1.3	
AFout3	32	110	1.0*10 ⁶	26 ^{a)} , 49 ^{b)}	4.7	7.7	1.0	1.9	2.1	1.5	
Partitioning coefficient between compartments											
Kp _{uu,brain_{ECF}}	0.51	0.37	0.018	0.38 ^{a)} , 0.23 ^{b)}	0.50	0.26	1.5	1.1	0.80	0.80	0.97
Kp _{uu,CSF_{IV}}	0.51	0.37	0.0066	0.38 ^{a)} , 0.23 ^{b)}	0.50	0.26	1.5	1.1	0.80	0.80	0.97
Kp _{uu,CSF_{CM}}	0.51	0.37	0.0024	0.38 ^{a)} , 0.23 ^{b)}	0.50	0.26	1.5	1.1	0.80	0.80	0.97
Kp	1.0	0.94	NA	1.3	1.3	2.3	13	11	5.5	5.5	2.1
Free fraction											
f _{u,p}	0.81	0.91	0.45	0.83	0.080	0.090	0.14	0.070	0.74	0.74	0.070
f _{u,b}	0.80	0.90	NA	0.76	0.065 ^{d)}	0.080	0.090	0.13	0.57 ^{e)}	0.57 ^{e)}	0.065
Physicochemical properties											
Molecular weight	151	266	454	285	426	252	324	347	371	410	410
log P	0.5	0.2	-1.9	0.9	1.8	2.5	3.4	1.3	2.1	2.5	2.5
pKa (Acid)	9.5	14.1	3.4	10.3	13.7	9.5	13.9	5.9	13.1	13.1	13.1
pKa (Base)	-4.4	9.7	2.8	9.1	8.8	-9.0	9.1	9.0	8.4	8.4	8.8
Charge class	Neutral	Base	Acid	Base	Base	Neutral	Base	Zwitterion	Base	Base	Base

^{a)} 4 mg/kg, ^{b)} 10, 40 mg/kg, ^{c)} calculated from $V_{u,brain}$ and $K_{p,uu,cell}$, ^{d)} assumed to be the same as risperidone

AF, asymmetry factor

AFin1-3 and AFout1-3 were calculated from $K_{p,uu,brain_{ECF}}$, $K_{p,uu,CSF_{IV}}$ and $K_{p,uu,CSF_{CM}}$, respectively.

Impact of cerebral blood flow (Q_{CBF})

Q_{CBF} is 1.2 mL/min (40). Therefore, for strong lipophilic compounds, for instance quinidine, the drug transport clearance from plasma to the brain_{ECF} (BBB permeability) is limited by Q_{CBF} since Q_{BBB_in} and Q_{BBB_out} of quinidine were 9.1 and 5.1 mL/min, respectively (**Table III and Table V**).

Impact of distinct paracellular and transcellular pathways on total diffusion at the BBB and BCSFB (Q_{BBB} , Q_{BCSFB1} and Q_{BCSFB2})

The Q_{BBB} , Q_{BCSFB1} and Q_{BCSFB2} were determined by the combination of paracellular and transcellular diffusion in the model. Even though the SA of BBB for paracellular diffusion (SA_{BBBp}) is very small compared to the SA of BBB for transcellular diffusion (SA_{BBBt}) (0.006: 99.8), paracellular diffusion had an impact on the values of Q_{BBB} , Q_{BCSFB1} and Q_{BCSFB2} especially for hydrophilic compounds. For instance, the values of transcellular diffusion (Qt_{BBB}) and paracellular diffusion (Qp_{BBB}) for methotrexate, which is the most hydrophilic compound in this study, were 0.000080 and 0.087 mL/min, respectively (**Table V**). Thus, Q_{BBB} of methotrexate was determined mainly by paracellular diffusion. For quinidine, which is the most lipophilic compound in the study, Q_{BBB} was mainly determined by CBF limited transcellular diffusion (Qt_{BBB} and Qp_{BBB} were 7.6 and 0.10 mL/min, respectively).

Rate limiting drug transport clearance for intra-extracellular exchange (Q_{BCM_in} and Q_{BCM_out})

The Q_{BCM_in} and Q_{BCM_out} were higher than Q_{BBB_in} and Q_{BBB_out} for acetaminophen, paliperidone, phenytoin, quinidine, raclopride, remoxipride and risperidone. Q_{BCM_in} and Q_{BCM_out} are lower than Q_{BBB_in} and Q_{BBB_out} for methotrexate (**Table V**). This suggests that the transport clearance from brain_{MV} via brain_{ECF} to brain_{ICF} is limited by Q_{BBB_in} and Q_{BBB_out} for acetaminophen, paliperidone, phenytoin, quinidine, raclopride, remoxipride and risperidone, whereas it is limited by Q_{BCM_in} and Q_{BCM_out} for methotrexate.

Surface area of BCSFB to determine the paracellular and transcellular diffusion clearance around CSF_{LV} and CSF_{TFV}

In our model, we assumed that the SA of the BCSFB around CSF_{LV} (SA_{BCSFB1}) and CSF_{TFV} (SA_{BCSFB2}) are equal in size (50% of the total SA_{BCSFB} for each). SA is one of the key factors that determines the paracellular and transcellular diffusion clearance across the BCSFB1 and BCSFB2. However, the early-time predictions for CSF_{LV} for acetaminophen, quinidine and remoxipride indicate an over-prediction of the paracellular and transcellular diffusion clearance (**Figure 2 and Supplementary Figure S1**), suggesting that the SA of BCSFB1 is less than 50% of the total SA_{BCSFB} .

Impact of active transporters to determine the extent of drug exposure in the CNS compartments

Active transporters govern the extent of drug exposure in the brain and CSFs. For most of the compounds, the impact of active transporters among $K_{p,uu,brain_{ECF}}$, $K_{p,uu,CSF_{LV}}$ and $K_{p,uu,CSF_{CM}}$ was assumed to be identical, except for methotrexate. Different $K_{p,uu,CSF_{LV}}$ (0.0066) and $K_{p,uu,CSF_{CM}}$ (0.0024) were observed for methotrexate, which were taken into account in the PBPK model by asymmetry factors AF_{out2} and AF_{out3} . The extent of drug entry into the brain and CSF was predicted well for all compounds, except for morphine at the 4 mg/kg dose (**Supplementary Figure S1**).

DISCUSSION

The developed CNS PBPK model resulted in adequate predictions of concentration-time courses for 10 diverse drugs in the $brain_{ECF}$, CSF_{LV} , CSF_{CM} , and total brain tissue with less than two-fold prediction error. In comparison, QSPR studies that predict $K_{p,uu,brain_{ECF}}$ of drugs have similar prediction error magnitudes, even though only one parameter was predicted (5,6). Therefore, the two-fold prediction error is considered to be a good result.

A small under-prediction was observed in $brain_{ECF}$ and CSF_{CM} for risperidone, and in $brain_{ECF}$ for morphine at the 4 mg/kg dose. The under-prediction of risperidone $brain_{ECF}$ and CSF_{CM} concentrations (**Figure 2**) likely results from difficulties in the plasma PK modeling of risperidone, which leads to propagation of an error in the PBPK model. Risperidone plasma PK data appeared to follow a 2-compartment PK model but data were insufficient to describe this 2-compartment kinetics. The small under-prediction for morphine $brain_{ECF}$ profiles at a dosage of 4 mg/kg might be related to a large inter-study variability for morphine, since the predictions for morphine at the other dosage groups could adequately capture the observations (**Supplementary Figure S1 and Table S1**).

This is the first time that the transcellular and paracellular diffusion clearance at the BBB/BCSFB were addressed separately, by using the information of the intercellular space and the effective pore size. As the contribution of these pathways may depend on the condition of the barriers (i.e. in certain disease conditions the tight junctions may become less tight), the assessment of these system-specific parameters is important. From the electron microscopic cross-section picture of brain capillary (12), the intercellular space was measured to be 0.03 μm , which is comparable to the 0.02 μm width reported (46). Based on the relationship of the pore size and TEER, which were obtained from *in vitro*

studies (15), we assumed the effective pore size of the BBB and BCSFB to be 0.0011 μm and 0.0028 μm , respectively. The effective pore size derived for the rat BBB (0.0011 μm) is within the range reported in literature (0.0007-0.0018 μm) (47,48). Therefore, it is reasonable to assume that our estimations for these system-specific parameter values are appropriate. In this study, no compound with sole paracellular transport (such as mannitol) has been used, as no such data were available in literature.

For the PBPK model, the drug-specific parameters were obtained from *in silico* predictions using the compounds' physicochemical properties, except for AF values. AF values were calculated using $K_{p,uu}$ values, as obtained from the previously published *in vivo* animal experiments (3). It should be noted that $K_{p,uu}$ values can also be obtained from several published QSPR models using the compound's physicochemical properties (4–6).

Unlike previously developed PBPK models for the CNS (2), our PBPK model contains a number of key relevant physiological processes and compartments.

We discriminated between paracellular and transcellular diffusion processes. The relative impact of the paracellular diffusion on Q_{BBB} or Q_{BCSFB} for each compound varied from around 100% (methotrexate) to 1.3% (quinidine). For hydrophilic compounds, Q_{BBB} and Q_{BCSFB} were impacted most by paracellular diffusion, whereas transcellular diffusion largely determined the Q_{BBB} and Q_{BCSFB} of lipophilic compounds. The separation of the two processes is expected to be meaningful for the prediction of the CNS drug concentrations in disease conditions, since pathophysiological conditions may differently affect paracellular and transcellular diffusion.

We also demonstrated the relevance of considering CBF-limited kinetics on the drug transfer at the BBB. For the lipophilic compounds, $Q_{\text{BBB}_{in}}$ and $Q_{\text{BBB}_{out}}$ are higher than Q_{CBF} indicating that the drug transfer clearance on the BBB is largely determined by Q_{CBF} .

The importance of the separation between $\text{brain}_{\text{ECF}}$ and $\text{brain}_{\text{ICF}}$ compartments was shown. $Q_{\text{BCM}_{in}}$ and $Q_{\text{BCM}_{out}}$ were either higher or lower than $Q_{\text{BBB}_{in}}$ and $Q_{\text{BBB}_{out}}$, depending on the molecular weight, the log P and the pKa of the compound, which led to differences in drug distribution into $\text{brain}_{\text{ICF}}$ from brain_{MV} .

We identified differences in methotrexate drug concentration in CSF_{LV} and CSF_{CM} (23). Therefore, it is expected that the expression level (function) of some of the active transporters may be different between the BCSFB around CSF_{LV} and CSF_{TFV} . Methotrexate is known to be a substrate of various transporters, such as RFC1, MRP, BCRP, OATP and

OAT transporters (23), even though there is no detailed information about their exact location. Therefore, we incorporated this in our model by including Q_{BCSFB1} and Q_{BCSFB2} to describe transport for methotrexate.

All of the parameters for our CNS PBPK model can be derived from either literature or *in silico* predictions. Therefore, the model can be used to assess newly developed CNS drugs without *in vivo* data and contributes to the “refinement, reduction and replacement” of animals in drug research. Although the reported values of the system-specific parameters for human are sparse and variable (2), theoretically the model can be scaled to humans by replacing the system-specific parameters to predict target-site concentrations in human brain, representing an important tool for translational development of new CNS drugs.

REFERENCES

1. Kola I, Landis J. Can the pharmaceutical industry reduce attrition rates? *Nat Rev Drug Discov.* 2004;3:1–5.
2. Yamamoto Y, Danhof M, de Lange ECM. Microdialysis : the Key to Physiologically Based Model Prediction of Human CNS Target Site Concentrations. *AAPS J.* 2017;19(4):891–909.
3. Yamamoto Y, Väilitalo PA, van den Berg D-J, Hartman R, van den Brink W, Wong YC, et al. A Generic Multi-Compartmental CNS Distribution Model Structure for 9 Drugs Allows Prediction of Human Brain Target Site Concentrations. *Pharm Res.* 2017;34(2):333–51.
4. Fridén M, Winiwarter S, Jerndal G, Bengtsson O, Wan H, Bredberg U, et al. Structure-brain exposure relationships in rat and human using a novel data set of unbound drug concentrations in brain interstitial and cerebrospinal fluids. *J Med Chem.* 2009;52(20):6233–43.
5. Loryan I, Sinha V, Mackie C, van Peer A, Drinkenburg WH, Vermeulen A, et al. Molecular properties determining unbound intracellular and extracellular brain exposure of CNS drug candidates. *Mol Pharm.* 2015;12(2):520–32.
6. Chen H, Winiwarter S, Fridén M, Antonsson M, Engkvist O. In silico prediction of unbound brain-to-plasma concentration ratio using machine learning algorithms. *J Mol Graph Model.* 2011;29(8):985–95.
7. Jones H, Rowland-Yeo K. Basic concepts in physiologically based pharmacokinetic modeling in drug discovery and development. *CPT pharmacometrics Syst Pharmacol.* 2013;2:1–12.
8. Engelhardt B, Sorokin L. The blood-brain and the blood-cerebrospinal fluid barriers: Function and dysfunction. *Semin Immunopathol.* 2009;31(4):497–511.
9. Nguyen T-H-T, Mouksassi M-S, Holford N, Al-Huniti N, Freedman I, Hooker AC, et al. Model evaluation of continuous data pharmacometric models: Metrics and graphics. *CPT pharmacometrics Syst Pharmacol.* 2016;(1):1–20.
10. Nicholson C, Sykova E. Extracellular space structure revealed by diffusion analysis. *Trends Neurosci.* 1998;21(5):207–15.
11. Hardin J, Bertoni GP, Kleinsmith LJ. *Becker's World of the Cell*, 8th Edition. San Francisco: Pearson Education Inc.; 2011.
12. Weiss N, Miller F, Cazaubon S, Couraud PO. The blood-brain barrier in brain homeostasis and neurological diseases. *Biochim Biophys Acta.* 2009;1788(4):842–57.
13. Crone C, Olesen SP. Electrical resistance of brain microvascular endothelium. *Brain Res.* 1982;241(1):49–55.
14. Olesen SP, Crone C. Electrical resistance of muscle capillary endothelium. *Biophys J.* 1983;42(1):31–41.

15. Adson A, Raub TJ, Burton PS, Barsuhn CL, Hilgers AR, Ho NFH, et al. Quantitative approaches to delineate paracellular diffusion in cultured epithelial cell monolayers. *J Pharm Sci.* 1994;83(11):1529–36.
16. Avdeef A, Nielsen PE, Tsinman O. PAMPA - A drug absorption in vitro model: 11. Matching the in vivo unstirred water layer thickness by individual-well stirring in microtitre plates. *Eur J Pharm Sci.* 2004;22(5):365–74.
17. Grumetto L, Russo G, Barbato F. Immobilized Artificial Membrane HPLC Derived Parameters vs PAMPA-BBB Data in Estimating in Situ Measured Blood-Brain Barrier Permeation of Drugs. *Mol Pharm.* 2016;13(8):2808–16.
18. Fridén M, Bergström F, Wan H, Rehngren M, Ahlin G, Hammarlund-Udenaes M, et al. Measurement of unbound drug exposure in brain: Modeling of pH partitioning explains diverging results between the brain slice and brain homogenate methods. *Drug Metab Dispos.* 2011;39(3):353–62.
19. Henderson LJ. Concerning the Relationship between the Strength of Acids and Their Capacity to Preserve Neutrality. *Am J Physiol.* 1908;21:173–9.
20. Henderson LJ. The Theory of Neutrality Regulation in the Animal Organism. *Am J Physiol.* 1908;21:427–48.
21. Berezhkovskiy LM. Volume of distribution at steady state for a linear pharmacokinetic system with peripheral elimination. *J Pharm Sci.* 2004;93(6):1628–40.
22. Poulin P, Theil F-P. Prediction of pharmacokinetics prior to in vivo studies. II. Generic physiologically based pharmacokinetic models of drug disposition. *J Pharm Sci.* 2002;91(5):1358–70.
23. Westerhout J, van den Berg D-J, Hartman R, Danhof M, de Lange ECM. Prediction of methotrexate CNS distribution in different species - Influence of disease conditions. *Eur J Pharm Sci.* 2014;57:11–24.
24. Westerhout J, Ploeger B, Smeets J, Danhof M, de Lange ECM. Physiologically based pharmacokinetic modeling to investigate regional brain distribution kinetics in rats. *AAPS J.* 2012;14(3):543–53.
25. de Lange ECM, Danhof M, de Boer AG, Breimer DD. Critical factors of intracerebral microdialysis as a technique to determine the pharmacokinetics of drugs in rat brain. *Brain Res.* 1994;666(1):1–8.
26. Groenendaal D, Freijer J, de Mik D, Bouw MR, Danhof M, de Lange ECM. Population pharmacokinetic modelling of non-linear brain distribution of morphine: influence of active saturable influx and P-glycoprotein mediated efflux. *Br J Pharmacol.* 2007;151(5):701–12.
27. Bouw MR, Gårdmark M, Hammarlund-Udenaes M. Pharmacokinetic-pharmacodynamic modelling of morphine transport across the blood-brain barrier as a cause of the antinociceptive effect delay in rats - a microdialysis study. *Pharm Res.* 2000;17(10):1220–7.

28. Westerhout J, Smeets J, Danhof M, de Lange ECM. The impact of P-gp functionality on non-steady state relationships between CSF and brain extracellular fluid. *J Pharmacokinet Pharmacodyn.* 2013;40(3):327–42.
29. Wong Y, Ilkova T, van Wijk R, de Lange ECM. Development of a population pharmacokinetic model to predict brain distribution and dopamine D2 receptor occupancy of raclopride in non-anesthetized rat. Prep.
30. Stevens J, Ploeger BA, van der Graaf PH, Danhof M, de Lange ECM. Systemic and direct nose-to-brain transport pharmacokinetic model for remoxipride after intravenous and intranasal administration. *Drug Metab Dispos.* 2011;39(12):2275–82.
31. Kawakami J, Yamamoto K, Sawada Y, Iga T. Prediction of brain delivery of ofloxacin, a new quinolone, in the human from animal data. *J Pharmacokinet Biopharm.* 1994;22(3):207–27.
32. Cserr H, Cooper D, Suri P, Patlak C. Efflux of radiolabeled polyethylene glycols and albumin from rat brain. *Am J Physiol.* 1981;240(4):319–28.
33. Thorne RG, Hrabe S, Nicholson C, Robert G. Diffusion of Epidermal Growth Factor in Rat Brain Extracellular Space Measured by Integrative Optical Imaging. *J Neurophysiol.* 2004;92(6):3471–81.
34. Condon P, Wyper D, Grant R, Patterson J, Hadley D, Teasdale G, et al. Use of magnetic resonance imaging to measure intracranial cerebrospinal fluid volume. *Lancet.* 1986;327(8494):1355–7.
35. Kohn MI, Tanna NK, Herman GT, Resnick SM, Mozley PD, Gur RE, et al. Analysis of brain and cerebrospinal fluid volumes with MR imaging. Part I. Methods, reliability, and validation. *Radiology.* 1991;178(1):115–22.
36. Robertson EG. Developmental defects of the cisterna magna and dura mater. *J Neurol Neurosurg Psychiatry.* 1949;12(1):39–51.
37. Adam R, Greenberg JO. The mega cisterna magna. *J Neurosurg.* 1978;48(2):190–2.
38. Bass NH, Lundborg P. Postnatal development of bulk flow in the cerebrospinal fluid system of the albino rat: clearance of carboxyl-(14C)inulin after intrathecal infusion. *Brain Res.* 1973;52:323–32.
39. Liu X, Smith BJ, Chen C, Callegari E, Becker SL, Chen X, et al. Use of a Physiologically Based Pharmacokinetic Model to Study the Time to Reach Brain Equilibrium: An Experimental Analysis of the Role of Blood-Brain Barrier Permeability, Plasma Protein Binding, and Brain Tissue Binding. *J Pharmacol Exp Ther.* 2005;313(3):1254–62.
40. Sasaki Y, Wagner HN. Measurement of the distribution of cardiac output in unanesthetized rats. *J Appl Physiol.* 1971;30(6):879–84.
41. Neuwelt E, Abbott NJ, Abrey L, Banks WA, Blakley B, Davis T, et al. Strategies to advance translational research into brain barriers. *Lancet Neurol.* 2008;7(1):84–96.
42. Patabendige A, Skinner RA, Abbott NJ. Establishment of a simplified in vitro porcine blood-brain barrier model with high transendothelial electrical resistance. *Brain Res.* 2013;1521:1–15.

43. Strazielle N, Gherzi-Egea JF. Choroid plexus in the central nervous system: biology and physiopathology. *J Neuropathol Exp Neurol.* 2000;59(7):561–74.
44. Trapa PE, Belova E, Liras JL, Scott DO, Steyn SJ. Insights from an Integrated Physiologically Based Pharmacokinetic Model for Brain Penetration. *J Pharm Sci.* 2016;105(2):965–71.
45. Cornford EM, Hyman S. Localization of brain endothelial luminal and abluminal transporters with immunogold electron microscopy. *NeuroRx.* 2005;2(1):27–43.
46. Farquhar MG, Palade GE. Junctional complexes in various epithelia. *J Cell Biol.* 1963;17:375–412.
47. Crone C. Lack of selectivity to small ions in paracellular pathways in cerebral and muscle capillaries of the frog. *J Physiol.* 1984;353:317–37.
48. Zhang T-T, Li W, Meng G, Wang P, Liao W. Strategies for transporting nanoparticles across the blood-brain barrier. *Biomater Sci.* 2015;(2):219–29.
49. Stevens J, Ploeger BA, Hammarlund-Udenaes M, Osswald G, van der Graaf PH, Danhof M, et al. Mechanism-based PK-PD model for the prolactin biological system response following an acute dopamine inhibition challenge: Quantitative extrapolation to humans. *J Pharmacokinet Pharmacodyn.* 2012;39(5):463–77.
50. Srikanth CH, Chaira T, Sampathi S, Sreekumar VB, Bambal RB. Correlation of in vitro and in vivo plasma protein binding using ultracentrifugation and UPLC-tandem mass spectrometry. *Analyst.* 2013;138(20):6106–16.
51. Stain F, Barjavel MJ, Sandouk P, Plotkine M, Scherrmann J-M, Bhargava HN. Analgesic Response and Plasma and Brain Extracellular Pharmacokinetics of Morphine and Morphine-6-f3-D-Glucuronide in the Rat Fluid of opiates effects. *J Pharmacol Exp Ther.* 1995;274(2):852–7.
52. Widman M, Nilsson L, Bryske B, Lundström J. Disposition of remoxipride in different species. Species differences in metabolism. *Arzneimittelforschung.* 1993;43(3):287–97.

SUPPLEMENTARY MATERIAL

S1. Algebraic solutions for calculating AFs and BF using Maxima Computer Algebra System.

The algebraic solutions for calculating drug-specific parameters AFin1, AFin2, AFin3, AFout1, AFout2, AFout3, and BF were obtained as follows. If the Kp,uu values were larger than 1 (net active influx), AFin1, AFin2 and AFin3 were calculated using the following equations, while AFout1-3 were fixed to 1. If the Kp,uu values were smaller than 1 (net active efflux), AFout1, AFout2 and AFout3 were calculated using the following equations, while AFin1-3 were fixed to 1. All parameter values in the equations for each compound are provided in Table III, Table IV and Table V.

$$AFin1 = \frac{AFout1 \times Kp,uu, brain_{ECF} \times PHF1 \times Qt_{BBB} + (Kp,uu, brain_{ECF} \times PHF1 - 1) \times Qp_{BBB} + Kp,uu, brain_{ECF} \times Q_{ECF}}{Kp,uu, brain_{ECF} \times PHF1 \times Qt_{BBB}}$$

$$AFout1 = \frac{AFin1 \times Qt_{BBB} + (1 - Kp,uu, brain_{ECF} \times PHF1) \times Qp_{BBB} + Kp,uu, brain_{ECF} \times Q_{ECF}}{Kp,uu, brain_{ECF} \times PHF1 \times Qt_{BBB}}$$

$$A = (AFin1 \times AFout2 \times Kp,uu, CSF_{LV} \times PHF2 \times Qt_{BBB} + AFout2 \times Kp,uu, CSF_{LV} \times PHF2 \times Qp_{BBB} + AFout2 \times Kp,uu, CSF_{LV} \times Q_{CBF} \times PHF2) \times Qt_{BCSFB1}$$

$$B = ((AFin1 \times Kp,uu, CSF_{LV} \times PHF2 - AFout1 \times Kp,uu, brain_{ECF} \times PHF1) \times Qp_{BCSFB1} - AFin1 \times Kp,uu, brain_{ECF} \times Q_{ECF} + AFin1 \times Kp,uu, CSF_{LV} \times Q_{CSF}) \times Qt_{BBB}$$

$$C = ((Kp,uu, CSF_{LV} \times PHF2 - Kp,uu, brain_{ECF} \times PHF1) \times Qp_{BBB} - Kp,uu, brain_{ECF} \times Q_{ECF} + (Kp,uu, CSF_{LV} \times PHF2 - 1) \times Q_{CBF}) \times Qp_{BCSFB1}$$

$$D = (Kp,uu, CSF_{LV} \times Q_{CSF} - Kp,uu, brain_{ECF} \times Q_{ECF}) \times Qp_{BBB}$$

$$AFin2 = \frac{A + B + C + D - Kp,uu, brain_{ECF} \times Q_{CBF} \times Q_{ECF} + Kp,uu, CSF_{LV} \times Q_{CBF} \times Q_{CSF}}{(AFout1 \times Kp,uu, brain_{ECF} \times Qt_{BBB} + Kp,uu, brain_{ECF} \times Qp_{BBB} + Kp,uu, brain_{ECF} \times Q_{ECF} + Q_{CBF}) \times Qt_{BCSFB1}}$$

$$E = (AFout1 \times AFin2 \times Kp,uu, brain_{ECF} \times PHF1 \times Qt_{BBB} + AFin2 \times Kp,uu, brain_{ECF} \times PHF1 \times Qp_{BBB} + AFin2 \times Kp,uu, brain_{ECF} \times Q_{ECF} + AFin2 \times Q_{CBF}) \times Qt_{BCSFB1}$$

$$F = ((AFout1 \times Kp,uu, brain_{ECF} \times PHF1 - AFin1 \times Kp,uu, CSF_{LV} \times PHF2) \times Qp_{BCSFB1} + AFin1 \times Kp,uu, brain_{ECF} \times Q_{ECF} - AFin1 \times Kp,uu, CSF_{LV} \times Q_{CSF}) \times Qt_{BBB}$$

$$G = ((Kp,uu, brain_{ECF} \times PHF1 - Kp,uu, CSF_{LV} \times PHF2) \times Qp_{BBB} + Kp,uu, brain_{ECF} \times Q_{ECF} + (1 - Kp,uu, CSF_{LV} \times PHF2) \times Q_{CBF}) \times Qp_{BCSFB1}$$

$$H = (Kp,uu, brain_{ECF} \times Q_{ECF} - Kp,uu, CSF_{LV} \times Q_{CSF}) \times Qp_{BBB}$$

$$\begin{aligned}
\text{AFout2} &= \frac{E + F + G + H + Kp, uu, \text{brain}_{ECF} \times Q_{CBF} \times Q_{ECF} - Kp, uu, \text{CSF}_{LV} \times Q_{CBF} \times Q_{CSF}}{(AFin1 \times Kp, uu, \text{CSF}_{LV} \times PHF2 \times Q_{t_{BBB}} + Kp, uu, \text{CSF}_{LV} \times PHF2 \times Q_{CBF}) \times Q_{t_{BCSFBB1}}} \\
I &= (AFin1 \times AFout3 \times Kp, uu, \text{CSF}_{CM} \times PHF3 \times Q_{p_{BBB}} + AFout3 \times Kp, uu, \text{CSF}_{CM} \times PHF3 \times Q_{CBF}) \times Q_{t_{BCSFBB2}} \\
J &= ((AFin1 \times Kp, uu, \text{CSF}_{CM} \times PHF3 - AFout1 \times Kp, uu, \text{brain}_{ECF} \times PHF1) \times Q_{p_{BCSFBB2}} + (AFin1 \times Kp, uu, \text{CSF}_{CM} - AFin1 \times Kp, uu, \text{CSF}_{LV}) \times Q_{CSF}) \times Q_{t_{t_{BBB}}} \\
K &= ((Kp, uu, \text{CSF}_{CM} \times PHF3 - Kp, uu, \text{brain}_{ECF} \times PHF1) \times Q_{p_{BBB}} - Kp, uu, \text{brain}_{ECF} \times Q_{ECF} + (Kp, uu, \text{CSF}_{CM} \times PHF3 - 1) \times Q_{CBF}) \times Q_{p_{BCSFBB2}} \\
L &= (Kp, uu, \text{CSF}_{CM} - Kp, uu, \text{CSF}_{LV}) \times Q_{CSF} \times Q_{p_{BBB}} \\
\text{AFin3} &= \frac{I + J + K + L + (Kp, uu, \text{CSF}_{CM} - Kp, uu, \text{CSF}_{LV}) \times Q_{CBF} \times Q_{CSF}}{(AFout1 \times Kp, uu, \text{brain}_{ECF} \times PHF1 \times Q_{t_{BBB}} + Kp, uu, \text{brain}_{ECF} \times PHF1 \times Q_{p_{BBB}} + Kp, uu, \text{brain}_{ECF} \times Q_{ECF} + Q_{CBF}) \times Q_{t_{BCSFBB2}}} \\
M &= (AFout1 \times AFin3 \times Kp, uu, \text{brain}_{ECF} \times PHF1 \times Q_{t_{BBB}} + AFin3 \times Kp, uu, \text{brain}_{ECF} \times PHF1 \times Q_{p_{BBB}} + AFin3 \times Q_{CBF} + AFin3 \times Q_{CBF}) \times Q_{t_{BCSFBB2}} \\
N &= ((AFout1 \times Kp, uu, \text{brain}_{ECF} \times PHF1 - AFin1 \times Kp, uu, \text{CSF}_{CM} \times PHF3) \times Q_{p_{BCSFBB2}} + (AFin1 \times Kp, uu, \text{CSF}_{LV} - AFin1 \times Kp, uu, \text{CSF}_{CM}) \times Q_{CSF}) \times Q_{t_{t_{BBB}}} \\
O &= ((Kp, uu, \text{brain}_{ECF} \times PHF1 - Kp, uu, \text{CSF}_{CM} \times PHF3) \times Q_{p_{BBB}} + Kp, uu, \text{brain}_{ECF} \times Q_{ECF} + (1 - Kp, uu, \text{CSF}_{CM} \times PHF3) \times Q_{CBF}) \times Q_{p_{BCSFBB2}} \\
P &= (Kp, uu, \text{CSF}_{LV} - Kp, uu, \text{CSF}_{CM}) \times Q_{CSF} \times Q_{p_{BBB}} \\
\text{AFout3} &= \frac{M + N + O + P + (Kp, uu, \text{CSF}_{LV} - Kp, uu, \text{CSF}_{CM}) \times Q_{CBF} \times Q_{CSF}}{(AFin1 \times Kp, uu, \text{CSF}_{CM} \times PHF3 \times Q_{t_{BBB}} + Kp, uu, \text{CSF}_{CM} \times PHF3 \times Q_{p_{BBB}} + Kp, uu, \text{CSF}_{CM} \times PHF3 \times Q_{CBF}) \times Q_{t_{BCSFBB2}}} \\
\text{BF} &= \frac{V_{tot} \times PHF2 \times PHF7 \times Kp + (-Kp, uu, \text{brain}_{ECF} \times V_{ECF} \times PHF2 - Kp, uu, \text{brain}_{ECF} \times V_{ICF} \times PHF1) \times PHF7 - Kp, uu, \text{brain}_{ECF} \times V_{LysO} \times PHF1 \times PHF6}{Kp, uu, \text{brain}_{ECF} \times V_{tot} \times PHF2 \times PHF7}
\end{aligned}$$

S2. General animal surgery and experimental setting.

Animals

All of the animal study protocols were approved by the Animal Ethics Committee of Leiden University (all approval numbers are given in Table S1). All animal experiments were performed in accordance with the Dutch Law of Animal Experimentation. Male Wistar rats with a weight range 225-275 g (Charles River, The Netherlands) were housed in groups for a few days (5-13 days) under standard environmental conditions with ad libitum access to food (Laboratory chow, Hope Farms, Woerden, The Netherlands) and acidified water. Between surgery and experiments, the animals were kept individually in Makrolon type 3 cages for 1 week to recover from surgical procedures.

Surgery

Rats were anesthetized (5% isoflurane for induction, 1-2% as maintenance). Subsequently cannulas were implanted in the femoral artery for serial blood sampling, and in the femoral vein for drug administration, respectively. Microdialysis guides were inserted into brain and several CSF locations. One day before the experiment, the microdialysis dummies were replaced by microdialysis probes. For details on the microdialysis guides, probes and locations are summarized in **Table S1**.

Drug administration

Experiments generally started at 9:00 a.m. to minimize the influence of circadian rhythms. Before the start of drug administration microdialysis probes were continuously flushed with microdialysis perfusion fluid until equilibration was reached. Drugs were intravenously administered for 1-30 mins.

Bioanalytical methods for remoxipride total brain tissue data

Remoxipride brain tissue was extracted at the end of the animal experiment in which plasma, brain_{ECF} data were sampled (3). The remoxipride brain samples were quantified with a validated liquid chromatography tandem mass spectrometry (LC-MS/MS) method (30), with slight adaptations for the 0.7 mg/kg group as follows: the trifluoroacetic acid was added to the solvents of the on-line solid phase extraction and mobile phases were replaced with formic acid in order to reach the required pH while maintaining a satisfactory peak shape, and to eliminate the signal suppression caused by trifluoroacetic acid. Also, raclopride-d5 hydrochloride (Toronto Research Chemicals, North York, Canada) was used as the internal standard.

SUPPLEMENTARY FIGURES

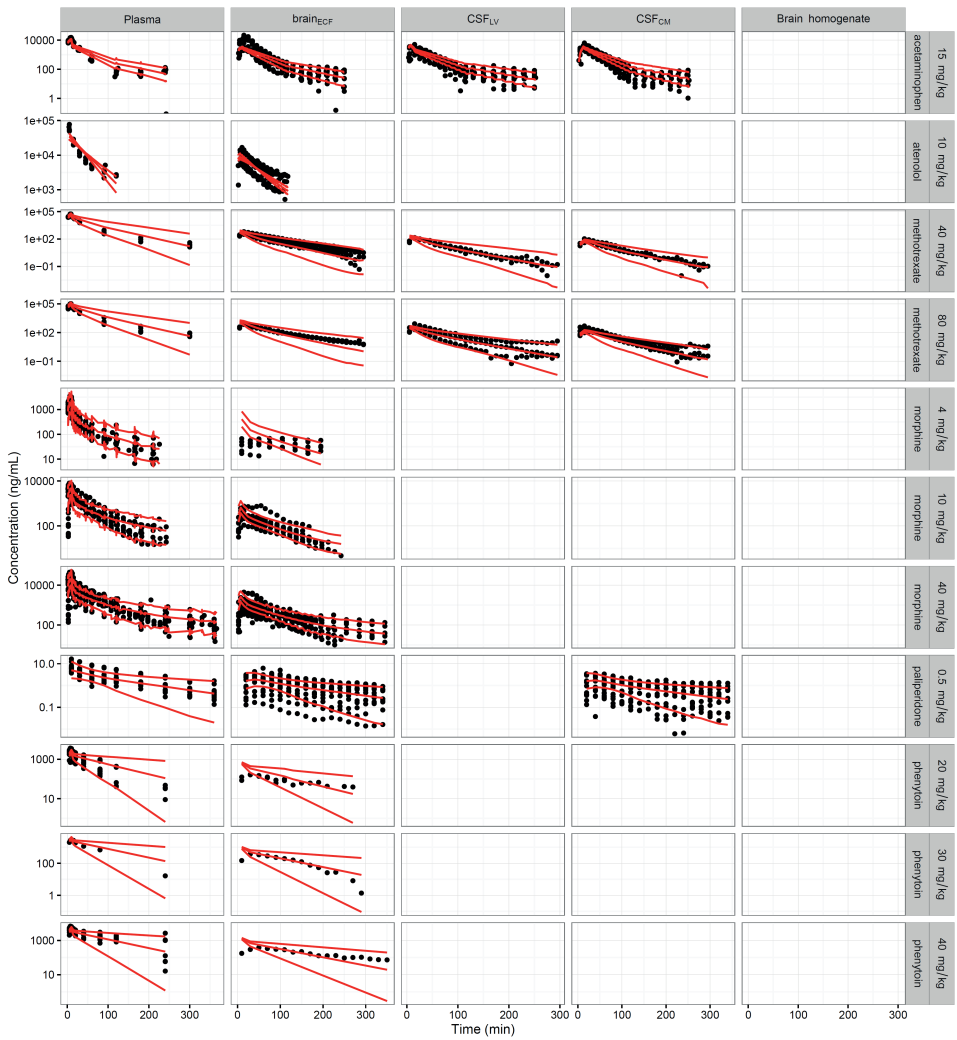


Figure S1. Prediction of the PBPK model. Individual observed drug concentrations (dots) and 95 % prediction interval (red lines). Unbound concentration (ng/mL) versus time (min) profiles for 10 compounds.

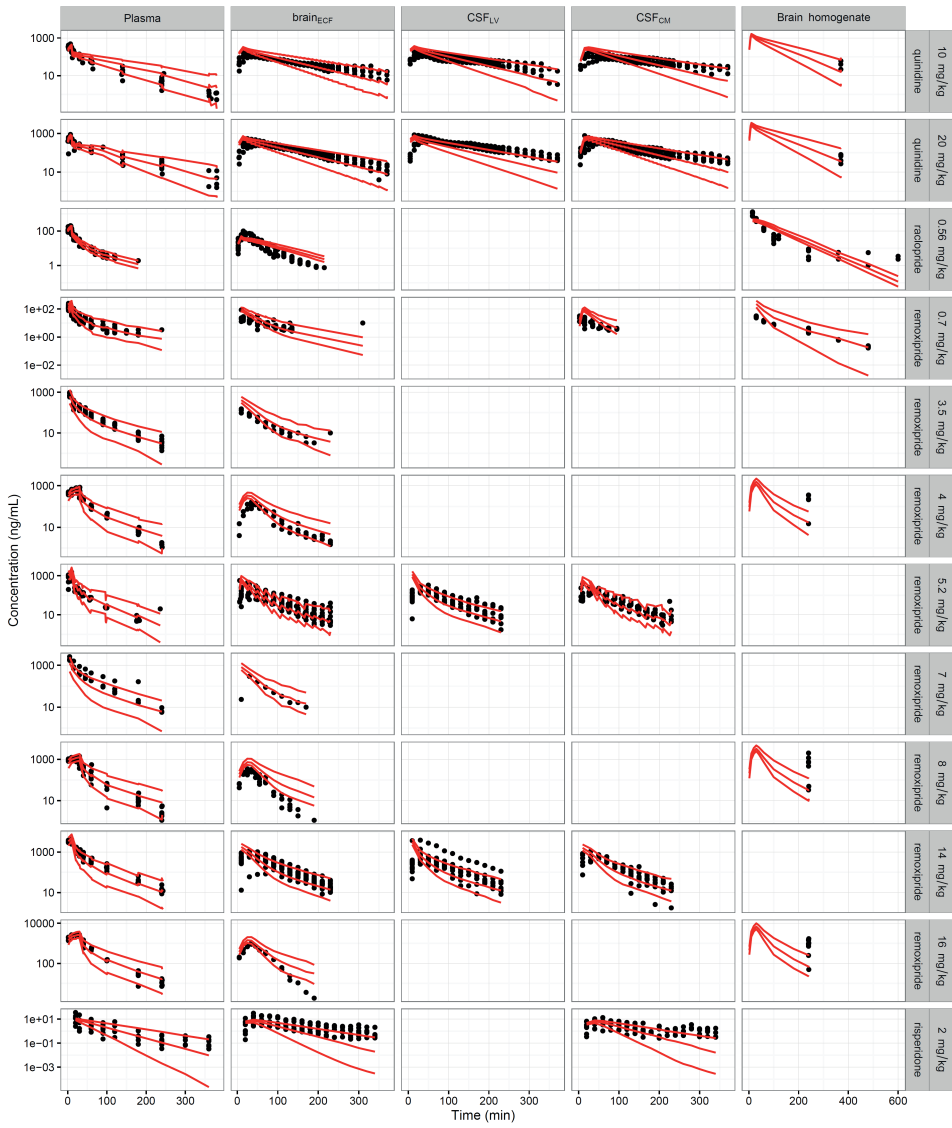


Figure S1. (continued)

SUPPLEMENTARY TABLES

Table S1. Summary of the *in vivo* experimental set-up for rat data

Study design	Acetaminophen	Atenolol	Methotrexate	Morphine	Morphine	Morphine	Paliperidone	Phenytoin	Quinidine	Raclopride	Remoxipride	Remoxipride	Risperidone
plasma sampling points	-5, 2, 7, 10, 15, 30, 60, 120, 180, 240 min	0, 5, 15, 30, 45, 60, 90, 120 min	-5, 2, 7, 9, 10, 12, 17, 30, 90, 180, 300 min	0, 8, 20, 70, 130, 190 min	15 samples up to 360 min	0, 8, 20, 70, 130, 190 min	-15, 10/20, 30, 60, 90, 120, 180, 240, 300, 360 min	10 samples up to 480 min	-5, 2, 7, 10, 12, 17, 30, 60, 140, 240, 360 min	-20, 2, 7, 10, 15, 22, 40, 60, 120, 240 min	-5, 5, 10, 20, 35, 60, 90, 120, 150, 240 min	0, 2, 7, 10, 16, 22, 40, 150 and 240 min	-15, 10/20, 30, 60, 90, 120, 180, 240, 300, 360 min
dialysate sampling points	every 10 min up to 120 min, every 20 min from 120 to 240 min	up to 120 min	every 10 min up to 300 min	every 5 min during infusion, 10 min from 10 to 60 min, every 20 min from 60 to 180 min	25 and 30 dialysate samples up to 360 min	every 5 min during infusion, 10 min from 10 to 60 min, every 20 min from 60 to 180 min	every 20 min up to 240 min	every 10 min up to 480 min	every 10 min up to 240 min, every 20 min from 240 to 360 min	every 20 mins up to 240 mins	every 10 min up to 120 min, every 20 min from 120 to 240 min	every 20 min up to 240 min	every 20 min up to 240 min
DEC approval number	7068	2112	10094	3008	NA (from literature)	NA (from literature)	12049	11092	7142	14051	6132	13186	12049
Microdialysis setting													
probe material	A	B	C	D	NA (from literature)	NA (from literature)	C	C	C	C	A	C	C
probe supplier	E	F	E	E	E	E	E	E	E	E	E	E	E
PF	G	H	G	H	H	H	H	H	G	H	H	H	H
flow rate	2 μ L/min	7 μ L/min	2 μ L/min	2 μ L/min	2 μ L/min	2 μ L/min	1 μ L/min	2 μ L/min	2 μ L/min	1 μ L/min	2 μ L/min	1 μ L/min	1 μ L/min
fu,p (%)	81%	91%	45%	83%	83%	83%	8%	9%	14%	37%	74%	74%	7%

Table S1. (continued)

	Acetaminophen	Atenolol	Methotrexate	Morphine	Morphine	Paliperidone	Phenytoin	Quinidine	Raclopride	Remoxipride	Remoxipride	Risperidone
<i>in vivo</i> recovery (loss %)	Brain _{ECF} : 12.0 % CSF _{IV} : 8.10% CSF _{CSF} : 8.60%	Brain _{ECF} : 13.0 %	Brain _{ECF} : 22.1 % CSF _{IV} : 28.1% CSF _{CSF} : 35.9 %	Brain _{ECF} (4mg/kg): 16.1 % Brain _{ECF} (40mg/kg): 20.3 %	Plasma: 40.9 % Brain _{ECF} : 8.40 %	Brain _{ECF} : 18.0 % CSF _{CSF} : 10.0 %	Brain _{ECF} : 35.0 %	Brain _{ECF} : 9.10 % CSF _{IV} : 2.90% CSF _{CSF} : 3.50 %	Brain _{ECF} : 28 %	Brain _{ECF} : 20 %	Brain _{ECF} : 11.0 % CSF _{IV} : 7.00 % CSF _{CSF} : 5.00%	Brain _{ECF} : 22.0 % CSF _{CSF} : 10.0 %
<i>In vivo</i> recovery references	(24)	(25)	(23)	(26)	(27)	(3)	(3)	(28)	(49)	(3)	(3)	(3)
f.u.p. references	(24)	(50)	(23)	(51)	(51)	(3)	(50)	(28)	(52)	(52)	(52)	(3)

A: Polycarbonate, B: Cellulose acetate, C: Polyarylethersulphone (PAES), D: Polycarbonate-poly-ether (PC-PE) co-polymeric membrane, E: CMA Microdialysis AB, Kista, Sweden, F: Homemade, G: 140.3 mM sodium, 2.7 nM potassium, 1.2 mM calcium, 1.0 mM magnesium and 147.7 mM chloride, H: NaCl 145 mM, KCl 0.6 mM, MgCl₂ 1.0 mM, CaCl₂ 1.2 mM and ascorbic acid 0.2 mM in 2 mM phosphate buffer (pH 7.4)

PF: microdialysis perfusion fluid

f.u.p.: free fraction in plasma



Prediction of human CNS pharmacokinetics using a physiologically based pharmacokinetic modeling approach

Y Yamamoto, P A Väliälä, Y C Wong, D R Huntjens, J H Proost, A Vermeulen, W Krauwinkel, M W Beukers, H Kokki, M Kokki, M Danhof, J G C van Hasselt, E C M de Lange

Submitted for publication

ABSTRACT

Knowledge of drug concentration-time profiles at the central nervous system (CNS) target-site is critically important for rational development of CNS targeted drugs. Our aim was to translate a recently published comprehensive CNS physiologically based pharmacokinetic (PBPK) model from rat to human, and to predict drug concentration-time profiles in multiple CNS compartments on available human data of four drugs (acetaminophen, oxycodone, morphine and phenytoin).

Values of the system-specific parameters in the rat CNS PBPK model were replaced by corresponding human values. The contribution of active transporters for the four selected drugs was scaled based on differences in expression of the pertinent transporters in both species. Model predictions were evaluated with available pharmacokinetic (PK) data in human brain extracellular fluid and/or cerebrospinal fluid, obtained under physiologically healthy CNS conditions (acetaminophen, oxycodone, and morphine) and under pathophysiological CNS conditions where CNS physiology could be affected (acetaminophen, morphine and phenytoin).

The human CNS PBPK model could successfully predict their concentration-time profiles in multiple human CNS compartments in physiological CNS conditions within a 1.6-fold error. Furthermore, the model allowed investigation of the potential underlying mechanisms that can explain differences in CNS PK associated with pathophysiological changes. This analysis supports the relevance of the developed model to allow more effective selection of CNS drug candidates since it enables the prediction of CNS target-site concentrations in humans, which are essential for drug development and patient treatment.

INTRODUCTION

Development of drugs for central nervous system (CNS) diseases faces high attrition rates (1). A major factor for this high attrition rate is the lack of adequate information on unbound drug concentration-time profile at the CNS target-sites, which is the driving force for the drug-target interaction and subsequent drug effect (2).

Several factors govern the distribution of drug molecules into and within the CNS. Physiological CNS compartments include the brain microvascular space, the key drug-target site compartments being the brain extracellular fluid ($\text{brain}_{\text{ECF}}$), the brain intracellular fluid ($\text{brain}_{\text{ICF}}$), and also multiple cerebrospinal fluid (CSF) spaces. CNS drug distribution is governed by several processes including physiological fluid flows, passive and active membrane transport across the blood-brain barrier (BBB) and the blood-CSF barrier (BCSFB), extracellular-intracellular exchange, and pH differences (3). Physiological fluid flows include cerebral blood flow (CBF), $\text{brain}_{\text{ECF}}$ bulk flow, and CSF flow. The interplay between various processes complicates prediction of drug target-site concentrations. In addition, aging and pathophysiological conditions may alter CNS drug distribution. This happens for example via changes in properties of the BBB and BCSFB (e.g. tight junctions, active transporters), volumes of CNS compartments and CNS fluid flows (4,5), and should therefore be taken into account in CNS pharmacokinetics (PK) predictions.

To investigate CNS drug distribution, *ex vivo* techniques such as the brain homogenate and the brain slicing technique are currently used. With these techniques, steady state values of the unbound fraction in brain (6) and the volume of distribution of the unbound drug in brain (7) can be determined, from which also intracellular accumulation of the unbound drug can be derived. Unfortunately, these techniques cannot provide information on the unbound drug concentration-time profiles, and potential local concentration differences. Such information is very important for determining the rate and extent of processes in CNS drug distribution and understanding their interrelationships (systems pharmacokinetics). Time course data of unbound drug concentrations can only be obtained by *in vivo* intracerebral microdialysis (8–11), as other monitoring techniques like positron emission tomography measure total drug concentrations (12–14). However, though minimally invasive, the use of microdialysis in humans is highly restricted. Therefore, approaches that can predict time-dependent and CNS location-dependent unbound drug concentration in human are of great interest.

We recently developed a comprehensive physiologically based pharmacokinetic (PBPK) rat model to predict unbound drug concentration-time profiles for multiple CNS compartments (15). This rat PBPK model allows prediction of CNS PK profiles without the need of *in vivo* PK data. The purpose of the present study was to scale the rat CNS PBPK model to predict drug PK profiles in multiple CNS compartments in human. The human CNS PBPK model was evaluated using available human brain_{ECF} and/or CSF PK data in physiological and/or pathophysiological CNS conditions, on acetaminophen, oxycodone, morphine, and phenytoin.

MATERIALS AND METHODS

The previously developed rat CNS PBPK model (15), which consisted of a plasma PK and a CNS PBPK component, was scaled to predict human CNS PK by substitution of rat CNS physiological parameter values by the human values (**Figure 1**). Human plasma PK models for the drugs investigated (acetaminophen, oxycodone, morphine, phenytoin) were either obtained from literature or developed using available human plasma data.

All analyses were performed using NONMEM version 7.3 (16). The predictive performance of the developed model was evaluated using available human data on the concentrations of acetaminophen, oxycodone, morphine and phenytoin in brain_{ECF} and/or CSF, obtained under physiological and/or pathophysiological CNS conditions.

Human plasma and CNS data

The details of the clinical PK studies of acetaminophen, oxycodone, morphine and phenytoin, which were used for the evaluation of the human PBPK model predictions, are summarized in **Table I**.

Acetaminophen

Human acetaminophen PK data in plasma and in CSF in the lumbar region (CSF_{SAS_LUMBAR}) were obtained from healthy subjects (study A1) and from patients with nerve-root compression pain (study A2) (17,18). These CNS conditions were considered to be physiological CNS conditions, i.e. without likely effects on CNS PK. In study A3, human CSF samples from the lateral ventricle (CSF_{LV}) were obtained by extra-ventricular drainage (EVD) (CSF_{EVD}) from patients with traumatic brain injury (TBI), which was considered to be a pathophysiological CNS condition (19). For all datasets, total plasma concentrations for acetaminophen were converted to unbound plasma concentrations using the free fraction (85%) obtained from literature for healthy subjects (20).

Oxycodone

Oxycodone human plasma and CSF_{SAS_LUMBAR} PK data (study O1) were obtained from patients under elective gynecological surgery (21), where a CNS condition considered to be physiological. Unbound plasma concentrations for oxycodone were extrapolated from the total plasma concentrations using the free fraction (59%) obtained from literature for healthy subjects (22,23).

Morphine

Morphine human PK data in plasma and in brain_{ECF} (study M1 and M2) were obtained from bilateral microdialysis measurements from both the injured and uninjured brain sides of TBI patients, thereby providing a comparison of physiological and pathophysiological conditions (24,25). For both datasets, the unbound plasma concentrations were reported in these original publications.

Phenytoin

Phenytoin human PK data in plasma and in CSF_{SAS_LUMBAR} (study P1) were obtained from epileptic patients, which was considered a pathophysiological CNS condition (26). Unbound plasma concentrations for phenytoin were extrapolated from the total plasma concentrations using the free fraction (13%) obtained from literature for healthy subjects (27).

Human plasma PK models

For acetaminophen (study A3) and morphine (study M1 and M2), we used published human plasma PK models (19). For acetaminophen (study A1 and A2), oxycodone (study O1) and phenytoin (study P1), plasma PK models were systematically developed with a mixed effects modeling approach using available individual human plasma data, since there is no plasma PK model from literature or the existing plasma PK model did not adequately describe the data (19) (see Table I). One-, two- and three-compartment models were evaluated for their utility to describe the data. Inter-individual variability was incorporated on each PK parameter, using an exponential model. Proportional and combined additive-proportional residual error models were tested. Model selection was guided by a likelihood ratio test with $p < 0.05$, the precision of the parameter estimates, assessment of the parameter correlation matrix, and graphical evaluation of the plots for observations *versus* predictions, weighted residuals *versus* time, and weighted residuals *versus* predictions (28).

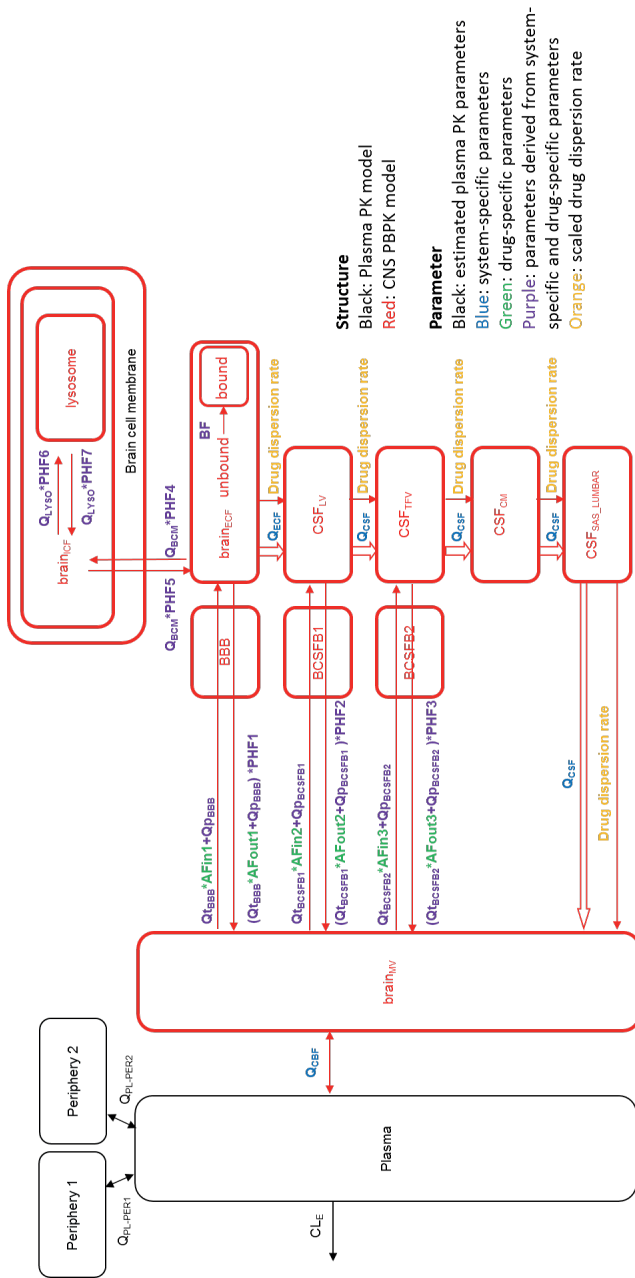


Figure 1. The human PBPK model structure.

The model consists of a plasma PK model and a CNS PBPK model with estimated plasma PK parameters, and system-specific and drug-specific parameters (colors) for CNS. The plasma PK model was extended with peripheral compartments 1 and 2 in cases where these compartments were required to describe the plasma data adequately. $Brain_{mv}$: brain microvascular, BBB: blood-brain barrier, BCSFB: blood-CSF barrier, $brain_{ecf}$: brain extra cellular fluid, $brain_{icf}$: brain intra cellular fluid, CSF_{LV} : CSF in the lateral ventricle, CSF_{TV} : CSF in the third and fourth ventricle, CSF_{OI} : CSF in the cisterna magna, CSF_{SAS_LUMBAR} : CSF in the subarachnoid space and lumbar region, Q_{BBB} : cerebral blood flow, Q_{t_BBB} : transcellular diffusion clearance at the BBB, Q_{t_BBB} : paracellular diffusion clearance at the BBB, Q_{t_BCSFB1} : transcellular diffusion clearance at the BCSFB1, Q_{p_BCSFB1} : paracellular diffusion clearance at the BCSFB1, Q_{t_BCSFB2} : transcellular diffusion clearance at the BCSFB2, Q_{p_BCSFB2} : paracellular diffusion clearance at the BCSFB2, Q_{BCSFB2} : passive diffusion clearance at the brain cell membrane, Q_{LVS0} : passive diffusion clearance at the lysosomal membrane, Q_{ECF} : $brain_{ECF}$ flow, Q_{CSF} : CSF flow, A_{Fin1-3} : asymmetry factor into the CNS compartments 1-3, $A_{Fout1-3}$: asymmetry factor out of the CNS compartments 1-3, $PHF1-7$: pH-dependent factor 1-7, BF : binding factor.

Table I. Summary of human plasma, brain and CSF data sources for the PBPK model evaluation

		Acetaminophen		Oxycodone		Morphine		Phenytoin	
		Study A1	Study A2	Study A3	Study O1	Study M1	Study M2	Study P1	
Study design									
Condition of patients	Healthy subjects	Patients with nerve-root compression	Patients with traumatic brain injury	Patients undergoing elective gynecological surgery	Patients with traumatic brain injury	Patients with traumatic brain injury	Patients with traumatic brain injury	epileptic patients	
Nr of subjects	1 (mean values)	1 (mean values)	7	12	2	1	6		
Dosage	1 g, 15 min infusion	2g (propacetamol), short infusion	1 g, 30 min infusion	0.1 mg/kg, 5min infusion	10 mg, 10min infusion	10 mg, 10min infusion	13 mg/kg, 100mg/min		
Nr of samples (sampling time, h)	plasma	11 (0-12h)	38 (0-6h)	133 (0-24h)	23 (0-3h)	11 (0-3h)	24 (0-1.25h)		
	brain _{E_{CF}} ^a or CSF	11 (0-13h)	54 (0-5.5h)	116 (0-24h)	74 (0-3h)	37 (0-3h)	20 (0-1.25h)		
Data									
plasma	X	X	X	X	X	X	X	X	X
brain _{E_{CF}}						X^e, X^f	X^e, X^f		
CSF _{EVD} ^b			X						
CSF _{SAS LUMBAR} ^c	X	X		X				X	
data references	(18)	(17)	(19)	(21)	(24)	(25)	(26)		
fup ^d	85%			59%	-	-	13%		
fup references	(20)			(22)(23)			(27)		

^a brain extracellular fluid compartment, ^b compartment of cerebrospinal fluid in EVD, ^c compartment of cerebrospinal fluid in subarachnoid space and lumbar region, ^d free fraction in plasma, ^e better side of brain tissue, ^f injured side of brain tissue

blue: data was obtained under physiological CNS conditions, red: data was obtained under pathophysiological CNS conditions

Scaling of the rat CNS PBPK model to humans

The previously developed rat CNS PBPK model (15) (**Figure 1**) consists of nine compartments, being plasma, brain microvessels (brain_{MV}), brain_{ECF} , brain_{ICF} , lysosomes, CSF_{LV} , CSF in the third and fourth ventricle (CSF_{TFV}), CSF in the cisterna magna (CSF_{CM}) and CSF_{SAS_LUMBAR} . The model parameters are either system- or drug-specific.

This rat CNS PBPK model was scaled to humans by 1) substitution of the rat system-specific parameters values by their corresponding human equivalents, 2) rat to human conversion of the contribution of active transport at the BBB and the BCSFB based on reported differences in the expression of active transporters, and 3) adding the rate of drug dispersion in the CNS.

System-specific parameters

Literature values were used for the physiological volumes for all CNS compartments, CBF, brain_{ECF} bulk flow, CSF flow, surface area (SA) of the BBB (SA_{BBB}), SA of the BCSFB (SA_{BCSFB}), the ratio of SA_{BBB} and SA_{BCSFB} for transcellular and paracellular diffusion, the diameter of brain parenchyma cells, the diameter of lysosomes, the cross-width of the BBB cells and the effective pore size (29–44). The SA_{BCSFB} was divided into SA_{BCSFB1} which is the SA around CSF_{LV} and SA_{BCSFB2} which is SA around CSF_{TFV} , like those in the rat CNS PBPK model (15). The total volume of lysosomes was calculated using the volume ratio of the lysosomes to the brain intracellular fluid of brain parenchyma cells (1:80) (45). The SA of total brain parenchymal cell membrane and the SA of total lysosomes were calculated using the diameter of brain parenchyma cells and the volume of brain_{ICF} and diameter of lysosomes and the total volume of lysosomes, respectively. The values of the system-specific parameters used in the model are summarized in **Table II**.

Drug-specific parameters

The calculation of drug-specific parameters including the aqueous diffusivity coefficient and BBB transmembrane permeability of the compound was performed as described previously (15) and the details for the calculation are described in **Supplementary Material S1**. The influence of the net effect of active transporters on the drug exchange at the BBB and BCSFB was incorporated into the model using three asymmetry factors (AFin1-3 or AFout1-3, which can be calculated from $K_{p,uu}$ values (unbound brain/CSF-to-plasma concentration ratio), such that they produced the same $K_{p,uu}$ values within the model). If the net transport is influx of the drug, AFin1-3 were used, while AFout1-3 were fixed to 1. If the net transport is efflux of the drug, AFout1-3 were used, while AFin1-3 were fixed to 1 (15).

Table II. System-specific parameters of the human PBPK model in healthy condition

	Description	Parameter	Human value	Reference
Volumes	Brain	V_{tot}	1400 mL	(29)
	Brain _{ECF}	$V_{brain_{ECF}}$	240-280mL (260 was used in the model)	(30,31)
	Brain _{ICF}	$V_{brain_{ICF}}$	960 mL	(31)
	Total lysosome	V_{LYSO}	12 mL	calculated ^d
	CSF _{IV}	$V_{CSF_{IV}}$	20-25 mL (22.5 was used in the model)	(32,33)
	CSF _{TFV}	$V_{CSF_{TFV}}$	20-25 mL (22.5 was used in the model)	(32,33)
	CSF _{CM}	$V_{CSF_{CM}}$	7.5 mL	(34,35)
	CSF _{SAS_LUMBAR}	$V_{CSF_{SAS_LUMBAR}}$	90-125 mL (90 was used in the model)	(32,33)
Flows	Brain microvascular	V_{MV}	150 mL	(42)
	Cerebral blood flow	Q_{CBF}	610-860 mL/min (735 was used in the model)	(36–38)
	Brain _{ECF} bulk flow	Q_{ECF}	0.15-0.2 mL/min (0.175 was used in the model)	(39)
Surface areas	CSF flow	Q_{CSF}	0.3–0.4 mL/min (0.35 was used in the model)	(39)
	BBB	SA_{BBB}	12-18 m ² ^a (12 was used in the model)	(40,41)
	BCSFB	SA_{BCSFB}	6-9 m ² ^{b,c} (7.5 was used in the model)	calculated (assumed 50% of BBB_{SA})
	Total BCM	SA_{BCM}	228 m ²	calculated ^e
Width	Total lysosomal membrane	SA_{LYSO}	180 m ²	calculated ^f
	BBB	$Width_{BBB}$	0.3-0.5 μ m (0.5 was used in the model)	(43)
effective pore size	BBB		0.0007-0.0009 μ m (0.0007 was used in the model)	(44)

CSF, cerebrospinal fluid; BBB, blood-brain barrier; BCSFB, blood-cerebrospinal barrier; BCM, brain cell membrane

^a 99.8 % of SA_{BBB} was used for transcellular diffusion, and 0.004 % of SA_{BBB} was used for paracellular diffusion, ^b 99.8 % of SA_{BCSFB} was used for transcellular diffusion and 0.016 % of SA_{BCSFB} was used for paracellular diffusion, ^c SA_{BCSFB1} and SA_{BCSFB2} was both assumed to be 3.75cm², ^d based on the volume ratio of lysosomes to brain_{ICF} (1:80), ^e based on the number of brain parenchyma cells which was calculated using the total brain_{ICF} volume and diameter of each brain parenchyma cell (15 μ m) (46), ^f based on the lysosome number per cell which was calculated using the total lysosomal volume and diameter of each lysosome (0.5-1.0 μ m) (47).

As no direct information is available on the values of AFs for human, we used two different approaches to obtain the values depending on the information available for the active transporters for each compound. We propose a workflow and decision tree to obtain human AF values for the individual compounds, based on availability of literature information (**Figure 2**), as follows:

- 1) A literature search was performed for the main transporters involved in the BBB/BCSFB transport of the compounds in humans.
- 2) If relevant active transporters were reported, a literature search was performed on species differences in transporter protein expression / activity of the main active transporters.
- 3) If information on the inter-species differences was available, rat AF values were converted to human AF values using a conversion factor as calculated from the differences in transporter protein expression and/or activity of the main active transporters between rats and humans (**Method 1**).

- 4) If information of the inter-species differences was not available for the compound, we searched information available from other compounds whose transfer are predominantly mediated by the same transporters, and then step 2 was repeated (**Method 2**).
- 5) If an active transporter was not reported, we searched for *in vitro* data able to derive the net contribution of active transport component on the overall permeability. If no indications of active transport could be found, the human AF values were fixed to 1 (**Method 3**). The details of the calculation methods to obtain human AF values from the *in vitro* data are described in **Supplementary Material S3**.

Below we describe in detail the rationale for selection of AF values for each compound.

- *Acetaminophen*

Acetaminophen is reported to be transported across the human BBB by passive diffusion only, (48), therefore we fixed the AF values for acetaminophen to 1 (**Method 3**).

- *Oxycodone*

An active influx transporter for oxycodone at the BBB has been reported; pyrilamine-sensitive proton-coupled organic cation (H⁺/OC) antiporter (49,50). Even though information on species difference in its protein expression level and its activity is not directly available for oxycodone, the transporter activity can be deduced from the *in vitro* observations on pyrilamine transfer, of which the exchange at the BBB is predominantly mediated by this transporter (49,50). Therefore, **Method 2** was applied for oxycodone. According to the *in vitro* studies on pyrilamine in the human BBB model (hCMEC/D3 cells), the Km and Vmax values of active uptake are comparable to those in the rat BBB model (TR-BBB13 cells) (50). Moreover, the weaker active uptake of oxycodone comparing to that of pyrilamine in the human BBB model (50) is in line with the observations in the rat BBB model (49). It thus appears reasonable to assume that the BBB influx mediated by this transporter is comparable between rat and human, and therefore the human AFs were considered to be similar to rat AFs. The human AF at the BBB, AF_{in1}, was 2.3, which was calculated using a $K_{puu,brain_{ECF}}$ (unbound brain_{ECF}-to-plasma concentration ratio) value of 1.7 (51). The human AFs at the BCSFB, AF_{out2} and AF_{out3}, were assumed to be 1.9 and 2.3, respectively, which were calculated from a $K_{puu,CSF}$ (unbound CSF-to-plasma concentration ratio) value of 1 (21).

- *Morphine*

Permeability glycoprotein (P-gp) and multidrug resistance-associated proteins (MRPs) are reported to be the active efflux transporters for morphine at the rat BBB (52,53). Furthermore, an involvement of active influx transporters has also been suggested in rat

BBB (54). Even though morphine is reported to be a substrate of P-gp (55) for humans, other efflux and influx transporters have not been clearly identified. The P-gp protein concentration in rat brain endothelial cells is about 19 fmol/mg protein, which is about three-fold higher than that in humans (6 fmol/mg protein) (56). Regarding the P-gp activity for morphine, no inter-species difference has been observed (57). Therefore, the rat-to-human conversion factor of AFs was set to 3 for morphine. The rat AFout1, AFout2 and AFout3 are 20, 38 and 49, respectively (15), and therefore in this study human AFout1, AFout2 and AFout3 were assumed to be 6.6, 13 and 16, respectively (**Method 1**).

- Phenytoin

P-gp and MRPs are suggested to be the active efflux transporters for phenytoin at the rat BBB (58,59). However, many *in vitro* studies, including the studies using human hCMEC/D3 cells and other cells expressing human P-gp and human MRPs, have shown that phenytoin is neither a substrate for human P-gp nor human MRP2 (60–63). Even though the reasons for these differences between the *in vivo* rat studies and the *in vitro* experiments using human P-gp and MRPs are not clear, inter-species differences in the activity by P-gp for phenytoin (63) and MRP2 have been reported (64). Therefore, **Method 3** was applied to predict AFs for phenytoin. In this study, we assumed that the human AFs for phenytoin are equal to 1.

Use of system-specific and drug-specific parameters in the model

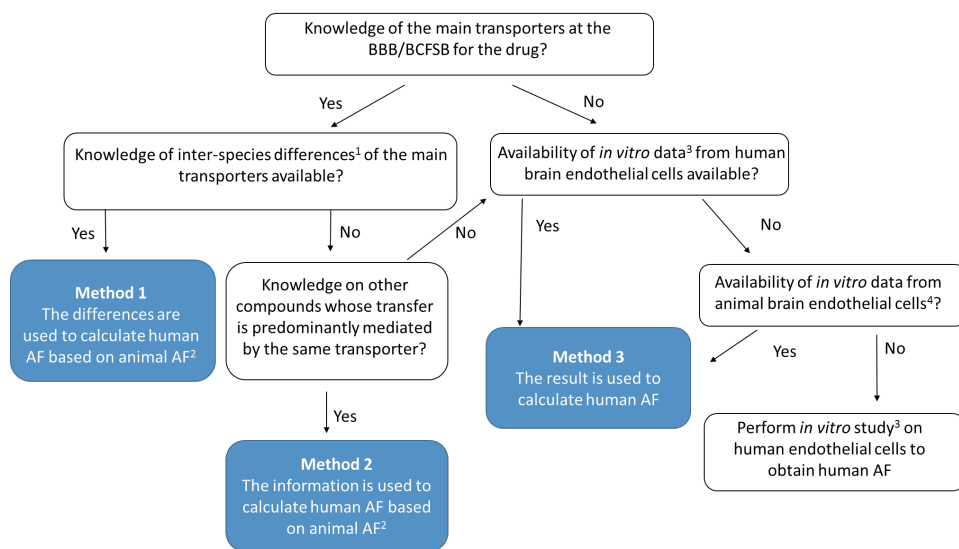
Drug transport at the BBB and BCSFB, brain cellular distribution, acidic subcellular distribution and drug binding were derived by using drug-specific parameter values and system-specific parameters using the equations which were described previously (15) and are provided in **Supplementary Material S2**.

Scaling of the dispersion rate

Previously the values of the system-specific drug dispersion rate within the brain and CSF have been estimated based on rat microdialysis data of nine compounds (19). This dispersion rate is defined as a combination of CSF flow, brain_{ECF} bulk flow and turbulence flow of the drug molecules. For the scaling of the drug dispersion rate to humans we used the following allometric scaling equation.

$$P_{human} = P_{rat} \times \left(\frac{BW_{human}}{BW_{rat}} \right)^{0.75} \quad (1)$$

where P_{human} is the scaled human parameter, P_{rat} is the estimated rat parameter from the model, BW_{human} is the average human body weight (75 kg), and BW_{rat} is the average rat body weight (250 g).



1. Inter-species differences of the expression level and activity/function of the main transporters, are needed.
2. The methods to calculate the rat AF were reported (15). In short, rat AF was calculated using the $K_{p,uu}$ values which were obtained from *in vivo* studies or *in silico* predictions.
3. *In vitro* data which is able to derive active transport component of the overall permeability are needed. The details are provided in supplementary material S3.
4. The assumption is made that the overall active transport characteristics of animal and human BBB are similar.

Figure 2. Decision tree to obtain human AF.

Evaluation of the human CNS PBPK model

The predictions of the scaled human CNS PBPK model were evaluated by comparing of model predictions to observed human PK data in brain_{ECP}, CSF_{SAS_LUMBAR} and/or CSF_{EVD}. The accuracy of the prediction was evaluated with symmetric mean absolute percentage error (SMAPE) (Eq. 2) using population prediction (PRED). We also performed 200 simulations for each compound, then calculated 2.5 % tile, median and 97.5 % tile of the simulated concentrations and plotted these together with the observations.

$$SMAPE = \frac{1}{N} \sum_{k=1}^N \left| \frac{Y_{OBS,ij} - Y_{PRED,ij}}{(Y_{OBS,ij} + Y_{PRED,ij})/2} \right| \times 100 \quad (2)$$

where $Y_{OBS,ij}$ is the j th observation of the i th subject, $Y_{PRED,ij}$ is the j th mean prediction of the i th subject, and N is the number of observations.

Simulated impact of different pathophysiological conditions on CNS PK

Under pathophysiological CNS conditions, several CNS system-specific parameter values, such as CBF, BBB characteristics, BCSFB characteristics, brain_{ECF} bulk flow, CSF flow and active transporters, have been reported to be changed (**Supplemental Table SI**). The following data were available from literature: acetaminophen concentrations in CSF_{EVD} and morphine concentrations in brain_{ECF} which were obtained from TBI patients, and phenytoin data in CSF_{SAS_LUMBAR} which were obtained from epileptic patients (**Table I**).

In TBI patients, a decrease in CBF, an increase in paracellular permeability due to the disruption of the tight junction complexes, and changes in activity/expression of active transporters (such as a decreased expression of P-gp) have been reported (65–67). For epileptic conditions, studies have indicated regional decreases in CBF, increased paracellular permeability due to the opening of the tight junction proteins, and an increase in some active efflux transporters such as P-gp and MRPs (68–71).

To investigate the impact of such pathological changes on each compound's PK profiles, we simulated the PK upon such changes. In the simulations, the system-specific parameter values were varied within a range of 20-500% of their original values (i.e. 5 times lower or higher).

If the changes in the values of the system-specific parameters had a relevant impact on PK profiles, the model predictions were performed again by adapting values of system-specific parameters identified in the literature, and subsequently compared to the observed PK data.

RESULTS

Plasma PK parameter values

The plasma PK parameters used in the analysis for acetaminophen, morphine, oxycodone, and phenytoin are summarized in **Supplemental Table SII**. For acetaminophen (study A3) and morphine (study M1 and M2), the plasma PK parameter values were obtained from literature (19). For acetaminophen (study A1 and study A2), oxycodone (study O1) and phenytoin (study O1), the descriptive plasma PK model was developed using available plasma data. The plasma PK parameter values were obtained with acceptable precision (relative standard error <66%) and could adequately describe the plasma PK data (**Figure 3** and **Figure 5**).

Prediction of CNS PK in physiological CNS conditions

System-specific and drug-specific parameters in physiological CNS conditions are summarized in **Table II** and **Table III**, respectively. The parameters derived from human system-specific and drug-specific parameters are summarized in **Table IV**. The drug dispersion rate for human was calculated to be 1.6 mL/min based on allometric scaling. The model could adequately predict the PK profiles in brain_{ECF} for morphine and the PK profiles in CSF_{SAS_LUMBAR} for acetaminophen and oxycodone under physiological CNS conditions (**Figure 3**), with an SMAPE of brain_{ECF} and CSF_{SAS_LUMBAR} of 49% and 54%, respectively.

Prediction of CNS PK in TBI and epileptic conditions

To explore the impact of each system-specific parameters, which were altered in pathological CNS conditions of TBI and epilepsy on the PK profiles for acetaminophen, morphine and phenytoin, simulations were performed by changing the values of the CBF, and paracellular diffusion. The influence of the active efflux transporters was also simulated for morphine. The impact on model predictions after changing the values of CBF, paracellular diffusion and the influence of the active efflux transporters within a range of 20-500% of their original values are shown in **Figure 4**. It can be seen that the impact of pathological changes on PK profiles is drug-dependent and CNS compartment-dependent. For acetaminophen, the PK profiles in CSF_{LV} were not sensitive to the changes in CBF nor to the changes in paracellular diffusion across the BBB/BCSFB. In contrast, for morphine brain_{ECF} concentrations increased with an increase in paracellular diffusion, and decreased with an increase in active efflux transport. For phenytoin, no change was observed in PK profiles in CSF_{SAS_LUMBAR} with the changes in CBF and paracellular diffusion.

Since TBI and epilepsy conditions did not influence acetaminophen PK profiles in CSF_{LV} and phenytoin PK profiles in CSF_{SAS_LUMBAR} to a significant extent, the model prediction for these PK data was performed using the physiological values of the system-specific parameters (**Figure 5**). The model predictions captured the acetaminophen PK data in CSF_{EVD} and the phenytoin PK data in CSF_{SAS_LUMBAR} well even if the concentrations are slightly over-predicted around the early sampling time for the acetaminophen PK data in CSF_{EVD}.

On the other hand, we found that the values of paracellular diffusion and the influence of the active efflux transporters needed to be adjusted to capture the morphine concentrations in brain_{ECF} in TBI patients (**Figure 4**). Morphine PK data in brain_{ECF} in TBI patients were captured well when paracellular diffusion was upregulated and active efflux transport was downregulated (**Figure 6**).

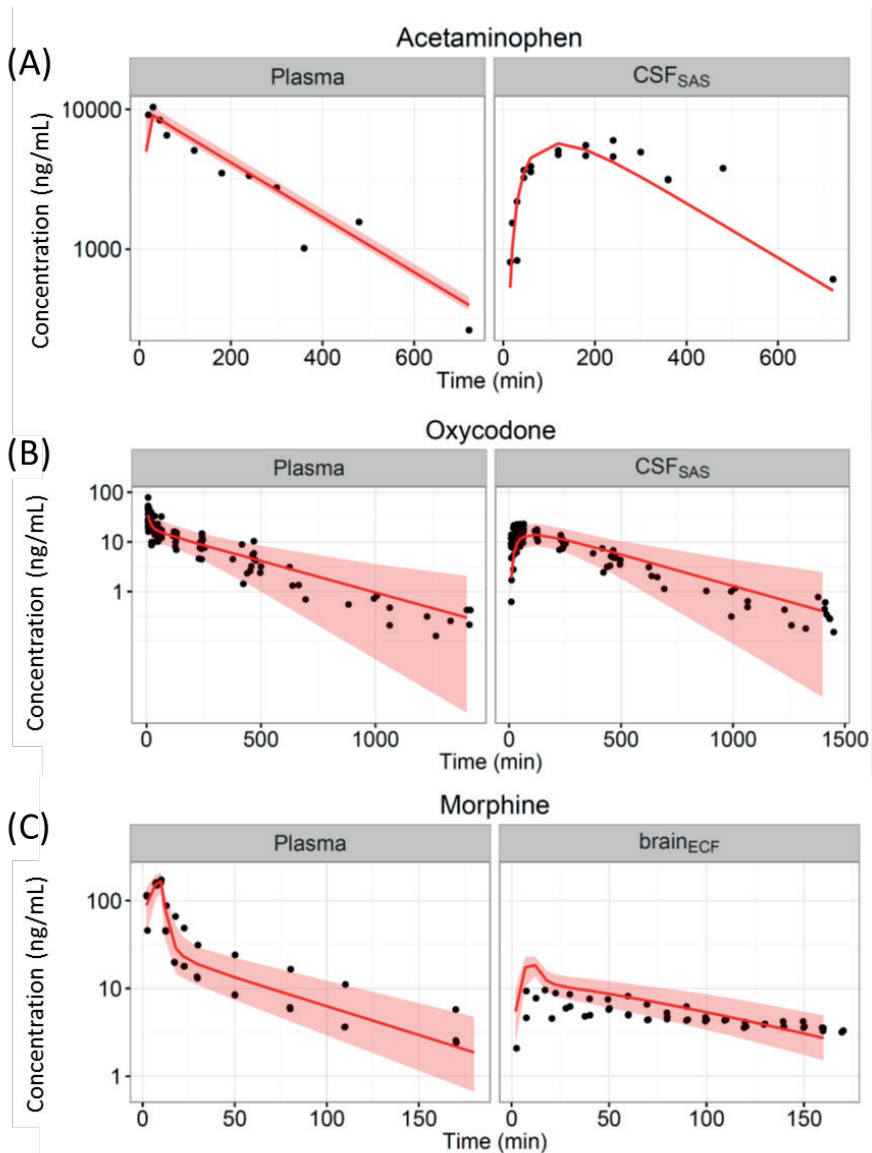


Figure 3. Predicted (red lines: median, shaded area is 95 % prediction interval) and observed (circles) concentration-time profiles in physiological CNS compartments. (A) Plasma and CSF in the lumbar region (CSF_{SAS_LUMBAR}) data for acetaminophen which were obtained from both healthy subjects and patients with nerve-root compression, (B) plasma and CSF_{SAS_LUMBAR} data for oxycodone which were obtained from patients undergoing elective gynecological surgery and (C) plasma and $brain_{ECF}$ data for morphine which were obtained from the uninjured side of the brain in traumatic brain injury (TBI) patients. The x-axis represents the time in minutes and the y-axis represents the concentration in ng/mL.

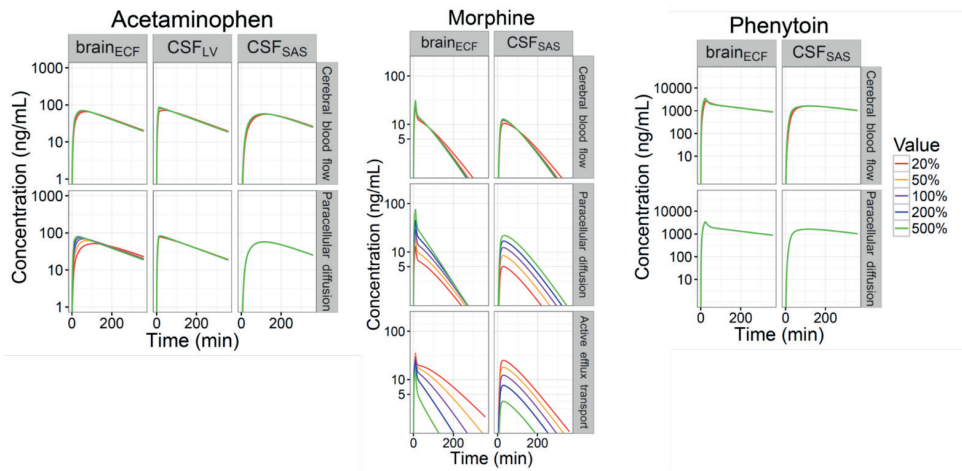


Figure 4. Simulation of the concentration-time profiles for acetaminophen, morphine and phenytoin using the human CNS PBPK model. The values of CBF, paracellular diffusion and an influence of active transports (if applicable) were varied within the range of 20-500% of their original values (colors). The plots were stratified by the CNS compartments (panels). The x-axis represents the time in minutes and the y-axis represents the concentration in ng/mL.

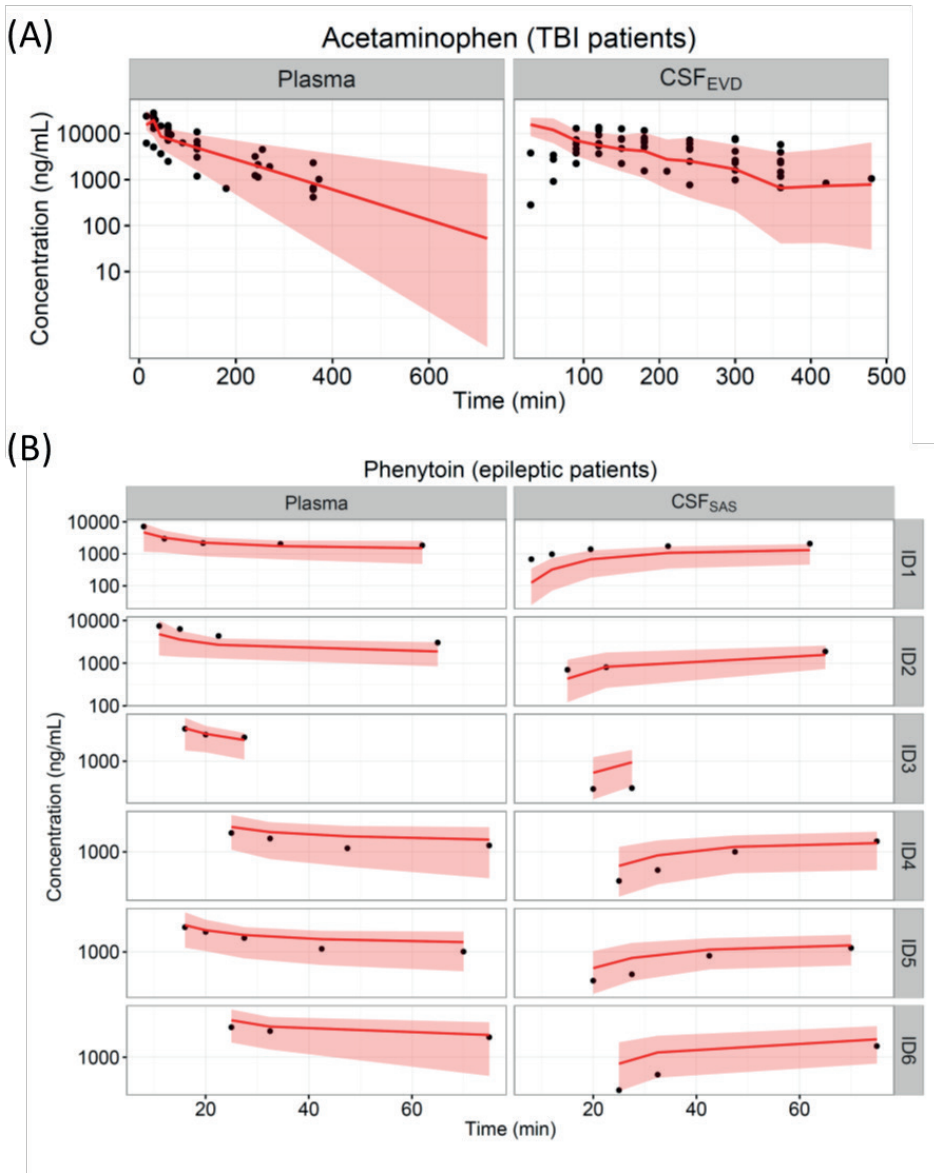


Figure 5. Model prediction (red lines: median, shaded area is 95% prediction interval) versus concentration-time profiles (circles) for each pathophysiological condition. (A) Acetaminophen data was obtained from plasma and CSF in the lateral ventricle collected by extra-ventricular drainage (CSF_{EVD}) from traumatic brain injury (TBI) patients, (B) phenytoin data was obtained from plasma and CSF in the lumbar region (CSF_{SAS_LUMBAR}) from epileptic patients. The x-axis represents the time in minutes and the y-axis represents the concentration in ng/mL.

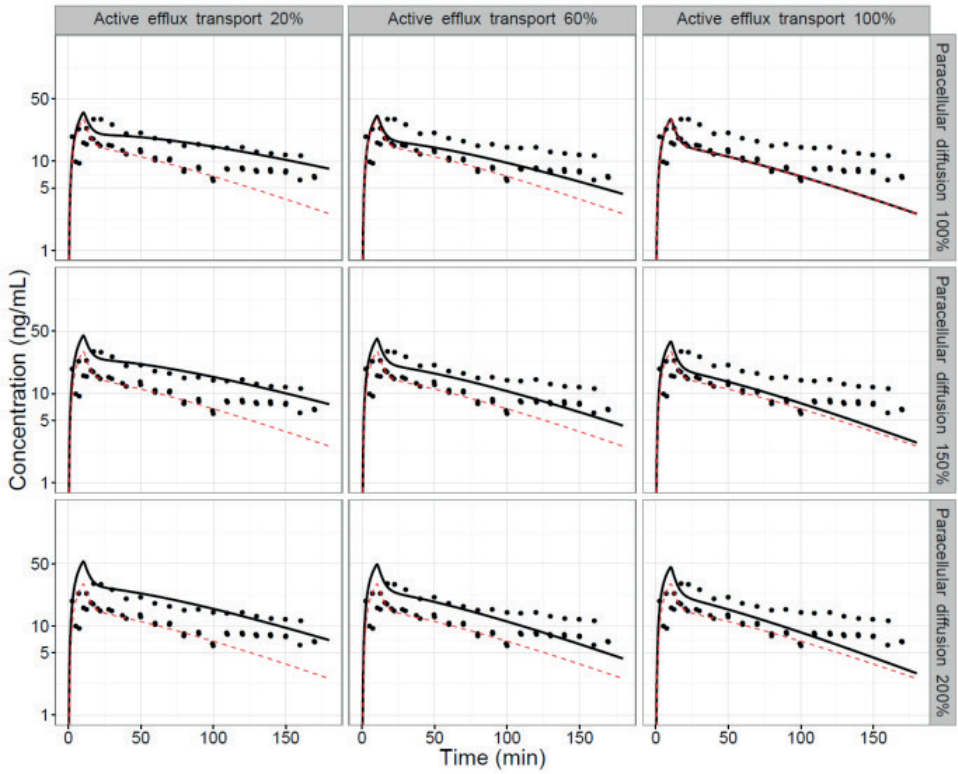


Figure 6. Model prediction (black lines) versus concentration-time profiles (circles) for morphine in brain_{ECF} in TBI patients. The plots were stratified by the change in the values of the system-specific parameters. The red dotted lines were the model predicted concentration-time profile for morphine in brain_{ECF} in healthy subjects. The x-axis represents the time in minutes and the y-axis represents the concentration in ng/mL.

Table III. Drug-specific parameters of the PBPK model

		Acetaminophen	Oxycodone	Morphine	Phenytoin
Drug specific parameters					
Transmembrane permeability	cm/min	1.1*10 ⁻⁴	3.5*10 ⁻⁴	2.5*10 ⁻⁴	0.0077
Aqueous diffusivity coefficient (Paracellular diffusion)	cm ² /min	4.6*10 ⁻⁴	3.3*10 ⁻⁴	3.4*10 ⁻⁴	3.6*10 ⁻⁴
AF	AFin1	1	2.3	1	1
	AFin2	1	1	1	1
	AFin3	1	1	1	1
	AFout1	1	1	6.6	1
	AFout2	1	1.9	13	1
	AFout3	1	2.3	16	1
Free fraction					
fu,p		0.85	0.59	0.11	0.13
fu,b		-	0.39 (72)	0.45 (72)	-
Physicochemical properties					
Molecular weight		151	315	285	252
log P		0.5	0.3	0.9	2.5
pKa (Acid)		9.5	13.6	10.3	9.5
pKa (Base)		-4.4	8.2	9.1	-9.0
Charge class		Neutral	Base	Base	Neutral

AF, asymmetry factor

AFin1-3 and AFout1-3 were converted from the rat AFs or obtained from *in vitro* study.

Table IV. Parameters derived using system-specific and drug-specific parameters in the PBPK model

Parameter	Unit	Acetaminophen	Oxycodone	Morphine	Phenytoin
Q_{BBB_in}	mL/min	72	120	64	510
Q_{BBB_out}	mL/min	72	68	130	510
Q_{t_BBB}	mL/min	6.5	21	15	460
Q_{p_BBB}	mL/min	66	47	50	52
PHF1		1.0	0.82	0.80	1.0
Q_{BCSFB1_in}	mL/min	57	47	46	190
Q_{BCSFB1_out}	mL/min	57	46	98	190
Q_{t_BCSFB1}	mL/min	2.0	6.6	4.7	140
Q_{p_BCSFB1}	mL/min	55	39	41	43
PHF2		1.0	0.82	0.80	1.0
Q_{BCSFB2_in}	mL/min	57	47	46	190
Q_{BCSFB2_out}	mL/min	57	46	98	190
Q_{t_BCSFB2}	mL/min	2.0	6.6	4.7	140
Q_{p_BCSFB2}	mL/min	55	39	41	43
PHF3		1.0	0.82	0.80	1.0
Q_{BCM_in}	mL/min	250	650	461	18000
Q_{BCM_out}	mL/min	250	360	230	18000
PHF4		1.0	0.82	0.80	1.0
PHF5		1.0	0.43	0.40	1.0
Q_{LYSO_in}	mL/min	120	170	120	8800
Q_{LYSO_out}	mL/min	130	1.8	1.2	8900
PHF6		1.0	0.43	0.40	1.0
PHF7		1.0	0.0046	0.0041	1.0
BF		-	0.01	1	-

$$Q_{BBB_in} = Q_{p_BBB} + Q_{t_BBB} * A_{Fin1}, Q_{BBB_out} = (Q_{p_BBB} + Q_{t_BBB} * A_{Fout1}) * PHF1,$$

$$Q_{p_BBB} = (\text{Aqueous diffusivity coefficient}/\text{Width}_{BBB}) * SA_{BBBp},$$

$$Q_{t_BBB} = 1/2 * \text{Transmembrane permeability} * SA_{BBBt},$$

$$Q_{BCSFB1_in} = Q_{p_BCSFB1} + Q_{t_BCSFB1} * A_{Fin2},$$

$$Q_{BCSFB1_out} = (Q_{p_BCSFB1} + Q_{t_BCSFB1} * A_{Fout2}) * PHF2,$$

$$Q_{p_BCSFB1} = (\text{Aqueous diffusivity coefficient}/\text{Width}_{BCSFB1}) * SA_{BCSFB1p},$$

$$Q_{t_BCSFB1} = 1/2 * \text{Transmembrane permeability} * SA_{BCSFB1t},$$

$$Q_{BCSFB2_in} = Q_{p_BCSFB2} + Q_{t_BCSFB2} * A_{Fin3},$$

$$Q_{BCSFB2_out} = (Q_{p_BCSFB2} + Q_{t_BCSFB2} * A_{Fout3}) * PHF3,$$

$$Q_{p_BCSFB2} = (\text{Aqueous diffusivity coefficient}/\text{Width}_{BCSFB2}) * SA_{BCSFB2p},$$

$$Q_{t_BCSFB2} = 1/2 * \text{Transmembrane permeability} * SA_{BCSFB2t},$$

$$Q_{BCM_in} = \text{Transmembrane permeability} * SA_{BCM} * PHF4,$$

$$Q_{BCM_out} = \text{Transmembrane permeability} * SA_{BCM} * PHF5$$

$$Q_{LYSO_in} = \text{Transmembrane permeability} * SA_{LYSO} * PHF6$$

$$Q_{LYSO_out} = \text{Transmembrane permeability} * SA_{LYSO} * PHF7$$

PHF1, PHF2, PHF3, PHF4, PHF5, PHF6, and PHF7 were calculated from the pKa of each compound and pH of the respective compartment.

BF was calculated from the Kp of each compound.

DISCUSSION

We developed a human CNS PBPK model to predict unbound drug PK of four model compounds in multiple CNS compartments. Under physiological CNS conditions, good predictions of observed human data were achieved within a 1.6-fold error. Furthermore, the model showed its ability to be used for building a better understanding of the key system properties that may explain the changes on drug concentration-time profiles under pathophysiological CNS conditions.

The human CNS PBPK model can be applied to any (existing or new) compounds once the physicochemical properties and information on the involvement of active transporters at the BBB and the BCSFB are available. Such information can be obtained from *in silico* predictions and/or *in vitro* studies.

The model uses plasma PK data as input to build a plasma PK model. In our study we either used plasma PK models that have been published or we developed the plasma PK model separately on the basis of existing plasma PK data. It should be noted that even in the absence of a plasma PK model or data, the CNS PBPK model can be used in conjunction with plasma PK simulations by using the existing whole-body PBPK platforms. Thus, the human CNS PBPK model does not require any *in vivo* data to predict unbound drug PK at target-site in the human CNS.

Gathering as much information as possible about unbound drug PK in the CNS is important to improve CNS drug development and CNS drug treatment, because it is the driver for drug-target binding kinetics and therewith for the drug effect profile. In contrast to the *ex vivo* techniques, such as brain homogenate and brain slicing techniques, as well as *in silico* approaches like quantitative structure-activity relationship models (73,74) that can provide information on unbound concentrations in the brain at steady state conditions, the CNS PBPK model predicts the unbound drug concentration time course. This is an important improvement since even during chronic dosing, variations in drug concentrations will still be present and may influence the target occupancy-time profile (75).

The human CNS PBPK model allows prediction of the unbound drug PK in multiple physiologically relevant CNS compartments. This is crucial as the PK profiles in different CNS compartments are known to be different, even for drugs that are not subjected to active transport (9). Moreover, the model could be used to investigate the impact on PK profiles in the different CNS compartments as a result of pathological processes, which have shown to be drug-dependent as well as CNS compartment-dependent (**Figure**

5 and 6). To our best knowledge, such integration of multiple aspects has not been reported earlier, and it will substantially contribute to an increased insight into CNS PK changes in pathological conditions in relation to the CNS effects.

A key feature of drug transport across the BBB and BCSFB is the contribution of active transporters. In PBPK modeling, expression levels and activity of each active transporter should ideally be separately incorporated. The major transporters such as P-gp and MRP are investigated well with regard to their inter-species differences of expression levels and transporters activity; however, such information is currently lacking for the other transporters (56,76).

Therefore, in our human CNS PBPK model, instead of using information on individual transporters, we used the “net contribution of the active transport” approach. This is a useful approach in situations where active transporters, which have not yet been widely investigated, are involved in the process of drug exchange at the BBB/BCSFB. In this study, we investigated a method to convert the “net contribution of the active transport (AFs)” at the BBB and BCSFB from rat to human, or obtain it from *in vitro* studies. We propose a workflow and decision tree to derive human “net contribution of the active transport (AFs)” (**Figure 2**).

In the rat PBPK model, we derived the “net contribution of the active transport (AFs)” from K_{puu} values (15). The translation method of AFs values from rat to human depends on the available information about the transporters involved in the processes. If the existing literature information is not sufficient to support the conversion of the rat AFs to human AFs, we proposed alternative methods to obtain human AFs directly from *in vitro* study using preferably human brain endothelial cells, such as hCMEC/D3 cells. Thus, either way, theoretically we do not need any *in vivo* data to obtain human AFs.

We have shown the potential of the model to be adapted according to literature information of pathophysiological changes and to explore the impact of the pathophysiological changes on PK profiles in each CNS compartment. For PK data for acetaminophen in CSF_{EVD} under TBI condition and PK data for phenytoin in CSF_{SAS_LUMBAR} under epileptic conditions, the impact of the conditions did not lead to significant alterations of CNS PK, hence no changes to the model were needed to obtain reasonable predictions. For morphine, the simulations showed that the model could describe the drug concentration in $brain_{ECF}$ in TBI patients if the paracellular diffusion at the BBB and BCSFB was increased by more than 50% and AFs at the BBB and BCSFB were decreased by more than 40%. Our findings align with the reported 40% decrease in expression of P-gp in TBI patients (67). This demonstrates how the model could provide quantitative

mechanistic insights of clinically observed alterations in CNS PK which are supported by additional external evidence. In the future, additional human data, for example from the accessible CSF lumbar region, can provide further information to validate the model in other pathophysiological conditions, and can better inform the human CNS PBPK model about what system-specific parameter values has actually changed or how much the system-specific parameter values need to be adjusted.

Due to the lack of information for the drug dispersion rate in the CSF, we used allometric scaling of the drug dispersion rate in rats using body weight to obtain the drug dispersion rate for humans. Since the drug dispersion rate may be different depending on the physiological components such as the length of spine and size of the tube of spine, an allometric scaling can be considered as an appropriate approach to scale the value among species. In this study, the average drug dispersion rate value in rat for the nine compounds was used for the scaling (19). At least for acetaminophen, oxycodone, morphine and phenytoin, the average drug dispersion rate was sufficient to capture the PK profiles of the compounds in the CNS. However, the drug dispersion rate may depend on not only the physiological components (which have already been taken into account by the allometric scaling), but also on the physicochemical properties such as molecular weight and lipophilicity. Therefore, further investigations are needed to optimize the drug dispersion rate for each compound in human.

CONCLUSIONS

A human CNS PBPK model was developed to predict the concentration-time profiles of four model compounds in human CNS compartments. All model parameters were either derived from *in silico* predictions, literature data or based on *in vitro* information. Therefore, the model can provide the concentration-time profiles in multiple physiologically relevant compartments in human CNS without the need of *in vivo* PK data. We demonstrated that the model could predict the brain_{ECF} and CSF_{SAS_LUMBAR} concentrations-time profiles under physiological CNS conditions. We also showed how the model can provide quantitative understanding of the impact of pathophysiological conditions on PK profiles in each CNS location. This human CNS PBPK model provides the basis to link CNS PK with drug-target binding kinetics and the biological effect(s) of the drug. As such, the developed model will have a substantial role in the selection of CNS drug candidates, in the prediction of target-site concentrations in humans, and to support the assessment of drug efficacy and safety in the early stage of the drug development.

REFERENCES

1. Arrowsmith J, Miller P. Trial Watch: Phase II and Phase III attrition rates 2011–2012. *Nat Rev Drug Discov.* 2013;12(8):569–569.
2. Danhof M, de Jongh J, de Lange ECM, Della Pasqua O, Ploeger BA, Voskuyl RA. Mechanism-Based Pharmacokinetic-Pharmacodynamic Modeling: Biophase Distribution, Receptor Theory, and Dynamical Systems Analysis. *Annu Rev Pharmacol Toxicol.* 2007;47(1):357–400.
3. Westerhout J, Danhof M, de Lange ECM. Preclinical Prediction of Human Brain Target Site Concentrations : Considerations in Extrapolating to the Clinical Setting. *J Pharm Sci.* 2011;100(9):3577–93.
4. Deo AK, Theil F-P, Nicolas J-M. Confounding parameters in preclinical assessment of blood-brain barrier permeation: an overview with emphasis on species differences and effect of disease states. *Mol Pharm.* 2013;10(5):1581–95.
5. Yamamoto Y, Danhof M, de Lange ECM. Microdialysis : the Key to Physiologically Based Model Prediction of Human CNS Target Site Concentrations. *AAPS J.* 2017;19(4):891–909.
6. Kalvass JC, Maurer TS. Influence of nonspecific brain and plasma binding on CNS exposure: Implications for rational drug discovery. *Biopharm Drug Dispos.* 2002;23(8):327–38.
7. Friden M, Gupta A, Antonsson M, Bredberg U, Hammarlund-Udenaes M. In Vitro Methods for Estimating Unbound Drug Concentrations in the Brain Interstitial and Intracellular Fluids. *Drug Metab Dispos.* 2007;35:1711–9.
8. de Lange ECM, Danhof M, de Boer AG, Breimer DD. Critical factors of intracerebral microdialysis as a technique to determine the pharmacokinetics of drugs in rat brain. *Brain Res.* 1994;666(1):1–8.
9. Westerhout J, Ploeger B, Smeets J, Danhof M, de Lange ECM. Physiologically based pharmacokinetic modeling to investigate regional brain distribution kinetics in rats. *AAPS J.* 2012;14(3):543–53.
10. Westerhout J, Smeets J, Danhof M, de Lange ECM. The impact of P-gp functionality on non-steady state relationships between CSF and brain extracellular fluid. *J Pharmacokinet Pharmacodyn.* 2013;40(3):327–42.
11. Westerhout J, van den Berg D-J, Hartman R, Danhof M, de Lange ECM. Prediction of methotrexate CNS distribution in different species - Influence of disease conditions. *Eur J Pharm Sci.* 2014;57:11–24.
12. Dresel S, Tatsch K, Dahme I, Mager T, Scherer J, Hahn K. Iodine-123-Iodobenzamide SPECT assessment of dopamine D2 receptor occupancy in risperidone treated schizophrenia patients. *J Nucl Med.* 1998;39(7):1138–42.
13. Mamo D, Kapur S, Shammi CM, Papatheodorou G, Mann S, Therrien F, et al. A PET Study of Dopamine D2 and Serotonin 5-HT2 Receptor Occupancy in Patients with Schizophrenia Treated with Therapeutic Doses of Ziprasidone. *Am J Psychiatry.* 2004;161(5):818–25.

14. Neuwelt E, Abbott NJ, Abrey L, Banks WA, Blakley B, Davis T, et al. Strategies to advance translational research into brain barriers. *Lancet Neurol.* 2008;7(1):84–96.
15. Yamamoto Y, Väilitalo PA, Huntjens DR, Proost JH, Vermeulen A, Krauwinkel W, et al. Predicting drug concentration-time profiles in multiple relevant CNS compartments using a comprehensive physiologically based pharmacokinetic model. in press. *CPT Pharmacometrics Syst Pharmacol.* 2017. In press
16. Beal S, Sheiner L, Boeckmann A, Bauer R. *NONMEM User's Guides.* Icon Development Solutions, Ellicott City. 2010.
17. Bannwarth B, Netter P, Lopicque F, Gillet P, Péré P, Boccard E, et al. Plasma and cerebrospinal fluid concentrations of paracetamol after a single intravenous dose of propacetamol. *Br J Clin Pharmacol.* 1992;34(1):79–81.
18. Singla NK, Parulan C, Samson R, Hutchinson J, Bushnell R, Beja EG, et al. Plasma and Cerebrospinal Fluid Pharmacokinetic Parameters After Single-Dose Administration of Intravenous, Oral, or Rectal Acetaminophen. *Pain Pract.* 2012;12(7):523–32.
19. Yamamoto Y, Väilitalo PA, van den Berg D-J, Hartman R, van den Brink W, Wong YC, et al. A Generic Multi-Compartmental CNS Distribution Model Structure for 9 Drugs Allows Prediction of Human Brain Target Site Concentrations. *Pharm Res.* 2017;34(2):333–51.
20. Gazzard B, Ford-Hutchinson A, Smith M, Williams R. The binding of paracetamol to plasma proteins of man and pig. *J Pharm Pharmacol.* 1973;25(12):964–7.
21. Kokki M, Väilitalo P, Kuusisto M, Ranta VP, Raatikainen K, Hautajärvi H, et al. Central nervous system penetration of oxycodone after intravenous and epidural administration. *Br J Anaesth.* 2014;112(1):133–40.
22. Dean M. Opioids in renal failure and dialysis patients. *J Pain Symptom Manage.* 2004;28(5):497–504.
23. Kirvela M, Lindgren L, Seppala T, Olkkola KT. The pharmacokinetics of oxycodone in uremic patients undergoing renal transplantation. *J Clin Anesth.* 1996;8(1):13–8.
24. Ederoth P, Tunblad K, Bouw R, Lundberg CJ, Ungerstedt U, Nordstrom CH, et al. Blood-brain barrier transport of morphine in patients with severe brain trauma. *Br J Clin Pharmacol.* 2003;57(4):427–35.
25. Bouw R, Ederoth P, Lundberg J, Ungerstedt U, Nordström C-H, Hammarlund-Udenaes M. Increased blood-brain barrier permeability of morphine in a patient with severe brain lesions as determined by microdialysis Case report. *Acta Anaesthesiol Scand.* 2001;45(3):390–2.
26. Wilder BJ, Ramsay RE, Willmore LJ, Feussner GF, Perchalski RJ, Shumate JB. Efficacy of intravenous phenytoin in the treatment of status epilepticus: Kinetics of central nervous system penetration. *Ann Neurol.* 1977;1(6):511–8.
27. Fraser DG, Ludden TM, Evens RP, Sutherland EW. Displacement of phenytoin from plasma binding sites by salicylate. *Clin Pharmacol Ther.* 1980;27(2):165–9.

28. Nguyen T-H-T, Mouksassi M-S, Holford N, Al-Huniti N, Freedman I, Hooker AC, et al. Model evaluation of continuous data pharmacometric models: Metrics and graphics. *CPT pharmacometrics Syst Pharmacol*. 2016;(1):1–20.
29. Dekaban A, Sadowsky D. Changes in brain weights during the span of human life: relation of brain weights to body heights and body weights. *Ann Neurol*. 1978;4(4):345–56.
30. Begley DJ, Bradbury MW, Kreuter J. *The Blood-Brain Barrier and Drug Delivery to the CNS*. New York: Marcel Dekker, Inc. 2000.
31. Thorne RG, Hrabe S, Nicholson C, Robert G. Diffusion of Epidermal Growth Factor in Rat Brain Extracellular Space Measured by Integrative Optical Imaging. *J Neurophysiol*. 2004;92(6):3471–81.
32. Sakka L, Coll G, Chazal J. Anatomy and physiology of cerebrospinal fluid. *Eur Ann Otorhinolaryngol Head Neck Dis*. 2011 Dec;128(6):309–16.
33. Pardridge WM. Drug transport in brain via the cerebrospinal fluid. *Fluids Barriers CNS*. 2011;8(7):1–7.
34. Robertson EG. Developmental defects of the cisterna magna and dura mater. *J Neurol Neurosurg Psychiatry*. 1949;12(1):39–51.
35. Adam R, Greenberg JO. The mega cisterna magna. *J Neurosurg*. 1978;48(2):190–2.
36. Stange K, Greitz M, Ingvar T, Hindmarsh T, Sollevi A. Global cerebral blood flow during infusion of adenosine in humans: assessment by magnetic resonance imaging and positron emission tomography. *Acta Physiol Scand*. 1997;160(2):117–22.
37. Ito H, Inoue K, Goto R, Kinomura S, Taki Y, Okada K, et al. Database of normal human cerebral blood flow measured by SPECT: I. Comparison between I-123-IMP, Tc-99m-HMPAO, and Tc-99m-ECD as referred with O-15 labeled water PET and voxel-based morphometry. *Ann Nucl Med*. 2006;20(2):131–8.
38. Fagerholm U. The highly permeable blood-brain barrier: an evaluation of current opinions about brain uptake capacity. *Drug Discov Today*. 2007;12(23–24):1076–82.
39. Kimelberg HK. Water homeostasis in the brain: basic concepts. *Neuroscience*. 2004 Jan;129(4):851–60.
40. Wong AD, Ye M, Levy AF, Rothstein JD, Bergles DE, Searson PC. The blood-brain barrier: an engineering perspective. *Front Neuroeng*. 2013;6:1–22.
41. Abbott NJ, Patabendige AAK, Dolman DEM, Yusof SR, Begley DJ. Structure and function of the blood-brain barrier. *Neurobiol Dis*. 2010;37(1):13–25.
42. Rengachary SS, Ellenbogen RG. *Principles of Neurosurgery*. Edinburgh: Elsevier Mosby; 2005.
43. Cornford EM, Hyman S. Localization of brain endothelial luminal and abluminal transporters with immunogold electron microscopy. *NeuroRx*. 2005;2(1):27–43.
44. Monteiro J, Goraksha S. 'ROSE concept' of fluid management: Relevance in neuroanaesthesia and neurocritical care. *J Neuroanaesth Crit Care*. 2017;4(1):10.

45. Loryan I, Sinha V, Mackie C, van Peer A, Drinkenburg W, Vermeulen A, et al. Mechanistic Understanding of Brain Drug Disposition to Optimize the Selection of Potential Neurotherapeutics in Drug Discovery. *Pharm Res.* 2014;32(8):2203–19.
46. Trapa PE, Belova E, Liras JL, Scott DO, Steyn SJ. Insights from an Integrated Physiologically Based Pharmacokinetic Model for Brain Penetration. *J Pharm Sci.* 2016;105(2):965–71.
47. Hardin J, Bertoni GP, Kleinsmith LJ. *Becker's World of the Cell*, 8th Edition. San Francisco: Pearson Education Inc.; 2011.
48. Mabondzo A, Bottlaender M, Guyot AC, Tsaouin K, Deverre JR, Balimane P V. Validation of in vitro cell-based human blood-brain barrier model using clinical positron emission tomography radioligands to predict in vivo human brain penetration. *Mol Pharm.* 2010;7(5):1805–15.
49. Okura T, Hattori A, Takano Y, Sato T, Hammarlund-udenaes M, Terasaki T, et al. Involvement of the Pylramine Transporter, a Putative Organic Cation Transporter, in Blood-Brain Barrier Transport of Oxycodone. *Drug Metab Dispos.* 2008;36(10):2005–13.
50. Shimomura K, Okura T, Kato S, Couraud P-O, Schermann J-M, Terasaki T, et al. Functional expression of a proton-coupled organic cation (H⁺/OC) antiporter in human brain capillary endothelial cell line hCMEC/D3, a human blood-brain barrier model. *Fluids Barriers CNS.* 2013;10(1):8.
51. Kitamura A, Okura T, Higuchi K, Deguchi Y. Cocktail-Dosing Microdialysis Study to Simultaneously Assess Delivery of Multiple Organic-Cationic Drugs to the Brain. *J Pharm Sci.* 2016;105(2):935–40.
52. Tunblad K, Jonsson EN, Hammarlund-udenaes M. Morphine Blood-Brain Barrier Transport Is Influenced by Probenecid Co-Administration. 2003;20(4):618–23.
53. Letrent SP, Polli JW, Humphreys JE, Pollack GM, Brouwer KR, Brouwer KLR. P-glycoprotein-mediated transport of morphine in brain capillary endothelial cells. *Biochem Pharmacol.* 1999;58(6):951–7.
54. Groenendaal D, Freijer J, de Mik D, Bouw MR, Danhof M, de Lange ECM. Population pharmacokinetic modelling of non-linear brain distribution of morphine: influence of active saturable influx and P-glycoprotein mediated efflux. *Br J Pharmacol.* 2007;151(5):701–12.
55. Wandel C, Kim R, Wood M, Wood A. Interaction of morphine, fentanyl, sufentanil, alfentanil, and loperamide with the efflux drug transporter P-glycoprotein. *Anesthesiology.* 2002;96(4):913–20.
56. Aday S, Cecchelli R, Dehouck MP, Ferreira L. Stem Cell-Based Human Blood-Brain Barrier Models for Drug Discovery and Delivery. *Trends Biotechnol.* 2016;34(5):382–93.
57. Feng B, Mills JB, Davidson RE, Mireles RJ, Janiszewski JS, Troutman MD, et al. In vitro P-glycoprotein assays to predict the in vivo interactions of P-glycoprotein with drugs in the central nervous system. *Drug Metab Dispos.* 2008;36(2):268–75.
58. Potschka H, Löscher W. In vivo evidence for P-glycoprotein-mediated transport of phenytoin at the blood-brain barrier of rats. *Epilepsia.* 2001;42(10):1231–40.

59. Potschka H, Löscher W. Multidrug resistance-associated protein is involved in the regulation of extracellular levels of phenytoin in the brain. *Neuroreport*. 2001;12(11):2387–9.
60. Dickens D, Yusof SR, Abbott NJ, Weksler B, Romero IA, Couraud PO, et al. A Multi-System Approach Assessing the Interaction of Anticonvulsants with P-gp. *PLoS One*. 2013;8(5).
61. Zhang C, Kwan P, Zuo Z, Baum L. In vitro concentration dependent transport of phenytoin and phenobarbital, but not ethosuximide, by human P-glycoprotein. *Life Sci*. 2010;86(23–24):899–905.
62. Luna-Tortós C, Fedrowitz M, Löscher W. Evaluation of transport of common antiepileptic drugs by human multidrug resistance-associated proteins (MRP1, 2 and 5) that are overexpressed in pharmaco-resistant epilepsy. *Neuropharmacology*. 2010;58(7):1019–32.
63. Baltés S, Gastens AM, Fedrowitz M, Potschka H, Kaefer V, Löscher W. Differences in the transport of the antiepileptic drugs phenytoin, levetiracetam and carbamazepine by human and mouse P-glycoprotein. *Neuropharmacology*. 2007;52(2):333–46.
64. Li M, Yuan H, Li N, Song G, Zheng Y, Baratta M, et al. Identification of interspecies difference in efflux transporters of hepatocytes from dog, rat, monkey and human. *Eur J Pharm Sci*. 2008;35(1–2):114–26.
65. Greve MW, Zink BJ. Pathophysiology of traumatic brain injury. *Mt Sinai J Med*. 2009;76(2):97–104.
66. Chodobski A, Zink BJ, Szmydynger-Chodobska J. Blood-Brain Barrier Pathophysiology in Traumatic Brain Injury. *Transl Stroke Res*. 2011;2(4):492–516.
67. Pop V, Sorensen DW, Kamper JE, Ajao DO, Murphy MP, Head E, et al. Early brain injury alters the blood-brain barrier phenotype in parallel with b-amyloid and cognitive changes in adulthood. *J Cereb Blood Flow Metab*. 2013;33:205–14.
68. Appel S, Duke ES, Martinez AR, Khan OI, Dustin IM, Reeves-Tyer P, et al. Cerebral blood flow and fMRI BOLD auditory language activation in temporal lobe epilepsy. *Epilepsia*. 2012;53(4):631–8.
69. Bednarczyk J, Lukasiuk K. Tight junctions in neurological diseases. *Acta Neurobiol Exp*. 2011;71(4):393–408.
70. Lazarowski A, Czornyj L, Lubienieki F, Girardi E, Vazquez S, D’Giano C. ABC transporters during epilepsy and mechanisms underlying multidrug resistance in refractory epilepsy. *Epilepsia*. 2007;48:140–9.
71. Löscher W, Potschka H. Role of multidrug transporters in pharmaco-resistance to antiepileptic drugs. *J Pharmacol Exp Ther*. 2002;301(1):7–14.
72. Ball K, Bouzom F, Scherrmann J-M, Walther B, Declèves X. Development of a physiologically based pharmacokinetic model for the rat central nervous system and determination of an in vitro-in vivo scaling methodology for the blood-brain barrier permeability of two transporter substrates, morphine and oxycodone. *J Pharm Sci*. 2012;101(11):4277–92.

73. Loryan I, Sinha V, Mackie C, van Peer A, Drinkenburg WH, Vermeulen A, et al. Molecular properties determining unbound intracellular and extracellular brain exposure of CNS drug candidates. *Mol Pharm*. 2015;12(2):520–32.
74. Chen H, Winiwarter S, Fridén M, Antonsson M, Engkvist O. In silico prediction of unbound brain-to-plasma concentration ratio using machine learning algorithms. *J Mol Graph Model*. 2011;29(8):985–95.
75. de Witte WEA, Danhof M, van der Graaf PH, de Lange ECM. In vivo Target Residence Time and Kinetic Selectivity: The Association Rate Constant as Determinant. *Trends Pharmacol Sci*. 2016;37(10):831–42.
76. Ohtsuki S, Ikeda C, Uchida Y, Sakamoto Y, Miller F, Glacial F, et al. Quantitative targeted absolute proteomic analysis of transporters, receptors and junction proteins for validation of human cerebral microvascular endothelial cell line hCMEC/D3 as a human blood-brain barrier model. *Mol Pharm*. 2013;10(1):289–96.
77. Avdeef A, Nielsen PE, Tsinman O. PAMPA - A drug absorption in vitro model: 11. Matching the in vivo unstirred water layer thickness by individual-well stirring in microtitre plates. *Eur J Pharm Sci*. 2004;22(5):365–74.
78. Grumetto L, Russo G, Barbato F. Immobilized Artificial Membrane HPLC Derived Parameters vs PAMPA-BBB Data in Estimating in Situ Measured Blood-Brain Barrier Permeation of Drugs. *Mol Pharm*. 2016;13(8):2808–16.
79. Berezhkovskiy LM. Volume of distribution at steady state for a linear pharmacokinetic system with peripheral elimination. *J Pharm Sci*. 2004;93(6):1628–40.
80. Poulin P, Theil F-P. Prediction of pharmacokinetics prior to in vivo studies. II. Generic physiologically based pharmacokinetic models of drug disposition. *J Pharm Sci*. 2002;91(5):1358–70.
81. Aanerud J, Borghammer P, Chakravarty MM, Vang K, Rodell AB, Jónsdóttir KY, et al. Brain energy metabolism and blood flow differences in healthy aging. *J Cereb Blood Flow Metab*. 2012;32(7):1177–87.
82. Serot JM, Béné MC, Foliguet B, Faure GC. Altered choroid plexus basement membrane and epithelium in late-onset Alzheimer's disease: An ultrastructural study. *Ann N Y Acad Sci*. 1997;826:507–9.
83. Shimada A, Hasegawa-Ishii S. Senescence-accelerated Mice (SAMs) as a Model for Brain Aging and Immunosenescence. *Aging Dis*. 2011;2(5):414–35.
84. Silverberg GD, Miller MC, Messier AA, Majmudar S, Machan JT, Donahue JE, et al. Amyloid deposition and influx transporter expression at the blood-brain barrier increase in normal aging. *J Neuropathol Exp Neurol*. 2010;69(1):98–108.
85. Palmer JC, Baig S, Kehoe PG, Love S. Endothelin-converting enzyme-2 is increased in Alzheimer's disease and up-regulated by Abeta. *Am J Pathol*. 2009;175(1):262–70.
86. Bowman G, Quinn J. Alzheimer's disease and the blood-brain barrier: past, present and future. *Aging health*. 2008;4(1):47–57.

87. Cipolla MJ, Sweet JG, Chan S-L. Cerebral vascular adaptation to pregnancy and its role in the neurological complications of eclampsia. *J Appl Physiol.* 2011;110(2):329–39.
88. Dutheil F, Jacob A, Dauchy S, Beaune P, Scherrmann J-M, Declèves X, et al. ABC transporters and cytochromes P450 in the human central nervous system: influence on brain pharmacokinetics and contribution to neurodegenerative disorders. *Expert Opin Drug Metab Toxicol.* 2010;6(10):1161–74.
89. Hsu JL, Jung TP, Hsu CY, Hsu WC, Chen YK, Duann JR, et al. Regional CBF changes in Parkinson's disease: A correlation with motor dysfunction. *Eur J Nucl Med Mol Imaging.* 2007;34(9):1458–66.
90. van Vliet EA, Araújo SDC, Redeker S, van Schaik R, Aronica E, Gorter JA. Blood-brain barrier leakage may lead to progression of temporal lobe epilepsy. *Brain.* 2007;130(2):521–34.
91. Ingrisch M, Sourbron S, Morhard D, Ertl-Wagner B, Kümpfel T, Hohlfeld R, et al. Quantification of Perfusion and Permeability in Multiple Sclerosis. *Invest Radiol.* 2012;47(4):252–8.
92. Weiss N, Miller F, Cazaubon S, Couraud PO. The blood-brain barrier in brain homeostasis and neurological diseases. *Biochim Biophys Acta.* 2009;1788(4):842–57.

SUPPLEMENTARY MATERIAL

S1. Calculation for the drug-specific parameters in the model.

The drug-specific parameters in the model were calculated using the following equations.

Aqueous diffusivity coefficient. The aqueous diffusivity coefficient was calculated using the molecular weight of each compound with the following equation (77).

$$\log Daq = -4.113 - 0.4609 \times \log MW \quad (1)$$

where Daq is the aqueous diffusivity coefficient (in cm^2/s) and MW is the molecular weight (in g/mol).

Permeability. Transmembrane permeability was calculated using the $\log P$ of each compound with the following equation (78).

$$\log P_0^{\text{transcellular}} = 0.939 \times \log P - 6.210 \quad (2)$$

where $P_0^{\text{transcellular}}$ is the transmembrane permeability (in cm/s), $\log P$ is the *n*-octanol lipophilicity value.

Active transport. The impact of the net effect of active transporters on the drug exchange at the BBB and BCSFB was incorporated into the model using asymmetry factors (AFin1-3 and AFout1-3). The AFs were calculated from $K_{p,uu,brain_{ECP}}$, $K_{p,uu,CSF_{LV}}$ (unbound CSF_{LV} -to-plasma concentration ratio) and $K_{p,uu,CSF_{CM}}$ (unbound CSF_{CM} -to-plasma concentration ratio), such that they produced the same $K_{p,uu}$ values within the PBPK model at the steady state. The AFs were therefore dependent on both the $K_{p,uu}$ values and the structure and parameters of the PBPK model. If the $K_{p,uu}$ values were larger than 1 (i.e. net active influx), then AFin1, AFin2 and AFin3 were derived from $K_{p,uu,brain_{ECP}}$, $K_{p,uu,CSF_{LV}}$ and $K_{p,uu,CSF_{CM}}$ respectively, while AFout1-3 were fixed to 1. If the $K_{p,uu}$ values were smaller than 1 (i.e. net active efflux), then AFout1, AFout2 and AFout3 were derived from $K_{p,uu,brain_{ECP}}$, $K_{p,uu,CSF_{LV}}$ and $K_{p,uu,CSF_{CM}}$ respectively, while AFin1-3 were fixed to 1. In the analysis, $K_{p,uu,brain_{ECP}}$, $K_{p,uu,CSF_{LV}}$ and $K_{p,uu,CSF_{CM}}$ were derived from previous *in vivo* animal experiments (15). The steady state differential equations in the PBPK model were solved using the Maxima Computer Algebra System (<http://maxima.sourceforge.net>) to obtain algebraic solutions for calculating AFs from the $K_{p,uu}$ values.

S2. Calculation for the parameters using the system-specific and drug-specific parameters.

The parameters in the model were calculated using the following equations.

Passive diffusion across the brain barriers. Passive diffusion clearance at the BBB and BCSFB (Q_{BBB} and Q_{BCSFB} , respectively) was obtained from a combination of paracellular and transcellular diffusion, Q_p and Q_t , respectively (Eq.3).

$$Q_{BBB/BCSFB} (mL/min) = Q_{p_{BBB/BCSFB}} + Q_{t_{BBB/BCSFB}} \quad (3)$$

where $Q_{BBB/BCSFB}$ represents the passive diffusion clearance at the BBB/BCSFB, $Q_{p_{BBB/BCSFB}}$ represents the paracellular diffusion clearance at the BBB/BCSFB, and $Q_{t_{BBB/BCSFB}}$ represents the transcellular diffusion clearance at the BBB/BCSFB.

The paracellular diffusion clearance was calculated with the aqueous diffusivity coefficient (Daq), $Width_{BBB/BCSFB}$ and SA_{BBBp} or SA_{BCSFBp} using equation 4.

$$Q_{p_{BBB/BCSFB}} (mL/min) = \frac{Daq}{Width_{BBB/BCSFB}} \times SA_{BBBp/BCSFBp} \quad (4)$$

The transcellular diffusion clearance was calculated with the transmembrane permeability and SA_{BBBt} or SA_{BCSFBt} using equation 5.

$$Q_{t_{BBB/BCSFB}} (mL/min) = \frac{1}{2} * P_0^{transcellular} \times SA_{BBBt/BCSFBt} \quad (5)$$

where the factor 1/2 is the correction factor for passage over two membranes instead of one membrane in transcellular passage.

Active transport across the brain barriers. To take into account the net effect of the active transporters at the BBB and BCSFB, AFs were added on $Q_{t_{BBB/BCSFB}}$ (Eq.6 and 7).

$$Q_{BBB/BCSFB_in} (mL/min) = Q_{p_{BBB/BCSFB}} + Q_{t_{BBB/BCSFB}} * AF_{in} \quad (6)$$

$$Q_{BBB/BCSFB_out_withoutPHF} (mL/min) = Q_{p_{BBB/BCSFB}} + Q_{t_{BBB/BCSFB}} * AF_{out} \quad (7)$$

where $Q_{\text{BBB/BCSFB}_{\text{in}}}$ represents the drug transport clearance from brain_{MV} to $\text{brain}_{\text{ECF}}/\text{CSFs}$, and $Q_{\text{BBB/BCSFB}_{\text{out_withoutPHF}}}$ represents the drug transport clearance from $\text{brain}_{\text{ECF}}/\text{CSFs}$ to brain_{MV} without taking into account the pH-dependent kinetics (to be taken into account separately; see below).

Cellular and subcellular distribution. Passive diffusion at the BCM (Q_{BCM}) and at the lysosomal membrane (Q_{LYSO}) was described with the transmembrane permeability together with SA_{BCM} or SA_{LYSO} respectively (Eq.8 and 9).

$$Q_{\text{BCM}}(\text{mL}/\text{min}) = P_0^{\text{transcellular}} \times SA_{\text{BCM}} \quad (8)$$

$$Q_{\text{LYSO}}(\text{mL}/\text{min}) = P_0^{\text{transcellular}} \times SA_{\text{LYSO}} \quad (9)$$

where Q_{BCM} represents the passive diffusion clearance at the BCM, and Q_{LYSO} represents the passive diffusion clearance at the lysosomal membrane.

pH-dependent partitioning. We considered the differences in pH in plasma (pH 7.4) and in relevant CNS compartments, namely $\text{brain}_{\text{ECF}}$ (pH_{ECF} 7.3), CSF (pH_{CSF} 7.3), $\text{brain}_{\text{ICF}}$ (pH_{ICF} 7.0), and lysosomes (pH_{LYSO} 5.0) (Friden, 2011). The impact of pH differences on the passive diffusion clearance from $\text{brain}_{\text{ECF}}$ to brain_{MV} (PHF1), from CSF_{LV} to brain_{MV} (PHF2), from CSF_{TFV} to brain_{MV} (PHF3), from $\text{brain}_{\text{ECF}}$ to $\text{brain}_{\text{ICF}}$ (PHF4), from $\text{brain}_{\text{ICF}}$ to $\text{brain}_{\text{ECF}}$ (PHF5), from $\text{brain}_{\text{ICF}}$ to lysosomes (PHF6), and from lysosomes to $\text{brain}_{\text{ICF}}$ (PHF7) were described by pH-dependent factors, which were defined as the ratio of the un-ionized fraction of each compound at the pH in a particular compartment and the un-ionized fraction in plasma. The PHFs were calculated from the pKa of each compound and the pH of a particular compartment. The equations are developed using the classical Henderson-Hasselbalch equation (Henderson, 1908 and Henderson, 1908), and are based on the assumption that there is no active transport.

$$PHF_{\text{base}1} = PHF_{\text{base}4} = \frac{10^{\text{pKa}-7.4+1}}{10^{\text{pKa}-\text{pH}_{\text{ECF}}+1}} \quad (10)$$

$$PHF_{\text{base}2} = PHF_{\text{base}3} = \frac{10^{\text{pKa}-7.4+1}}{10^{\text{pKa}-\text{pH}_{\text{CSF}}+1}} \quad (11)$$

$$PHF_{\text{base}5} = PHF_{\text{base}6} = \frac{10^{\text{pKa}-7.4+1}}{10^{\text{pKa}-\text{pH}_{\text{ICF}}+1}} \quad (12)$$

$$PHF_{\text{base}7} = \frac{10^{\text{pKa}-7.4+1}}{10^{\text{pKa}-\text{pH}_{\text{LYSO}}+1}} \quad (13)$$

$$PHF_{acid1} = PHF_{acid4} = \frac{10^{7.4-pK_{a+1}}}{10^{pH_{ECF}-pK_{a+1}}} \quad (14)$$

$$PHF_{acid2} = PHF_{acid3} = \frac{10^{7.4-pK_{a+1}}}{10^{pH_{CSF}-pK_{a+1}}} \quad (15)$$

$$PHF_{acid5} = PHF_{acid6} = \frac{10^{7.4-pK_{a+1}}}{10^{pH_{ICF}-pK_{a+1}}} \quad (16)$$

$$PHF_{acid7} = \frac{10^{7.4-pK_{a+1}}}{10^{pH_{LYSO}-pK_{a+1}}} \quad (17)$$

where $PHF_{base1-7}$ are PHF1-7 for basic compounds, $PHF_{acid1-7}$ are PHF1-7 for acidic compounds, and 7.4 is the pH in the plasma compartment.

The impact of pH differences on the drug distribution among $brain_{ECF}$, CSF, $brain_{ICF}$ and lysosomes was added on Q_{BCM} and Q_{LYSO} using PHFs with the following equations 18-24, based on the assumption that the transport clearance is proportional to the un-ionized fraction of each compound.

$$Q_{BBB_{out}}(mL/min) = Q_{BBB_{out}_{withoutPHF}} \times PHF1 \quad (18)$$

$$Q_{BCSFB1_{out}}(mL/min) = Q_{BCSFB_{withoutPHF}} \times PHF2 \quad (19)$$

$$Q_{BCSFB2_{out}}(mL/min) = Q_{BCSFB_{withoutPHF}} \times PHF3 \quad (20)$$

$$Q_{BCM_{in}}(mL/min) = Q_{BCM} \times PHF4 \quad (21)$$

$$Q_{BCM_{out}}(mL/min) = Q_{BCM} \times PHF5 \quad (22)$$

$$Q_{LYSO_{in}}(mL/min) = Q_{LYSO} \times PHF6 \quad (23)$$

$$Q_{LYSO_{out}}(mL/min) = Q_{LYSO} \times PHF7 \quad (24)$$

where $Q_{BBB_{out}}$ represents the drug transport clearance from $brain_{ECF}$ to $brain_{MV}$, $Q_{BCSFB1_{out}}$ represents the drug transport clearance from CSF_{LV} to $brain_{MV}$, $Q_{BCSFB2_{out}}$ represents the drug transport clearance from CSF_{TFV} to $brain_{MV}$, $Q_{BCM_{in}}$ represents the drug transport clearance from $brain_{ECF}$ to $brain_{ICF}$ and $Q_{BCM_{out}}$ represents the drug transport clearance from $brain_{ICF}$ to $brain_{ECF}$, $Q_{LYSO_{in}}$ represents the drug transport clearance from $brain_{ICF}$ to lysosomes, and $Q_{BCM_{out}}$ represents the drug transport clearance from lysosomes to $brain_{ICF}$.

Drug binding. Drug binding to brain tissue components was taken into account in the model using a binding factor (BF) under the assumption that drug binding to the tissue happens instantly. The BF was calculated from Kp (total brain-to-plasma concentration ratio) by solving the BF that results in the same Kp value in the model, using the Maxima program as described above (**Supplementary Material S1**). The Kp for each compound was calculated using the compounds' log P, the composition of brain tissue and plasma, fu,p (free fraction in plasma) and fu,b (free fraction in brain) with the following equation (79).

$$Kp = \frac{[10^{\log P} \times (Vnlb + 0.3 \times Vphb) + 0.7 \times Vphb + Vwb / fu,b]}{[10^{\log P} \times (Vnlp + 0.3 \times Vphp)] + 0.7 \times Vphp + Vwp / fu,p} \quad (25)$$

where Vnlb, Vphb, Vwb, Vnlp, Vphp, and Vwp represent the rat volume fractions of brain neutral lipids (0.0392), brain phospholipids (0.0533), brain water (0.788), plasma neutral lipids (0.00147), plasma phospholipids (0.00083), and plasma water (0.96), respectively (80).

S3. Calculation for the active transport component of the overall permeability from *in vitro* data.

The asymmetry factors (AFs) can be derived from *In vitro* data such as efflux ratio data and cell uptake kinetics data (72).

Efflux ratio data. AFs can be derived from the information of apparent permeability (P_{app}) from apical to basolateral ($P_{app,A:B}$) and basolateral to apical ($P_{app,B:A}$), or the information of efflux ratio (ER). The active transport component of the overall permeability can be derived using the following equation (in this case, the active transporters mediate a net efflux of the drug).

$$CL_{eff,active} = (P_{app,B:A} - P_{app,A:B}) * SA_{BBB} * \text{scaling factor} \quad (26)$$

$$ER_{eff,active} = (P_{app,B:A} / P_{app,A:B}) \quad (27)$$

where the scaling factor is used to convert values obtained from *in vitro* experiments to *in vivo* BBB values.

Cell uptake kinetics data. AFs can be derived from the information of Vmax and Km. The active transport component of the overall permeability can be derived using the following equation (in this case, the active transporters mediate a net influx of the drug).

$$CL_{uptake} = \left(\frac{Km}{Vmax + C_{u,BM}} \right) * \text{the milligrams of protein per gram of brain} * \text{brain weight} \quad (28)$$

$$CL_{inf,active} = \left(CL_{uptake} - P_{passive} * SA_{BBB} * \left(1 - \frac{C_{u,BM}}{C_{u,Plasma}} \right) \right) * \text{scaling factor} \quad (29)$$

where $C_{u,BM}$ is free drug concentration in brain microvascular compartment, $C_{u,plasma}$ is free drug concentration in plasma compartment, $P_{passive}$ is passive permeability.

In the PBPK model, $CL_{eff,active}$, $ER_{eff,active}$, $CL_{inf,active}$ and $ER_{inf,active}$ can be derived using the following equation :

$$CL_{eff,active} = Qt_{BBB} * (PHF1 * AFout1 - 1) + Qp_{BBB} * (PHF1 - 1) \quad (30)$$

$$ER_{eff,active} = \frac{(Qt_{BBB} * AFout1 + Qp_{BBB}) * PHF1}{(Qt_{BBB} + Qp_{BBB})} \quad (31)$$

$$CL_{inf,active} = Qt_{BBB} * (AFin1 - PHF1) + Qp_{BBB} * (1 - PHF1) \quad (32)$$

$$ER_{inf,active} = \frac{(Qt_{BBB} + Qp_{BBB}) * PHF1}{(Qt_{BBB} * AFin1 + Qp_{BBB})} \quad (33)$$

where Qt_{BBB} is the transcellular diffusion rate at the BBB, Qp_{BBB} is the paracellular diffusion rate at the BBB.

Using equations 26 and 30, for example, AFout1 can be calculated from *in vitro* data.

SUPPLEMENTARY TABLES

TABLE S1. Impact of pathophysiological change on the system-specific parameters of the CNS

Pathophysiological condition	cerebral blood flow (CBF)		BBB characteristics		BCSFB characteristics		brain _{ECF} bulk flow		CSF flow		Active transporters	
	CBF		Paracellular diffusion		Paracellular and transcellular diffusion		Drug dispersion		Drug dispersion		AFs	
Aging	decrease of the regional CBF (81)				thinner of the height of CP epithelial cells and thicker of the choroid plexus (CP) epithelial basement (82)				decrease in CSF production, increase in CSF outflow resistance (83)		loss of the function of LRP-1 and P-gp (84)	
Traumatic injury	CBF reduced by 50% (65)		increase of the paracellular permeability due to the disruption of the tight junction complexes and the integrity of the basement membranes (66)								increase of pinocytotic vesicle transport across the BBB (66), decrease of the expression of P-gp (67)	
Epilepsy	regional decrease of the CBF (68)		increase of the paracellular permeability due to the opening of tight junctions decrease in some tight junction proteins (e.g., occluding, ZO-1) and increase of the pinocytosis (69)								increase of the expression of P-gp and MRPs (70,71)	
Alzheimer's disease (AD)	regional decrease of the CBF (85)		increase of permeability due to the abnormal opening of tight junctions (86)		thinner of the height of CP epithelial cells and thicker of the CP epithelial basement (82)		blockade of brain _{ECF} flow (87)		decrease in CSF production, CSF turnover and increase in CSF volume (81)		decrease of ABCB1 (P-gp) and upregulation of ABCG2 (88)	
Parkinson's disease (PD)	increase/decrease of the CBF depending on the brain region and the state of the disease (89)		increase of the paracellular permeability due to the decrease of some tight junction proteins (e.g., occluding, ZO-1) (90)									
Multiple sclerosis (MS)	increase of the CBF (91)		increase of the paracellular permeability due to the opening of tight junctions and decrease of some tight junction proteins (e.g., occluding, ZO-1, VE-cadherin) (92)								decrease of the expression of P-gp (91)	

TABLE SII. Plasma PK parameter values

		Parameter estimates (RSE, %)					
		Acetaminophen		Oxycodone	Morphine	Phenytoin	
		Study 1 and Study 2	Study 3	Study 1	Study 1 and Study 2	Study 1	
CL_{PL}	mL/min	495	562 (20.1)	1030 (17.9)	3070 (15.8)	802 (65.6)	
$Q_{PL,PER1}$	mL/min	NA	2060 (31.1)	7270 (52.1)	3030 (0.60)	7690 (12.3)	
V_{PL}	mL	108000	9880 (41.1)	166000 (31.0)	16000 (35.3)	105000 (35.8)	
V_{PER1}	mL	NA	51900 (18.3)	147000 (24.7)	95400 (2.50)	2000000 (5.00)	
inter individual variability^{a)}							
$\omega_{CL_{PL}}$	%	NA	49.0 (30.2)	34.1 (30.4)	27.1 (19.9)	107.7 (44.8)	
$\omega_{Q_{PL,PER1}}$	%	NA	NA	NA	NA	21.1 (18.8)	
$\omega_{V_{PL}}$	%	NA	NA	47.2 (41.9)	59.6 (20.0)	81.0 (26.3)	
$\omega_{V_{PER1}}$	%	NA	23.5 (22.5)	NA	NA	NA	
residual error^{b)}							
$\sigma_{\text{plasma proportional}}$	%	23.9	25.0 (8.20)	15.0 (23.4)	9.60 (22.9)	8.00 (30.5)	
Ref			(15)		(15)		

CL_{PL} : clearance from the central compartment, $Q_{PL,PER1}$: inter-compartmental clearance between the central compartment and the peripheral compartment 1, RSE: relative standard error, distribution volume of the peripheral compartment 1, V_{PL} : distribution volume of the central compartment, V_{PER1} : distribution volume of the peripheral compartment 1, V_{PER2} : distribution volume of the peripheral compartment 2.

a) $\theta = \theta_0 \times e^{\lambda \cdot \eta_j}$, where θ_0 represents the parameters of the i th subject, θ represents the population mean value of the parameter, η_j is the random effect of the j th subject under the assumption of a normal distribution with a mean value of 0 and variance of ω^2 .

b) $C_{ij} = Y_{i,PER(j)} \times (1 + \epsilon_{ij})$, where C_{ij} represents the j th observed concentration of the i th subject, $Y_{i,PER(j)}$ represents the j th individual prediction of the i th subject, and ϵ_{ij} is the random effect of the j th observed concentration of the i th subject under the assumption of a normal distribution with a mean value of 0 and variance of σ^2 .



General discussion and future perspectives

Drug development for central nervous system (CNS) indications has been particularly challenging and suffers from high attrition rate due to safety concerns or lack of efficacy during clinical development (1,2). Knowledge of unbound drug concentration-time profiles at the target-site in the CNS is crucial to understand drug concentration-effect relationships and to determine whether relevant CNS drug concentrations relative to the target affinity have been reached (3). This is relevant specifically for the CNS, because drug concentrations in the CNS can be significantly different from drug concentrations in plasma due to the presence of the blood-brain and the blood-cerebrospinal fluid barriers (BBB and BCSFB, respectively) (4), and intra-brain distribution processes. However, since measurement of the drug concentration in human CNS is highly limited due to ethical and practical constraints, plasma concentrations are typically used in CNS drug development to quantify drug pharmacodynamics (PD) for selection of optimal dose regimens.

The purpose of our research was to develop novel approaches to predict the unbound drug pharmacokinetics (PK) in the CNS. To achieve this, a comprehensive CNS physiologically based pharmacokinetic (PBPK) model has been developed. The resulting model includes expressions describing key CNS physiology and drug distribution processes to predict unbound drug PK in multiple CNS compartments. Specifically, in this thesis we present:

- 1) A comprehensive overview of key physiological variables for prediction and translation of CNS PK (**Chapter 2**)
- 2) A generic multi-compartmental CNS PK distribution model (**Chapter 3**)
- 3) A comprehensive rat CNS PBPK model (**Chapter 4**)
- 4) Scaling the comprehensive rat CNS PBPK model to humans (**Chapter 5**)

The systems pharmacokinetic models, which have been developed in the thesis, is summarized in **Table I**, focusing on the characteristics of each model.

Table I. Summary of the developed systems pharmacokinetic models

		generic multi-compartmental CNS PK distribution model	comprehensive CNS PBPK model	
		Chapter 3	Chapter 4	Chapter 5
model structure		plasma, brain _{ECF} , brain _{ICF} , CSF _{IV} , CSF _{TPV} , CSF _{CM} and CSF _{SAS}	plasma, brain _{MV} , brain _{ECF} , brain _{ICF} , lysosome, CSF _{IV} , CSF _{TPV} , CSF _{CM} and CSF _{SAS}	
model parameter	system-specific	rat or human CNS systems information (literature)	rat CNS systems information (literature)	human CNS systems information (literature)
	drug-specific	estimated (<i>in vivo</i> animal PK data)	calculated using physicochemical properties (<i>in silico</i> prediction), and if necessary obtained (literature and/or <i>in vitro</i> studies)	
applicable condition	species	rat and human	rat	human
	physiological /pathophysiological	physiological CNS conditions (recommended)	physiological and pathophysiological CNS conditions	
purpose of the modeling		1. identify a generally applicable CNS PK model structure	1. predict drug PK in multiple CNS compartments in rats 2. develop a comprehensive PBPK model structure which can be scaled to humans	1. predict drug PK in multiple CNS compartments in humans 2. improve CNS drug development success rate

brain_{ECF}: brain extra cellular fluid compartment, brain_{ICF}: brain intracellular fluid compartment, CSF_{IV}: cerebrospinal fluid compartment in the lateral ventricle, CSF_{TPV}: cerebrospinal fluid compartment in the third and fourth ventricle, CSF_{CM}: cerebrospinal fluid compartment in the disterna magna, CSF_{SAS}: cerebrospinal fluid compartment in the subarachnoid space, brain_{MV}: brain microvascular compartment

A COMPREHENSIVE OVERVIEW OF KEY PHYSIOLOGICAL VARIABLES FOR PREDICTION AND TRANSLATION OF CNS PK

To predict the PK of drugs at multiple sites within the CNS, it is necessary to consider the complexity of the CNS physiology and drug distribution processes that underlie the drug PK at these sites. In **Chapter 2**, we described the key CNS physiological variables that determine the drug PK in the CNS.

The relevant CNS physiological compartments are the brain microvascular space, the cells of the barriers in the CNS (i.e. the BBB and BCSFB), the brain parenchymal cells, the brain extracellular fluid (brain_{ECF}), the brain intracellular fluid (brain_{ICF}), cerebrospinal fluid (CSF) in the lateral ventricle (CSF_{LV}), CSF in the cisterna magna (CSF_{CM}) and CSF in subarachnoid space (CSF_{SAS}). Additional physiological parameters are physiological fluid flows including the cerebral blood flow (CBF), brain_{ECF} bulk flow, and CSF flow within the CNS. Together with these physiological variables, drug properties are the important factors that govern the drug PK, specifically drug transport across the BBB and the BCSFB, which results in drug dependent rate and extent of drug distribution in the CNS. With regard to drug transport across the BBB and the BCSFB, a distinction needs to be made between transcellular and paracellular passive diffusion since the BBB and the BCSFB are comprised of cells that are interconnected by tight junctions (5). Moreover, we addressed the role of drug binding to the brain tissue components (such as proteins and lipids) and the influence of pH differences among the physiological compartments (pH partition theory) (6–9). These CNS system-specific parameters and drug-specific parameters are the basis of a comprehensive CNS PBPK model structure.

A GENERIC MULTI-COMPARTMENTAL CNS PK DISTRIBUTION MODEL

The purpose of **Chapter 3** was to develop a generally applicable CNS PK model structure that can be used to predict unbound drug concentration-time profiles in multiple CNS compartments in rats and humans. We used published and newly generated rich brain_{ECF} and CSF unbound concentration-time datasets in rats for nine drugs (acetaminophen, atenolol, methotrexate, morphine, paliperidone, phenytoin, quinidine, remoxipride and risperidone) that were obtained by microdialysis experiments.

The developed model could adequately describe the rat PK data of these nine structurally highly diverse drugs in multiple CNS compartments. This model includes descriptors of all relevant CNS physiological compartments with two drug-specific parameters: drug

exchange process at the BBB (Q_{PL_ECF}) and drug dispersion through brain_{ECF} and CSF compartments (Q_{DIFF}). These parameter values were estimated using available brain_{ECF} and/or CSF PK data in rats under physiological CNS condition. Interestingly, the value of Q_{DIFF} was comparable among the nine drugs, indicating this parameter value could be potentially fixed and used for other small molecules. Altogether, it means that the model requires only plasma PK data and brain_{ECF} or CSF PK data to estimate model parameters in the model for each drug, which makes this model relatively easy to use.

The model was scaled to predict unbound drug concentration-time profiles in human CNS by replacing the values of the rat system-specific parameters by the corresponding human values and allometric scaling of the drug-specific parameters. Generally, under physiological CNS conditions, the scaled model predicted the available drug PK data in multiple human CNS compartments very well.

In summary, a generic multi-compartmental CNS PK distribution model that could predict unbound drug PK profiles in multiple CNS compartments in rats and humans, was developed. The model structure formed the base model structure for the development of the comprehensive PBPK models for rats and humans as introduced in the successive chapters 4 and 5.

An important limitation of the use of this model to predict drug PK in the CNS is the requirement of *in vivo* PK data. Moreover, this model is not ideal for the investigation of the effect of pathophysiological conditions on drug PK in the CNS because the drug-specific parameters in the model were estimated using PK data under physiological CNS condition.

A COMPREHENSIVE RAT CNS PBPK MODEL

In **Chapter 4**, we developed a comprehensive rat CNS PBPK model to predict unbound drug concentration-time profiles in multiple CNS compartments. In contrast to the generic multi-compartmental CNS PK distribution model (**Chapter 3**), the comprehensive CNS PBPK model is able to predict unbound drug PK profiles in multiple CNS physiological compartments in the rat without the need to have PK data from *in vivo* animal studies.

The PBPK model includes descriptors of all physiologically relevant CNS compartments and drug distribution processes, with parameters that can be derived from either literature and/or through *in silico* predictions. The model was evaluated using rat PK data in brain_{ECF}, CSF_{LV}, CSF_{CM}, and brain tissue for ten drugs (acetaminophen, atenolol,

methotrexate, morphine, paliperidone, phenytoin, quinidine, raclopride, remoxipride and risperidone), resulting in adequate predictions of the PK data, within only a two-fold error.

This model is the first model to include two separate expressions to explicitly distinguish between paracellular and transcellular diffusion at the BBB and the BCSFB. The relative contributions of paracellular and transcellular diffusion to the total passive diffusion varied between individual drugs. The separation of these two passive transport processes appeared to be important for the prediction of the CNS drug concentrations under pathophysiological conditions that may differently affect paracellular and transcellular diffusion.

In conclusion, the rat CNS PBPK model is a valuable tool to predict unbound drug concentration-time profiles in the CNS for newly developed (CNS) drugs without the need for *in vivo* PK data. Furthermore, this CNS PBPK model is powerful in deciphering changes in CNS drug distribution due to variations in the values of system-specific parameters (for example by pathophysiological conditions) or variation in the values of drug-specific parameters (such as drug physiochemical properties). By doing this, we are able to investigate the influence of particular system- and drug-specific parameters on drug distribution in the CNS, thus bringing useful information in the stage of the drug candidate selection in drug discovery.

SCALING THE COMPREHENSIVE RAT CNS PBPK MODEL TO HUMANS

The rat CNS PBPK model was scaled to predict concentration-time profiles in human CNS by replacing the values of the rat system-specific parameters to their corresponding human values and by scaling the contribution of active transport from rat to human on the basis of information on differences in the protein expression level and activity/function of these transporters (**Chapter 5**).

The accuracy of the scaled human CNS PBPK model was evaluated by comparison with reference human PK data in brain_{ECF} and/or in CSF for acetaminophen, oxycodone and morphine, as paradigm compounds, which were obtained from physiological CNS conditions. It was demonstrated that the model could adequately predict these PK profiles in humans, within only a 1.6-fold error.

CNS drugs are often used under patient conditions in which CNS physiology may be altered (10–28) and changes in CNS physiology may have impact on drug PK in the CNS. We investigated how the developed CNS PBPK model can be used to quantitatively understand physiological determinants that may explain altered CNS PK under pathophysiological conditions. For this analysis we used PK data from traumatic brain injury (TBI) patients (acetaminophen and morphine), and epileptic patients (phenytoin). In TBI patients, a decrease in CBF, an increase in paracellular permeability, and changes in activity/expression of active transporters have been reported. For epileptic conditions, a decrease in CBF, an increase in paracellular permeability, and increases in some active efflux transporters such as P-glycoprotein (P-gp) and multidrug resistance-associated proteins (MRPs) have been reported. Therefore, the influence of these conditions on the drug distribution into and within the CNS was investigated. The CNS PBPK model captured PK profiles of acetaminophen in CSF for TBI patients and PK profiles of phenytoin in CSF for epileptic patients, by using the same system-specific parameters values as in the physiological condition. This indicated that acetaminophen and phenytoin PK profiles in CSF were not affected by TBI or epileptic conditions, respectively. For morphine, the CNS PBPK model did not capture the PK profiles in $\text{brain}_{\text{ECF}}$ in TBI patients. However, by varying the values of system-specific parameters, based on literature likely to be associated with these brain injuries, we were able to quantitatively investigate the influence of the TBI condition on the morphine PK data.

In summary, the scaled human CNS PBPK model could predict the unbound drug-concentration profiles in several CNS compartments in human without the need of clinical PK data. This is valuable because it allows obtaining human CNS PK profiles in a very early stage of the drug development process. Furthermore, we demonstrated how the developed human CNS PBPK model could be a useful tool to investigate the quantitative influence of each pathophysiological condition on drug PK in the CNS. This is extremely important as it allows us to gain an understanding on the impact of pathophysiological conditions on CNS system-specific parameters, and thereby on CNS drug distribution under these conditions.

FUTURE PERSPECTIVES

Due to the generic structure of the model, it could be further refined to an ever more robust and more widely applicable CNS PBPK model along the following ideas;

1) Further evaluation and refinement of the model using PK data of additional drugs in multiple species.

The developed CNS PBPK model was evaluated using ten compounds data in rats and four compounds data in humans. By including PK data of additional drugs with a wider range of physicochemical properties, obtained from multiple species, the model can be further validated and refined. Also, if deemed necessary, the model could be used for the extrapolation to species other than human. This is of particular interest for animal species with a high homology of disease characteristics with human. An example is the rhesus monkey, which is used in the research on modulators of the amyloid precursor protein in the treatment of Alzheimer's disease (29).

2) Mechanism-based investigation of the impact of various disease conditions on CNS PK.

The impact of various pathophysiological conditions on CNS physiology and subsequent CNS PK could be further systematically investigated and implemented in the CNS PBPK model. This could be done by using PK data obtained from other disease conditions such as inflammation (30) and/or different stages of disease processes that may affect CNS PK.

3) Systems-based investigation of the impact of population-specific properties on CNS PK.

The proposed CNS PBPK model has been developed using PK data obtained from adults only, while also the model application to pediatric and elderly patients could be of great relevance. For example, for pediatric patients, the model could be adapted by modification of system-specific parameters such as size of brain and volume of CSF. Also, developmental changes in expression (maturation) of membrane proteins such as transporters, receptors, and junctional proteins at the BBB, need to be considered (31).

To improve the CNS drug development success rate, the prediction of CNS drug effects in humans is essential. Our view is, that the development of a CNS PBPK- Pharmacodynamic (PBPK-PD) model on the basis of *in silico* predictions, literature information, and/or *in vitro* studies, would be an important milestone on the way towards this goal.

The developed CNS PBPK model could be integrated with target-mediated drug disposition and target association/dissociation kinetic submodels to support predictions of target occupancy (32). Since the target occupancy induces signal transduction processes, it may create the basis for the following PBPK-PD relationship (33). Recently it has been found that drug-target binding kinetics not only influences the time-dependent target occupancy, but also influences the drug target-site concentrations when drug target affinities are high or target protein concentrations in the target-site are high (34). This is an important finding since concentrations of target proteins may substantially differ between CNS locations (35). Furthermore, it has been shown that target binding has an impact on drug plasma concentrations as well when concentrations of target proteins or drug target affinities are high enough (36). Thus, integrating these factors into one model framework is important in order to take into account the contributions of individual factors for specific CNS locations to determine the PK and PD of drugs.

In summary, the developed CNS PBPK model offers a robust way to enhance CNS drug development and can be further extended to predict drug efficacy by integrating the information of drug-target binding kinetics, target occupancy, target activation, transduction, homeostatic feedback, and disease processes altogether.

CONCLUSION

We developed a comprehensive CNS PBPK model for prediction of unbound drug concentration-time profiles in multiple CNS compartments in both rats and humans. The CNS PBPK model is useful to investigate the impact of pathophysiological CNS conditions on the CNS drug distribution.

The CNS PBPK model only requires knowledge of physicochemical properties of the drugs and the influence of the net active transporters on the drug exchange at the BBB and the BCSFB, which could be obtained from *in silico* predictions, literature information and *in vitro* studies (if needed). Because of this it is a powerful tool to predict drug PK in the CNS in the early stage of the drug development, as well in later stage of drug development or even in drug treatment regimens of diseases using existing drugs.

REFERENCES

1. Kola I, Landis J. Can the pharmaceutical industry reduce attrition rates? *Nat Rev Drug Discov.* 2004;3:1–5.
2. Hurko O, Ryan JL. Translational Research in Central Nervous System Drug Discovery. *J Am Soc Exp Neurother.* 2005;2(4):671–82.
3. Danhof M, de Jongh J, De Lange ECM, Della Pasqua O, Ploeger BA, Voskuyl RA. Mechanism-Based Pharmacokinetic-Pharmacodynamic Modeling: Biophase Distribution, Receptor Theory, and Dynamical Systems Analysis. *Annu Rev Pharmacol Toxicol.* 2007;47(1):357–400.
4. Hammarlund-Udenaes M, Paalzow LK, De Lange ECM. Drug equilibration across the blood-brain barrier - Pharmacokinetic considerations based on the microdialysis method. *Pharm Res.* 1997;14(2):128–34.
5. Engelhardt B, Sorokin L. The blood-brain and the blood-cerebrospinal fluid barriers: Function and dysfunction. *Semin Immunopathol.* 2009;31(4):497–511.
6. Fridén M, Bergström F, Wan H, Rehngren M, Ahlin G, Hammarlund-Udenaes M, et al. Measurement of unbound drug exposure in brain: Modeling of pH partitioning explains diverging results between the brain slice and brain homogenate methods. *Drug Metab Dispos.* 2011;39(3):353–62.
7. Touitou E, Barry BW. Enhancement in Drug Delivery. 2006. 575-591 p.
8. Shen DD, Artru AA, Adkison KK. Principles and applicability of CSF sampling for the assessment of CNS drug delivery and pharmacodynamics. *Adv Drug Deliv Rev.* 2004;56(12):1825–57.
9. Mindell JA. Lysosomal acidification mechanisms. *Annu Rev Physiol.* 2012;74:69–86.
10. Serot JM, Béné MC, Foliguet B, Faure GC. Altered choroid plexus basement membrane and epithelium in late-onset Alzheimer's disease: An ultrastructural study. *Ann N Y Acad Sci.* 1997;826:507–9.
11. Aanerud J, Borghammer P, Chakravarty MM, Vang K, Rodell AB, Jónsdóttir KY, et al. Brain energy metabolism and blood flow differences in healthy aging. *J Cereb Blood Flow Metab.* 2012;32(7):1177–87.
12. Shimada A, Hasegawa-Ishii S. Senescence-accelerated Mice (SAMs) as a Model for Brain Aging and Immunosenescence. *Aging Dis.* 2011;2(5):414–35.
13. Silverberg GD, Miller MC, Messier A a, Majmudar S, Machan JT, Donahue JE, et al. Amyloid deposition and influx transporter expression at the blood-brain barrier increase in normal aging. *J Neuropathol Exp Neurol.* 2010;69(1):98–108.
14. Greve MW, Zink BJ. Pathophysiology of traumatic brain injury. *Mt Sinai J Med.* 2009;76(2):97–104.
15. Chodobski A, Zink BJ, Szymdynger-Chodobska J. Blood-Brain Barrier Pathophysiology in Traumatic Brain Injury. *Transl Stroke Res.* 2011;2(4):492–516.

16. Pop V, Sorensen DW, Kamper JE, Ajao DO, Paul Murphy M, Head E, et al. Early brain injury alters the blood – brain barrier phenotype in parallel with b-amyloid and cognitive changes in adulthood. *J Cereb Blood Flow Metab.* 2012;(May):1–10.
17. Appel S, Duke ES, Martinez AR, Khan OI, Dustin IM, Reeves-Tyer P, et al. Cerebral blood flow and fMRI BOLD auditory language activation in temporal lobe epilepsy. *Epilepsia.* 2012;53(4):631–8.
18. Bednarczyk J, Lukasiuk K. Tight junctions in neurological diseases. *Acta Neurobiol Exp.* 2011;71(4):393–408.
19. Lazarowski A, Czornyj L, Lubienieki F, Girardi E, Vazquez S, D’Giano C. ABC transporters during epilepsy and mechanisms underlying multidrug resistance in refractory epilepsy. *Epilepsia.* 2007;48(SUPPL. 5):140–9.
20. Löscher W, Potschka H. Role of multidrug transporters in pharmacoresistance to antiepileptic drugs. *J Pharmacol Exp Ther.* 2002;301(1):7–14.
21. Palmer JC, Baig S, Kehoe PG, Love S. Endothelin-converting enzyme-2 is increased in Alzheimer’s disease and up-regulated by Abeta. *Am J Pathol.* 2009;175(1):262–70.
22. Bowman G, Quinn J. Alzheimer’s disease and the blood–brain barrier: past, present and future. *Aging health.* 2008;4(1):47–57.
23. Cipolla MJ, Sweet JG, Chan S-L. Cerebral vascular adaptation to pregnancy and its role in the neurological complications of eclampsia. *J Appl Physiol.* 2011;110(2):329–39.
24. Dutheil F, Jacob A, Dauchy S, Beaune P, Scherrmann J-M, Declèves X, et al. ABC transporters and cytochromes P450 in the human central nervous system: influence on brain pharmacokinetics and contribution to neurodegenerative disorders. *Expert Opin Drug Metab Toxicol.* 2010;6(10):1161–74.
25. Hsu JL, Jung TP, Hsu CY, Hsu WC, Chen YK, Duann JR, et al. Regional CBF changes in Parkinson’s disease: A correlation with motor dysfunction. *Eur J Nucl Med Mol Imaging.* 2007;34(9):1458–66.
26. Van Vliet EA, Araújo SDC, Redeker S, Van Schaik R, Aronica E, Gorter JA. Blood-brain barrier leakage may lead to progression of temporal lobe epilepsy. *Brain.* 2007;130(2):521–34.
27. Ingrisch M, Sourbron S, Morhard D, Ertl-Wagner B, Kümpfel T, Hohlfeld R, et al. Quantification of Perfusion and Permeability in Multiple Sclerosis. *Invest Radiol.* 2012;47(4):252–8.
28. Weiss N, Miller F, Cazaubon S, Couraud PO. The blood-brain barrier in brain homeostasis and neurological diseases. *Biochim Biophys Acta - Biomembr.* 2009;1788(4):842–57.
29. van Dam D, de Deyn PP. Non human primate models for Alzheimer’s disease-related research and drug discovery. *Expert Opin Drug Discov.* 2017;12(2):187–200.
30. Luissint A, Artus C, Glacial F, Ganeshamoorthy K. Tight junctions at the blood brain barrier : physiological architecture and disease-associated dysregulation. *Fluids Barriers CNS.* 2012;9(23):1–12.

31. Ito K, Uchida Y, Ohtsuki S, Aizawa S, Kawakami H, Katsukura Y, et al. Quantitative membrane protein expression at the blood-brain barrier of adult and younger cynomolgus monkeys. *J Pharm Sci.* 2011;100(9):3939–50.
32. de Witte WEA, Wong YC, Nederpelt I, Heitman LH, Danhof M, van der Graaf PH, et al. Mechanistic models enable the rational use of in vitro drug-target binding kinetics for better drug effects in patients. *Expert Opin Drug Discov.* 2016;11(1):45–63.
33. Danhof M, de Lange ECM, Della Pasqua OE, Ploeger BA, Voskuyl RA. Mechanism-based pharmacokinetic-pharmacodynamic (PK-PD) modeling in translational drug research. *Trends Pharmacol Sci.* 2008;29(4):186–91.
34. de Witte WEA, Danhof M, van der Graaf PH, de Lange ECM. In vivo Target Residence Time and Kinetic Selectivity: The Association Rate Constant as Determinant. *Trends Pharmacol Sci.* 2016;37(10):831–42.
35. Ares-Santos S, Granado N, Moratalla R. The role of dopamine receptors in the neurotoxicity of methamphetamine. *Journa Intern Med.* 2013;273:437–53.
36. Yamazaki S, Shen Z, Jiang Y, Smith BJ, Vicini P. Application of Target-Mediated Drug Disposition Model to Small Molecule Heat Shock Protein 90 Inhibitors. *Drug Metab Dispos.* 2013;41:1285–94.



Appendix

ENGLISH SUMMARY

Clinical development of drugs for central nervous system (CNS) disorders has been particularly challenging and still suffers from high attrition rates. This high attrition is mainly due to lack of efficacy during clinical development. To improve the prediction of CNS drug effects, knowledge of the unbound drug concentration at the CNS target-site is indispensable, as these unbound drug concentrations at the target-site drive the effects of the drug. Unfortunately, measuring drug concentrations in the human CNS has major practical and ethical constraints. Plasma concentrations are therefore still the mainstay in the selection of optimal dose regimens in clinical CNS drug development, although these concentrations may substantially differ from the CNS target-site drug concentrations. This is due to the impact of blood-brain barrier (BBB) transport, the blood-cerebrospinal fluid barrier (BCSFB) transport and intra-brain distribution processes. Therefore, alternative approaches to predict the drug pharmacokinetics (PK) at the target-site(s) in the human CNS should be searched for.

The CNS is a very complex organ. Drug PK in the CNS is governed by drug properties and multiple system variables (**Chapter 2**). Firstly, the poorly penetrable BBB and BCSFB limit passage of unbound drugs from the systemic circulation into the brain. These barriers are associated with limited paracellular passive diffusion due to the presence of the tight junctions between the barrier cells. In addition, various active influx and efflux transport mechanisms on these barriers may increase or decrease drug distribution in the CNS, respectively. Secondly, the CNS can be subdivided into several distinct physiological compartments. These include the brain microvascular space, the cells of the barriers in the CNS (i.e. the BBB and BCSFB), the brain parenchymal cells, the brain extracellular fluid ($\text{brain}_{\text{ECF}}$), the brain intracellular fluid ($\text{brain}_{\text{ICF}}$), cerebrospinal fluid (CSF) in the lateral ventricle (CSF_{LV}), CSF in the cisterna magna (CSF_{CM}) and CSF in subarachnoid space (CSF_{SAS}). The specific drug disposition characteristics across these specific compartments further determines local drug PK in the CNS. Thirdly, CNS drug PK are influenced by physiological flows, including the cerebral blood flow (CBF), $\text{brain}_{\text{ECF}}$ bulk flow, and CSF flow. Lastly, drug protein and tissue binding and the pH in the various CNS physiological compartments further affect ultimate unbound drug PK in the CNS.

Several approaches have been taken to investigate CNS drug distribution (**Chapter 2**). For animals, *ex vivo* techniques such as the brain homogenate and the brain slicing technique, which have focused on steady state conditions, are used. Since, even in chronic dosing, drug concentrations in plasma and CNS will vary over time, and transport processes are time-dependent, we need information over drug concentrations in a time-dependent manner to understand the drug PK in the CNS. For human, non-invasive

monitoring techniques such as positron emission tomography and single-photon emission computed tomography, are currently used. These techniques, however, cannot distinguish between total and unbound drug concentrations, while in particular providing information on unbound drug concentrations is a prerequisite since it drives the drug effects.

Furthermore, as it has been recently demonstrated that (unbound) drug concentrations may vary between different locations in the CNS, it is also important to have information on the unbound drug PK at different locations within the CNS. Microdialysis is a highly valuable technique, as it allows the *in vivo* measurement of unbound drug concentration-time data, at different CNS locations. However, though minimally invasive, the use of microdialysis in humans is highly restricted and is only allowed in certain disease conditions, such as traumatic brain injury (TBI), where it can be used to monitor endogenous compounds to inform clinicians on the status of the patient earlier than clinical signs. This indicates that information on unbound drug PK in human CNS has to be obtained indirectly.

Mathematical PK modeling is an interesting tool to predict time- and location-dependent drug concentrations. Of all the mathematical PK modeling approaches that have been proposed to predict drug PK in the CNS, none has so far captured satisfactorily CNS systems complexity. To build and/or validate the mathematical PK models that enable the prediction of unbound drug PK in the CNS, the data obtained by microdialysis are indispensable, even though such data can be mainly obtained from animals. This indicates the need for the development of more comprehensive mathematical PK model, which includes descriptors of all physiologically relevant CNS compartments and drug distribution processes, and is able to be scaled from animals to humans to predict unbound drug PK in the human CNS.

Physiologically based pharmacokinetic (PBPK) modelling represents one of the most promising approaches for the prediction of CNS drug concentrations. PBPK models mathematically describe relevant physiological, physicochemical, and biochemical processes that determine the drug PK in tissues. In PBPK models, drug-specific and system-specific parameters are typically distinguished, therefore enabling predictions across drugs, species and disease conditions.

The ultimate goal of this research was to develop a comprehensive PBPK model for the prediction of concentration-time profiles of small molecule drugs in multiple CNS compartments in humans, only based on the physicochemical properties of the drug that can be obtained without the need for animal experiments.

Development of a generic multi-compartmental CNS PK distribution model

A generic multi-compartmental CNS PK distribution model was developed in **Chapter 3**. The purpose of this study was to identify a generally applicable CNS PK model structure that can be used to predict unbound drug concentration-time profiles in multiple CNS locations in rats and humans. For this study, in addition to published rat data on the time course of the concentrations for acetaminophen, atenolol, methotrexate, morphine, quinidine and remoxipride, we used newly generated rich rat datasets for paliperidone, phenytoin, remoxipride and risperidone to broaden the range of physicochemical properties and chemical structures. Ultimately, detailed datasets for nine drugs were available.

The developed model consisted of plasma and main CNS physiological compartments ($\text{brain}_{\text{ECF}}$, $\text{brain}_{\text{ICF}}$ and four different CSF sites) that could adequately describe the rat PK data of these nine structurally highly diverse drugs in multiple CNS compartments. This model includes descriptors of all relevant CNS physiological compartments with two drug-specific parameters: drug exchange process at the BBB ($Q_{\text{PL_ECF}}$) and drug dispersion through $\text{brain}_{\text{ECF}}$ and CSF compartments (Q_{DIFF}). These parameter values were estimated using available $\text{brain}_{\text{ECF}}$ and/or CSF PK data in rats under physiological CNS condition. Interestingly, the values of Q_{DIFF} that were obtained were comparable among the nine drugs, indicating this parameter value could be potentially fixed and used for predictions of the concentrations of other small molecules. Altogether, the proposed multi-compartmental CNS PK distribution model requires only plasma PK data and $\text{brain}_{\text{ECF}}$ or CSF PK data to estimate model parameters in the model for each drug, which makes this model relatively easy to use.

The model was scaled to predict unbound drug concentration-time profiles in human CNS by replacing the values of the rat system-specific parameters to the corresponding human values, and by allometric scaling of the drug-specific parameters. The scaled model predicted the available drug PK data in multiple human CNS locations very well under physiological CNS conditions.

In summary, a generic multi-compartmental CNS PK distribution model that could predict unbound drug PK profiles in multiple CNS compartments in rats and humans, was developed. The model structure formed the base model structure for the development of the comprehensive PBPK models for rats and humans as described in the successive **Chapters 4 and 5**.

An important limitation of the use of this model to predict drug PK in the CNS is the requirement of *in vivo* PK data. Moreover, this model is not ideal for the investigation of the effect of pathophysiological conditions on drug PK in the CNS because the drug-specific parameters in the model were estimated using PK data under physiologically healthy CNS condition.

Development of a comprehensive CNS PBPK model in rat

A comprehensive rat CNS PBPK model was developed in **Chapter 4**, to predict unbound drug concentration-time profiles in multiple CNS compartments using descriptors of the physicochemical characteristics of the drugs that were obtained either by computational methods or by *in vitro* screening. The rat CNS PBPK model structure was based on the previously developed generic multi-compartmental CNS PK distribution model structure. The model includes descriptors of all physiologically relevant CNS compartments and drug distribution processes, with parameters that can be derived from either literature and/or through *in silico* predictions. The model was evaluated using rat PK data in brain_{ECP}, CSF_{LV}, CSF_{CM} and brain tissue for ten drugs (acetaminophen, atenolol, methotrexate, morphine, paliperidone, phenytoin, quinidine, raclopride, remoxipride and risperidone), resulting in adequate predictions of the PK data, within only a two-fold error.

This model is the first model to include two separate expressions to explicitly distinguish between paracellular and transcellular diffusion at the BBB and the BCSFB. The relative contributions of paracellular and transcellular diffusion to the total passive diffusion varied between individual drugs. The separation of these two passive transport processes appeared to be important for the prediction of the CNS drug concentrations under pathophysiological conditions that may differently affect paracellular and transcellular diffusion.

In conclusion, the rat CNS PBPK model is a valuable tool to predict unbound drug concentration-time profiles in the CNS for newly developed (CNS) drugs without the need of *in vivo* PK data. Furthermore, this CNS PBPK model is powerful in deciphering changes in CNS drug distribution due to variations in the values of system-specific parameters (for example by pathophysiological conditions) or variation in the values of drug-specific parameters (such as drug physicochemical properties). By doing this, we are able to investigate the influence of particular system- and drug-specific parameters on drug distribution in the CNS, thus bringing useful information at the stage of the drug candidate selection in drug discovery.

Scaling of the comprehensive rat CNS PBPK model to humans

In **Chapter 5**, the rat CNS PBPK model was scaled to predict concentration-time profiles in human CNS by replacing the values of the rat system-specific parameters to their corresponding human values and by scaling the contribution of active transport from rat to human on the basis of information on differences in the protein expression level and activity/function of these transporters.

The scaled human CNS PBPK model was evaluated by comparison of the model predictions with available human PK data in brain_{ECF} and/or in CSF for acetaminophen, oxycodone and morphine, which were obtained under physiological CNS conditions. The human CNS PBPK model could adequately predict these PK profiles, within only a 1.6-fold error.

CNS drugs are often used under patient conditions in which CNS physiology may be altered and changes in CNS physiology may have impact on drug PK in the CNS. We investigated how the developed CNS PBPK model can be used to quantitatively understand physiological determinants that may explain altered CNS PK under pathophysiological conditions. For this analysis we used PK data from TBI patients (acetaminophen and morphine), and epileptic patients (phenytoin). In TBI patients, a decrease in CBF, an increase in paracellular permeability, and changes in activity/expression of active transporters have been reported. For epileptic conditions, a decrease in CBF, an increase in paracellular permeability, and increases in some active efflux transporters such as P-glycoprotein (P-gp) and multidrug resistance-associated proteins (MRPs) have been reported. Therefore, the influence of these conditions on the drug distribution into and within the CNS were investigated. The CNS PBPK model captured well the PK profiles of acetaminophen in CSF for TBI patients and PK profiles of phenytoin in CSF for epileptic patients, by using the same system-specific parameters values as in the physiological condition. This indicated that acetaminophen and phenytoin PK profiles in CSF were not affected by TBI or epileptic conditions, respectively. For morphine, the CNS PBPK model did not capture the PK profiles in brain_{ECF} in TBI patients. However, by varying the values of system-specific parameters, based on literature likely to be associated with these brain injuries, we were able to quantitatively investigate the influence of the TBI condition on the morphine PK data.

In summary, the scaled human CNS PBPK model could predict the unbound drug-concentration profiles in several CNS compartments in human under physiological CNS conditions without the need of clinical PK data. This is valuable because it allows obtaining human CNS PK profiles in a very early stage of the drug development process. Furthermore, we demonstrated how the developed human CNS PBPK model could

be a useful tool to investigate the quantitative influence of each pathophysiological condition on drug PK in the CNS. This is extremely important as it allows us to gain an understanding on the impact of pathophysiological conditions on CNS system-specific parameters, and thereby on CNS drug distribution under these conditions.

FUTURE PERSPECTIVES

Due to the generic structure of the model, it could be further refined to an ever more robust and more widely applicable CNS PBPK model along the following ideas;

1. further evaluation and refinement of the model using PK data of additional drugs in multiple species.
2. mechanism-based investigation of the impact of various disease conditions on CNS PK using PK data obtained from other disease conditions beyond TBI and epilepsy.
3. systems-based investigation of the impact of population-specific properties on CNS PK using PK data obtained from pediatric and elderly patients.

To improve the CNS drug development success rate, the prediction of CNS drug effects in humans is essential. Our view is, that the development of a CNS PBPK- Pharmacodynamic (PBPK-PD) model on the basis of *in silico* predictions, literature information, and/or *in vitro* studies, would be an important milestone on the way towards this goal.

The developed CNS PBPK model could be used to integrate target-mediated drug disposition and target association/dissociation kinetic submodels and to support predictions of target occupancy. Since the target occupancy induces signal transduction processes, it may create the basis for the following PBPK-PD relationship.

In summary, the developed CNS PBPK model offers a robust way to enhance CNS drug development and can be further extended to predict drug efficacy by integrating the information of drug-target binding kinetics, target occupancy, target activation, transduction, homeostatic feedback, and disease processes altogether within one model framework.

CONCLUSION

A comprehensive CNS PBPK model for prediction of unbound drug concentration-time profiles in multiple CNS compartments was developed for both rats and humans. This model is useful to investigate the impact of pathophysiological CNS conditions on the CNS drug distribution.

The CNS PBPK model only requires knowledge of physicochemical properties of the drugs, with the influence of the net active transporters on the drug exchange across the BBB and the BCSFB that can be obtained from *in silico* predictions, literature information and *in vitro* studies (if needed). Because of this, the developed CNS PBPK model is a powerful tool to predict drug PK in the CNS in the early stage of the drug development, as well in later stage of drug development or even in drug treatment regimens of diseases using existing drugs.

NEDERLANDSE SAMENVATTING

Het ontwikkelen van geneesmiddelen voor de behandeling van ziekten van de hersenen is nog altijd een grote uitdaging. Tijdens de ontwikkeling van deze geneesmiddelen valt een groot aantal van de verbindingen af met name doordat zij uiteindelijk in de mens onvoldoende werkzaam blijken te zijn.

Aangezien alleen het ongebonden geneesmiddel in staat te binden aan het aangrijpingspunt (zoals bijvoorbeeld een receptoreiwit), en de concentratie van het ongebonden geneesmiddel daardoor bepalend is voor de werking, is het van groot belang om kennis te vergaren over de vrije (ungebonden) geneesmiddelconcentratie op de plaats van werking in de hersenen. Echter, vanuit praktisch en ethisch gezichtspunt is het helaas in de regel niet mogelijk om bij mensen de geneesmiddelconcentratie in hun hersenen te meten. Daarom wordt nog altijd de geneesmiddelconcentratie in plasma gebruikt als basis voor het opstellen van de optimale doseerschema's tijdens de klinische onderzoeksfase, ook al kunnen concentraties in bloedplasma substantieel verschillen van de concentraties op de plaats van werking in de hersenen.

Deze concentratieverschillen tussen plasma en hersenen ontstaan als gevolg van het transport van geneesmiddelen over de bloed-hersenbarrière en de bloed-liquorbarrière, alsook als gevolg van de distributie van het geneesmiddel in de hersenen zelf. Omdat een directe bepaling van geneesmiddelconcentratie in de hersenen bij mensen in de regel niet mogelijk is, is het belangrijk alternatieve methoden te ontwikkelen waarmee het concentratie-tijd verloop van geneesmiddelen op de plaats van werking in de menselijke hersenen voorspeld kan worden.

De hersenen zijn zeer complex en het concentratie-tijdsverloop van een geneesmiddel (op verschillende locaties) in de hersenen hangt enerzijds af van de eigenschappen van het geneesmiddel en anderzijds van de eigenschappen van de het "biologische systeem" (**Hoofdstuk 2**). Bij het voorspellen van geneesmiddelconcentraties in de hersenen is het noodzakelijk een onderscheid te maken tussen stof-specifieke en systeem-specifieke parameters. De systeem-specifieke parameters hangen samen met de anatomie en de fysiologie van de hersenen. Voor de hersen-systeemeigenschappen zijn dat de barrières die bepalend zijn voor het transport van het bloed naar de hersenen. Deze barrières, de bloed-hersenbarrière en de bloed-liquorbarrière, worden gevormd door respectievelijk de endotheelcellen in de bloedvatwand in de hersenen en de epitheel cellen van de choroid plexus. Door de aanwezigheid van zogenaamde *tight junctions* is de ruimte tussen deze cellen erg klein, waardoor de passieve diffusie van geneesmiddelen via deze zogenoemde para-cellulaire route sterk wordt beperkt. Daarnaast hebben de

cellen van deze barrières verschillende actieve influx en efflux transportmechanismen die eveneens het transport van geneesmiddelen van plasma naar hersenen en *vice versa* kunnen beïnvloeden. Als tweede omvatten de hersensysteem-eigenschappen de volumes en oppervlakten van verschillende fysiologische hersen compartimenten, zoals de zojuist beschreven hersen bloedvat endotheelcellen en choroid plexus epitheelcellen, maar ook de hersenparenchym cellen, de extracellulaire vloeistof (*brain extracellular fluid*; $\text{brain}_{\text{ECF}}$), de intracellulaire vloeistof (*brain intracellular fluid*; $\text{brain}_{\text{ICF}}$), de cerebrospinale vloeistof (*cerebrospinal fluid*, CSF) in de laterale ventrikels (CSF_{LV}), de cisterna magna (CSF_{CM}) en de subarachnoïdale ruimten (CSF_{SAS}). De verdeling van het geneesmiddel over deze fysiologische hersencompartimenten is mede bepalend voor de lokale concentratie-tijdprofielen van geneesmiddelen in de hersenen. Als derde komen er in de hersenen vloeistofstromen voor. Dat zijn de cerebrale bloedstroom, de stroom van het $\text{brain}_{\text{ECF}}$ en ook die van de CSF. Tot slot is de binding van het geneesmiddel aan eiwitten en vetten in het hersenweefsel, alsook de invloed van zuurgraad op de verdeling van een geladen geneesmiddelmolecuul over verschillende fysiologische hersencompartimenten, van belang voor het uiteindelijk concentratieverloop van een geneesmiddel op een bepaalde locatie in de hersenen.

Om geneesmiddeldistributie naar de hersenen te onderzoeken zijn verschillende methoden ontwikkeld (**Hoofdstuk 2**). Bij onderzoek in proefdieren is het mogelijk om *ex vivo* methoden te gebruiken; daarbij is de analyse van hersenweefsel-homogenaten of hersenweefsel-plakjes meestal gericht op onderzoek naar concentraties onder evenwichtscondities. Echter, omdat er zelfs bij herhaalde toediening van het geneesmiddel geen sprake is van evenwichtscondities zullen we rekening moeten houden met geneesmiddelconcentraties in plasma en hersenen die variëren in de tijd en deze dan ook kunnen bepalen of voorspellen.

Voor hersenonderzoek in de mens kan gebruik gemaakt worden van niet-invasieve technieken zoals positron-emissie tomografie (PET) en single-photon emission computed tomography (SPECT), waarmee het tijdsverloop van locale concentraties van geneesmiddelen in de hersenen bepaald kunnen worden, maar het is daarmee helaas niet mogelijk om een onderscheid te maken tussen de totale en de ongebonden geneesmiddelconcentratie, terwijl juist deze informatie van belang is voor het effect.

Recent is aangetoond dat de (vrije) geneesmiddelconcentratie niet voor iedere locatie in de hersenen dezelfde is. Daarom is het ook belangrijk om de vrije geneesmiddelconcentratie op diverse locaties in de hersenen te kunnen bepalen. Dit kan met behulp van de microdialyse techniek. Alhoewel microdialyse een minimaal invasieve methode is, is het gebruik hiervan voor onderzoek bij mensen slechts in uitzonderlijke

gevallen toegestaan. Zo wordt microdialyse bijvoorbeeld toegepast bij patiënten met traumatisch hersenletsel om de concentraties van endogene stoffen te meten die de behandelend arts belangrijke informatie geeft over de toestand van de patiënt. In sommige gevallen is het daarbij toegestaan een deel van de microdialysemonsters te gebruiken voor het bepalen van ongebonden geneesmiddelconcentraties. Dit betekent dat we dus geen beschikking hebben over een algemeen te gebruiken methode om geneesmiddelconcentraties in de hersenen van mensen direct te bepalen en is daarmee dus het zoeken naar een indirecte methode.

Door middel van wiskundige modelering van concentratie-tijd profielen van geneesmiddelen (farmacokinetische modellering; PK modellering) is het in principe mogelijk om tijds- en locatie-afhankelijke geneesmiddelconcentraties te voorspellen. Tot nu toe is er nog geen wiskundig PK model beschikbaar dat de ongebonden geneesmiddelconcentraties in de verschillende fysiologische compartimenten van de hersenen goed kan voorspellen. Hiervoor zijn de gegevens uit microdialyse studies onmisbaar. Omdat het alleen mogelijk is om microdialyse studies in proefdieren uit te voeren is het noodzakelijk om een PK model te ontwikkelen waarin alle fysiologisch relevante hersencompartimenten en distributieprocessen opgenomen zijn, én waarmee het mogelijk is de vertaalslag van proefdier naar mensen te maken, zodat vrije geneesmiddelconcentraties in de diverse compartimenten van de hersenen in de mens kunnen worden voorspeld.

Op fysiologie-gebaseerde farmacokinetische (*physiology-based pharmacokinetics*, PBPK) modellering is een wiskundige methode, waarmee door onderscheid te maken tussen geneesmiddel-specifieke en systeem-specifieke eigenschappen (fysiologische, fysisch-chemische en biochemische processen) geneesmiddelconcentraties in het lichaam kunnen worden voorspeld.

Het doel van het onderzoek beschreven in dit proefschrift was het ontwikkelen van een uitgebreid hersen PBPK model om het beloop van de concentratie van geneesmiddel moleculen in diverse fysiologische compartimenten in de hersenen te voorspellen op basis van de fysisch-chemische eigenschappen van dat geneesmiddel.

Ontwikkeling van een generiek multi-compartmenteel hersen PK model voor geneesmiddel distributie naar de hersenen

Het onderzoek beschreven in **hoofdstuk 3** had tot doel het ontwikkelen van een generiek multi-compartmenteel hersen PK model waarmee het beloop van de vrije geneesmiddelconcentraties op meerdere plaatsen in de hersenen voorspeld kan worden. Voor ontwikkeling van dit model hadden we de beschikking over gegevens van ongebonden en gebonden geneesmiddelconcentraties in plasma en verschillende hersencompartimenten, voor 9 geneesmiddelen met zeer verschillende fysisch-chemische eigenschappen. Voor paracetamol, atenolol, methotrexaat, morfine, kinidine en remoxipride waren gegevens over het beloop van de concentraties beschikbaar uit eerdere studies, terwijl voor paliperidon, fenytoïne, remoxipride, en risperidon gegevens uit nieuwe studies verkregen werden. Het ontwikkelde model was opgebouwd uit diverse compartimenten, waaronder plasma en de belangrijkste fysiologische hersencompartimenten ($\text{brain}_{\text{ECF}}$, $\text{brain}_{\text{ICF}}$ en 4 verschillende CSF-compartimenten) Dit generieke hersen PK model bevat wiskundige vergelijkingen voor de beschrijving van alle relevante fysiologische hersencompartimenten en bevat ook vergelijkingen voor 2 stof-specifieke parameters, te weten het geneesmiddeltransport over de bloed-hersenbarrière en de dispersie (een combinatie van flow en diffusie) van de geneesmiddelen door de brain ECF en CSF-compartimenten. Een interessante bevinding was dat de waarden van de dispersie voor de 9 verschillende stoffen vergelijkbaar waren.

Het ontwikkelde multi-compartmentele hersen PK model is relatief eenvoudig toe te passen omdat alleen *in vivo* plasma PK en brain ECF of CSF PK gegevens nodig zijn om voor een specifiek geneesmiddel de modelparameters te schatten. Echter, de noodzaak om beschikking te hebben over *in vivo* data is een beperking van dit model. Bovendien is dit model niet of beperkt geschikt om het effect van pathofysiologische condities op het concentratie- tijdprofiel van geneesmiddelen in de hersenen te voorspellen, omdat dit model uitgaat van fysiologische condities.

Tot slot hebben we aangetoond dat, onder fysiologische omstandigheden het multi-compartmentele hersen PK model kan worden gebruikt om het concentratie-tijdverloop van de vrije geneesmiddelconcentratie in de menselijke hersenen te voorspellen. Hiervoor werden de waarden van systeem-specifieke parameters van de rat vervangen door de corresponderende waarden van de mens en werd tevens gebruik gemaakt van allometrische schaling. Met het resulterende humane hersen PK model bleek het mogelijk om een adequate voorspelling te maken van het geneesmiddelconcentratie-tijdverloop in de verschillende fysiologische compartimenten van de menselijke hersenen.

Kort samenvattend heeft het onderzoek beschreven in dit hoofdstuk geleid tot een generiek multi-compartimenteel hersen PK model waarmee het beloop van de vrije geneesmiddelconcentratie in meerdere hersencompartimenten kan worden beschreven in zowel ratten als mensen. De gebruikte modelstructuur vormde vervolgens de basis voor het ontwikkelen van de PBPK hersen distributiemodellen voor ratten en mensen, zoals beschreven in de volgende hoofdstukken.

Ontwikkeling van een uitgebreid PBPK hersendistributie-model in ratten

Het onderzoek beschreven in **hoofdstuk 4** had tot doel om een integraal PBPK hersendistributiemodel te ontwikkelen waarmee het beloop van de ongebonden geneesmiddelconcentratie in meerdere compartimenten in de hersenen voorspeld kan worden op basis van alleen de fysisch-chemische eigenschappen van een geneesmiddel. De structuur van het hersen PBPK model voor de rat was gebaseerd op het eerder ontworpen generieke multi-compartimentele hersen PK model en bevat beschrijvingen van alle fysiologisch-relevante compartimenten in de hersenen en de geneesmiddel distributie processen. De waarden van de verschillende stof-specifieke en systeem-specifieke parameters voor dit model werden verkregen met behulp van *in silico* of *in vitro* methoden en/of uit de literatuur. Op basis van dit model werd een betrouwbare voorspelling verkregen van het tijdsverloop van de ongebonden concentratie van 10 verschillende geneesmiddelen (paracetamol, atenolol, methotrexaat, morfine, paliperidon, fenytoïne, kinidine, raclopride, remoxipride en risperidon) in $\text{brain}_{\text{ECF}}$, CSF_{LV} en CSF_{CM} waarbij een maximale afwijking slechts een factor 2 bedroeg.

Dit hersen PBPK model is het eerste model waarin expliciet onderscheid wordt gemaakt tussen paracellulair en transcellulair transport over de bloed-hersenbarrière en de bloed-liquorbarrière, waartoe twee aparte vergelijkingen in het model zijn opgenomen. De relatieve bijdrage van paracellulaire en transcellulaire diffusie aan de totale passieve diffusie was per geneesmiddel verschillend. Het onderscheid tussen deze twee passieve transportprocessen bleek van belang voor de voorspelling van geneesmiddelconcentraties in de hersenen in patho-fysiologische condities, omdat de relatieve bijdragen van deze transportprocessen eveneens in verschillende mate werden beïnvloed door patho-fysiologische condities.

Het door ons ontwikkelde hersen PBPK model is een waardevolle methode om het beloop van de vrije geneesmiddelconcentratie in de hersenen van ratten te voorspellen voor nieuwe geneesmiddelen, zonder dat er *in vivo* PK data beschikbaar hoeven te zijn. Bovendien kan met dit model worden aangetoond of verschillen in geneesmiddeldistributie naar de hersenen het gevolg zijn van variatie in de systeem-specifieke parameters (bijvoorbeeld in pathofysiologische situaties) of variatie in de

waarden van de stof-specifieke eigenschappen (bijvoorbeeld de fysische en chemische eigenschappen). Deze informatie kan vervolgens gebruikt worden bij de selectie van kandidaatmoleculen tijdens het onderzoek naar nieuwe geneesmiddelen.

Opschalen van het volledige PBPK hersendistributie-model van rat naar mens

De volgende stap in ons onderzoek was het opschalen van het volledige PBPK hersendistributiemodel van rat naar mens zodat we de geneesmiddelconcentraties in de hersenen van de mens kunnen voorspellen; dit is beschreven in **hoofdstuk 5**. Hiervoor hebben we de waarden van de systeem-specifieke parameters voor de ratten vervangen door de humane waarden. Ook hebben we de bijdrage van actieve transportereiwitten geschaald van rat naar mens op basis van verschillen in expressieniveaus en de activiteit/functionaliiteit van de betrokken transporteiwitten.

Door de voorspelde resultaten met het humane hersen PBPK hersendistributiemodel te vergelijken met beschikbare human PK gegevens voor paracetamol, oxycodon en morfine uit brainECF en/of CSF konden we het opgeschaalde model evalueren. De afwijking tussen de voorspelde PK profielen en de gemeten PK data was maximaal een factor 1,6 voor PK data die waren verkregen in een fysiologische situatie. Echter, geneesmiddelen voor neurologische aandoeningen worden juist gebruikt in situaties waarbij er sprake is van een patho-fysiologische conditie van de hersenen en ook dit kan van invloed zijn op het concentratie-tijd verloop van geneesmiddelen in de hersenen. Daarom hebben we literatuurgegevens gebruikt voor het onderzoek naar de invloed van pathologische condities op de PK van paracetamol en morfine voor patiënten met traumatisch hersenletsel en voor de PK van fenytoïne in patiënten met epilepsie. In patiënten met traumatisch hersenletsel is de doorbloeding van de hersenen afgenomen en is er een toename in para-cellulaire permeabiliteit. Ook zijn er veranderingen in de activiteit/expressioniveaus van de verschillende transportereiwitten gerapporteerd. In patiënten met epilepsie is er, naast de afname in cerebrale doorbloeding en de toename in para-cellulaire permeabiliteit, een toename in de activiteit van sommige efflux-transportereiwitten, zoals het P-glycoproteïne (P-gp) en de 'multidrug resistance-associated proteins' (MRPs) gerapporteerd. De invloed van deze veranderingen op geneesmiddeldistributie naar en in de hersenen zijn onderzocht met behulp van het humane hersen PBPK model.

Het concentratie-tijdprofiel van de paracetamol in CSF van patiënten met traumatisch hersenletsel en de fenytoïne concentratie in CSF van patiënten met epilepsie bleek goed beschreven te kunnen worden met het humane PBPK hersendistributiemodel waarbij dezelfde systeem-specifieke parameters werden gebruikt als voor de fysiologische

situatie. Hieruit kunnen we opmaken dat de farmacokinetiek van deze stoffen niet significant wordt beïnvloed door deze neurologische aandoeningen. Echter, het concentratie-tijdsverloop van morfine in brein_{ECV} van patiënten met traumatisch hersenletsel werd alleen goed beschreven als systeem-specifieke parameters werden aangepast voor de beschreven pathofysiologische veranderingen. Hierdoor konden we de invloed van traumatisch hersenletsel op de PK van morfine kwantitatief onderzoeken.

Samengevat kunnen we voor een fysiologische situatie met het humane hersen PBPK model de vrije geneesmiddelconcentraties in diverse compartimenten van de humane hersenen voorspellen zonder dat daarvoor (pre)klinische PK gegevens nodig zijn. Dit kan al in een vroeg stadium van het geneesmiddelontwikkelingsproces waardevolle informatie opleveren over de PK in de humane hersenen. Ook hebben we aangetoond dat het humane hersen PBPK model gebruikt kan worden om, op een kwantitatieve manier, de invloed van een pathofysiologische conditie op de geneesmiddel PK in de hersenen te onderzoeken. Dit is een belangrijke stap, omdat het informatie oplevert over de invloed van de pathofysiologische situatie op de systeem-specifieke hersenparameters en daarmee over geneesmiddeldistributie naar de hersenen bij verschillende neurologische aandoeningen.

TOEKOMSTPERSPECTIEF

Doordat ons model een generieke basisstructuur heeft kan het verder worden verfijnd en geoptimaliseerd tot een nog robuuster en breder toepasbaar hersen PBPK model. Hiervoor hebben we de volgende ideeën:

1. Verdere evaluatie en optimalisatie van het model met behulp van PK data van andere geneesmiddelen en/of diersoorten;
2. Een op mechanisme-gebaseerd onderzoek naar de invloed van verschillende neurologische aandoeningen op het concentratie-tijdsverloop van geneesmiddelen in de hersenen gebruik makend van gegevens voor hersenaandoeningen anders dan traumatisch hersenletsel en epilepsie;
3. Door in een systeembenadering de invloed van populatie-specifieke eigenschappen op het concentratie-tijdsverloop van geneesmiddelen in de hersenen te onderzoeken, waarbij gebruik gemaakt kan worden van PK data verkregen bij pediatrische en geriatrische patiënten.

De voorspelling van de effecten van geneesmiddelen in de hersenen is van groot belang om het succespercentage in de ontwikkeling van geneesmiddelen voor hersenaandoeningen te verbeteren. Wij zijn van mening dat de ontwikkeling van een

hersenen PBPK- farmacodynamisch (PBK-PD) model waarmee op basis van *in vitro* en *in silico* analyses de vrije geneesmiddelconcentraties van geneesmiddelen in relevante compartimenten in de hersenen kunnen worden voorspeld, een belangrijke mijlpaal is. Het ontwikkelde hersenen PBPK model kan dan worden geïntegreerd met, onder meer target associatie/dissociatie kinetiek (sub)modellen en modellen voor beschrijving van de target activatie, transductie en homeostatische feedback mechanismen, met als uiteindelijk doel de voorspelling van het beloop van het effect.

CONCLUSIE

Een uitvoerig hersenen PBPK model is ontwikkeld om de vrije geneesmiddelconcentraties in meerdere compartimenten van de hersenen te voorspellen, zowel in ratten als in mensen. Dit model kan ook worden gebruikt om voor stoffen met uiteenlopende fysisch-chemische eigenschappen het concentratie-tijdsverloop van geneesmiddelen in relevante compartimenten in het hersenen te voorspellen. Bovendien geeft het model inzicht in de invloed van hersenaandoeningen op de distributie naar en in de hersenen. Omdat voor de voorspelling van de concentraties van nieuwe geneesmiddelen in de hersenen uitsluitend gegevens uit *in vitro* en *in silico* studies nodig zijn, is het model bij uitstek geschikt voor toepassing in de vroege fases van het geneesmiddelenonderzoek en bij de selectie van kandidaatgeneesmiddelmoleculen. In de latere fases klinische fases kan het model worden toegepast om veranderingen in de verdeling naar de hersenen als gevolg van pathofysiologische processen te voorspellen.

ACKNOWLEDGEMENTS

First, I am grateful to my supervisor Dr. Elizabeth C.M. de Lange for all knowledge and experiences I have gained during my time in the University of Leiden. I would like to thank for the opportunities that she gave me, her brilliant ideas, her passion, and above all, for being patient and trusting in me.

I place on record, my sincere gratitude to Prof. Meindert Danhof for constantly encouraging and supporting me during this challenging journey. Our meetings were always important occasions to receive wise suggestions and useful feedback.

I wish to express my sincere thanks to Dr. Johan GC. van Hasselt, for supporting me with his excellent knowledge and experience, and for his enthusiasm that always encouraged me to get through all the difficult moments and help me to build confidence.

I am thankful to all staff, post-doc and PhD colleagues that I got to know during the years spent at the Division of Pharmacology of the University of Leiden, with whom I could exchange ideas and experiences and ask for support and collaboration. A special acknowledgment to Piry and Eric for giving me scientific advice, Dirk-Jan and Robin for producing beautiful animal data, Willem and Wilbert for having discussions related to my research.

This research was performed within the framework of project no. D2-501 of the former Dutch Top Institute Pharma, currently Lygature (Leiden, the Netherlands). I would like to thank all project members, Dymphy, Hans, An, Walter Suruchi and Margot to always giving me scientific advice.

Lastly, special thanks to my husband J-P and my daughter Sara, who always respect what I would like to do and kindly support me. Thank you for following my decisions and for always trusting in me.

CURRICULUM VITAE

Yumi Yamamoto (Emoto) was born on the 25th of November 1980 in Tokyo, Japan.

She graduated from Tokyo Institute of Technology, where she obtained her BSc in 2003. Subsequently she started her studies in Bioscience and Biotechnology at Tokyo Institute of Technology, where she obtained her MSc in 2005.

In April 2005, she started working at Chugai Pharmaceutical Co., Ltd., as a Clinical Pharmacologist and Pharmacokinetics/Pharmacodynamics Analyst. During that time she performed several phase I studies and pharmacological studies. At the same time, she performed broad range of non-linear mixed effect modeling such as population pharmacokinetic (PPK) analysis, pharmacokinetic/pharmacodynamic (PK/PD) analysis for clinical projects. In November 2009, she worked at F. Hoffmann-La Roche Ltd., as a pharmacometrician. During that time, she was exposed to more advanced system-based model of the glucose-insulin system to assess the PD of newly developed compounds for diabetes.

In May 2013, Yumi started her PhD research program at the Division of Pharmacology of the Leiden Academic Center for Drug Research with Dr. Elizabeth C.M. de Lange as a co-promoter and Prof. Meindert Danhof as a promoter, which led to this thesis. Her research theme was to develop a comprehensive physiologically based pharmacokinetic model which enables the prediction of drug concentration-time profiles in multiple CNS compartments in rats and humans.

LIST OF PUBLICATIONS

Yamamoto Y, Väliälto PA, Wong YC, Huntjens DR, Proost JH, Vermeulen A, et al. Prediction of human CNS pharmacokinetics using a physiologically based pharmacokinetic modeling approach. Submitted for publication.

Yamamoto Y, Väliälto PA, Huntjens DR, Proost JH, Vermeulen A, Krauwinkel W, et al. Predicting drug concentration-time profiles in multiple CNS compartments using a comprehensive physiologically based pharmacokinetic model. In press. CPT:PSP.

Yamamoto Y, Danhof M, de Lange ECM. Microdialysis : the Key to Physiologically Based Model Prediction of Human CNS Target Site Concentrations. AAPS J. 2017;19(4):891–909.

Yamamoto Y, Väliälto PA, van den Berg D-J, Hartman R, van den Brink W, Wong YC, et al. A Generic Multi-Compartmental CNS Distribution Model Structure for 9 Drugs Allows Prediction of Human Brain Target Site Concentrations. Pharm Res. 2017;34(2):333–51.

(Publications not in this thesis)

De Lange ECM, van den Brink W, **Yamamoto Y**, de Witte WEA, Wong YC. Novel CNS drug discovery and development approach: model-based integration to predict neuro-PK and PD. In press. Expert Opin Drug Discov.

Emoto-Yamamoto Y, Iida S, Kawanishi T, Fukuoka M. Population pharmacokinetics of erlotinib in Japanese patients with advanced non-small cell lung cancer. J Clin Pharm Ther. 2015;40(2):232–9.

Kervezee L, Hartman R, van den Berg D-J, Shimizu S, **Emoto-Yamamoto Y**, Meijer JH, et al. Diurnal variation in P-glycoprotein-mediated transport and cerebrospinal fluid turnover in the brain. AAPS J. 2014;16(5):1029–37.

Emoto Y, Wada H, Okamoto H, Kudo A, Imai Y. Retinoic acid-metabolizing enzyme Cyp26a1 is essential for determining territories of hindbrain and spinal cord in zebrafish. Dev Biol. 2005;278(2):415–27.

